Perpendicular Magnetic Anisotropy in Sputter-Deposited Fe/MgO(001)-Based Heterostructures

Yuki Iida

February 2021

Perpendicular Magnetic Anisotropy in Sputter-Deposited Fe/MgO(001)-Based Heterostructures

Yuki Iida

Doctoral Program in Materials Science and Engineering

Submitted to the Graduate School of

Pure and Applied Sciences

in Partial Fulfillment of the Requirements

for the Degree of Doctor of Philosophy in

Engineering

at the

University of Tsukuba

Table of Content

Chapter 1 Introduction

1.1 Spintronics

Spintronics is a field that aims to surpass conventional electronic devices based on semiconductor engineering by utilizing spin degrees of freedom in addition to charge degrees of freedom.[1] Particularly with respect to memory, attention has been paid to the magnetoresistive effect in which the resistivity changes by applying a magnetic field. Anisotropic magnetoresistance (AMR) is the effect of changing resistance in a ferromagnet depending on the direction of spontaneous magnetization. Giant magnetoresistance (GMR) is a fundamental phenomenon in spintronics and is different in quantity and quality from AMR.[2,3] It was used as a playback head for hard disk drives, leading to a dramatic increase in storage capacity. The GMR element has a structure in which two ferromagnetic layers are separated by a non-magnetic layer. Since the spin scattering differs depending on the relative angle of magnetization of the two layers, the resistivity changes. On the other hand, there is the tunnel magnetoresistance (TMR) effect, which is similar to GMR.[4-6] TMR effect is observed in magnetic tunnel junction (MTJ), composed of a ferromagnetic layer/insulating layer/ferromagnetic layer. Since the tunnel probability differs depending on the relative angle of magnetization of the ferromagnetic layer, the resistivity changes significantly. When the magnetization is parallel, the resistance becomes small, while when it is anti-parallel, the resistance becomes large. As shown in Figure 1.1, these corresponds to the binary data “1” and “0”. MTJs are not only used for a sensor like a GMR element, but also used as a memory cell in a magnetoresistive random access memory (MRAM). MRAM is a non-volatile memory, leading to low power consumption system, which is the advantage compared to static random access memory (SRAM) and dynamic random access memory (DRAM).[7,8] MRAM also has a high endurance. The write speed is not as good as SRAM, but comparable to DRAM. Since one memory cell is composed of one MTJ and one transistor, it is difficult to exceed the density of DRAM. MRAM is currently in practical use and is expected to replace DRAM in the future. There are several types of MRAM, which are introduced below.

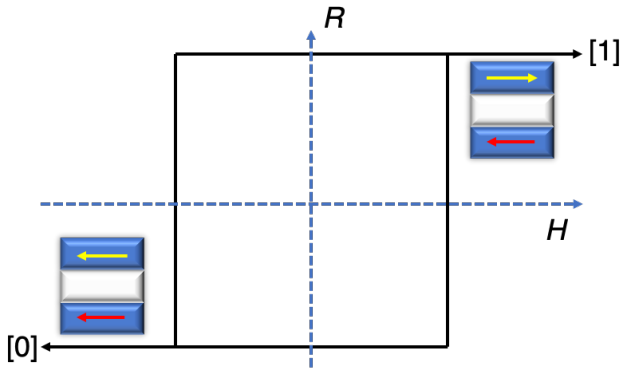

Figure 1.1 The resistance change in MTJ.

· Magnetic field MRAM

The magnetic field writing MRAM was initially proposed. It consists of MTJ, word line, and bit line. When current flows through the word line and bit line, a magnetic field is generated, which reverse the magnetization direction of the free layer. In the Storner-Wohlfarths model, the magnetic field required for inversion is expressed as follows.[7]

$$H_W+H_B=H_K^{2/3} \tag{1.1}$$

Here, H_W and H_B are magnetic fields generated from the word line and bit line, and H_k is an anisotropic magnetic field assuming that the free layer is a single domain. Even if current flows through either one, inversion does not occur unless the threshold value is exceeded, and the memory cell can be selectively changed. When trying to increase the recording density, there is a problem that the magnetization is reversed even with one of the currents and the error rate increases. Therefore, the recording density is small compared to other MRAMs.

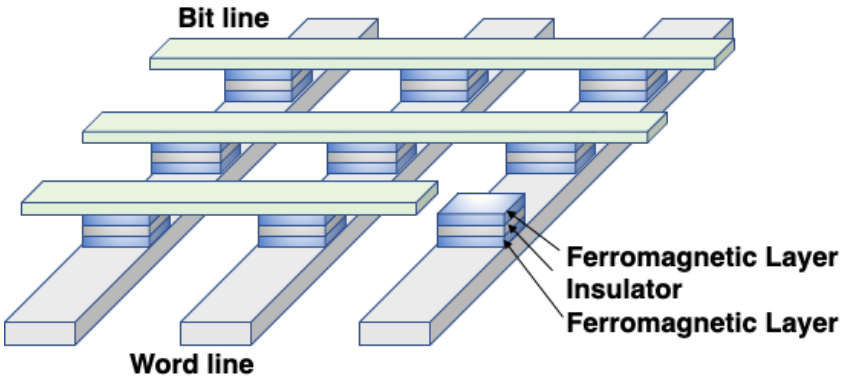

Figure 1.2 Magnetic field MRAM

· Spin transfer torque MRAM (STT-MRAM)

In order to increase the recording density, this model rotates the magnetization by the torque of the spin caused by passing an electric current instead of writing by a magnetic field.[9] To change the magnetization from antiparallel to parallel, when a current is passed from the pin layer side, only majority spins flow as a tunnel current, and the magnetization of the free layer is reversed by the torque. On the other hand, when changing from parallel to antiparallel, a current is passed from the free layer. The majority spins are tunneled, and the minority spins rebound at the barrier. The critical current density J_{c0} required to reverse the magnetization of the in-plane MTJ is expressed as follows.[9, 10]

$$J_{c0}=\frac{1}{\eta}\frac{2\alpha e}{\hbar}(M_s t)\left(\frac{1}{2}(4\pi M_{eff})+H_K\right) \tag{1.2}$$

Here, e is the charge of electrons, η is the spin transfer efficiency, α is the magnetic damping constant, M_s is the saturation magnetization, t is the thickness of the ferromagnetic layer, H_k is the anisotropy field, and $4\pi M_{eff}$ is the effective demagnetization field. Since the critical current

depends on the film thickness, only the magnetization of the free layer can be reversed by changing the film thickness of the pin layer and the free layer.

On the other hand, the critical current density of the perpendicular MTJ (p-MTJ) is expressed as follows.[10,11]

$$J_{c0} = \frac{1}{\eta}\frac{2\alpha e}{\hbar}(M_s t)H_K \quad (1.3)$$

Compared with in-plane MTJ, the energy corresponding to the shape magnetic anisotropy can be reduced. Moreover, it can also improve the recording density.

·Spin orbit torque MRAM (SOT-MRAM)

In SOT-MRAM, the magnetization is reversed by using the spin current generated from the spin Hall effect.[12] STT-MRAM has 2 terminals, but SOT-MRAM consists of 2 terminals on the bottom electrode and 1 terminal on the top electrode.[7] It consumes less power than STT-MRAM and has a faster writing speed, but its recording density is inferior because it has 3 terminals.

·Voltage-control MRAM

Large perpendicular magnetic anisotropy (PMA) energy prevents thermal fluctuation of magnetization but increases energy consumption during magnetization reversal. Therefore, research is being conducted to reduce the PMA energy by applying a voltage to reduce the energy consumption during magnetization reversal.[13]

In this study, materials development for voltage-control MRAM have been performed. Detailed explanation of voltage control magnetic anisotropy is given in Chapter 1.4.

1.2 Tunnel magnetoresistance (TMR)

TMR ratio is the most important factor for MTJ. In this section, the theory and history of TMR and actual materials is described. TMR ratio is expressed as follows.

$$\text{TMR}\ (\%) = \frac{R_{ap}-R_p}{R_p}\times 100 \quad (1.4)$$

Here, R_{ap} and R_p are the resistance when the magnetization directions of two ferromagnetic layers are antiparallel and parallel, respectively. Figure 1.3~1.10 show history of TMR and inverse TMR measured at room temperature and low temperature from 1995 to 2019.

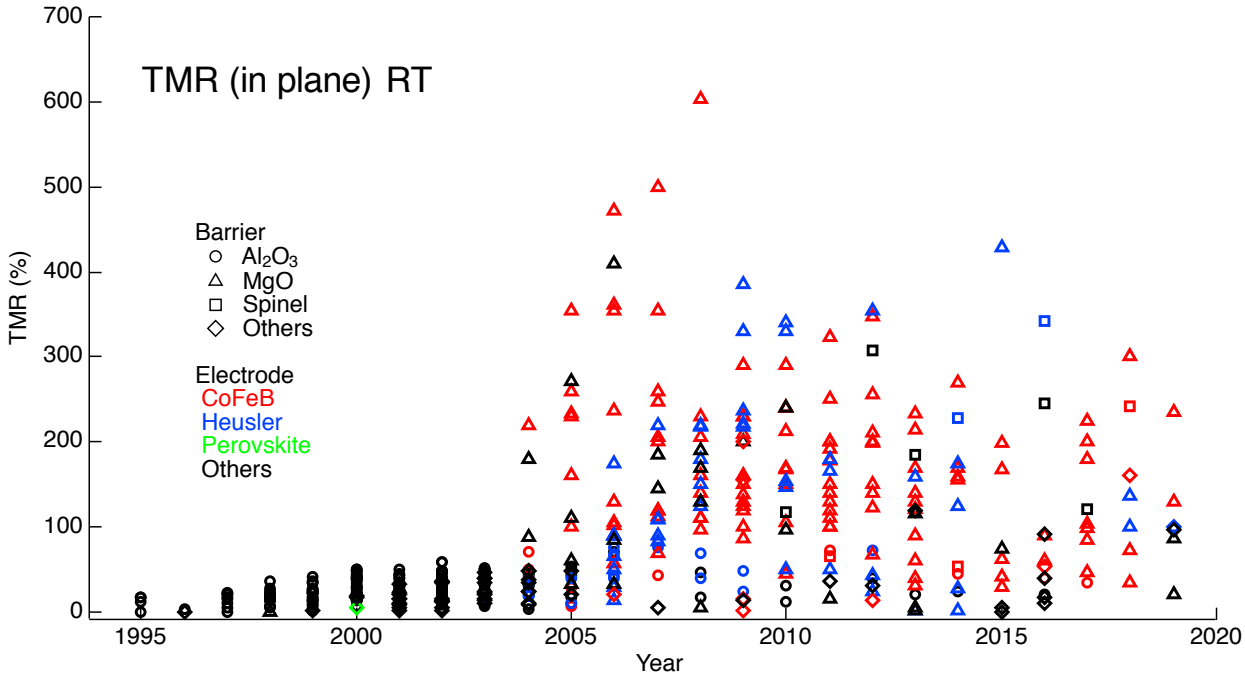

Figure 1.3 In-plane TMR measured at RT.

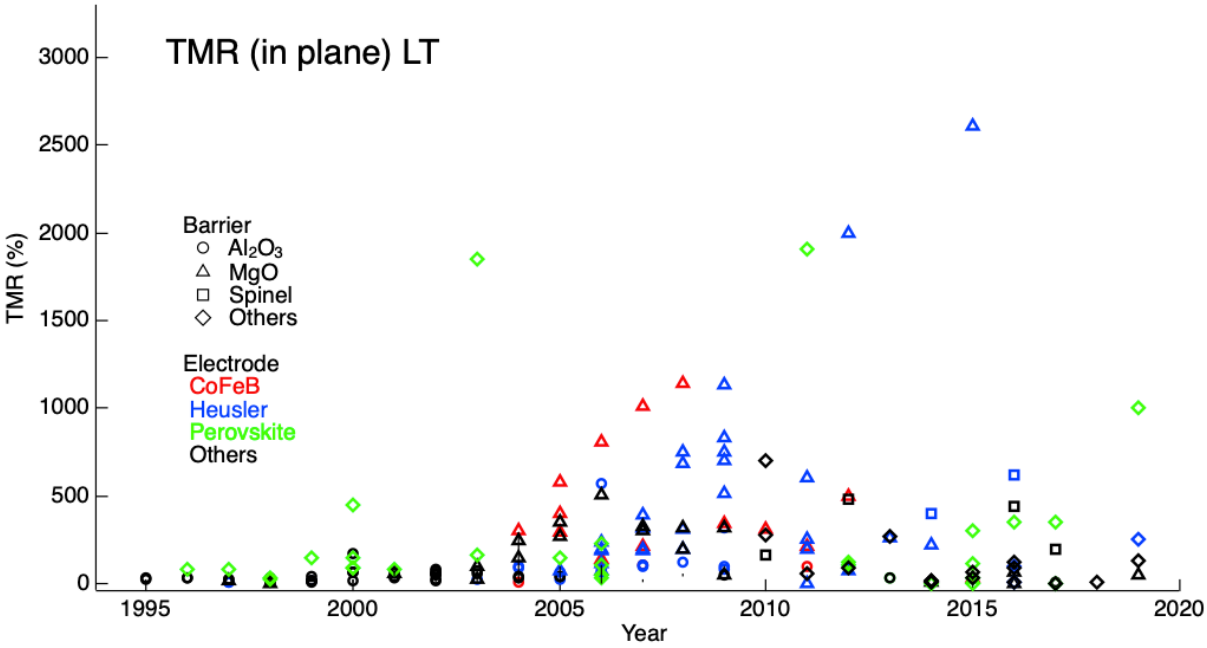

Figure 1.4 In-plane TMR measured at LT.

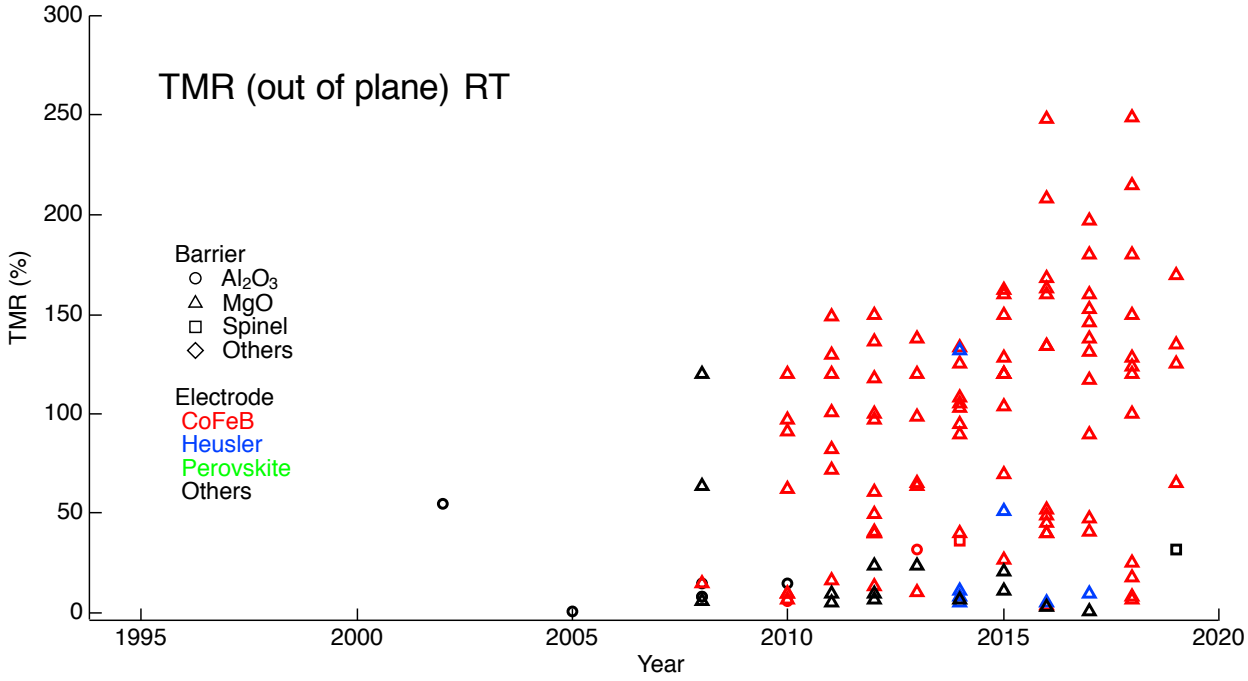

Figure 1.5 Out-of-plane TMR measured at RT.

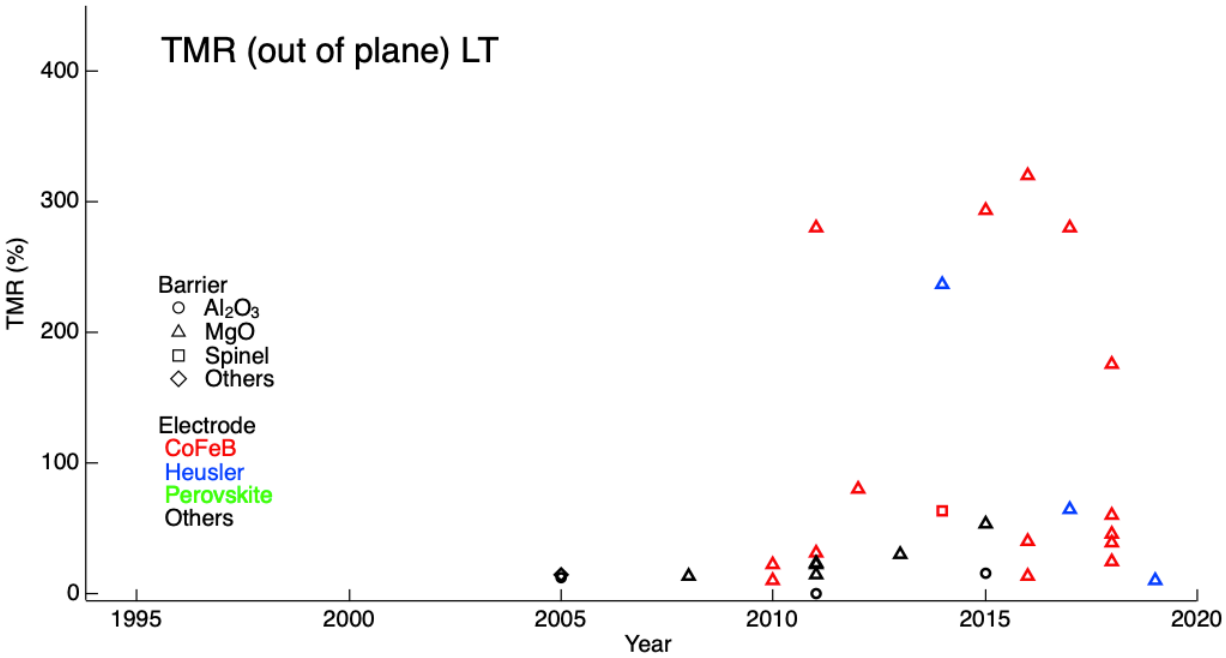

Figure 1.6 Out-of-plane TMR measured at LT.

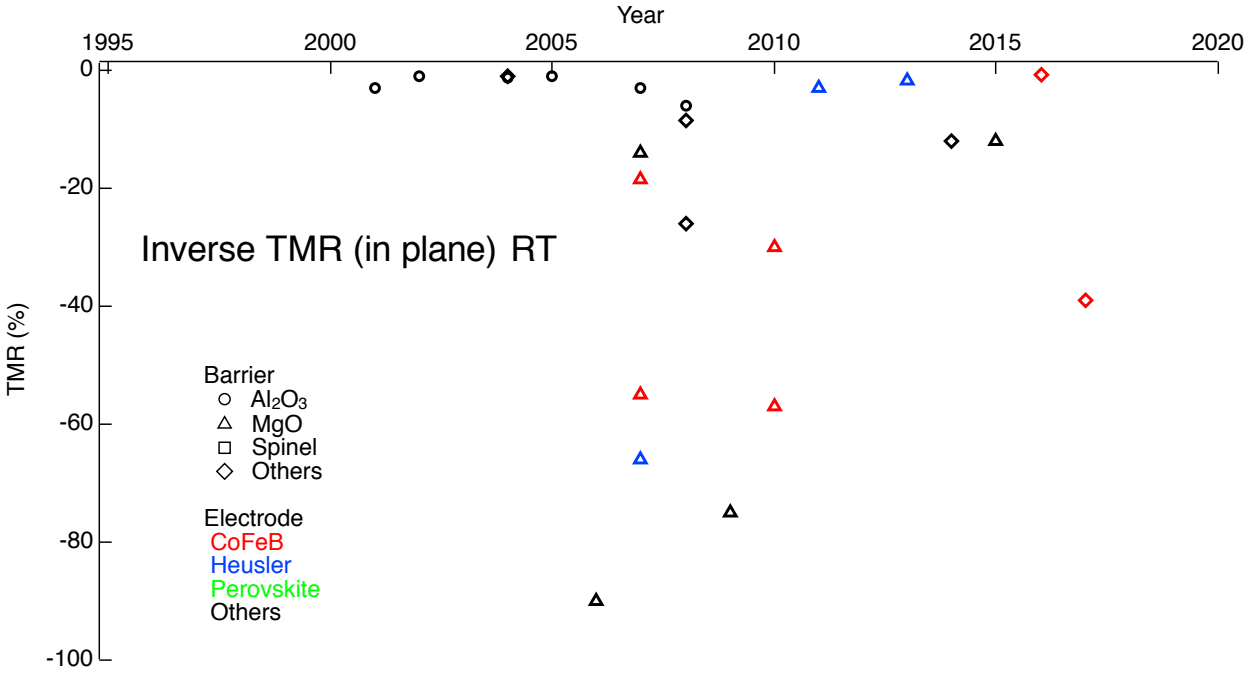

Figure 1.7 In-plane inverse TMR measured at RT.

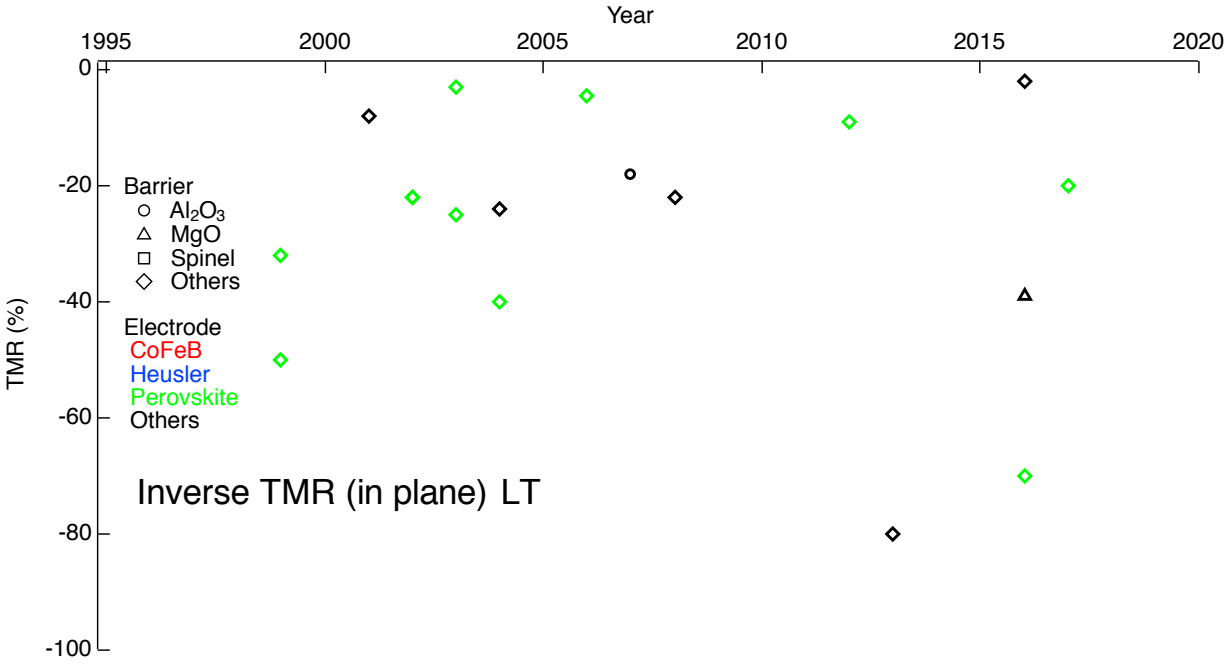

Figure 1.8 In-plane inverse TMR measured at LT.

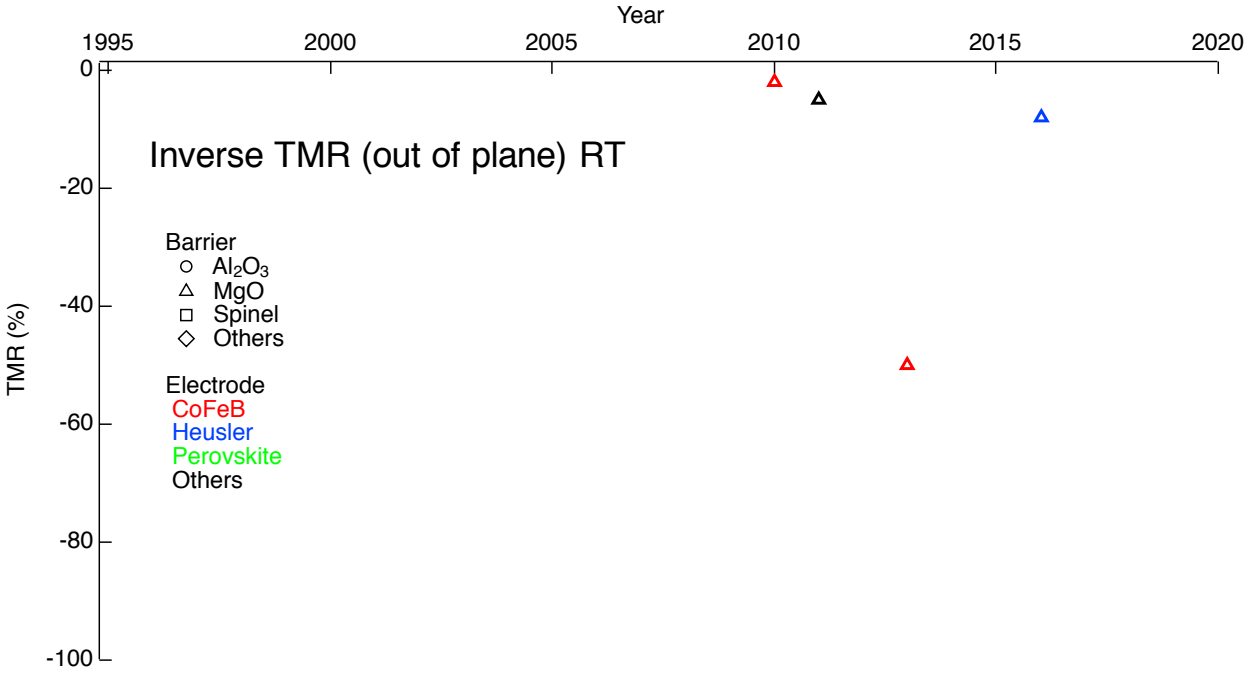

Figure 1.9 Out-of-plane inverse TMR measured at RT.

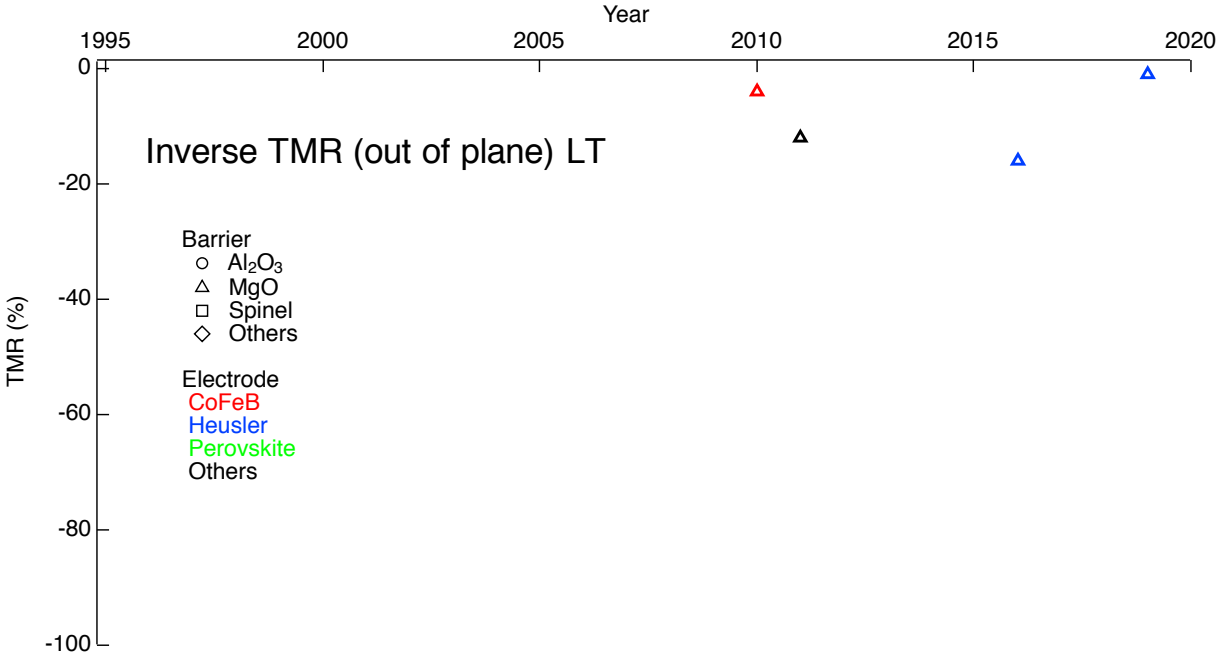

Figure 1.10 Out-of-plane inverse TMR measured at RT.

In Figure 1.3~1.10, the barrier is represented by a shape and the electrodes are represented by a color. Circles, triangles, squares, and diamonds represent Al_2O_3, MgO, Spinel, and Others, respectively. Red, blue, green and black represent CoFeB, Heusler, Perovskite and Others. If the material is different for the top and bottom electrodes, the priority of display priority in Figure 1.3~1.10 is Heusler, Perovskite, CoFeB, Others. For example, in the case of Co_2MnSi/MgO/CoFeB, it is represented by a blue triangle. Each reference, structure, TMR, and measured temperature are summarized in Appendix.

The TMR effect was reported by Julliere in 1975 in the structure of Fe/Ge/Co.[4] Its TMR ratio is 14 % at 4.2 K. Its theoretical interpretation is known as the Julliere model (Figure 1.11). The spin polarization is represented by P = 2a-1 and P' = 2a'-1, where a and a' are the existence probabilities of electrons at the Fermi level in each electrode. Assuming that spin flip does not occur in the electron tunneling process, the conductances G_p and G_{ap} when the magnetizations of the two electrodes are parallel and antiparallel are expressed as follows.

$$G_p \propto a \cdot a' + (1 - a) \cdot (1 - a') \quad (1.5)$$

$$G_{ap} \propto a \cdot (1 - a') + (1 - a) \cdot a' \quad (1.6)$$

Using (1.5) and (1.6), TMR ratio is expressed as follows.

$$\text{TMR}\ (\%) = \frac{R_{ap}-R_p}{R_p} = \frac{2PP'}{1-PP'} \quad (1.7)$$

Therefore, high spin polarization leads to be high TMR ratio.

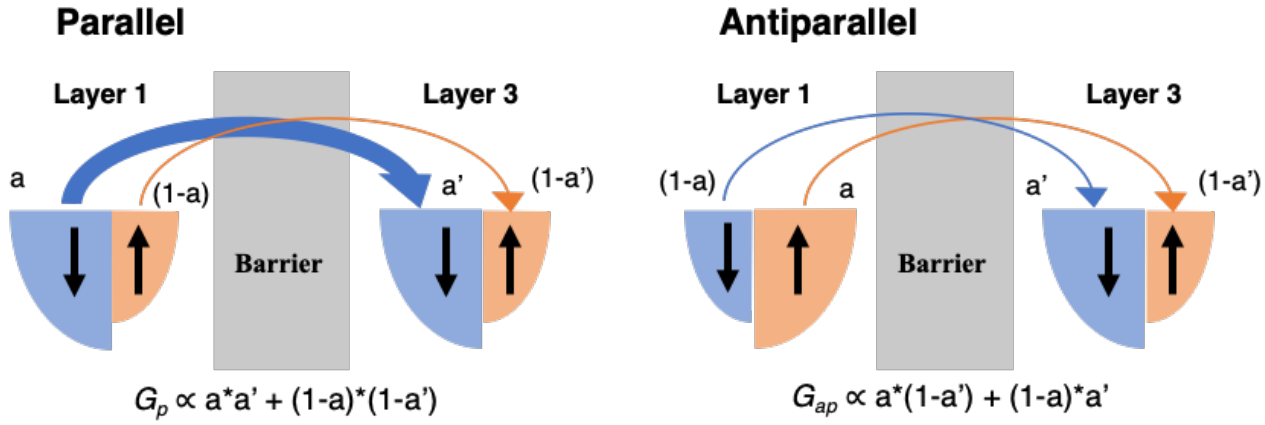

Figure 1.11 Julliere's model

The observation of TMR at room temperature by Moodere and Miyazaki in 1995 raised expectations for its application,[5,6] and a huge amount of research was conducted as shown in Figure 1.3~1.10. In 1995, TMR of 11.8% and 18% were obtained for CoFe/Al_2O_3/Co and Fe/Al_2O_3/Fe, respectively. As shown in Figure 1.3, research was conducted focusing on the Al_2O_3 barrier until the first half of 2000. Various barriers such as Ta oxides,[14-16] Hf oxides,[17-19] fluorides[20] and organics[21-23] were studied to obtain larger TMR. In these efforts, research on MgO barriers started,[24-29] and in 2004 there was a breakthrough in which a lager TMR of around 200% was achieved.[30,31] In the Fe/MgO/Fe MTJ, the spin polarization of Fe is not large,

so a large TMR cannot be expected in the Julliere model. Figure 1.12 shows tunneling density of states for Fe(100)/MgO/Fe(100).[32] Electrons with Δ_1 symmetry can be tunneled because of slow decay in MgO barrier. Moreover, since the electrons with Δ_1 symmetry are highly spin-polarized in Fe, a large TMR ratio can be obtained.

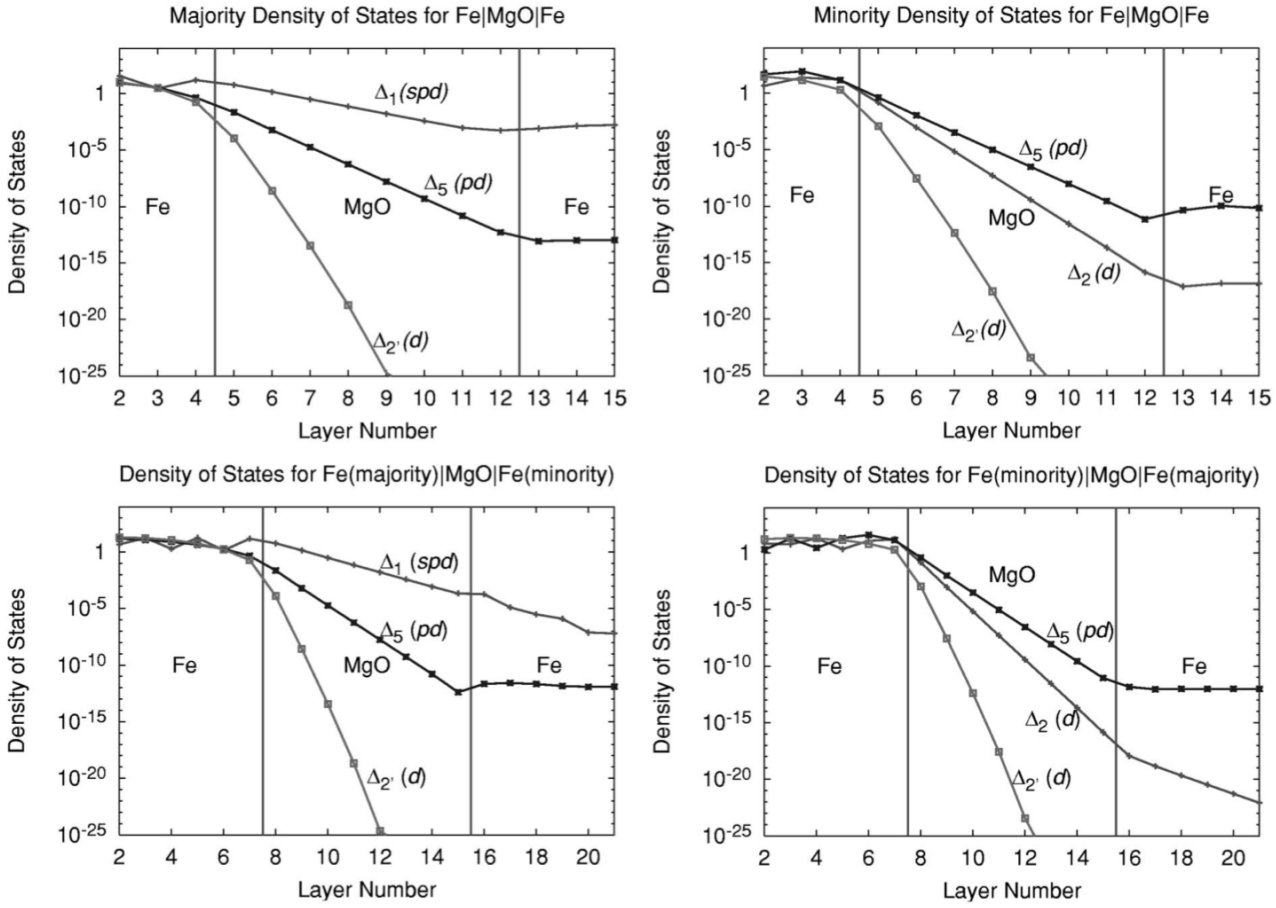

Figure 1.12 Tunneling density of states (DOS) Fe(100)/MgO/Fe(100). Upper figures show tunneling DOS in for parallel alignment of the magnetization and lower figures show tunneling DOS in for antiparallel alignment. Reprinted with permission from [32].

Normally, when using MTJ to MRAM, it is necessary to apply an exchange bias using IrMn or FeMn to create a pin layer.[33-36] However, since IrMn and FeMn are oriented toward the (111) plane, the Fe (001) plane cannot be made on it. Therefore, an amorphous electrode using CoFeB has been developed. The deposited CoFeB has an amorphous structure, and the MgO deposited on CoFeB becomes a polycrystal oriented in the (001) direction.[37] After annealing, CoFeB polycrystallizes along the MgO (001) direction. In addition, since CoFeB can be applied to various buffer layers, many studies have been conducted as shown in Figure 1.3~1.10.

Perovskite oxides such as $LaSrMnO_3$ (LSMO) show high spin polarizability.[38] Using $SrTiO_3$ (STO) as a barrier, which is also a perovskite oxide, a large TMR of over 1000% has been

experimentally obtained in the stack of LSMO/STO/LSMO.[39] However, since the Curie temperature of LSMO is lower than RT, TMR is achieved only at LT as shown in Figure 1.4. In order to use the material with high spin polarization at room temperature, Heusler alloy electrodes were developed. In CoMnFeSi/MgO/CoMnFeSi, TMR of 429 % and 2610 % was achieved at RT and LT.[40]

As described in Chapter 1.1, when the direction of the easy magnetization axis of MTJ became out-of-plane direction, the threshold current for the STT switching can be reduced, and the recording density is also improved. In order to make p-MTJs, the electrodes must have a PMA. In 2002, TMR of 55 % at room temperature was reported in the structure of GdFeCo/CoFe/Al_2O_3/CoFe/TbFeCo.[41] In this structure, GdFeCo and TbFeCo has PMA. After that, it was found that CoFeB/MgO interface show interface PMA.[42] In 2010, a CoFeB/MgO/CoFeB p-MTJ with TMR of 120% was achieved.[43] As shown in Fig. 1.5, most of p-MTJ is composed of CoFeB/MgO. This is thought to be due to the fact that CoFeB/MgO can easily achieve a large TMR and can be formed on various buffer layers, as is the case with in-plane MTJs. The MTJ currently in practical use for MRAM is based on CoFeB/MgO/CoFeB.

Inverse TMR is the effect observed when the spin polarization is a negative value.[44] The sign of TMR changes from positive to negative when an oxide electrode is used or when a bias voltage is applied. To date, as shown in Figure 1.7~1.10, no inverse TMR exceeding 100% has been reported. It is expected from the perspective of basic research.

1.3 Perpendicular magnetic anisotropy (PMA)

In order to make p-MTJs, the easy magnetization axis in the electrode should be out of plane. Table 1.1 summarizes the materials with PMA in the MTJs used in Figure 1.5, 1.6, 1.9, 1.10. GdFeCo and TbFeCo were adopted in the first p-MTJ created.[41] Co/Pd and Co/Pt multilayered stacks are known to exhibit large PMA and are now commonly used in pin layers.[45,46] These Co/Pd and Co/Pt have a large damping constant, which means that the critical current for switching becomes large. Therefore, it is not suitable for the free layer. Electrodes using Mn alloy for the free layer can achieve a low damping constant, but the problem of low TMR ratio remains.[47] Currently, the mainstream research toward the free layer is the interface magnetic anisotropy of the ferromagnetic layer and the oxide. Research on various electrodes and barriers has been conducted.

Table 1.1 Materials with PMA actually used in MTJs

Alloys	Stacks
・GdFeCo [41]	・Co/Pd multi stack [45]
・TbFeCo [41]	・Co/Pt multi stack [46]
・CoPt [48]	・CoFe/Pd multi stack [58]
・FePt [49]	・Ni/Co multi stack [59]
・FePd [50]	・CoFeB/MgO [43]
・$D0_{22}$-MnGa [51]	・Fe/MgO [60]
・$L1_0$-MnGa [47]	・$CoFeB/MgAl_2O_4$ [61]
・MnCoGa [52]	・Fe_2CrSi/MgO [62]
・GdFe [53]	・$Fe/MgAl_2O_4$ [63]
・Mn_3Ge [54]	・Co_2FeAl/MgO [64]
・Mn_2RuGa [55]	
・CoGa/MnGa [56]	
・MnGaN [57]	

・ Required PMA energy

Large PMA energy is required to prevent the magnetization from reversing naturally due to thermal fluctuation. The following relationships must be satisfied in order to retain the data for 10 years at room temperature.

$$\frac{K_{eff}V}{k_BT} > 60 \tag{1.8}$$

Here, K_{eff} is the effective PMA energy, V is the volume of the ferromagnetic material, K_B is the Boltzmann constant, and T is the temperature. The smaller the device size, the more PMA energy is required. Figure 1.13 shows the PMA energy required for MTJs whose shape is a pillar. The horizontal axis is the diameter and the vertical axis is the film thickness of the ferromagnetic layer. For example, when the diameter is 20 nm and the film thickness of the ferromagnetic layer is 1 nm, K_{eff} of 1 MJ/m^3 or more is required.

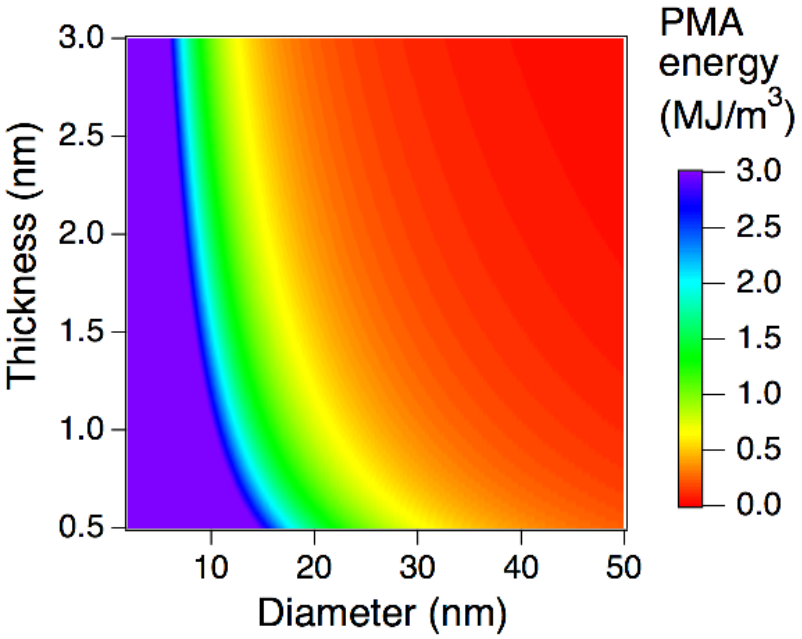

Figure 1.13 Required PMA energy depending on thickness and diameter of the ferromagnetic layer.

The relationship among the interface magnetic anisotropy energy K_i, the film thickness of the ferromagnetic layer t, the effective PMA energy K_{eff}, the shape magnetic anisotropy energy K_s, and the volume magnetic anisotropy energy K_v is described below.

$$K_{eff} \cdot t = (K_V - K_s) \cdot t + K_i \quad (1.9)$$

The contribution of K_v is small in the case of ultrathin films. Assuming the shape of the ferromagnetic layer as an infinite flat plate, K_s is proportional to the square of the saturation magnetization M_s. K_{eff} becomes a positive value when the film thickness is thin to reduce the negative contribution of K_s and the interface magnetic anisotropy is sufficiently large. For example, in Ta/CoFeB/MgO, when the film thickness of CoFeB is thick, the easy magnetization axis is in the in-plane direction, but when it is 1.5 nm or less, it becomes PMA.[43]

・Theory of magnetic anisotropy

Ferromagnetic single crystals such as Fe, Ni, and Co have magnetic anisotropy that depends on the crystal orientation. In the case of Fe with a body-centered cubic structure, the magnetization is saturated immediately when a magnetic field is applied in the [100] direction, while a large magnetic field is required to saturate the magnetization by applying a magnetic field in the [111] direction. This magnetic anisotropy is explained by the spin-orbit interaction.[65] If the overlap of orbitals changes depending on the crystal orientation, the strength of the exchange interaction also changes accordingly. The magnetic energy is minimized in the direction in which the exchange interaction is strongest, and the axis

becomes the easily magnetized axis.

In a thin film, unlike bulk, the effect of the surface or interface has a large effect on magnetic anisotropy. In the second order perturbation theory, the interface magnetic anisotropy is given as follows.[66]

$$K_i \propto E_{\uparrow\uparrow} + E_{\downarrow\downarrow} + E_{\uparrow\downarrow} + E_{\downarrow\uparrow} \cong E_{\downarrow\downarrow} + E_{\uparrow\downarrow} \tag{1.10}$$

$E_{\uparrow\uparrow}$, $E_{\downarrow\downarrow}$, $E_{\uparrow\downarrow}$, $E_{\downarrow\uparrow}$ are the spin-orbit interaction energy in each spin transition. The values of $E_{\uparrow\uparrow}$ and $E_{\downarrow\uparrow}$ are negligibly small. For example, up-down (↑↓) means a virtual excitation from an occupied up-spin state to an unoccupied down-spin state. Here, $E_{\uparrow\uparrow}$ and $E_{\downarrow\downarrow}$, are non-spin flip term, and $E_{\uparrow\downarrow}$ and $E_{\downarrow\uparrow}$are spin flip term.

In Bruno model, non-spin flip term corresponds to the anisotropy of the orbital moments ΔM_{orb} in the in-plane direction and the out of plane direction.[67]

$$E_{\downarrow\downarrow} = \frac{\xi}{4\mu_B}\left(M_{orb}{}^{\perp} - M_{orb}{}^{\parallel}\right) \tag{1.11}$$

Here, ξ is the spin-orbit interaction constant. If the contribution of the spin flip term is small, the interfacial magnetic anisotropy strongly depends on ΔM_{orb}. In the case of a monolayer, in-plane orbitals are quenched by Coulomb repulsion, but out-of-plane orbitals are not quenched and are localized.[68] Hence, anisotropy of the orbital moment arises.

As an example, consider the magnetic anisotropy of free-standing Co (111) monolayer and Au/Co monolayer/Au. In Co thin film, there are in-plane orbital states ($d_{x^2-y^2}$, d_{xy}) and out of plane orbital states (d_{xz}, d_{yz}, $d_{3z^2-r^2}$). Figure 1.14 shows DOS of a free-standing Co (111) monolayer.[69]

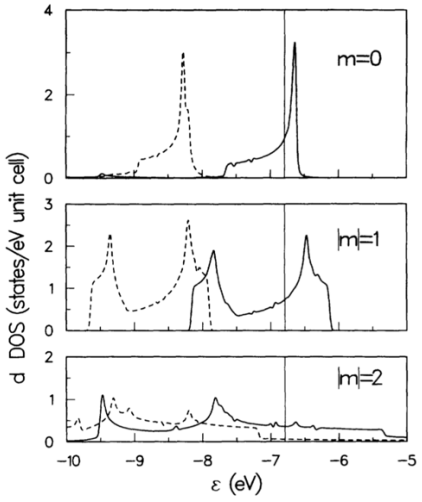

Figure 1.14 Majority (solid line) and minority (dashed line) DOS with m=0 ($d_{3z^2-r^2}$), |m|=1 (d_{xz}, d_{yz}), |m|= 2 (d_{xy}, $d_{x^2-y^2}$). Reprinted with permission from [69].

In-plane and out of plane orbital motion determines the out of plane and in-plane orbital magnetic moments, respectively. From the perturbation theory, M_{orb} is expressed by the

following relation.[68]

$$M_{orb} \propto \xi/W \tag{1.12}$$

W is the averaged bandwidth that separates the filled and empty states. The more localized DOS, the smaller W. As shown in Figure 1.14, the out of plane orbital DOS is small in the Co monolayer, so the in-plane M_{orb} becomes large. Therefore, in the Bruno model, K_i becomes in-plane magnetic anisotropy. Figure 1.15 shows the out of plane orbital DOS in Au/Co monolayer Au.[70]

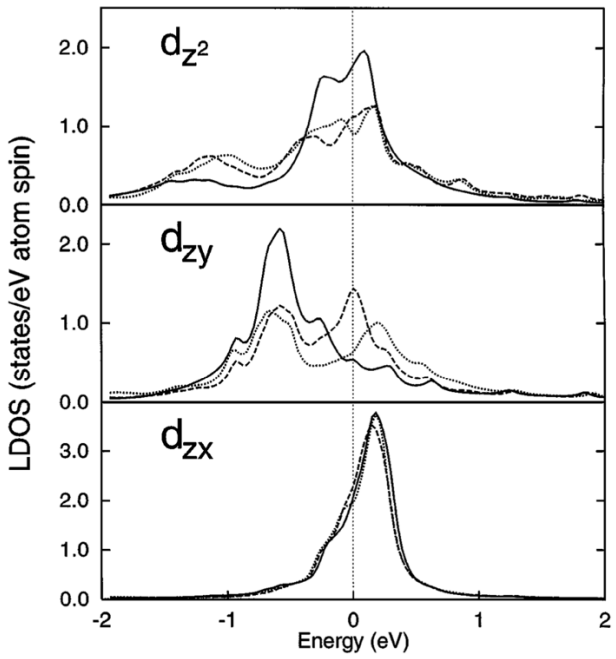

Figure 1.15 Minority DOS of d orbitals for Au/Co/Au(111) multilayers. Reprinted with permission from [70].

In Figure 1.15, the DOS of $d_{3z^2-r^2}$ in Au/Co/Au is wider than that of Co monolayer. Therefore, the in-plane orbital magnetic moment becomes small and K_i becomes positive.

Similarly, in the Fe surface, anisotropy of the orbital magnetic moment occurs due to symmetry breaking, and K_i becomes positive even in a free-standing Fe monolayer and Fe surface.[71,72] Table 1.2 shows M_{spin}, M_{orb} and interface magnetic anisotropy at Fe/X interface, where X are the non-magnetic metals. Consider the interface magnetic anisotropy between Fe and a metal with occupied and unoccupied d-orbitals. At the interface between Fe and a metal such as Ag with the occupied d-orbitals, the interface magnetic anisotropy tends to be positive as with the Fe surface because the overlap between the d-orbital of Fe and Ag is small. On the other hand, since the d-orbital overlap is large at the interface between Fe and a metal such as Pd with partially occupied d-orbital, a moment is induced in Pd, which contributes to in-plane magnetic anisotropy. Cr is often used as the buffer layer for Fe. Since the *d* orbital is partially occupied in Cr, in-plane magnetic anisotropy is predicted at the Fe/Cr interface.

Table 1.2 M_{spin}, M_{orb} and interface magnetic anisotropy in X/Fe. Reprinted with permission from [72].

	M_{spin} (μ_B)	$M_{orb}^{[001]}$ (μ_B)	ΔM_{orb} (μ_B)	E_{MCA} (mJ/m^2)
Hf/Fe	2.0	0.032	−0.014	1.5
Zr/Fe	2.2	0.053	0.000	0.15
Ti/Fe	1.7	0.037	0.000	−0.089
Ta/Fe	1.6	0.039	−0.005	−0.018
Nb/Fe	1.7	0.037	−0.006	−0.42
V/Fe	1.8	0.037	−0.002	−0.36
Ir/Fe	2.7	0.064	−0.021	−4.8
Rh/Fe	2.8	0.054	−0.009	−0.92
Pt/Fe	2.8	0.049	−0.003	−2.8
Pd/Fe	2.9	0.054	0.004	−0.62
Au/Fe	2.8	0.055	0.022	0.21
Ag/Fe	2.8	0.068	0.013	0.77
Cu/Fe	2.7	0.069	0.009	0.49
Zn/Fe	2.4	0.085	0.012	0.99
MgO/Fe	2.8	0.071	0.018	1.6
Fe surf.	3.0	0.072	0.011	0.85
Bulk Fe	2.2	0.046	0.00	0.00

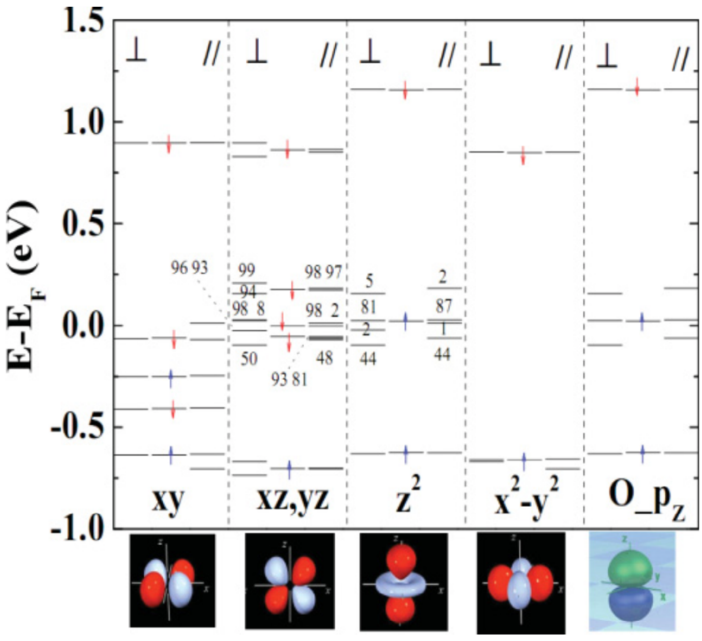

Figure 1.16 Band around the Fermi level with the Fe *d* and O *p* orbitals with or without spin orbit interaction. Reprinted with permission from [73].

At the Fe/MgO interface, the hybridization between Fe $3d_{z^2}$ and O $2p_z$ orbitals reduce the in-plane M_{orb}, leading to large interface PMA. The hybridization between d_{z^2} and $d_{xz,yz}$ confirmed due to the spin orbit interaction as shown in Figure 1.16, which also contribute to PMA. The oxidation states at Fe/MgO interface is an important factor for PMA.
As shown in Table 1.3, PMA decreases when the oxygen in MgO is deficient (underoxidized) or Fe is oxidized (overoxidized). Also, the PMA at the Co/MgO interface is very small. Therefore, in CoFeB/MgO, PMA in Fe-rich one is larger than that in Co-rich one. Ta/CoFeB/MgO shows K_{eff} of 0.5 MJ/m^3. In the case of single crystal Fe/MgO, K_{eff} of 1.4 MJ/m^3 has been achieved.[74]

Table 1.3 PMA energy (erg/cm^2) and magnetic moment in pure, underoxidized, and overoxidized Fe/MgO and Co/MgO. Reprinted with permission from [73].

	Fe|MgO			Co|MgO:
	Pure	Underoxidized	Overoxidized	pure
PMA	2.93	2.27	0.98	0.38
m (μ_B)				
Interfacial	2.73	2.14	3.33	1.67
Sublayer	2.54	2.41	2.70	1.84
Bulk	2.56	2.55	2.61	1.60

The Fe thin film rotates 45° with respect to the crystal plane of the MgO (100) substrate and grows epitaxially. There is a 4% lattice mismatch between Fe and MgO. On the other hand, at the Fe/$MgAl_2O_4$ interface, the lattice mismatch is small (~1 %),[75] and K_i of 1.7 mJ/m^2 is observed.[76]

Table 1.4 K_i, M_{spin} and M_{orb} of Fe/$MgAl_2O_4$ and Fe/MgO when the lattice constant is distorted to that of Fe or MgO. Reprinted with permission from [77].

System	K_i (mJ/m^2)	$E_{demag}t$ (mJ/m^2)	$K_{eff}t$ (mJ/m^2)	$\Delta M_{orb,i}$ (μ_B/atom)	$M_{spin,i}$ (μ_B/atom)
Fe/$MgAl_2O_4$	1.192	−0.895	0.296	0.026	2.81
Fe/MgO ($a = a_{MgO}/\sqrt{2}$)	1.617	−0.828	0.788	0.030	2.73
Fe/MgO ($a = a_{Fe}$)	1.552	−0.908	0.643	0.020	2.78

Table 1.4 shows interface PMA and ΔM_{orb} in Fe/$MgAl_2O_4$ and Fe/MgO with different lattice constant.[77] K_i in Fe/MgO is larger than that in Fe/$MgAl_2O_4$, on the other hand ΔM_{orb} in Fe/$MgAl_2O_4$ is larger than that in Fe/MgO, when lattice constant is distorted to Fe. Figure 1.17 shows the values of $E_{\uparrow\uparrow}$, $E_{\downarrow\downarrow}$, $E_{\uparrow\downarrow}$, $E_{\downarrow\uparrow}$ of each Fe layer. In Fe/MgO, in addition to ΔM_{orb} contribution, the spin flip term shows a large PMA.

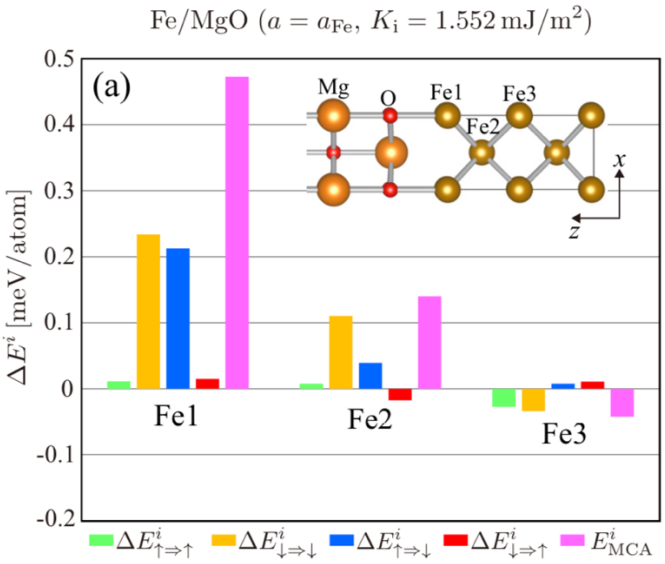

Figure 1.17 Values of $E_{\uparrow\uparrow}$, $E_{\downarrow\downarrow}$, $E_{\uparrow\downarrow}$, $E_{\downarrow\uparrow}$ of each Fe layer in Fe/MgO when the lattice constant was distorted to that of Fe. Reprinted with permission from [77].

These contributions of non-spin flip term and spin flip term are experimentally confirmed with X-ray circular magnetic dichroism (XMCD) and X-ray linear magnetic dichroism (XMLD).[78,79]

XMCD measurements are performed using right and left circularly polarized X-rays. M_{spin} and M_{orb} of each element were deduced according to the optical sum rules. Integrated XMCD signals is proportional to M_{orb}. Figure 1.18 shows X-ray absorption spectroscopy (XAS), XMCD and integrated XMCD intensities of Fe(0.7 nm)/MgO(2nm) with K_i of 2.0 mJ/m^2.[78] There is a difference in residual of integrated XMCD measured at normal incidence (NI) and grazing incidence (GI) setups, suggesting that anisotropy of orbital magnetic moments exist. ΔM_{orb} is deduced to be 0.09 μ_B, which corresponds to be K_i of 1.48 mJ/m^2.

Spin flip term $E_{\uparrow\downarrow}$ is expressed as follows.[79]

$$E_{\uparrow\downarrow}=\xi^2 \sum_{o\uparrow u\downarrow} \frac{|\langle o\uparrow|3l^2{}_z\text{-}l^2|u\downarrow\rangle|}{E(u\downarrow)\text{-}E(o\uparrow)} \tag{1.13}$$

$E(u\downarrow)$-$E(o\uparrow)$ is the exchange splitting between occupied up and unoccupied down 3d bands. The quadrupole tensor $Q_{zz} = 3l_z^2$-l^2 is proportional integrated XMLD intensity. Figure 1.19 shows XAS, XMCD and XMLD intensity for Fe(0.7nm)/MgO(2nm) with K_i of 1.85 mJ/m^2. The values of $E_{\uparrow\downarrow}$ are deduced to be 17 μeV from the XMCD sum rules, which is one order smaller than $E_{\downarrow\downarrow}$. Although the value of $E_{\uparrow\downarrow}$ is small, the contribution to PMA is experimentally confirmed.

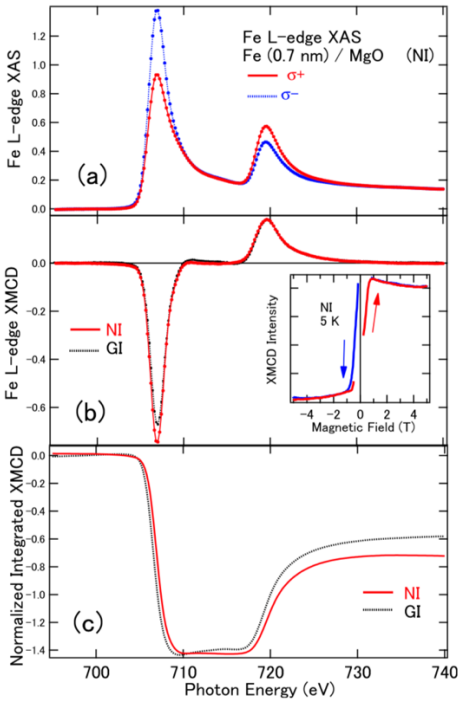

Figure 1.18 XAS, XMCD and normalized integrated XMCD spectra for Fe $L_{2,3}$ edges in Fe(0.7 nm)/MgO(2 nm) with K_{eff} = 1.4 MJ/m^3. Reprinted with permission from [78].

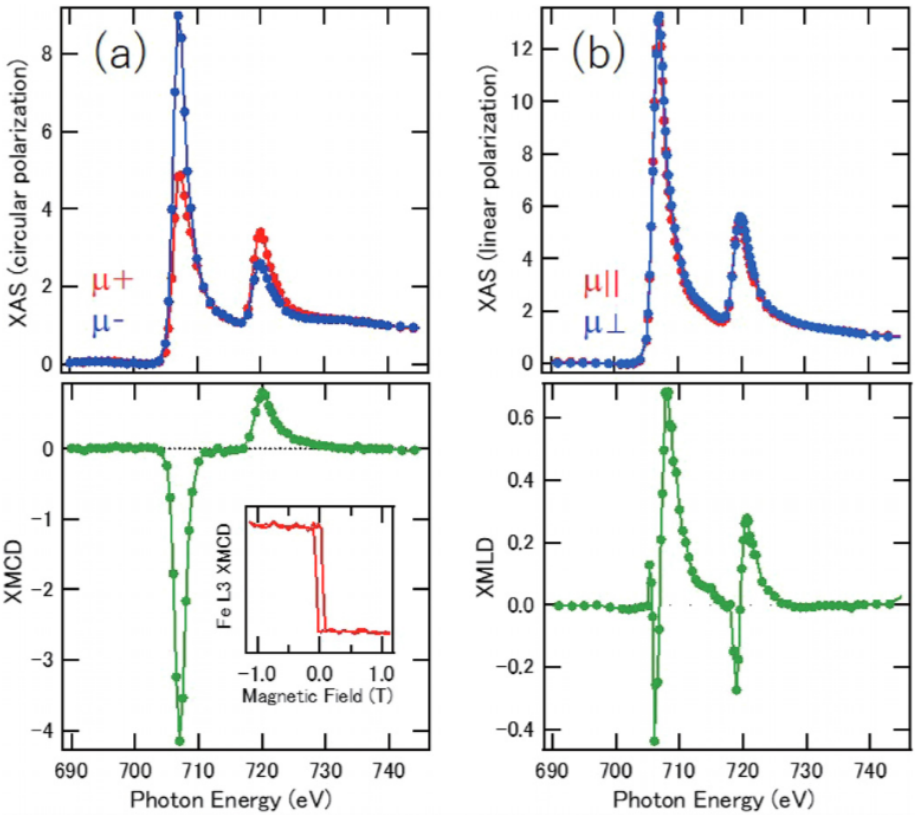

Figure 1.19 (a) XAS and XMCD spectra by circularly polarized x ray and (b) XAS and XMLD spectra by linearly polarized x ray for Fe $L_{2,3}$ edges in Fe(0.7 nm)/MgO(2 nm) with K_{eff} = 1.2 MJ/m^3. Reprinted with permission from [79].

1.4 Voltage control magnetic anisotropy (VCMA)

Larger PMA energy keeps the magnetization stronger in the out of plane direction but leads to an increase in energy consumption during magnetization switching. In order to reduce writing energy, a method of reducing PMA energy by applying an electric field has been proposed.[13] Compared to STT-MRAM, MRAM using the VCMA effect can reduce write energy by an order of magnitude.[80] Since the direction of magnetization cannot be determined simply by applying an electric field to lower the PMA energy, it is necessary to apply a pulse voltage to precess the magnetization.[81] The rate of change of PMA energy when an electric field is applied is called the VCMA coefficient. The required PMA energy and VCMA coefficient values differ depending on the type of memory. When controlling K_{eff}・t of 1 mJ/m^2 under an electric field of 1 V/nm, a VCMA coefficient of about 1000 fJ/V・m is required. Table 1.5 shows the VCMA coefficient for each material.

Table 1.5 VCMA coefficient in ferromagnetic/oxide.

Structures	**VCMA coefficient (fJ/V・m)**
Ta/CoFeB/MgO [82]	33
W/CoFeB/MgO [83]	50
Ir/CoFeB/MgO [84]	100
Cr/Fe/MgO [85]	290
Cr/Fe/Cr/MgO [86]	370
V/Fe/MgO [87]	1150
Pd/Co/Gd-oxide [88]	5000

Since the electric field is decayed in the metal, only the magnetic anisotropy occurred at the interface with the insulator can be controlled. The singlecrystalline Fe/MgO has a larger VCMA coefficient than CoFeB/MgO. The VCMA effect in Fe/MgO is due to charge accumulation at the interface. Large VCMA coefficients are obtained for V/Fe/MgO and Pd/Co/Gd-oxide, but high-speed switching cannot be expected because charge trapping and ion migration are the origins of the large VCMA effect in these materials.[87,88] Therefore, singlecrystalline Fe/MgO is expected as a material for MRAM utilizing the VCMA effect.

1.5 Purpose

As shown in Figure 1.3 and 1.5, almost MTJs consist of CoFeB/MgO/CoFeB. Actually, CoFeB/MgO-based MTJs are used in the MRAM on the market. Therefore, as a material research aiming at practical application, meaningful materials are as follows; (1) it has physical parameters (TMR, PMA, damping constants, etc.) comparable to CoFeB/MgO without significant drawbacks, and (2) it has at least one advantage over CoFeB/MgO.

Singlecrystalline Fe/MgO shows larger PMA and VCMA effect than those of CoFeB/MgO. Basic understanding of PMA in Fe/MgO has progressed theoretically and experimentally, and recently, large TMR of 400% was achieved in Fe/MgO/Fe in-plane MTJ.[89] Therefore, Fe/MgO heterostructures are promising for perpendicular MTJs, especially for voltage control MRAM.

The great advantage of CoFeB/MgO is that it can be realized on various buffer layers. Sputtering is generally used as a method for the deposition of CoFeB/MgO. Firstly, CoFeB is deposited as amorphous on the buffer. After that, MgO polycrystallizes on CoFeB in the (001) direction. By annealing, boron diffuses into the buffer layer and CoFeB crystallizes along the MgO (001) direction. Therefore, boron is considered to play an important role in the crystallization of CoFeB. Figure 1.20 shows the breakdown of the deposition methods for Fe/MgO and CoFe/MgO without boron. The 240 papers were investigated from 2004, when Fe/MgO began to attract attention as a material for MTJ, to 2018. These papers were collected with the search word “Fe/MgO” on google scholar. In Figure 1.20, 75% is EB or MBE, 15% is sputtering, and 10% is other film formation methods such as pulsed laser deposition (PLD). The breakdown in Figure 1.20 includes the deposition method of Fe/MgO prepared for structural analysis. All of studies for enhancing PMA, TMR and VCMA are only demonstrated in EB or MBE grown Fe/MgO.[31,74,85,90,91] The magnetic properties of sputter-deposited Fe/MgO is inferior to that of MBE-grown one. The inability to make high-quality samples by sputter-deposition is a major drawback compared to CoFeB/MgO.

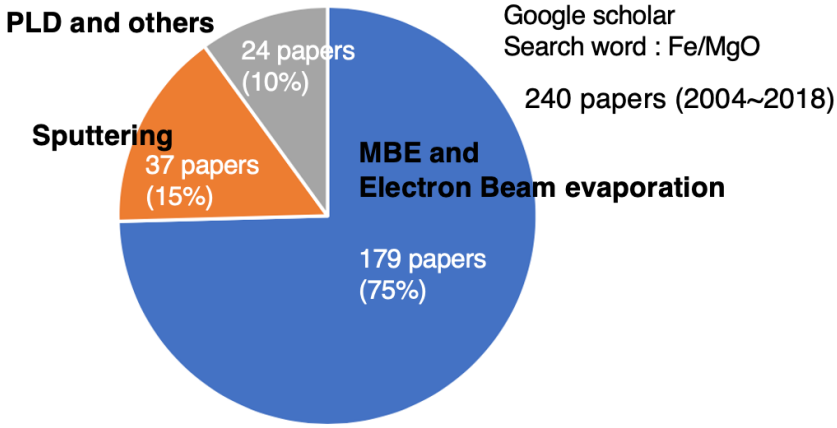

Figure 1.20 Breakdown of the deposition methods for Fe/MgO and CoFe/MgO

With the miniaturization of MTJ, larger interface magnetic anisotropy is required. An interface magnetic anisotropy of 2 mJ/m^2 has been achieved at the Fe/MgO interface,[74] but it seems difficult to obtain larger PMA energy at the Fe/oxide interface. In recent years, attempts have been performed to aim for larger PMA energy by doping the interface with metal atoms.[92] PMA and VCMA are increased when Ir and W are doped at the FeB/MgO interface. Even if these are inserted at the interface between the buffer layer and Fe, PMA may increase, but if they are not placed near the oxide interface, they cannot be modulated by voltage and do not become a large VCMA. PMA energy was calculated when the few monolayer of bcc W was inserted into the Fe/MgO and Fe/$MgAl_2O_4$ interface.[77] Figure 1.21 shows K_i in Fe/W/MgO and Fe/W/$MgAl_2O_4$ when the lattice constant was distorted to Fe, MgO or $MgAl_2O_4$. When the lattice constant of W is distorted to Fe or $MgAl_2O_4$, larger PMA energy can be expected than that in Fe/MgO. Since W is the transition metal with less than half d states, it has unoccupied majority spin states, which provides large positive contribution to the PMA. It is confirmed that W has an induced moment due to the proximity effect by XMCD measurement.[93] On the other hand, when the lattice constant of W is distorted to the MgO, K_i drastically decreases. Although the change of magnetic anisotropy from negative to positive was confirmed depending on the lattice constant of W,[94] large PMA predicted by the theory has not been achieved. In connection with the study of polycrystalline W-doped FeB/MgO,[92] it is worth studying W insertion into the single crystal Fe/MgO interface experimentally.

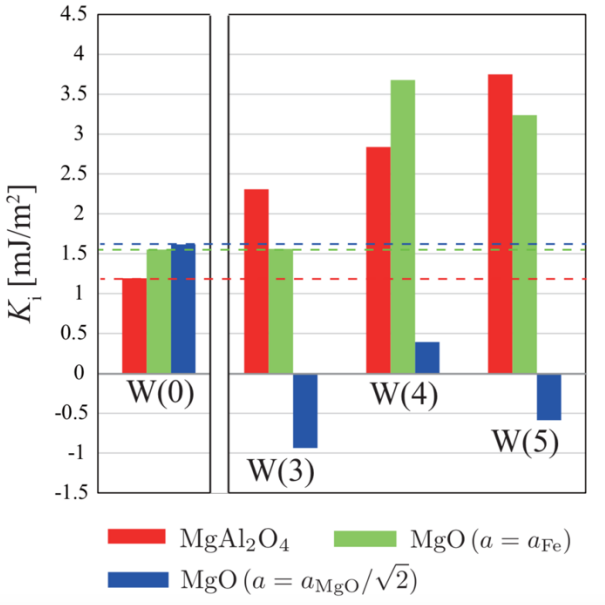

Figure 1.21 K_i in Fe/W/MgO and Fe/W/$MgAl_2O_4$ with different lattice constants. Reprinted with permission from [77].

The contribution of buffer layer for PMA is also important. As shown in Table 1.2, positive contribution can be expected depending on buffer layers. In CoFeB/MgO, various buffer layers have been studied for PMA and VCMA. So far, PMA has been achieved on various buffers such as Ti, V, Cr, Nb, Mo, Ru, Rh, Pd, Ag, Hf, Ta, W, Re, Os, Ir, Pt, Au, CuN.[42,43,83, 95-98] Table 1.6 shows the magnetic anisotropy in CoFeB/MgO on various buffer layers. While the annealing process plays an important role in obtaining PMA, it is obtained without annealing in some buffer materials. Actually, various buffer layer has been investigated, but there are still many unclear problems. It is thought that the electronegativity, elastic strain of the buffer layer, the hybridization of the 5d and 4f orbitals and the Fe and Co 3d orbitals affect the magnetic anisotropy.[96]

Table 1.6 Magnetic anisotropy in as deposited and annealed X/CoFeB/MgO.[96] ©2016IEEE

IVA	VA	VIA	VIIA	VIIIA	VIIIA	VIIIA	IB
22, Ti as: //, ann: // a = 2.59 c/a=1.59 2.0 1.54 $3d^2 4s^2$	23, V as: //, ann: // a= 3.02 1.92 1.63 $3d^3 4d^2$	24, Cr as: ⊥ , ann: // a = 2.88 1.85 1.66 $3d^5 4d^1$	25, Mn 1.55 $3d^5 4d^2$	26, Fe a=2.87 1.72 1.83 $3d^6 4d^2$	27, Co a=2.51 c=1.62 1.67 1.83 $3d^7 4d^2$	28, Ni a=3.53 1.62 1.88 $3d^8 4d^2$	29, Cu a=3.61 1.57 1.90 $3d^{10} 4d^1$
40, Zr as: //, ann: ⊥ a = 3.2 c/a=1.59 2.16 1.33 $4d^2 5s^2$	41, Nb as: //, ann: ⊥ a=3.3 2.08 1.6 $4d^4 5s^1$	42, Mo as: ⊥, ann: ⊥ a=3.15 2.01 2.16 $4d^5 5s^1$	43, Tc	44, Ru as: //, ann: // a=2.7 c/a=1.59 1.89 2.2 $4d^7 5s^1$	45, Rh as: //, ann: // a=3.8 1.83 2.28 $4d^8 5s^1$	46, Pd as: //, ann: ⊥ a=3.89 1.79 2.2 $4d^{10}$	47, Ag as: //, ann: // a=4.09 1.75 1.93 $4d^{10} 5s^1$
72, Hf as: ⊥, ann: ⊥ a= 3.2 c/a=1.58 2.16 1.3 $5d^2 6s^2$	73, Ta as: ⊥, ann: ⊥ a=3.31 2.09 1.5 $5d^3 6s^2$	74, W as: ⊥, ann: ⊥ a=3.16 2.02 1.7 $5d^4 6s^2$	75, Re as: ⊥, ann: ⊥ a= 2.76 c/a=1.62 1.97 1.9 $5d^5 6s^2$	76, Os as: //, ann: // a=2.74 c/a=1.58 1.92 2.2 $5d^6 6s^2$	77, Ir as: ⊥, ann: ⊥ a=3.84 1.87 2.2 $5d^7 6s^2$	78, Pt as: //, ann: ⊥ a=3.92 1.83 2.2 $5d^9 6s^1$	79, Au as: //, ann: // a=4.08 1.79 2.4 $5d^{10} 6s^1$

Even in Fe/MgO and CoFeB/MgO, which have been studied for a long time, there are some unclear problems. In this study, the purpose is to increase the knowledge of the ferromagnetic layer/oxide layer (mainly Fe/MgO) to bring it closer to practical use.

In Chapter 2, experimental methods are described. Deposition methods, microfabrication, magnetic measurement, X-ray absorption spectroscopy measurement and structural analyses are explained.

In Chapter 3, experiments of PMA in sputter-deposited Fe/MgO are described. The stacks of polycrystalline and singlecrystalline Fe/MgO was investigated. The problem of the oxidation of Fe caused by the MgO sputtering was tackled. The usefulness of W buffer and Tb cap and the new

structure Fe/CrO are described.

In Chapter 4, experiments of PMA in W-inserted Fe/MgO are described. Structural analyses revealed the actual structure, and magnetic properties were evaluated. The effectiveness of W insertion is discussed.

In Chapter 5, experiments of PMA in La and Tb buffers/CoFeB/MgO are described. These PMA were observed even in the stacks without post-annealing. The contribution of each layer is discussed.

In Chapter 6, Chapter 3 ~ 5 are summarized.

In this Ph. D. thesis, PMA was achieved in Fe/oxide heterostructures without boron by sputter deposition. The oxidation of the Fe layer during the sputter deposition of MgO was found to be a major problem. PMA was obtained by reduction of Fe-oxide using Tb and Cr. In addition, it was found that the deposition of W on Fe is difficult, and this is also same for other heavy metals. Moreover, the possibility of lanthanoids as the buffer layer was shown. These efforts provide the useful knowledge for p-MTJs.

Chapter 2 Experiment

2.1 Film preparation

In this section, the film deposition machines are introduced. The stacks made only by sputtering were prepared in 5 targets ultrahigh vacuum (UHV) magnetron rf-sputtering (Figure 2.1). W-inserted EB-grown Fe/MgO in Chapter 4 was prepared in the cluster system (10 targets UHV magnetron dc and rf sputtering and EB) (Figure 2.2). As an important thing, since the filament in EB chamber is made of W, W cannot be deposited by EB. Detailed deposition conditions are given in experiment section of each Chapter.

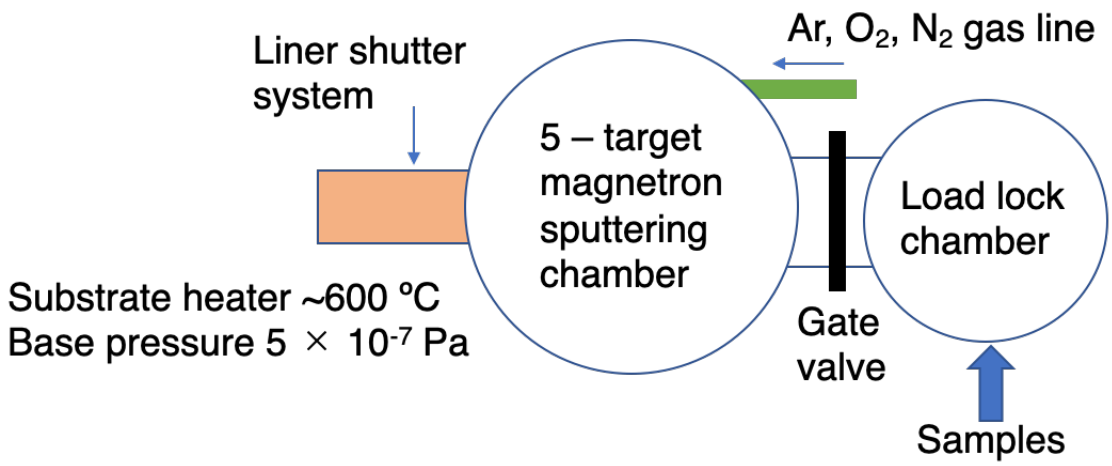

Figure 2.1 5 target UHV magnetron sputtering

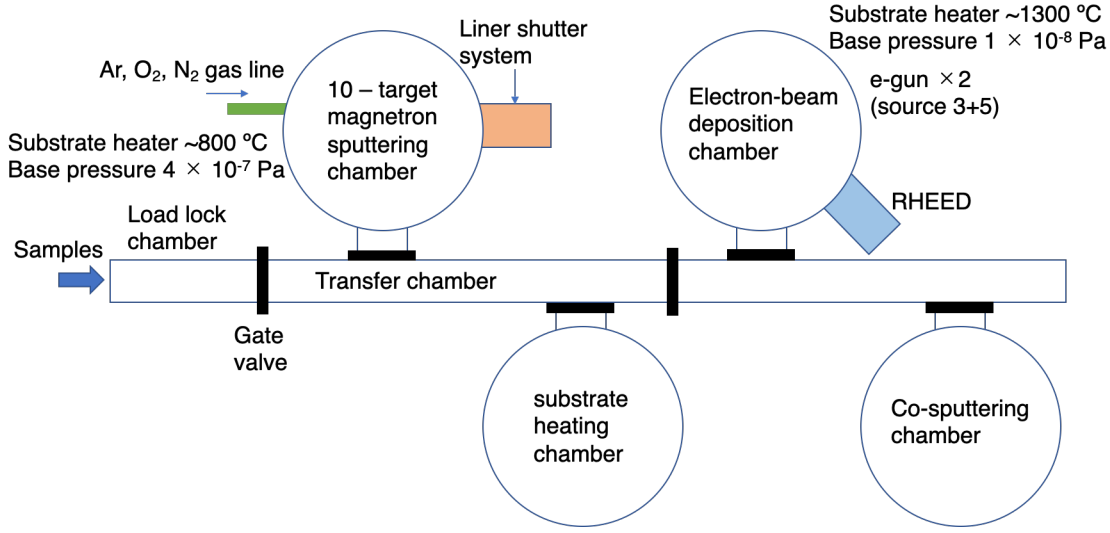

Figure 2.2 10 target Sputtering, EB, Co-sputtering cluster system.

2.2 Microfabrication

It is necessary to make MTJ to measure VCMA effect. The MTJ microfabrication process is as follows. As an example, the process of microfabrication of MgO substrate//Cr buffer(30 nm)/Fe(0.7 nm)/MgO(2 nm)/Fe(10 nm)/Ru-cap(10 nm) is shown.

[1] Bottom electrode
(1) Applying resist (Hexamethyldisilane; HDMS) to the sample
(2) Spin coater rotating at 3000 rpm + bake 2 min
(3) Apply resist (ma-N1407) to the sample
(4) Spin coater rotating at 3000 rpm + bake 1 min 30 sec
(5) 100 sec exposure with a photomask for Bottom
(6) Wash for 90 seconds with developer for ma-N1407
(7) After that, wash with water for 20 seconds
(8) Ar ion milling until Mg of substrate is detected
(9) Deposition of SiO_2 by sputtering
(10) Removal of the resist
Wash with N-Methyl-2-pyrrolidone (NMP) for 5 min and acetone for 5 min
Top view is as shown in Figure 2.3 (b).

[2] Pillar
(1) Wash the sample with butanone for 1 min
(2) Applying HDMS to the sample
(3) Spin coater rotating at 3000 rpm + bake 2 min
(4) Apply ma-N1407 to the sample
(5) Spin coater rotating at 3000 rpm + bake 1 min 30 sec
(6) 100 sec exposure with a photomask for Pillar
(7) Wash for 90 seconds with developer for ma-N1407
(8) After that, wash with water for 20 seconds
(9) Ar ion milling until MgO barrier is no longer detected
(10) Deposition of SiO_2 by sputtering
(11) Removal of the resist
Wash with NMP for 5 min and acetone for 5 min
Top view is as shown in Figure 2.3 (c).

[3] Contact hole
(1) Wash the sample with butanone for 1 min
(2) Applying HDMS to the sample
(3) Spin coater rotating at 3000 rpm + bake 2 min
(4) Apply ma-N1407 to the sample

(5) Spin coater rotating at 3000 rpm + bake 1 min 30 sec
(6) 100 sec exposure with a photomask for Contact hole
(7) Wash for 90 seconds with developer for ma-N1407
(8) After that, wash with water for 20 seconds
(9) Ar ion milling until Cr buffer is detected
(10) Deposition of Ta/Au by sputtering
(11) Removal of the resist
Wash with NMP for 5 min and acetone for 5 min
Top view is as shown in Figure 2.3 (d).

[4] SiO_2 Pad
(1) Wash the sample with butanone for 1 min
(2) Applying HDMS to the sample
(3) Spin coater rotating at 3000 rpm + bake 2 min
(4) Apply ma-N1407 to the sample
(5) Spin coater rotating at 3000 rpm + bake 1 min 30 sec
(6) 100 sec exposure with a photomask for SiO_2 pad
(7) Wash for 90 seconds with developer for ma-N1407
(8) After that, wash with water for 20 seconds
(9) Deposition of SiO_2 by sputtering
(10) Removal of the resist
Wash with NMP for 5 min and acetone for 5 min
Top view is as shown in Figure 2.3 (e).

[5] Top electrode
(1) Wash the sample with butanone for 1 min
(2) Applying HDMS to the sample
(3) Spin coater rotating at 3000 rpm + bake 2 min
(4) Apply ma-N1407 to the sample
(5) Spin coater rotating at 3000 rpm + bake 1 min 30 sec
(6) 100 sec exposure with a photomask for Top electrode
(7) Wash for 90 seconds with developer for ma-N1407
(8) After that, wash with water for 20 seconds
(9) Ar ion milling for 20 seconds
(10) Deposition of Ta/Au by sputtering
(11) Removal of the resist
Wash with NMP for 5 min and acetone for 5 min
Top view is as shown in Figure 2.3 (f).

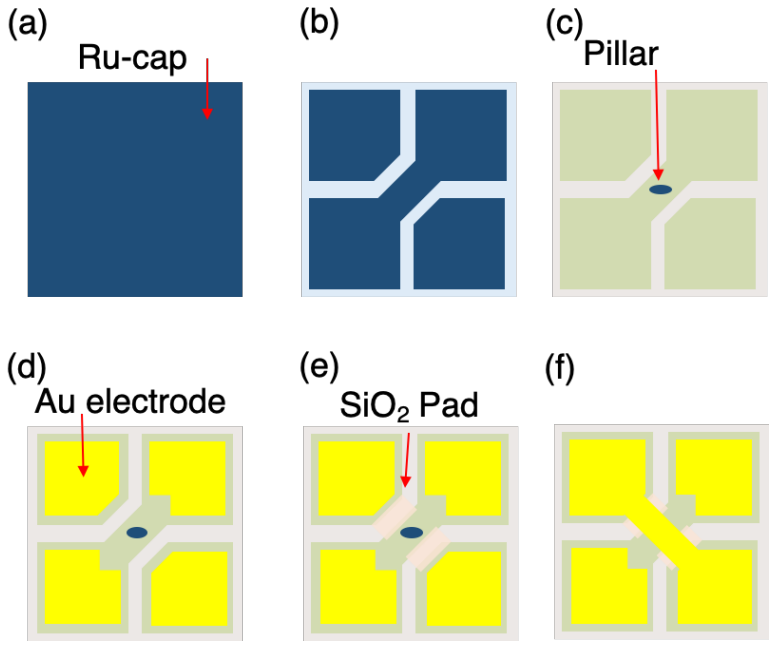

Figure 2.3 Process of microfabrication for MTJ.

2.3 Magnetization measurement

In this study, the saturation magnetization and anisotropic energy of the sample are evaluated using a vibrating sample magnetometer (VSM) and superconducting quantum interference device VSM (SQUID-VSM). The VSM in this laboratory can apply a magnetic field up to 1T. If a large magnetic field is required to saturate the magnetization hard axis direction, SQUID-VSM are used to investigate the anisotropic magnetic field. The evaluation method of saturation magnetization and anisotropic energy from the raw data obtained experimentally is described below. Here, the results of samples of MgO substrate//MgO(5 nm)/Cr(30 nm)/Fe(0.84 nm)/MgO(2 nm) are introduced as an example. Figure 2.4 (a) shows the magnetization curves obtained from the VSM when a magnetic field is applied in the in-plane direction and the out of plane direction. Since the components of the entire sample are measured, emu is converted to T in consideration of the size of the sample. When the background from the substrate and rod is removed, the *M*-*H* curve shown in Figure 2.4 (b) is obtained. The area surrounded by the easy and hard axes of magnetization corresponds to the magnetic anisotropy energy. When the easy axis is in the out of plane (in-plane) direction, the magnetic anisotropy energy is defined as positive (negative). Effective PMA energy K_{eff} is derived by integrating from H：0 to H_{a} of each M-H curve and taking the difference. Here, H_{a} is the anisotropy field.

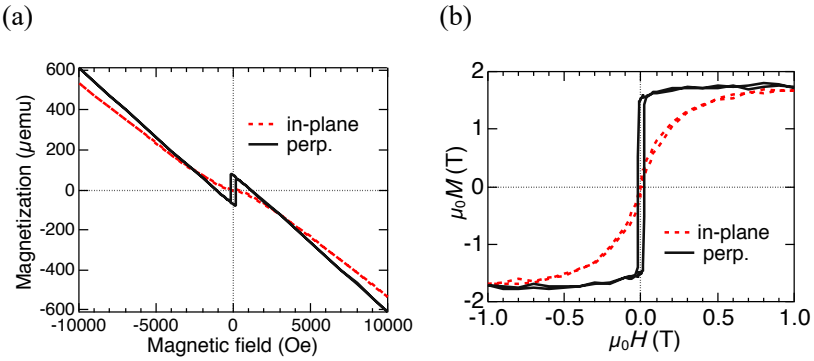

Figure 2.4 *M*-*H* curve obtained from VSM. (a) Raw data, (b) Corrected data.

2.4 X-ray magnetic circular dichroism (XMCD) measurement

In the XMCD measurement, the spin magnetic moment M_{spin} and orbital magnetic moment M_{orb} of the sample can be investigated for each element. Since the $L_{2,3}$ edges in Fe and Co reflect the levels with $l+s$ and $l-s$ due to spin-orbit interaction, M_{spin} and M_{orb} can be derived according to the XMCD sum rule.[68] When circularly polarized light is incident on the sample, the electron transitions from 2p to 3d states, and that amount of energy flows as an electric current. In the total electron yield mode, the current from the sample is measured. XMCD measurements were performed at BL-7A and 16A in Photon Factory, high-energy accelerator research organization (KEK). Magnetic field is applied parallel to the incident X-ray. The analyzing method of the obtained data is described below.

Figure 2.5 (a) shows the raw data of X-ray absorption spectroscopy intensities for Fe $L_{2,3}$ edges. μ_+ and μ_- indicates right and left hand circular polarized X-rays, respectively. The dashed lines are the noise caused by the dark current. Figure 2.5 (b) shows the spectra without dark current noises. Furthermore, the noises of step like function are removed. Finally, the spectra shown in Figure 2.5 (c) are obtained.

Figure 2.6 shows $\mu_+ + \mu_-$, $\mu_+ - \mu_-$ and their integrated spectra. From the XMCD sum rules, M_{orb} and M_{spin} are given as follows. [99]

$$M_{orb} = -\frac{4}{3}\frac{q}{r} n_h \mu_B \tag{2.1}$$

$$M_{spin} = -\frac{6p-4q}{r} n_h \mu_B \left(1+\frac{7\langle T_z\rangle}{2\langle S_z\rangle}\right)^{-1} \tag{2.2}$$

r, p, q are values shown in Figure 2.6 (b), (d). $\langle T_z\rangle$ is the expectation value of the magnetic dipole operator. $\langle S_z\rangle$ is equal to half of M_{spin} in Hartree atomic cell. $\langle T_z\rangle/\langle S_z\rangle$ can be neglected in (2.2). n_h is the hole number (3.39 for Fe, 2.49 for Co).

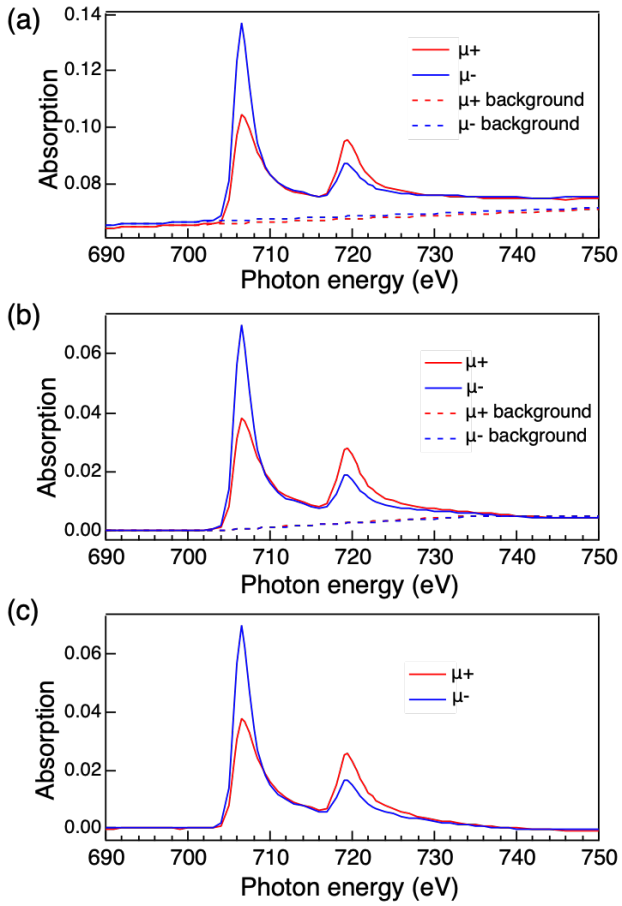

Figure 2.5 Removal method of the background. By removing the dashed line shown in (a), the spectrum shown in (b) is obtained. Also, by removing the dashed line shown in (b), the spectrum shown in (c) is obtained.

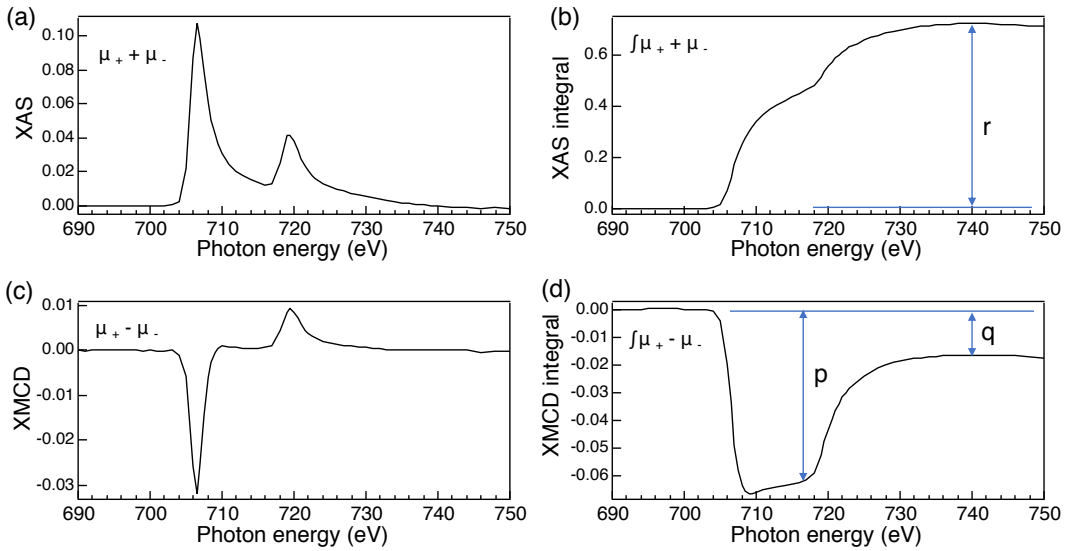

Figure 2.6 (a) XAS obtained in Figure 2.5, (b) XMCD and integrated (b) XAS, (d) XMCD spectra.

2.5 Structural analyses

·Reflection High Energy Electron Diffraction (RHEED)

Diffraction pattern is observed by emitting electron to the sample's surface. This is performed in vacuum so that the electrons are not affected by the atoms in the atmosphere. In-situ observation is possible, and especially in the case of EB, the surface can be observed during the growth of a film.

·X-ray diffraction (XRD)

Out of plane XRD measurement is performed for the Cr buffer layer. Other layers such as Fe and MgO are too thin to be evaluated by XRD.

·Atomic Force Microscope (AFM)

Surface morphology (average roughness; *Ra*, maximum peak to valley height; *P-V*) is evaluated with AFM. Roughness of the buffer layer is an important factor for PMA and TMR in thin films. The surface is measured by dynamic force mode (DFM).

·Transmission electron microscopy

Structure of samples is evaluated using aberration corrected scanning transmission electron microscopy (STEM) with energy dispersive X-ray spectroscopy (EDS). A dual beam system (FEI Helios G4UX) was used to prepare thin foil specimens for STEM observation by the standard lift-out method.

2.6 VCMA and TMR measurement

In the MTJ for VCMA measurement, the bottom electrode has PMA, on the other hand the top electrode has in-plane magnetic anisotropy. A magnetic field is applied in the in-plane direction and the voltage dependence of TMR is measured (Figure 2.7(a)).[100] If the magnetic anisotropy of the bottom electrode changes depending on the voltage, the magnetic field response of the TMR also changes.

The resistance $R(\theta)$ at a relative angle θ of the magnetization in both electrodes are as follows.

$$R(\theta) = \frac{R_{90} R_{\mathrm{p}}}{R_{\mathrm{p}} + (R_{90} - R_{\mathrm{p}}) \cdot \cos\theta} \tag{2.3}$$

R_{p} is the resistance when the direction of the magnetization of the bottom electrode is in-plane, and R_{90} is the resistance when $H = 0$ T. The ratio of the in-plane component of the magnetization $M_{\text{in-plane}}$ and the saturation magnetization M_{s} in bottom electrode are as follows.

$$\frac{M_{\text{in-plane}}}{M_s} = \cos\theta = \frac{R_{90} - R(\theta)}{R(\theta)} \frac{R_{\mathrm{p}}}{R_{90} - R_{\mathrm{p}}} \tag{2.4}$$

Shadow area in the inset of Figure 2.7 (b) corresponds to K_{eff} divided by saturation magnetization. If M_{s} is obtained from the result of VSM, K_{eff} can be derived.

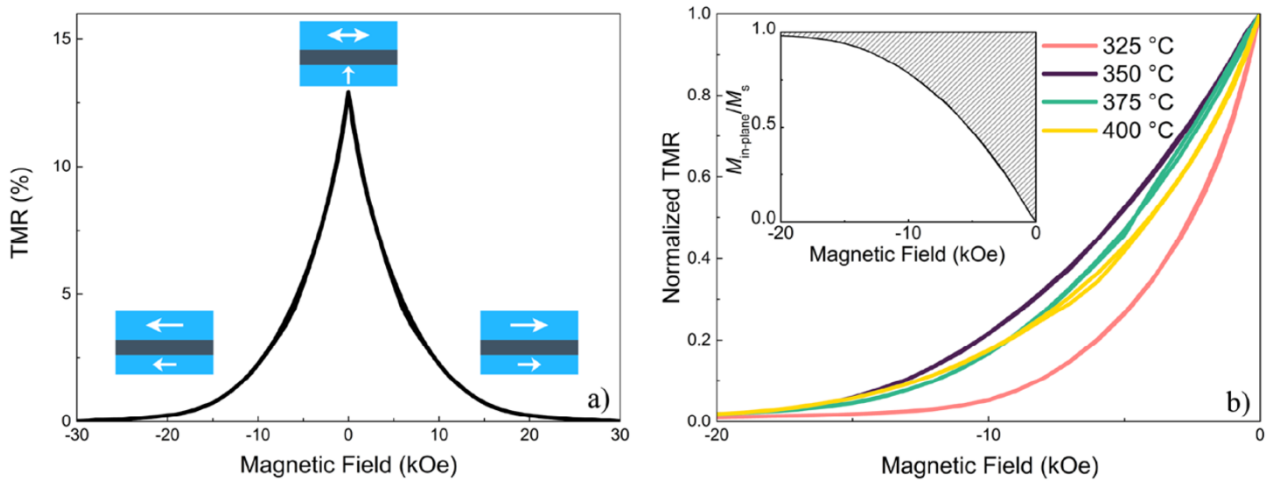

Figure 2.7 Evaluation of VCMA. (a) TMR in MTJ consisting of bottom electrode with PMA and top electrode with in-plane magnetic anisotropy. Shadow area in inset of (b) corresponds to the K_{eff} divided by saturation magnetization. Reprinted with permission from [100].

Chapter 3 Perpendicular magnetic anisotropy in sputter-deposited Fe/MgO

In this section, PMA of sputter-deposited polycrystalline (Chapter 3.1) and singlecrystalline (Chapter 3.2) Fe/MgO was studied. Polycrystalline Fe/MgO was prepared on thermally oxidized Si substrate (Si/SiO_2 substrate). On the other hand, singlecrystalline Fe/MgO was prepared on singlecrystalline MgO(001) substrate.

3.1 Polycrystalline Fe/MgO

3.1.1 Experiment

Fortunately, I found PMA in the stacks of Si/SiO_2 substrate/W/Fe/MgO/Tb from other experiments. In this section, the role of Tb capping and W buffer for PMA was studied.

An amorphous W buffer was formed on the Si/SiO_2 substrate, and Fe/MgO was deposited on the amorphous W buffer. As shown in Figure 3.1, when 3 nm W is formed on SiO_2 substrate, W becomes amorphous.[101] The crystallinity of this structure was investigated by RHEED. The specific structure is Si/SiO_2 substrate/W(t_W nm)/Fe (t_{Fe} nm)/MgO (t_{MgO} nm)/Tb (t_{Tb} nm) or Mg (t_{Mg} nm)/W (1 nm). Since the underlayer of MgO is easily oxidized in sputter-deposition compared with EB and MBE, Tb and Mg seems to be useful for adjusting the oxygen states. In order to obtain PMA in Fe/MgO, the oxidation state of the Fe/MgO interface is important. Figure 3.2 is Ellingham diagram for oxygen.[102] The Gibbs free energy of Tb-oxide is smaller than that of MgO, which means Tb can reduce MgO.

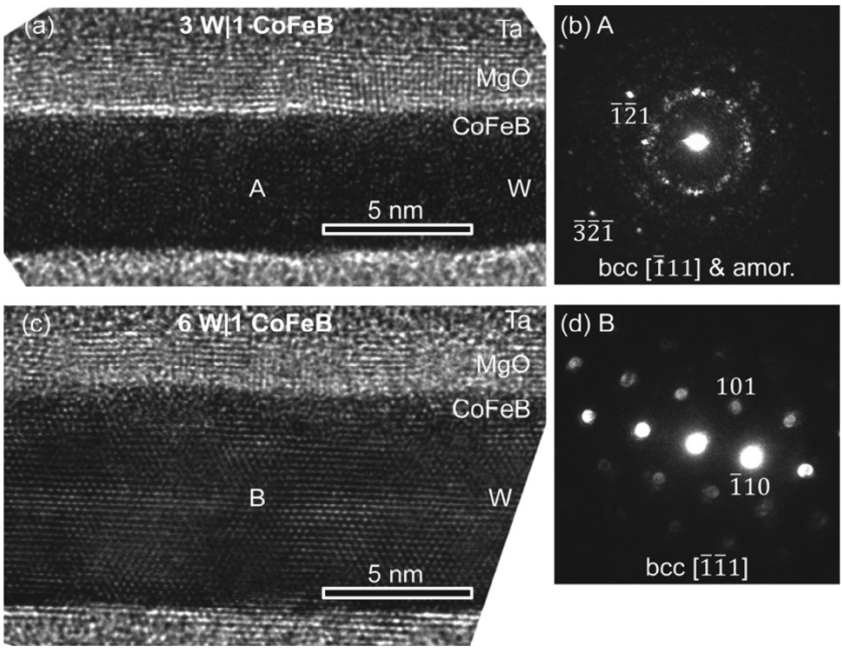

Figure 3.1 STEM images of W(3 or 6 nm)/CoFeB(1 nm)/MgO(2 nm)/Ta(1 nm) and NBD patterns of W buffer layers. Amorphous W is confirmed when the thickness of W is 3 nm. Reprinted with permission from [101].

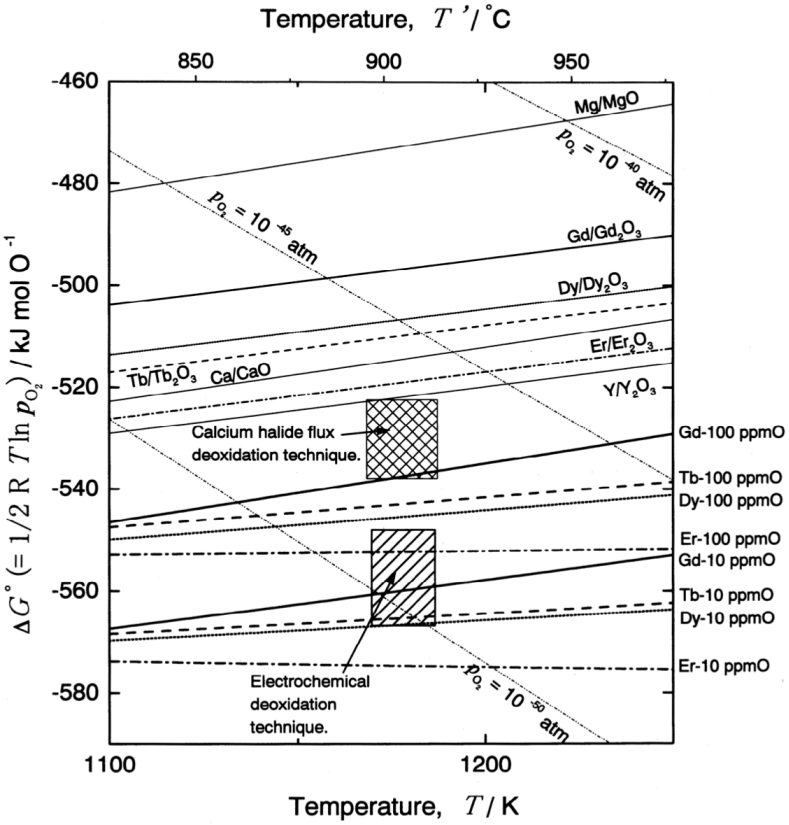

Figure 3.2 Ellingham diagram. Reprinted with permission from [102].

These experimental parts are divided as follows.

(1) Tb thickness dependence

(2) MgO and Mg thickness dependence

(3) W thickness dependence

(4) Fe thickness dependence

The surface structure was evaluated by RHEED. Magnetic properties were evaluated by VSM and poler magneto-optic Kerr effect (MOKE) measurements. XMCD measurements were performed to investigate the state of the interface in detail.

3.1.2 Result

First, the crystallinity of W(3 nm)/Fe (0.9 nm)/MgO (2 nm) formed on the Si/SiO_2 substrate was investigated. Figure 3.3 shows each RHEED pattern. In Fe layer on amorphous W buffer, halo patterns indicating amorphous-like structure was observed. It was also found that MgO became polycrystalline and was (001) oriented. It is considered that the Fe layer is polycrystallized along the orientation of MgO by annealing. Next, the magnetic properties of each structure were evaluated.

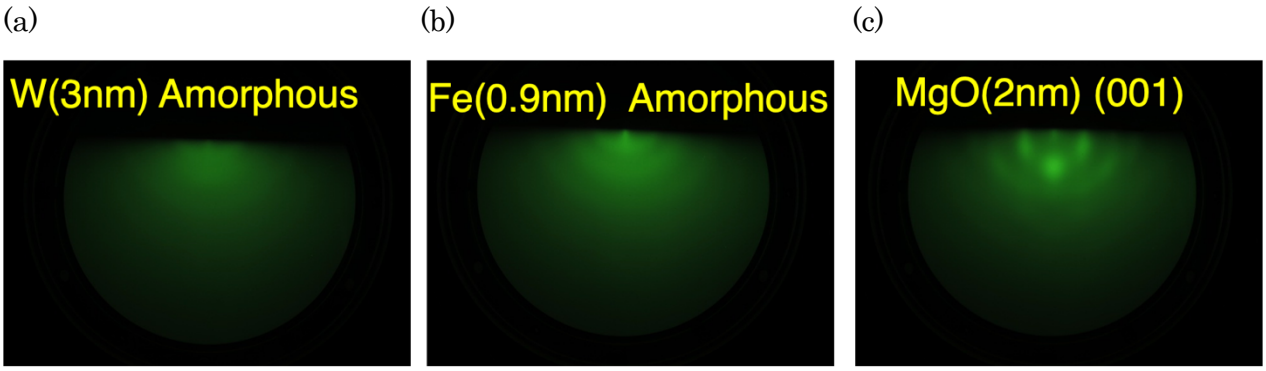

Figure 3.3 RHEED patterns of Si/SiO_2 substrate/W(3 nm)/Fe(0.9 nm)/MgO(2 nm). (a) amorphous W, (b) amorphous-like Fe, (c) MgO (001).

(1) Tb thickness dependence

Si/SiO_2 substrate//W (3 nm)/Fe (1 nm)/MgO (2 nm) /Tb (t_{Tb} nm)/W (1 nm) with the different Tb thickness and post-annealing temperature T_a were prepared. Post annealing was performed after the deposition. Saturation magnetization and magnetic anisotropy was evaluated by VSM. Figure 3.4 shows the schematic diagram of the structures.

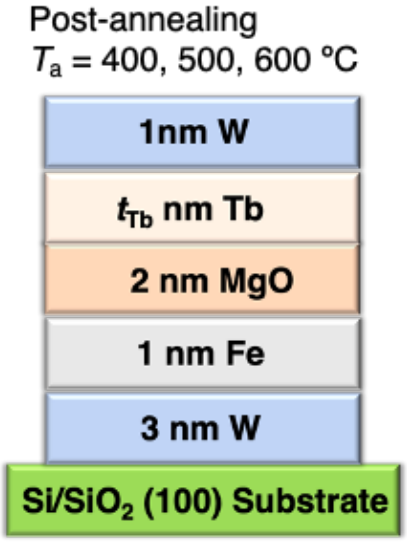

Figure 3.4 Schematic diagram of Si/SiO_2 substrate/W/Fe/MgO/Tb(t_{Tb} nm)/W.

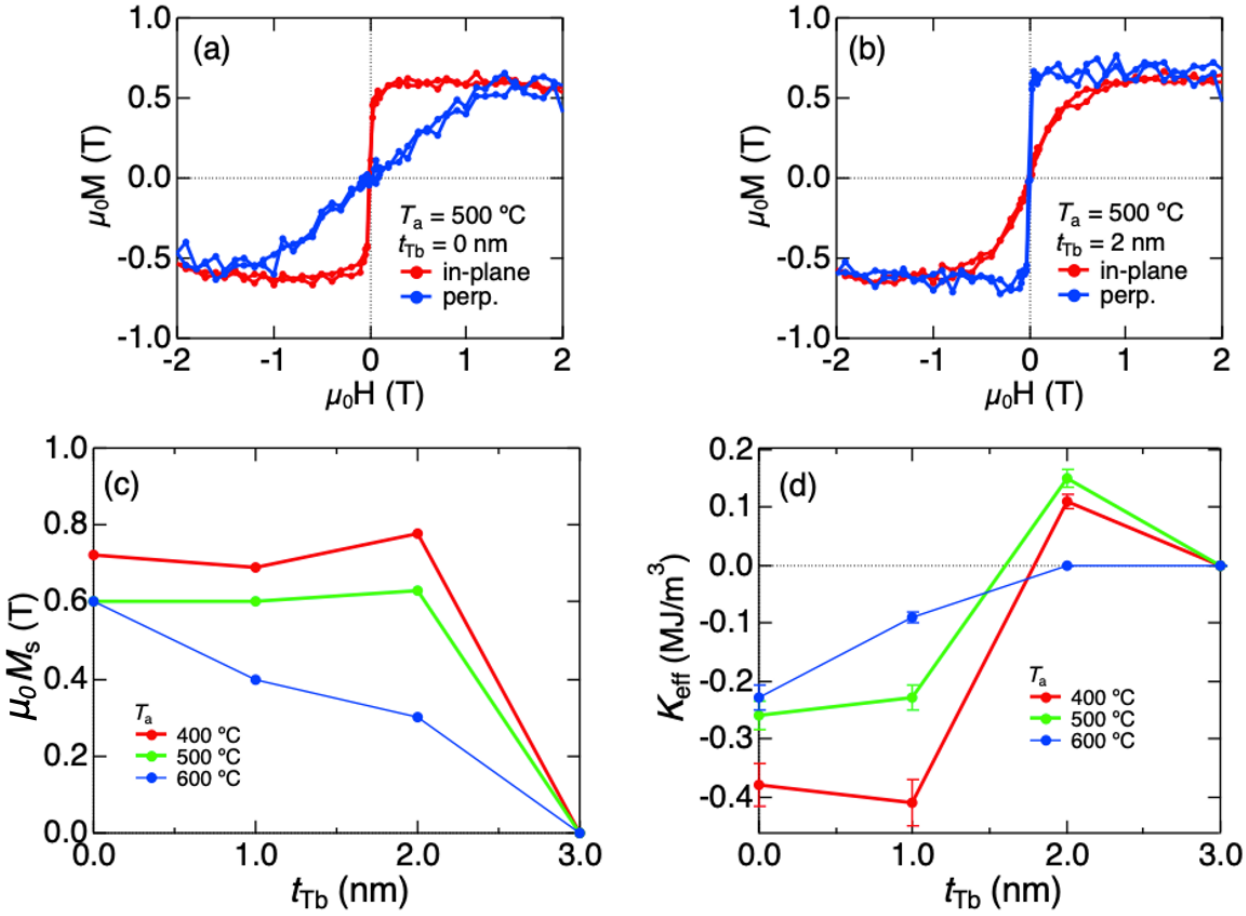

Figure 3.5 M-H curves for the stacks (a) without Tb and (b) with 2 nm Tb. t_{Tb} and T_a dependence of (c) $\mu_0 M_s$ and (d) K_{eff}.

Figure 3.5 shows the VSM results of the stacks without Tb and with t_{Tb} = 2 nm. It was found that the insertion of Tb provided effective PMA. Figure 3.5 (c) shows t_{Tb} and T_a dependences of $\mu_0 M_s$. It was found that $\mu_0 M_s$ decreases as the increasing of annealing temperature. When the thickness of Tb was 3 nm or more, the magnetization completely disappeared. It is considered that Tb diffused beyond the MgO barrier and mixed with Fe, leading to the decrease of $\mu_0 M_s$. Figure 3.5 (d) shows t_{Tb} and T_a dependence of K_{eff}. When t_{Tb} = 2 nm, effective PMA was achieved.

(2) MgO and Mg thickness dependence

Si/SiO_2 substrate//W(3 nm)/Fe(1 nm)/MgO(t_{MgO} nm)/Mg(t_{Mg} nm)/W(1 nm) were prepared. After the deposition of Mg, post annealing was performed at T_a = 500 °C. Figure 3.6 shows the schematic diagram and VSM result when t_{MgO} = 0.5 nm and t_{Mg} =1 nm.

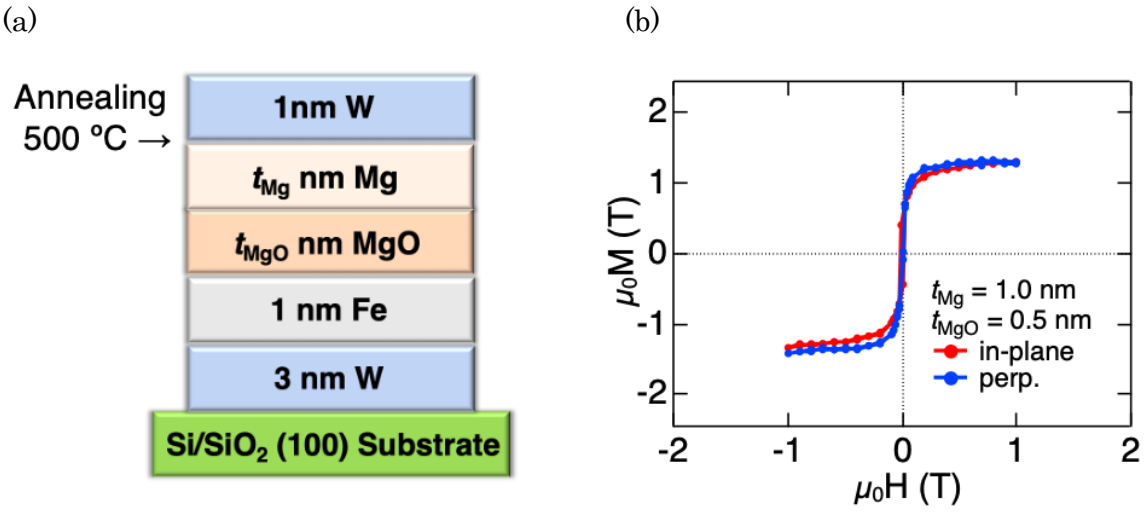

Figure 3.6 (a) Schematic diagram of Si/SiO_2 substrate/W/Fe/MgO(t_{MgO} nm)/Mg(t_{Mg} nm)/W. (b) M-H curves for the stack with t_{Mg} = 1.0 nm and t_{MgO} = 0.5 nm.

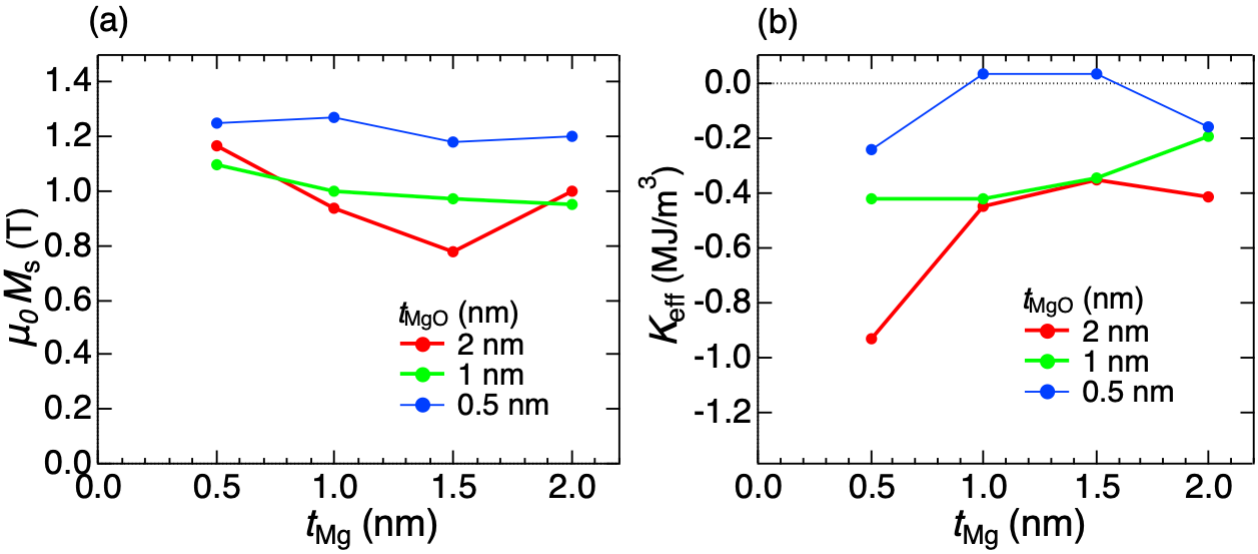

Figure 3.7 t_{Mg} and t_{MgO} dependence of (a) $\mu_0 M_s$ and (b) K_{eff}.

Figure 3.7 shows t_{MgO} and t_{Mg} dependence of $\mu_0 M_s$ and K_{eff}. In Figure 3.7 (a), it is considered that the large $\mu_0 M_s$ when t_{MgO} is 0.5 nm is due to the reduction of Fe by Mg. No significant change in $\mu_0 M_s$ was observed even when t_{Mg} increased. In Figure 3.7 (b), a change of K_{eff} can be seen as t_{Mg} increases. K_{eff} was a negative value when t_{MgO} was 1 or 2 nm. When t_{Mg} = 1 ~ 1.5 nm and t_{MgO} = 0.5 nm, the magnetic easy axis became the out of plane direction, however, the value of K_{eff} is almost zero. When the film thickness of MgO is thin, it is considered that there is a change in magnetic anisotropy because Mg slightly reduces oxidized Fe and changes the interface state. Compared with Tb insertion, PMA is smaller. The reason of larger K_{eff} in the case of Tb insertion is considered to be the stronger redox ability of Tb than Mg.

(3) W thickness dependence

Si/SiO_2 substrate//W (t_W nm)/Fe (1 nm)/MgO (2 nm) /Tb (2 nm)/W (1 nm) with the different W thickness were prepared. Post annealing was performed at T_a = 500 °C after the deposition.

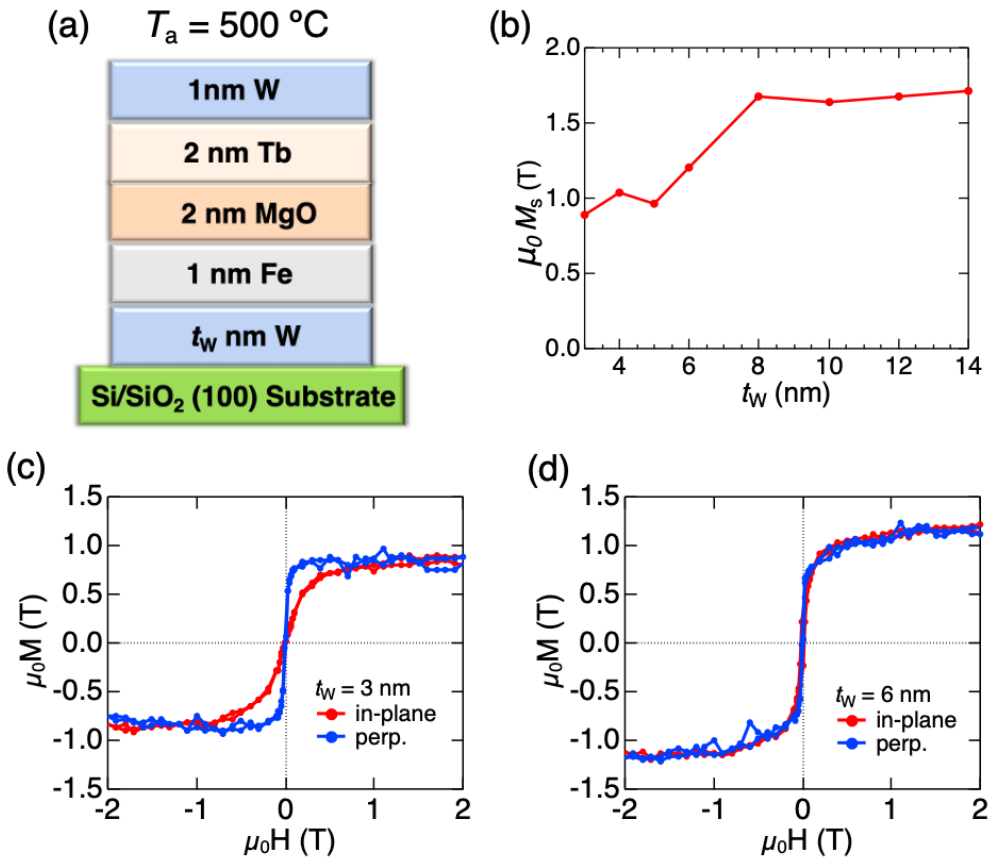

Figure 3.8 (a) Schematic diagram of Si/SiO_2 substrate/W(t_W nm)/Fe/MgO/Tb/W. (b) t_W dependence of $\mu_0 M_s$. (c), (d) M-H curves for t_W = 3 and 6 nm.

Figure 3.8 shows the schematic diagram, t_W thickness dependence of $\mu_0 M_s$, and the results of VSM when t_W = 3 and 6 nm. As shown in Figure 3.8 (b), the increase of $\mu_0 M_s$ was confirmed with the increase of t_W. K_{eff} was negative in the stacks with t_W above 6 nm. W becomes polycrystalline when the thickness reaches about 6 nm. It is considered that Fe on W also becomes polycrystalline, leading to the increase of $\mu_0 M_s$. Since the shape magnetic anisotropy is proportional to the square of M_s, which contribute to the in-plane magnetic anisotropy, K_{eff} decreases as a result.

(4) Fe thickness dependence

Si/SiO_2 substrate//W (3 nm)/Fe (t_{Fe} nm)/MgO (2 nm) /Tb (2 nm)/W (1 nm) were prepared. Figure 3.9 shows the schematic diagram. After the deposition, post annealing was performed at T_a = 500 or 550 °C. For the Kerr measurement, Fe-wedge samples were also prepared.

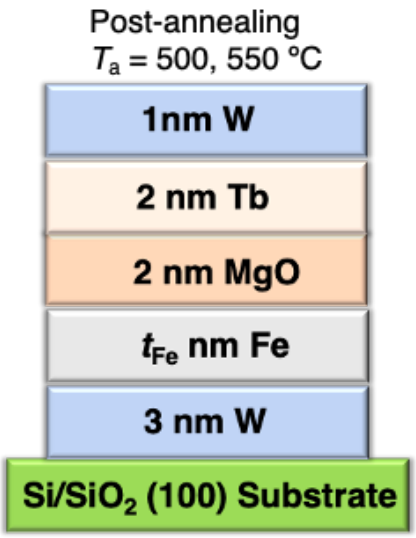

Figure 3.9 Schematic diagram of Si/SiO_2 substrate/Fe(t_{Fe} nm)/MgO/Tb/W.

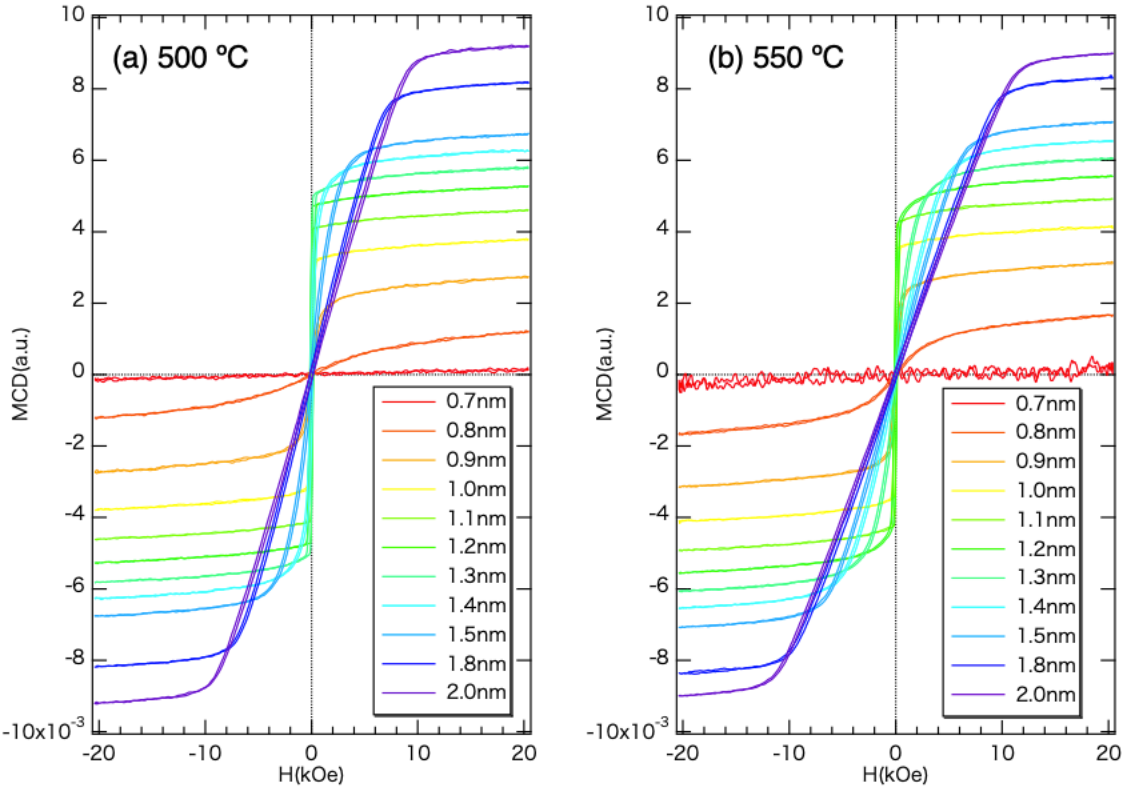

Figure 3.10 MOKE hysteresis curves for the stacks with T_a = (a) 500, (b) 550 °C.

Figure 3.10 shows the polar MOKE measurement result of the samples with T_a =500 and 550 °C. When t_{Fe} = 0.7 nm, the intensity was very weak, which indicates spontaneous magnetization is very small. PMA was confirmed until t_{Fe} = 1.2 ~ 1.3 nm. In the region with above t_{Fe} = 1.3 nm, the magnetic easy axis was in-plane direction.

Next, the interface PMA energy and magnetic dead layer were investigated for the stack with T_a = 550 °C.

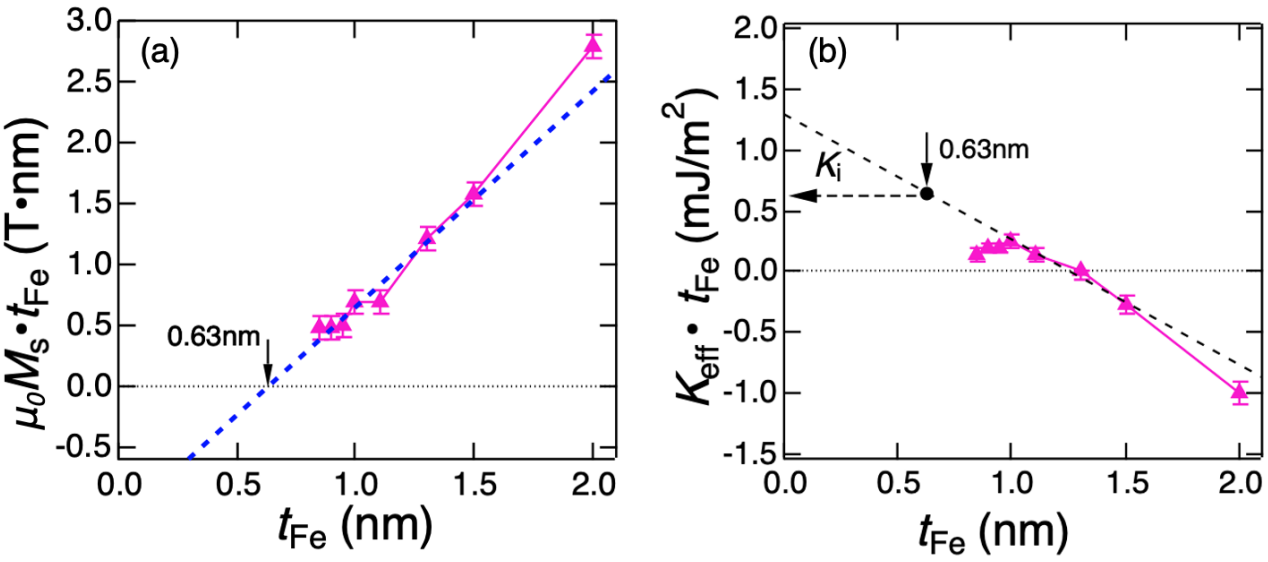

Figure 3.11 t_{Fe} dependence of (a) $\mu_0 M_s \cdot t_{Fe}$ and (b) $K_{eff} \cdot t_{Fe}$.

Figure 3.11 shows t_{Fe} dependence of $\mu_0 M_s \cdot t_{Fe}$ and $K_{eff} \cdot t_{Fe}$. From the fitting line in Figure 3.11 (a), magnetic dead layer t_{dead} of 0.63nm was deduced. K_i is estimated to be 0.64 mJ/m^2 in Figure 3.11 (b).

In order to evaluate the interface state in more detail, XAS and XMCD measurements were performed. Figure 3.12 shows the results of VSM, XAS and XMCD spectra for Fe $L_{2,3}$ edges in the stacks without Tb and with t_{Tb} = 2nm. As shown in Figure 3.12 (a) and (b), the stack with t_{Tb} = 2nm shows PMA, another one is in-plane magnetic anisotropy. Since the upper layer of the samples with Tb is thicker than the sample without Tb, XAS intensity in the sample with Tb is smaller than that in the sample without Tb. The difference between μ_+ and μ_- (XMCD) is larger in the sample with Tb. The XMCD intensity is proportional to the saturation magnetization. In Figure 3.12 (e), the difference between XMCD intensity in NI and GI direction was confirmed. In Figure 3.12 (d), the satellite in the Fe L_3 edges was confirmed, which indicates Fe layer is slightly oxidized. On the other hand, it was not confirmed in the stack with Tb. From these results, it was found that Fe layer is oxidized during the deposition of MgO, and Tb reduces Fe/MgO interface. The magnetic orbital moment M_{orb} is proportional to the integral of XMCD, which means there is an anisotropy in the magnetic orbital moments.[67] The anisotropy of the magnetic orbital moments was not confirmed in the stack without Tb. Interface magnetic anisotropy is proportional to the anisotropy of $M_{orb.}$, as expressed in (1.11). Since the PMA and ΔM_{orb} increased with the insertion of Tb, the interface PMA in Fe/MgO/Tb follows the Bruno relation.

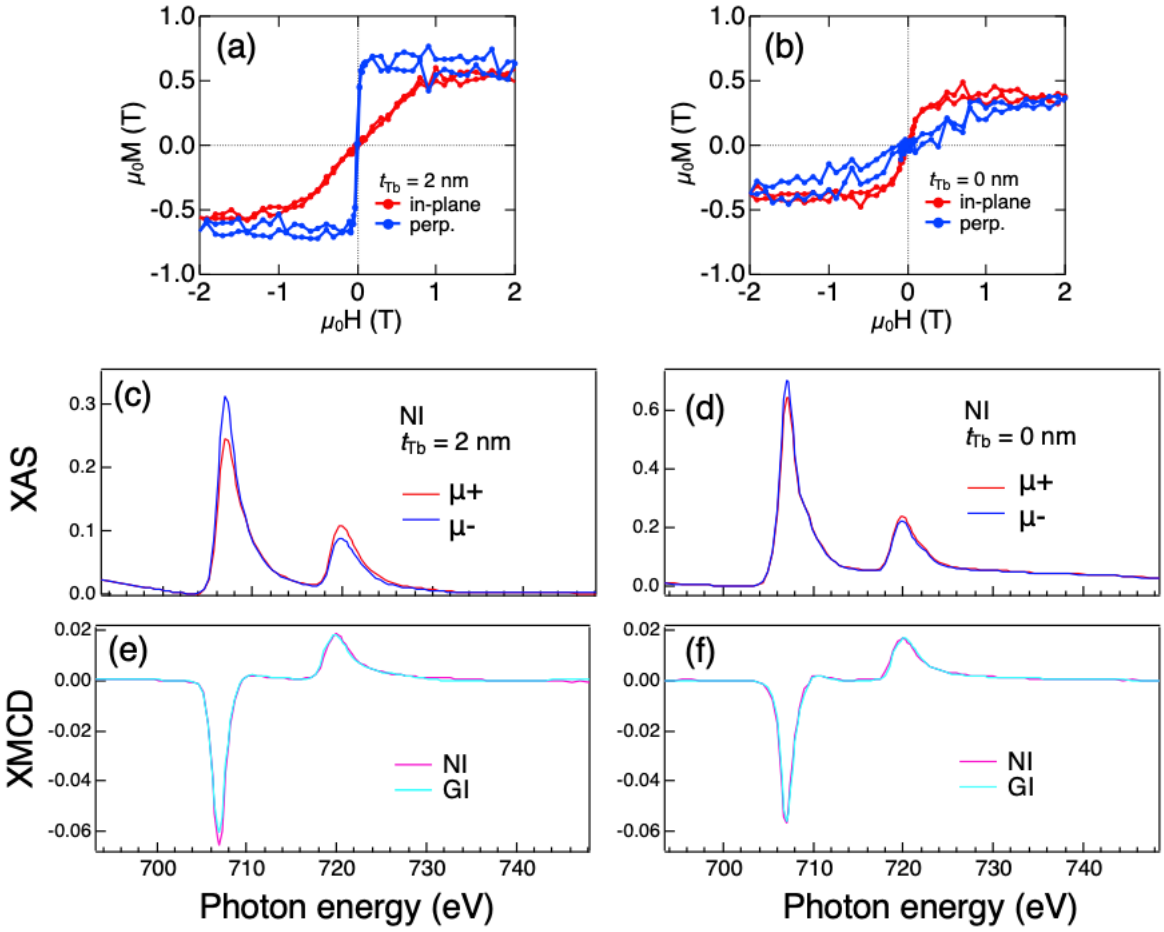

Figure 3.12 M-H curves, XAS, XMCD spectra of Fe $L_{2,3}$ edges for the stacks (a), (c), (e) with 2 nm Tb and (b), (d), (f) without Tb.

Figure 3.13 shows the XAS and XMCD intensity for Tb $M_{4,5}$ edges in Fe/MgO/Tb. Since Tb can reduce Fe-oxide and MgO, it should be Tb-oxide. However, since the 4f orbital are localized in the inner shell, the additional peaks due to the oxidation is not observed.[103] Also, the XMCD intensity of Tb was quite small, it was considered that Tb dose not diffuse to Fe layer.

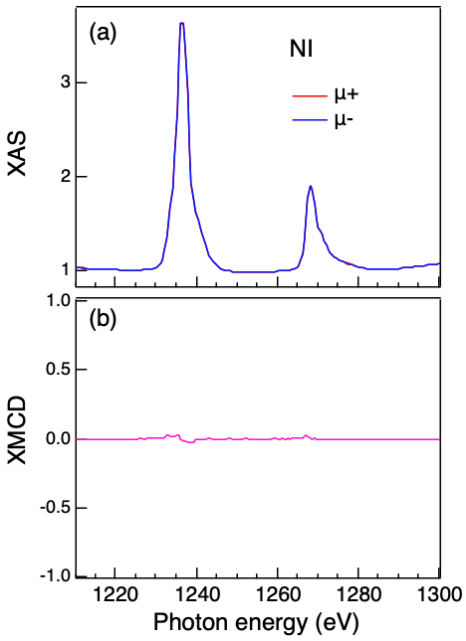

Figure 3.13 XAS and XMCD spectra of Tb $M_{4,5}$ edges.

3.1.3 Discussion

In this section, the magnetic dead layer and obtained PMA is considered. Figure 3.14 shows the images of as deposited and annealed samples. In as deposited sample, Fe layer is grown as amorphous structure on W buffer, and it is oxidized during the deposition of MgO. After the annealing, it is considered that a part of Fe layer became polycrystalline structure and the oxidation state at Fe/MgO interface was adjusted by Tb. Therefore, PMA was obtained, although K_i is small. Since it is considered that amorphous Fe remains even after annealing, the saturation magnetization is small.[104]

Figure 3.14 Images of as deposited and annealed samples.

Small M_s reduce the shape magnetic anisotropy which contribute to the in-plane magnetic anisotropy. Therefore, effective PMA was achieved although the interface PMA is small.

3.1.4 Summary

In summary, polycrystalline Fe/MgO was prepared by rf-sputtering. Amorphous W are used as buffer layer, and PMA was achieved by controlling oxidation state at the Fe/MgO interface using Tb capping layer. By adjusting the annealing temperature and the thickness of Tb, K_i of 0.64 mJ/m^2 was obtained. When the W buffer became polycrystalline, the M_s of Fe and the contribution of shape magnetic anisotropy increased, resulting in in-plane magnetic anisotropy. In addition, when Mg was used instead of Tb, the effect was not as good as that of Tb. This is because Tb has a higher redox ability than Mg, demonstrating the usefulness of Tb. In this experiment, it was found that PMA can be obtained even in polycrystalline Fe/MgO on a SiO_2 substrate by sputtering.

3.2 Singlecrystalline Fe/MgO (Fe/CrO/MgO)

3.2.1 Experiment

MgO(001) substrate//MgO-seed(5 nm)/Cr-buffer(30 nm)/Fe(0.7 nm)/MgO(2 nm) was prepared by rf-sputtering. All depositions were performed at room temperature. MgO substrate and Cr buffer were annealed at 500 ºC for 1 hour. After the deposition, post annealing was performed at different temperature T_a = 300, 400 or 500 ºC for 1 hour. As deposited sample was also prepared. As the sample for comparison, EB-grown sample with same nominal structure was prepared. In EB growth, MgO substrate, Cr buffer, Fe and MgO barrier were annealed at 800, 800, 250, 400 ºC, respectively, and the deposition was performed at 150 ºC. XRD measurements was performed for sputter deposited and EB grown samples. Structural analyses by STEM and magnetic measurements by VSM were performed for sputter-deposited samples. Interface magnetic anisotropy was investigated for the sample with T_a =500 ºC by changing the Fe layer thickness. XAS and XMCD measurements were performed in order to the oxidation states.

3.2.2 Result

Figure 3.15 shows the out of plane XRD for the sputter-deposited sample with T_a= 500 ºC and EB grown sample. As shown in Figure 3.15 (a) and (b), MgO(002) and MgO(004) peaks from MgO substrate and Cr(002) peaks can be observed, but Fe layer cannot be seen due to the thin thickness. Inset figures are the locking curves for Cr taken at θ= 32.25˚ and 32.31˚ for sputter and EB Fe/MgO, respectively. The full width at half maximum (FWHM) peak of Cr in sputter Fe/MgO is 0.689˚, which is almost same value of MBE of 0.553˚. This little difference seems to be due to the difference of the annealing temperature. Even in the sputter-deposited samples, same quality with EB was achieved in Cr-buffer.

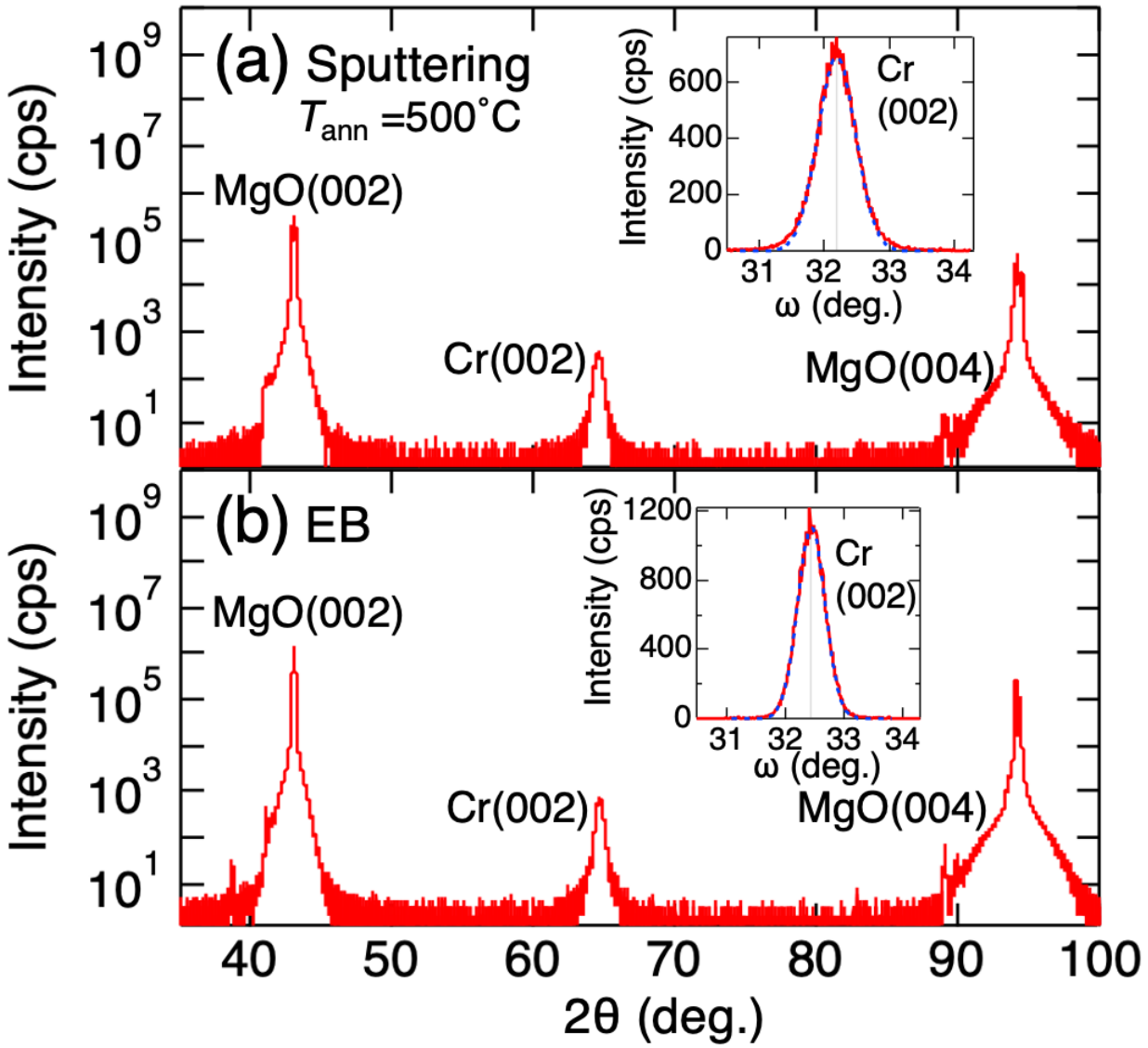

Figure 3.15 Out of plane θ-2θ scan for (a) sputtering and (b) EB. Inset shows rocking curve for Cr(002) peak. (c) FWHM of 0.689˚ taken at θ = 32.25˚. (d) FWHM of 0.553˚ taken at θ = 32.31˚.

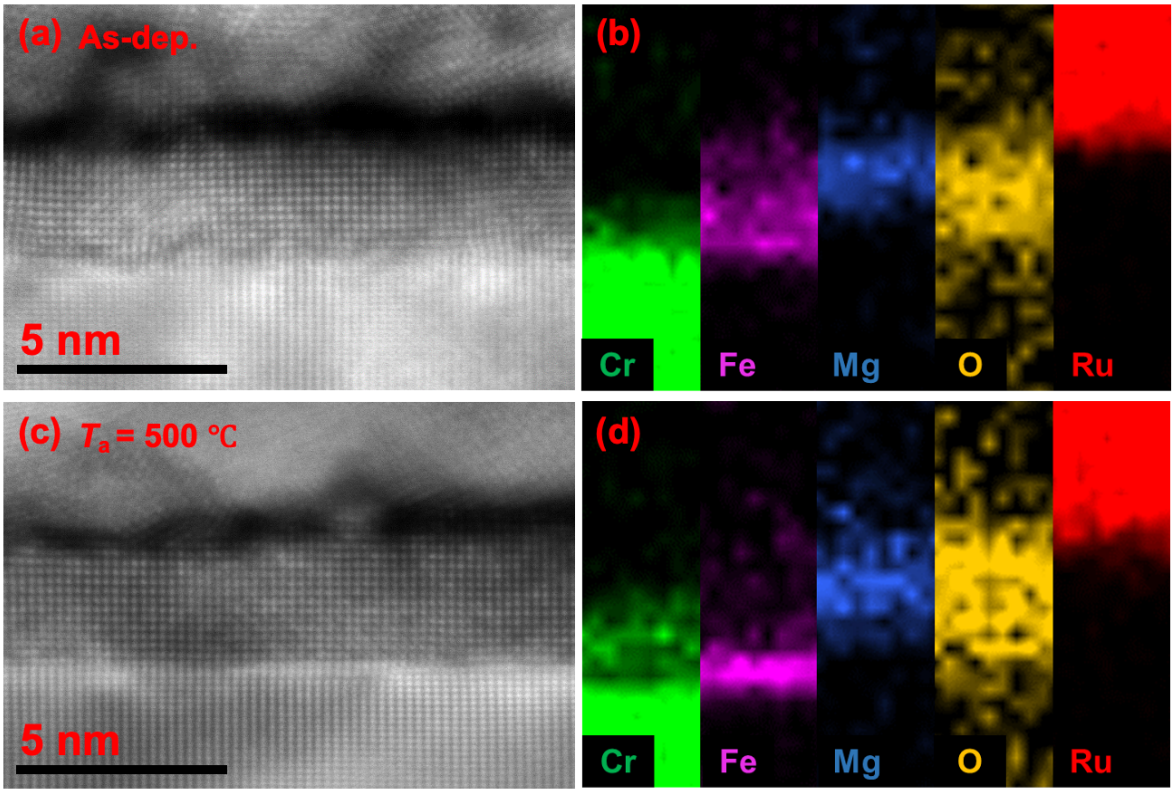

Figure 3.16 STEM images and EDS mappings for (a), (b) as deposited and (c), (d) T_a = 500 ℃ annealed samples.

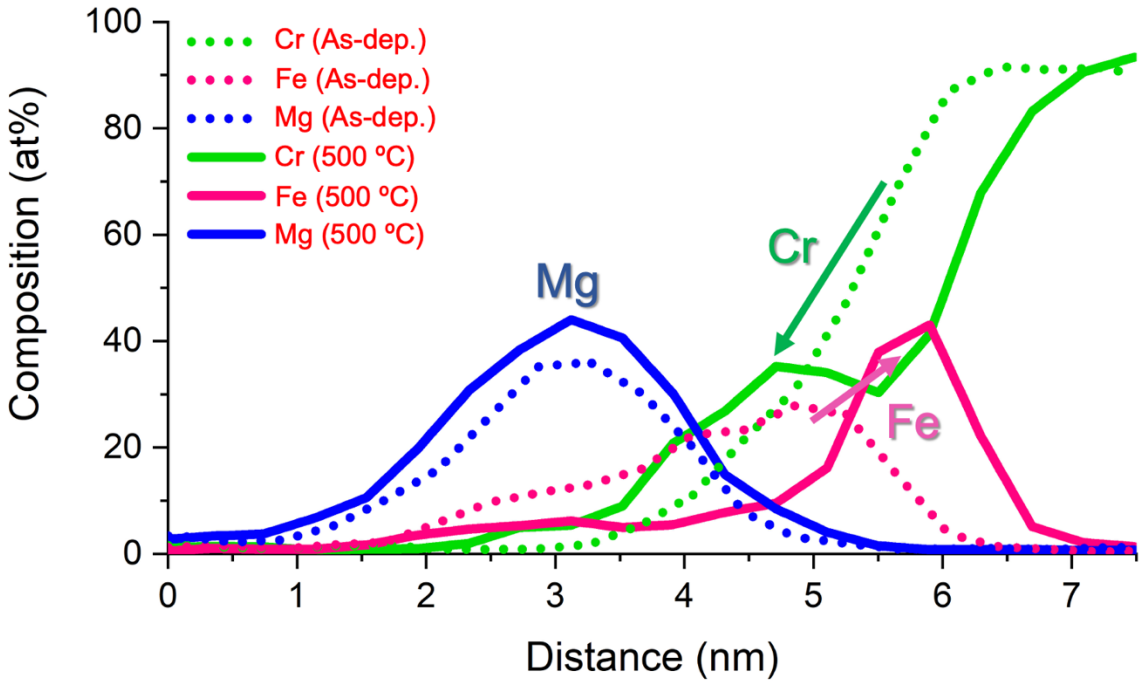

Figure 3.17 Composition profiles. Dotted line and solid line represent as deposited and T_a = 500 ℃ annealed samples.

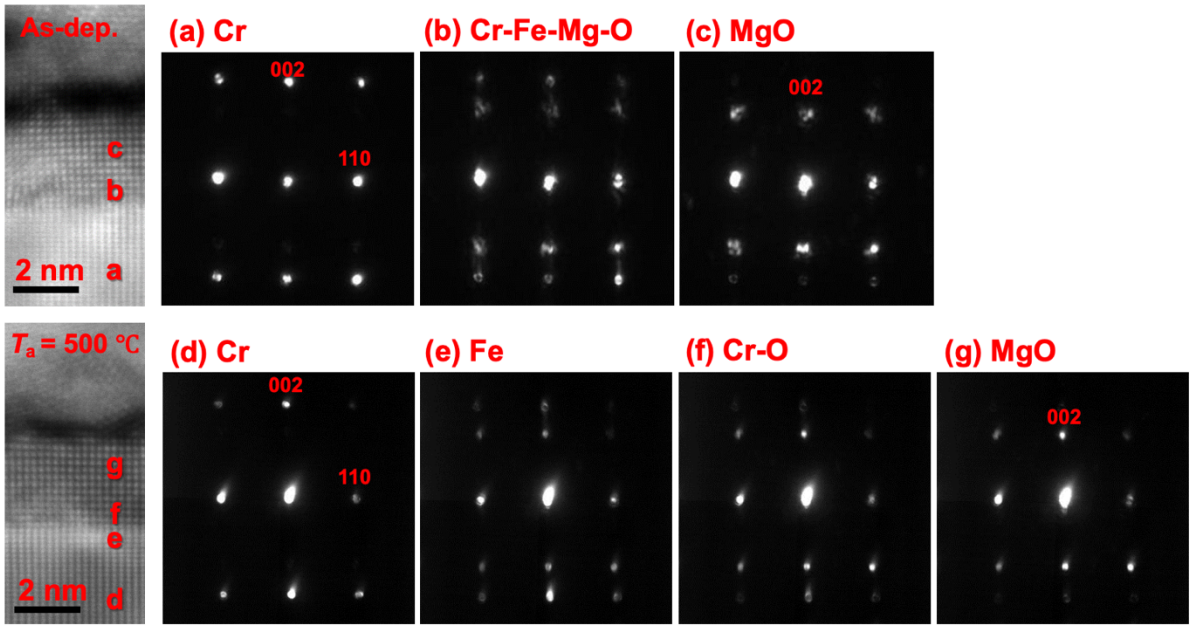

Figure 3.18 NBD patterns of as deposited and T_a = 500 °C annealed samples. As deposited sample; (a) Cr, (b) Cr-Fe-Mg-O, (c) MgO. T_a = 500 °C annealed sample; (d) Cr, (e) Fe, (f) CrO, (g) MgO.

Figure 3.16 shows the STEM images and EDS mapping for the sputter deposited sample without annealing and with T_a = 500 °C. Epitaxial growth of each layer was confirmed. As shown in Figure 3.16 (b), in as deposited sample, the mixing of Fe, Cr and Mg and the oxidation of underlayer was observed. These mixing was no reported in EB and MBE grown samples. Since the deposition energy of sputtering is much higher than EB and MBE, the mixing of Fe and Cr was caused. Also, the oxygen is released during the deposition of MgO, Fe layer is easily oxidized. In Figure 3.16 (d), diffused Fe became the film, and the formation of Cr-oxide between Fe and MgO was confirmed. Figure 3.17 shows composition profile. The peak position of Cr was changed before and after the post annealing. Figure 3.18 shows nanobeam electron diffraction (NBD) patterns. In an as deposited sample, the peaks from the region between Cr and MgO shows the mixing of Cr-Fe-Mg-O. After the annealing, the peak patterns of Cr-oxide were same with that of MgO, which means rock salt type CrO including Fe atoms. Cr_2O_3, CrO_2, $FeCr_2O_4$ can be considered as Fe and Cr compounds, but these are corundum, rutile, and spinel type structures, which are different from this NBD pattern. The most stable oxide of Cr is Cr_2O_3, but it is considered that CrO is stabilized by forming at the interface.

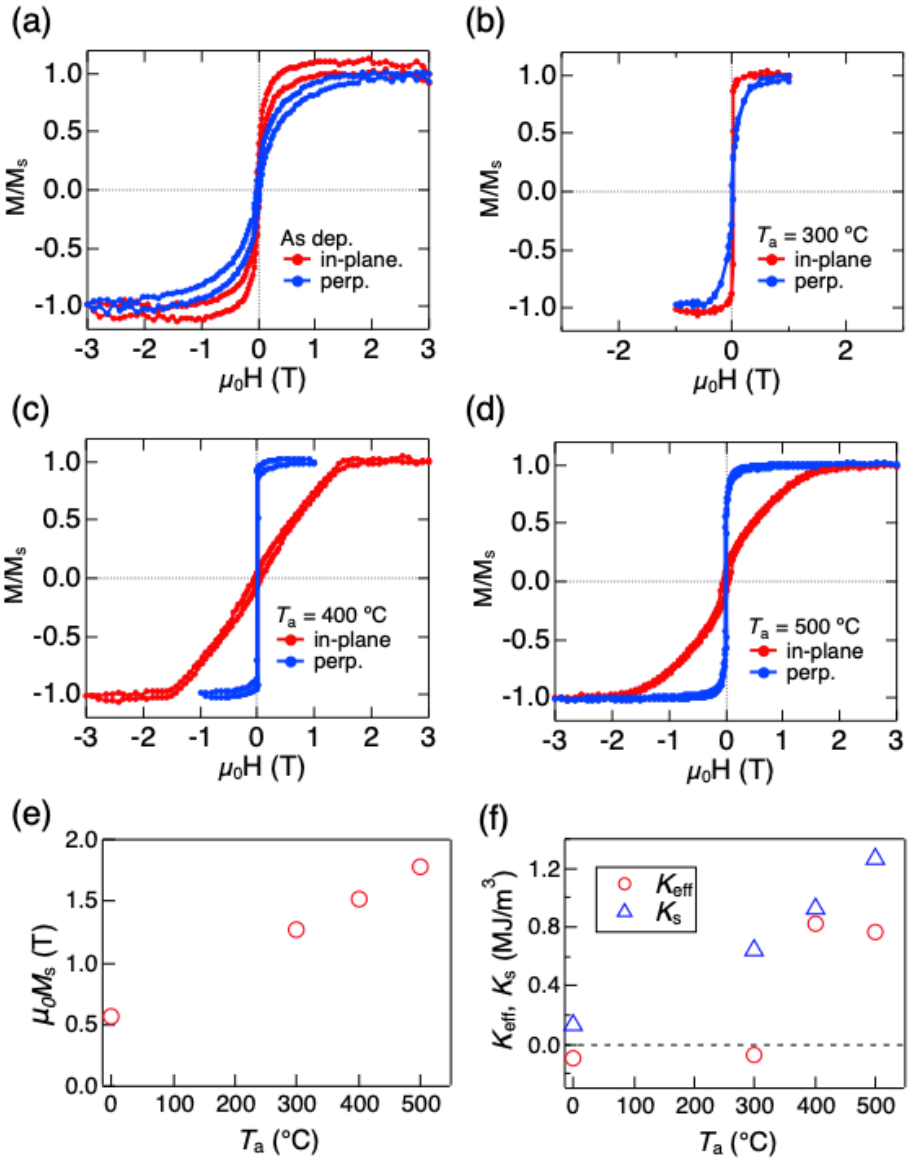

Figure 3.19 Normalized M-H curves for (a) as deposited, (b) T_a= 300 °C, (c) T_a= 400 °C, (d) T_a= 500 °C annealed samples. T_a dependence of (e) $\mu_0 M_s$ and (f) K_{eff}, K_s.

Figure 3.19 shows the M-H curves for the sputter-deposited samples with different T_a and $\mu_0 M_s$, K_{eff} and K_s. In the samples without annealing and with T_a = 300 °C, magnetic easy axis was in-plane direction. On the other hand, PMA was observed in the sample with T_a = 400 and 500 °C. As shown in Figure 3.19 (e), the increase of $\mu_0 M_s$ with the increase T_a was confirmed. Considering the STEM results, it seems that the magnetization was recovered because the oxidized Fe was reduced by annealing. K_{eff} of 0.82 and 0.77 MJ/m^3 was obtained in the samples with T_a = 400 and 500 °C, respectively. K_{eff} of the sample with T_a = 400 °C is larger than that with T_a = 500 °C, but interface PMA energy of the samples with T_a = 500 °C is larger than that with T_a =400 °C considering the contribution of K_s.

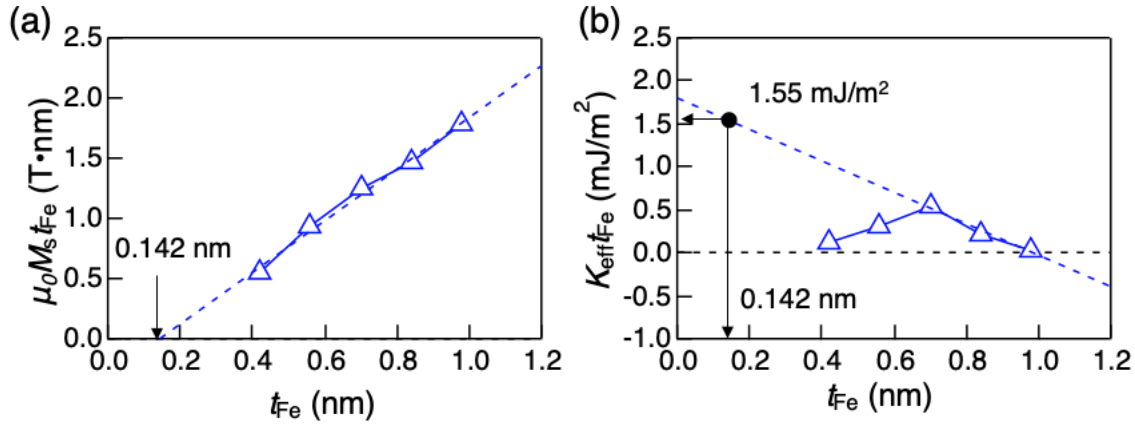

Figure 3.20 t_{Fe} dependence of (e) $\mu_0 M_s \cdot t_{Fe}$ and (f) $K_{eff} \cdot t_{Fe}$

Figure 3.20 shows the t_{Fe} dependence of $\mu_0 M_s \cdot t_{Fe}$ and $K_{eff} \cdot t_{Fe}$. As shown in Figure 3.20 (a), $t_{dead} = 0.142$ was confirmed which does not show the spontaneous magnetization. It is considered that the magnetic dead layer is due to the mixing of Fe and Cr and the oxidation of Fe layer. K_i was deduced to be 1.55 mJ/m² from the fitting line in Figure 3.20 (b) considering the magnetic dead layer. Since CrO exists between Fe and MgO layer as shown in Figure 3.17, this interface PMA occurred at Fe/CrO interface.

XAS and XMCD were performed for Fe and Cr $L_{2,3}$ edges in the sputter deposited and EB grown sample. Figure 3.21 shows XAS and XMCD spectra for Fe $L_{2,3}$ edges taken at NI configuration. The increase of XMCD intensity was confirmed with the increase of T_a, which results is consistent with the results of VSM because XMCD intensity is proportional to the M_s. Compared with the EB grown sample, the satellite was observed in the higher energy side of Fe L_3 edges in sputter-deposited samples. This means Fe layer was oxidized.

Figure 3.22 (a)-(d) and (f)-(i) show μ_+ and μ_- intensities for Fe and Cr $L_{2,3}$ edges taken at GI direction. Assuming that Fe and Cr of the EB grown sample were not oxidized at all, the difference from the spectrum of the sputter deposited sample was taken. Figure 3.22 (e) and (j) show the difference between sputter deposited and EB grown samples. In Figure 3.22 (e), the peaks at 707.5 eV are due to the oxidized Fe. It was confirmed that the peaks became smaller by post annealing, suggesting that Fe layer is reduced. On the other hand, the peaks at 576.75 eV due to the oxidized Cr was enhanced by the post annealing. These represent the fact that Cr reduces Fe-oxide.

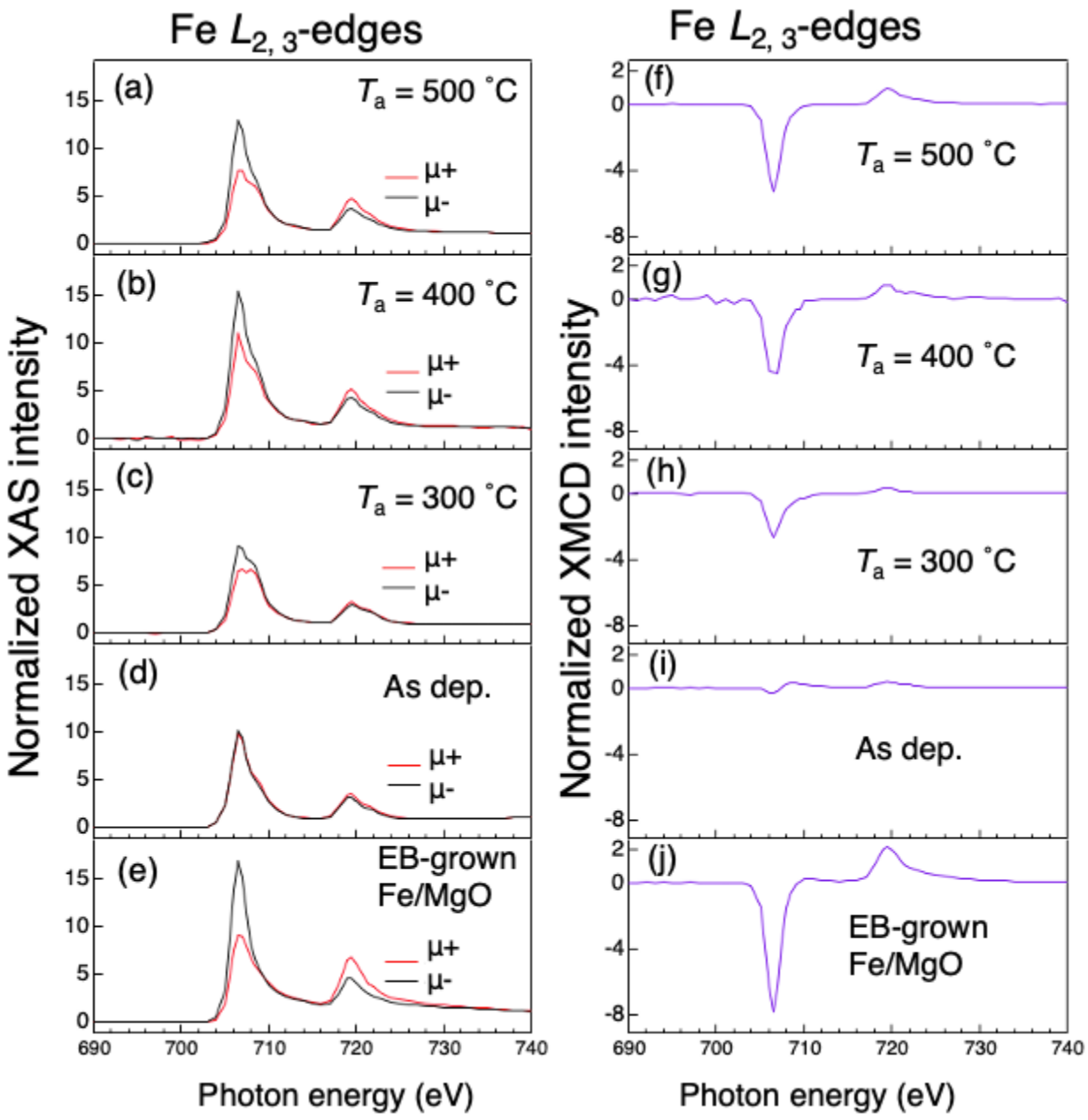

Figure 3.21 Normalized XAS and XMCD spectra for Fe $L_{2,3}$ edges. (a), (f) T_a = 500 ºC. (b), (g) T_a = 400 ºC. (c), (h) T_a = 300 ºC. (d), (i) as deposited. (e), (j) EB-grown Cr/Fe/MgO.

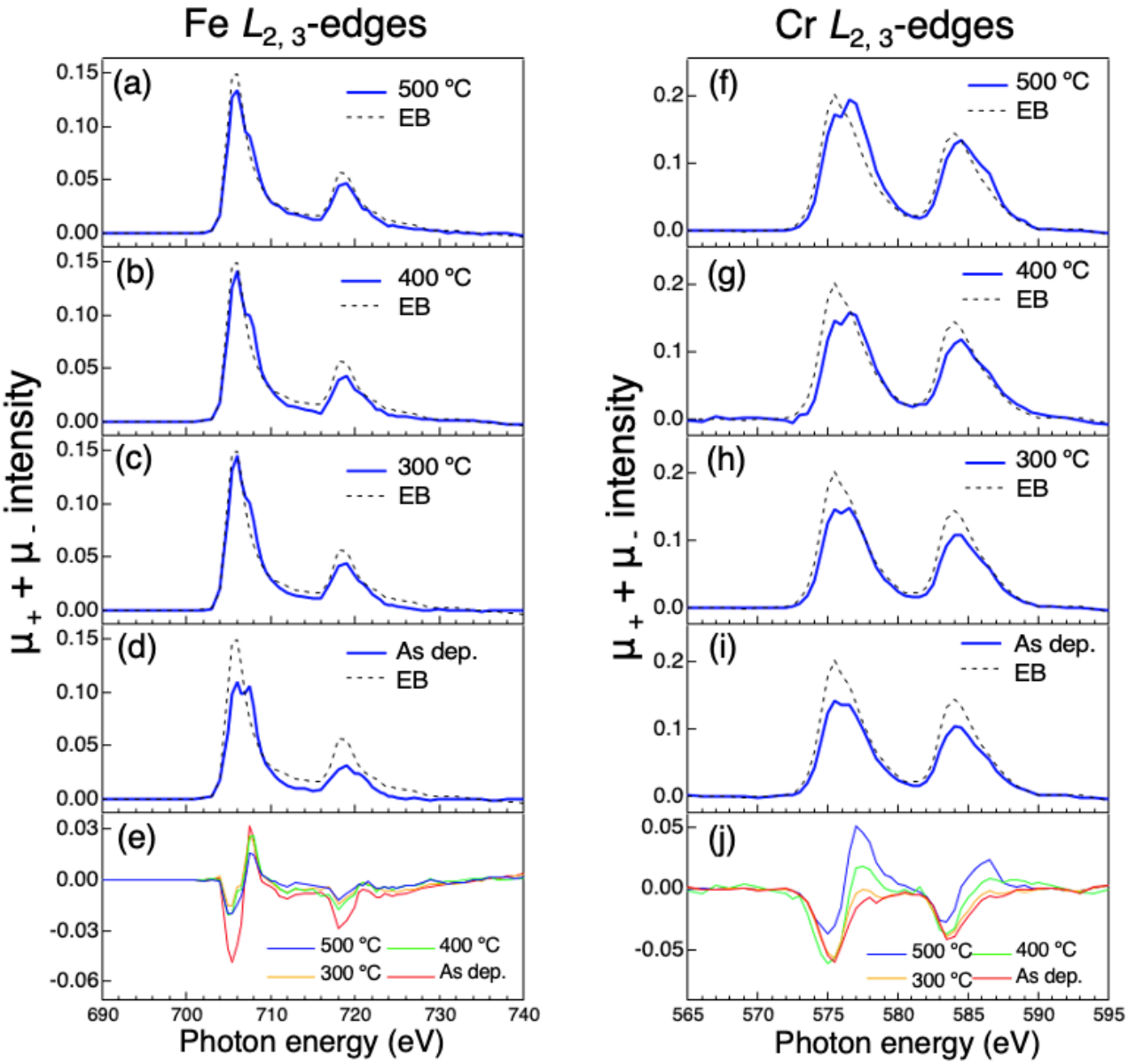

Figure 3.22 XAS (μ+ and μ-) spectra for Fe and Cr $L_{2,3}$ edges. (a), (f) T_a = 500 °C. (b), (g) T_a = 400 °C. (c), (h) T_a = 300 °C. (d), (i) as deposited. Dashed line represents the spectra in EB-grown Cr/Fe/MgO. (e), (j) differences between the spectra of sputter-deposited and EB-grown Cr/Fe/MgO.

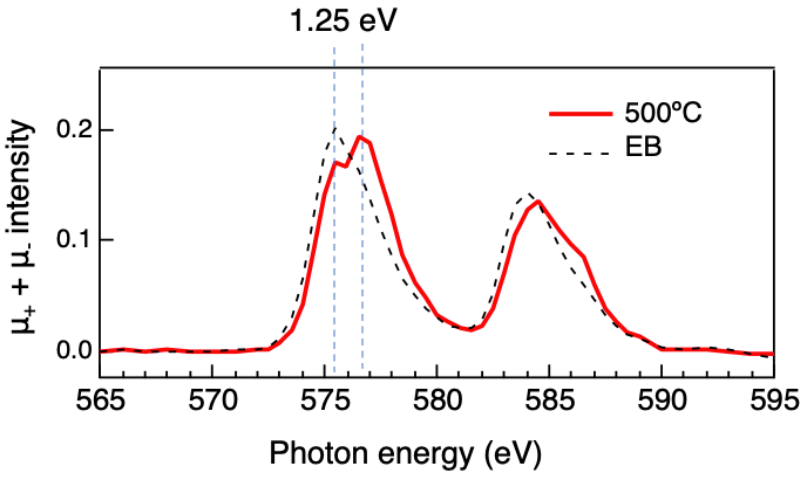

Figure 3.23 Peak shift between metallic and oxidized Cr.

The peak position of the oxidized Cr was 576.75 eV in the samples with T_a =500 °C, and that of pure Cr metal is 575.5 eV, as shown in Figure 3.23. The peak shift was deduced to be 1.25 eV, which is different from that of Cr_2O_3, CrO_2 and CrO_3.[105-107] Although it is difficult to evaluate the valence of Cr correctly, considering the structure of Cr oxide is rock salt in Figure 3.18 (f) and the peak shift of Cr2+ is 1.8 eV,[108] it is deduced to be 2+ or less. In particular, the lattice constant of $CrO_{0.87}$ is 0.404 nm,[109] which is lattice-matched with Fe, therefore it is possible that the CrO is oxygen-deficient.

Theory predicted that CrO is antiferromagnetic and has a local moment at Cr site,[110] but the magnetic properties have not been investigated because it is an unstable compound. In this experiment, XMCD was no observed at the peak of oxidized Cr, meaning that CrO does not possess ferromagnetism. In addition, in the case of Co/Cr_2O_3 and Fe/mono-layer-order Cr-oxide, the induced moment has been confirmed.[111,112] It was found that Fe did not induce a moment of Cr2+ at Fe/CrO interface.

3.2.3 Discussion

By annealing Cr/Fe-oxide/MgO, the stack of Cr/Fe/CrO/MgO was obtained. The process of the formation of CrO between Fe/MgO interface is discussed. This situation occurs as the metastable state.[113-115] In the case that high temperature or long-time annealing is performed, the formation of CrO does not occur because materials were completely mixed. In the field of semiconductor, there is the crystal growth method for Si-Al, Si-Ag, Ge-Al which exchange positions of layers.[116-118] These prevent the formation of compounds by annealing below the eutectic temperature. As an example, the process of exchanging the layers of an amorphous semiconductor and a metal layer such as Si-Al is introduced.[119] First, the semiconductor (Si) dissolves in the metal (Al) and form a nucleus. When the nucleus grows laterally, the metal is

pushed up and the layers are replaced. In the case of Fe/CrO, it is considered that the nucleus of CrO grows in Fe-oxide and finally Fe is pushed up by CrO. In the Ellingham diagram, Cr has a higher affinity for oxygen than Fe. Therefore, it is considered that the oxygen in Fe provide the driving force to diffuse into Fe layer for Cr.[114,115] It is considered that Fe/CrO/MgO was energetically more stable than oxygen moving into Cr to form a Cr-oxide/Fe/MgO structure. In the STEM image (Figure 3.17 (d)), the formation of 1 nm CrO was confirmed. If Cr completely reduces Fe-oxide, the diffusion of Cr is quenched. Therefore, in the stack of Cr/Fe-oxide/MgO, it is considered that CrO having same thickness with Fe-oxide segregate by post-annealing.

The layer exchange crystal growth method in semiconductors is mainly aimed at producing polycrystalline semiconductors on a glass substrate by low temperature annealing as compared with a normal deposition process, and it seems that much attention has not been paid to the characteristics of the obtained interface. In this study, Fe/CrO produced by the growth method in which the layers were replaced showed a large interface magnetic anisotropy of 1.55 mJ/m^2, which means the flatness of the interface is high enough for large PMA. In addition, unstable compound CrO could be stabilized by forming them into the interface.

Interface PMA energy of 2 mJ/m^2 is achieved at Fe/MgO and Fe/$MgAl_2O_4$.[74,76] Oxidation states at the interface is important for PMA. PMA at the Fe/FeO/MgO interface strongly depends on the composition of FeOx.[120] When the composition of FeOx is $FeO_{0.5}$, PMA is expected. PMA of Fe/CrO also seems to be dependent on the amount of oxygen in CrO.

PMA can be expected at the interface between Fe and the other 3*d* transition metal oxides such as CrO, FeO, and CoO. Since these 3*d* transition metals have a rock salt structure and have a lattice constant close to that of Fe and MgO,[121-124] an interface with little lattice mismatch can be achieved. These materials have different conductivity and magnetic moment, and if PMA can be realized between the Fe interface, functional p-MTJs can be created.

3.2.4 Summary

In summary, the structure and magnetic properties of sputter-deposited singlecrystalline Cr/Fe/MgO were investigated. In as-deposited samples, the mixing of Cr-Fe-Mg and the oxidation of Fe layer were confirmed. After the post-annealing, rock salt type CrO was formed at Fe/MgO interface. As the annealing temperature was increased, the saturation magnetization was recovered. In the stacks with T_a = 500 ºC, K_i of 1.55 mJ/m^2 was achieved, which means the interface PMA occurred at Fe/CrO interface. From the XAS measurement, redox reaction of Fe-oxide and Cr was confirmed. The valence of CrO was deduced to be 2+ or less form the peak shift in the XAS spectra and NBD patterns. Large PMA was obtained at the formed Fe/CrO interface, suggesting that PMA can be expected at the interface between Fe and other 3d transition metal oxide with rock salt type structures.

Chapter 4 Perpendicular magnetic anisotropy in W inserted Fe/MgO

In this section, the effect of W insertion for PMA was studied. W was inserted to the sputter deposited and EB grown Fe/MgO interface.

4.1 Experiment

· Sputter-deposition

MgO substrate//MgO(5 nm)/Cr(30 nm)/Fe(0.7 nm)/W(0, 0.05 nm)/MgO(2 nm) were prepared by rf-sputtering (Figure 4.1). All depositions were performed at room temperature. MgO substrate, Cr buffer and MgO barrier were annealed at 500 ºC for 1 hour. Magnetic properties were evaluated by VSM.

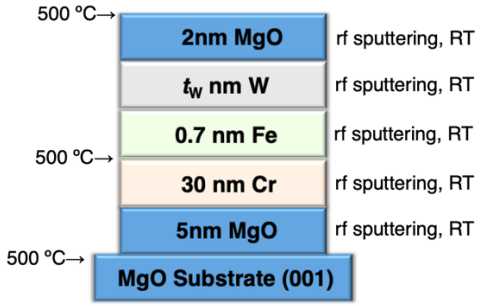

Figure 4.1 Schematic diagram of sputter deposited Fe/W/MgO.

·EB-growth (except for W)

MgO substrate//MgO(5 nm)/Cr(30 nm)/Fe(0.7 nm)/W(0, 0.05, 0.15 nm)/MgO(2 nm) were prepared by EB, except for W (Figure 4.2 (a)). EB growth were performed at 150 ºC. W is deposited by rf-sputtering at room temperature. MgO substrate, Cr buffer, Fe and MgO barrier were annealed at 800, 800, 250 and 400 ºC, respectively. Epitaxial growth of each layer was confirmed by RHEED. The spin and orbital magnetic moment were investigated by XMCD measurement. MTJ was made by adding top electrode Fe(10 nm)/Ru(10 nm) and the VCMA effect was evaluated (Figure 4.2 (b)). Top Fe layer was grown by EB at 150 ºC, and Ru-cap was deposited by dc sputtering at room temperature.

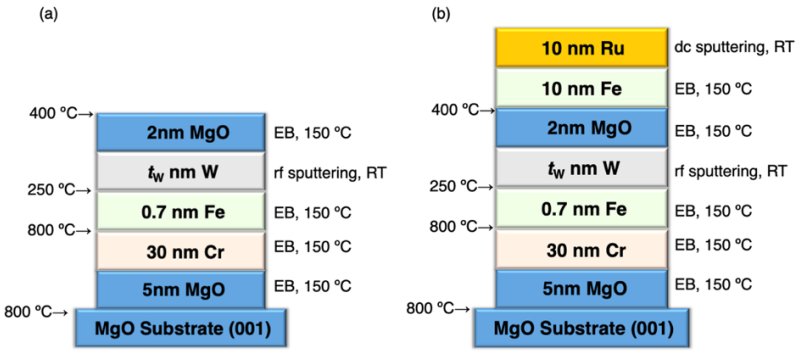

Figure 4.2 Schematic diagrams of EB grown Fe/W/MgO (except for W). (a) half stack MTJ for VSM, STEM. XMCD. (b) full stack MTJ for VCMA.

4.2 Result

· Sputter-deposition

Figure 4.3 shows the *M-H* curves for the stack without W and with t_W = 0.05 nm. K_{eff} of 1.0 and 0.4 MJ/m^3 was obtained for the stacks without W and with t_W = 0.05 nm, respectively. As shown in Chapter 3, the actual structure of Cr/Fe/MgO is Fe/CrO/MgO. By inserting W, K_{eff} decreased.

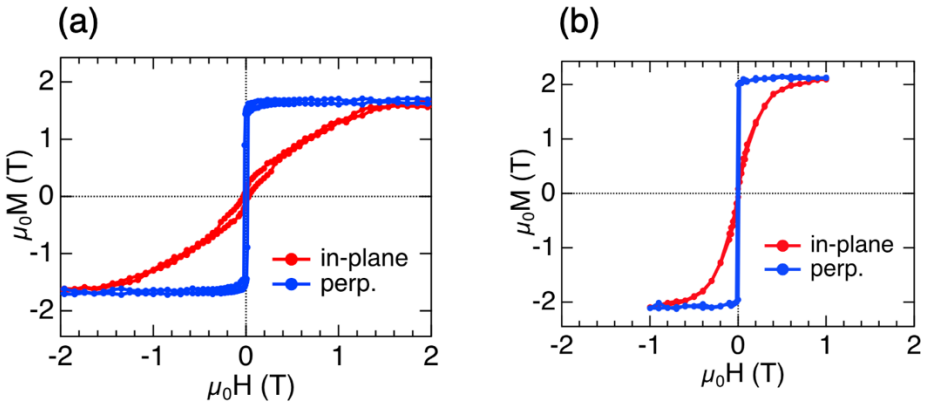

Figure 4.3 M-H curves for the stacks (a) without W and (b) with t_W = 0.05 nm.

· EB-growth (except for W)

Figure 4.4 shows the RHEED patterns for each layer taken at [100] direction of MgO substrate. The epitaxial growth of each layer was confirmed. Figure 4.5 shows STEM images, EDS mapping and composition profiles. As shown in Figure 4.5, the mixing of Fe and W is confirmed. Therefore, the structure proposed by theory was not obtained. Also, the diffusion of Cr to the Fe/MgO interface was confirmed. It is considered that the mixing of Cr and Fe was caused by the sputtering of W, and it was separated by post annealing. Since the Fe and W is mixed, RHEED patterns in Figure 4.4 (c) is FeW.

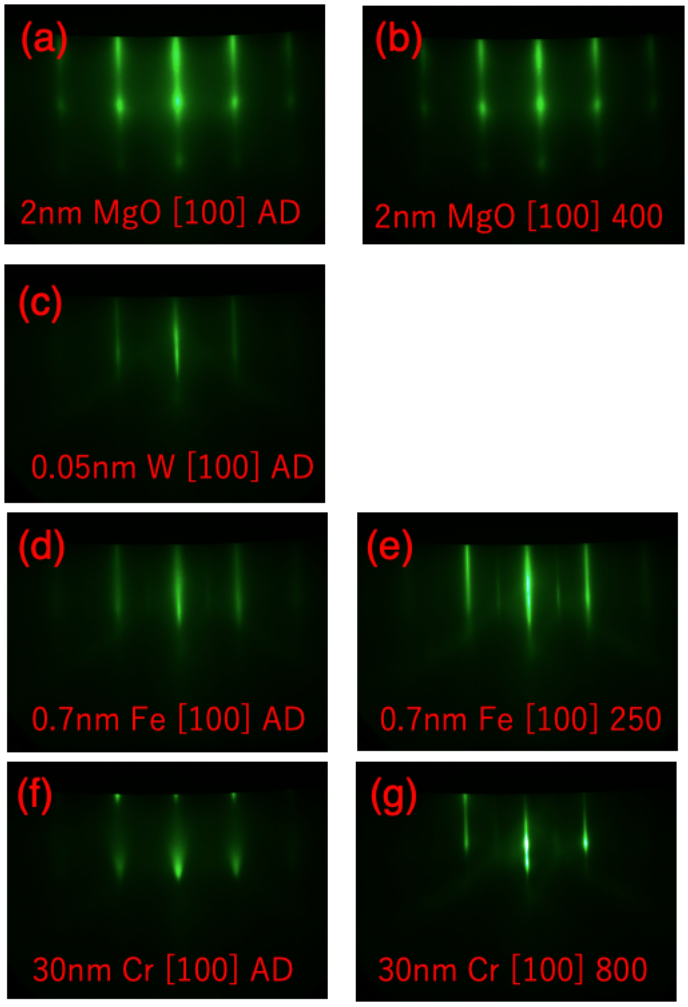

Figure 4.4 RHEED patterns of MgO substrate//MgO(5 nm)/Cr(30 nm)/Fe(0.7 nm)/W(0.05 nm)/MgO(2 nm). (a) as deposited top MgO. (b) 400 ºC annealed top MgO. (c) as deposited W. (d) as deposited Fe. (e) 250 º annealed Fe. (f) as deposited Cr. (g) 800 ºC annealed Cr.

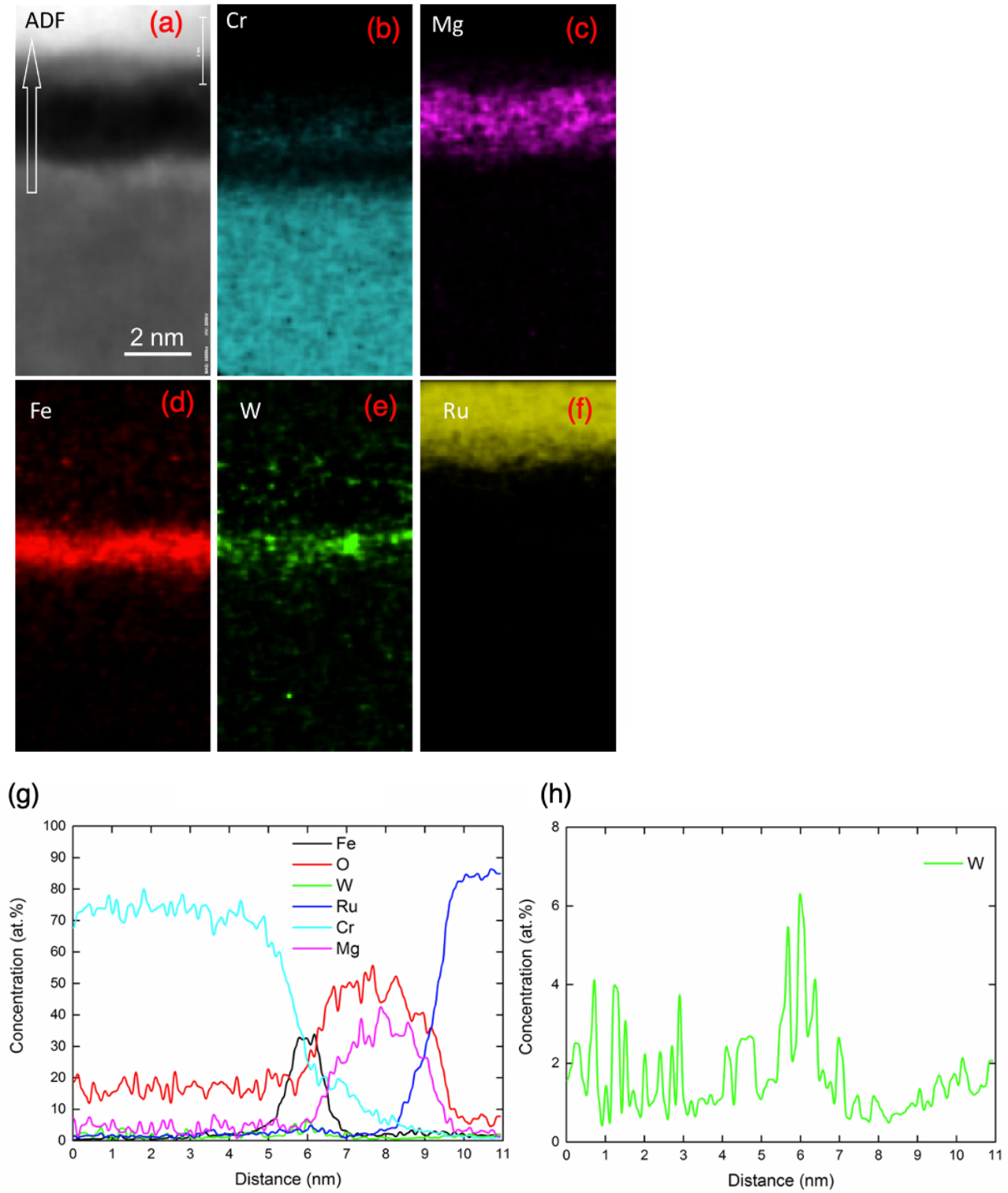

Figure 4.5 (a) STEM image, (b)-(f) EDS mapping and (g), (h) composition profiles of MgO substrate//MgO(5 nm)/Cr(30 nm)/Fe(0.7 nm)/W(0.05 nm)/MgO(2 nm).

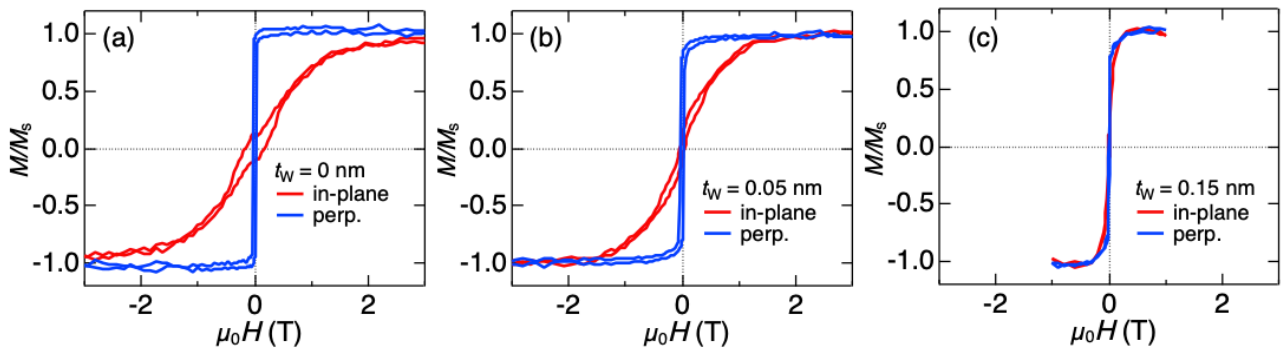

Figure 4.6 Normalized *M-H* curves for the sacks (a) without W, (b) with t_W = 0.05 nm and (c) t_W = 0.15 nm.

Figure 4.6 shows M-H curves for the stacks with t_W = 0, 0.05, 0.15 nm. K_{eff} was deduced to be 1.2, 0.76 and 0.05 MJ/m^3 and $\mu_0 M_s$ was 1.90, 1.78 and 1.70 T for t_W = 0, 0.05 and 0.15 nm. As can be seen from the STEM results, the mixture of Fe and W reduced both $\mu_0 M_s$ and K_{eff}.

XAS and XMCD measurements were performed on samples with different t_w. The magnetic field that can be applied is limited to 1T, and in the sample of t_w = 0, 0.05 nm, the GI direction cannot be completely saturated, so only the NI direction was measured. For samples with t_w = 0.15 nm, the measurements were performed in the NI and GI directions. Figure 4.7 shows the results of XAS and XMCD measurements at t_w = 0 and 0.15 nm. In the XMCD spectrum of the sample with t_w = 0.15 nm, a difference was confirmed in the NI direction and the GI direction. This means that there is anisotropy in M_{orb} in the NI and GI directions. These spin and orbital magnetic moments were calculated according to the XMCD sum rule. Table 4.1 shows M_{spin} and M_{orb} for each t_w. As shown in Table 4.1, it can be seen that the insertion of W reduces the M_{spin}, which is consistent with the decrease in magnetization. In Bruno's relation, K_i and ΔM_{orb} are in a proportional relationship, and both K_i and ΔM_{orb} are smaller than Fe/MgO. In the current situation where Fe and W are mixed, the interface between FeW and MgO is considered to be the origin of PMA.

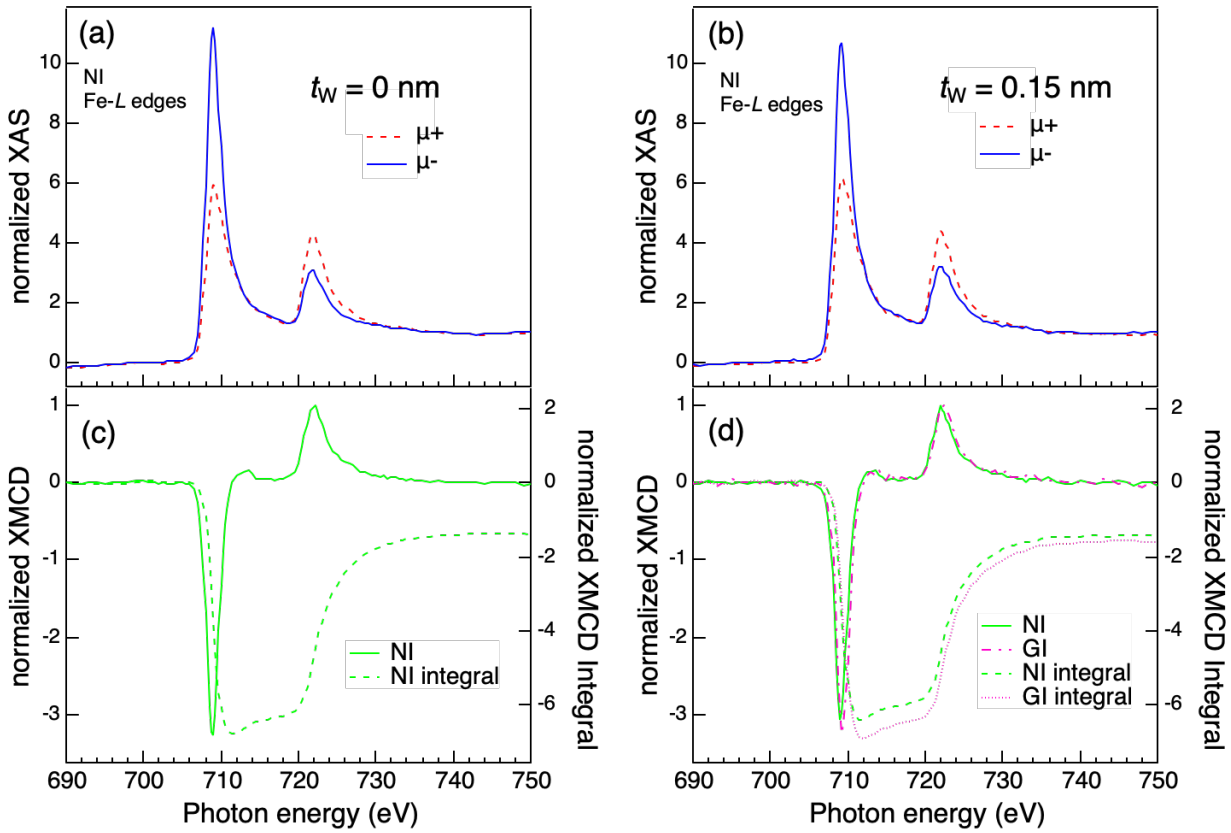

Figure 4.7 Normalized XAS and XMCD spectra for the stacks (a), (c) without W and (b), (d) with t_W = 0.15 nm.

Table 4.1 M_{spin}, M_{orb} and ΔM_{orb} in the stacks with different t_W.

t_W (nm)	0	0.05	0.15	
	NI	NI	NI	GI
M_{spin} (μ_B)	1.66	1.57	1.47	1.45
M_{orb} (μ_B)	0.095	0.073	0.093	0.093
ΔM_{orb} (μ_B)	…	…	< 0.01	

The electric field effect of MTJ composed of Fe(0.7 nm)/W (0.05 nm)/MgO (2 nm)/Fe (10 nm) was evaluated. The lower electrode shows PMA, on the other hand the upper electrode shows in-plane magnetic anisotropy. Figure 4.8 shows the VCMA effect of this structure.

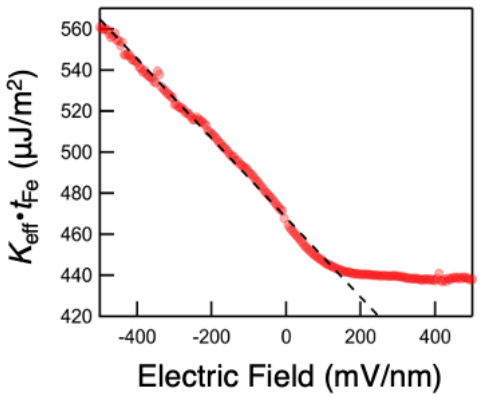

Figure 4.8 VCMA effect in Fe(0.7 nm)/W (0.05 nm)/MgO (2 nm).

In the positive electric field region, there was almost no change due to the electric field, but in the negative electric field region, VCMA coefficients of about 190 fJ/Vm were obtained. This value is small compared to normal Fe/MgO without W. In the results of this experiment, it seems that the interface condition was worse than that of pure Fe/MgO because Fe and W were mixed.

4.3 Discussion

In this experiment, the mixing of W and Fe and the decrease of magnetization was confirmed. It is known that in CoFeB/MgO, when W is deposited on CoFeB by sputtering, it is almost mixed.[125] On the other hand, when W/Fe/W is formed by MBE, no significant decrease in M_s is observed.[93] The deposition energy of sputtering is about two orders of magnitude higher than that of MBE. Since the atomic weight of W is large, the kinetic energy becomes large, and it seems that it penetrates Fe without epitaxial growth. In order to reduce the dead layer and epitaxially grow W on Fe, it seems necessary to make a film with MBE. As another method, the type of gas specified for sputtering seems to be important. Ar gas was used for this film formation, but a method of adjusting the kinetic energy of W by using Kr or Xe gas with different atomic weights is also conceivable.

When W or Ir was inserted at the FeB/Fe/MgO interface, both PMA and VCMA effect were larger than those without W and Ir.[92] In the case of Ir doping, it has been shown that PMA and VCMA are larger when Ir is diffused in Fe than those occurred at the Fe/Ir interface.[126] Theoretically, the effects of W-doping into Fe layer for PMA and VCMA have not been investigated, but as shown in the reference, polycrystalline FeW/MgO has a larger PMA than the polycrystalline Fe/MgO interface. However, since the PMA and VCMA of the

singlecrystalline Fe/MgO interface are originally large, no further increase can be expected with W doping. Therefore, in order to use W to achieve a larger PMA beyond Fe/MgO, it is better to create a perfect Fe/W/MgO interface or insert W into Fe where both effect of FeW and Fe/MgO can be expected.

4.4 Summary

In this study, W was inserted into the singlecrystalline Fe/MgO interface to investigate the magnetic properties. W was formed by sputtering, and the other layers were grown by EB. Structural analysis by STEM revealed that Fe and W were all mixed, and the designed structure could not be achieved. Since Fe and W are mixed, PMA, saturation magnetization, and VCMA effect are reduced. XMCD measurements also showed that ΔM_{orb} was also reduced. It was found that W doping to the singlecrystalline Fe/MgO interface does not increase PMA and VCMA unlike Ir doping. In order to obtain a large PMA or VCMA by inserting W, a complete layered structure of Fe/W/MgO and efforts to prevent mixing of Fe and W are required.

Chapter 5 Perpendicular magnetic anisotropy in (Tb, La)/CoFeB/MgO

In this section, PMA in CoFeB/MgO when Tb and La were used as buffer layer was studied. In particular, the PMA of the unannealed sample was mainly investigated.

5.1 Experiment

(1) Tb/CoFeB/MgO

Si/SiO_2 substrate//W(3 nm)/Tb(t_{Tb} nm)/$Co_{20}Fe_{60}B_{20}$(1 nm)/MgO(2 nm)/W(1 nm) was prepared. As deposited sample and annealed samples with T_a = 300, 500 ºC were prepared. t_{Tb} thickness and T_a dependence of magnetic properties were investigated.

(2) La/CoFeB/MgO

Si/SiO_2 substrate//W(3 nm)/La(t_{La} nm)/$Co_{20}Fe_{60}B_{20}$(1 nm)/MgO(2 nm)/W(1 nm) was prepared. All samples were as deposited. Magnetic properties were investigated for the samples with different t_{La}. Next, using same W buffers and cap, CoFeB thickness dependence in La(2 nm)/CoFeB(t_{CoFeB} nm)/MgO(2 nm), La(2 nm)/CoFeB(t_{CoFeB} nm)/La(2 nm), MgO(2 nm)/CoFeB(t_{CoFeB} nm)/MgO(2 nm) were investigated. XAS and XMCD measurements were performed on La(2 nm)/CoFeB(1 nm)/MgO(2 nm) samples. Measurements were performed in the NI and GI configurations, and the spin magnetic moment and the orbital magnetic moment were derived, respectively.

5.2 Result

(1) Tb/CoFeB/MgO

The samples with different t_{Tb} and T_a were measured by VSM. Figure 5.1 shows the M-H curves in as-deposited samples, K_{eff} and $\mu_0 M_s$.

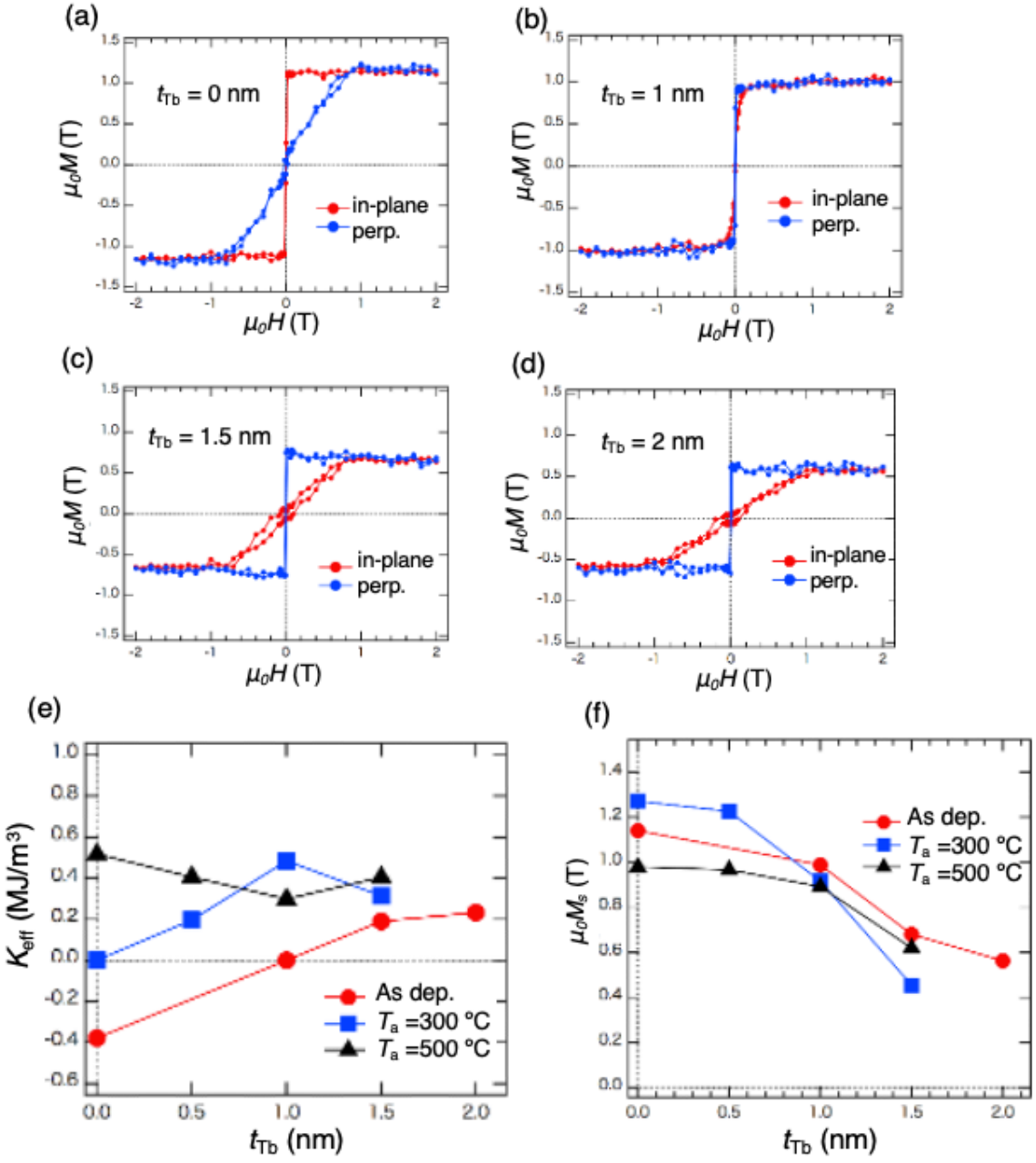

Figure 5.1 M-H curves for the as deposited stacks (a) without Tb, (b) with t_{Tb} = 1 nm, (c) with t_{Tb} = 1.5 nm, (d) with t_{Tb} = 2 nm. t_{Tb} and T_a dependence of (e) K_{eff} and (f) $\mu_0 M_s$.

As shown in Figure 5.1, the magnetic easy axis was an in-plane direction in the as deposited samples without Tb. On the other hand, PMA was observed in the as-deposited samples by inserting Tb. When annealed, PMA is obtained in the stack without Tb because W absorbs boron and CoFeB is polycrystalline in the (001) direction by solid state epitaxy. PMA was also obtained after annealing with Tb buffer layer, but annealing process did not enhance the PMA energy. It can be seen that M_s is reduced by inserting Tb. It is considered that this is because CoFeB and Tb are mixed, or because 4f orbitals of Tb is less than half and couples antiparallel to the 3d orbital of Fe. The mechanism of PMA in Tb/CoFeB/MgO without annealing is not clear. Possible factors are considered to be the absorption of boron without annealing, the effect of electronegativity, or the effect of the 4f orbital. Therefore, in order to remove the influence of the 4f orbital, an experiment using the La buffer is performed.

(2) La/CoFeB/MgO

Figure 5.2 shows the results of VSM for Si/SiO_2 substrate//W(3 nm)/La(t_{La} nm)/CoFeB(1 nm)/MgO(2 nm)/W(1 nm) without annealing. When the t_{La} exceeds 1.5 nm, PMA was obtained. Also, as with the Tb buffer result, it can be seen that M_s is decreasing. La, Tb and CoFeB are considered to be easier to mix than W. K_{eff} of 0.2 MJ/m^3 was achieved in the as deposited samples by using La buffer.

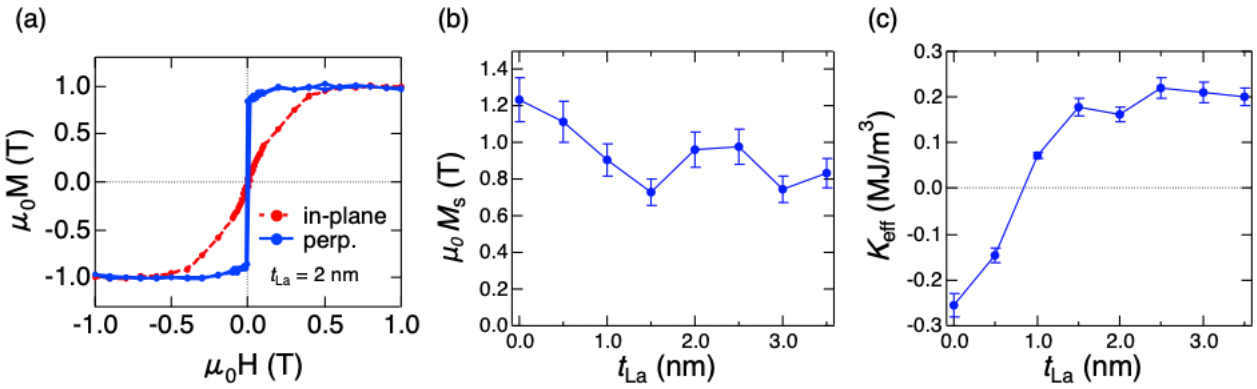

Figure 5.2 (a) M-H curve for the stack with t_{La} = 2 nm. t_{La} dependence of (b) $\mu_0 M_s$ and (c) K_{eff}.

Next, the investigation of the interface magnetic anisotropy in La(2 nm)/CoFeB(t_{CoFeB} nm)/MgO(2 nm), La(2 nm)/CoFeB(t_{CoFeB} nm)/La(2 nm), MgO(2 nm)/CoFeB(t_{CoFeB} nm)/MgO(2 nm) clarify which layer contribute to PMA. Figure 5.3 shows t_{CoFeB} dependence of K_{eff} ・ t_{CoFeB} and $\mu_0 M_s$ ・ t_{CoFeB}.

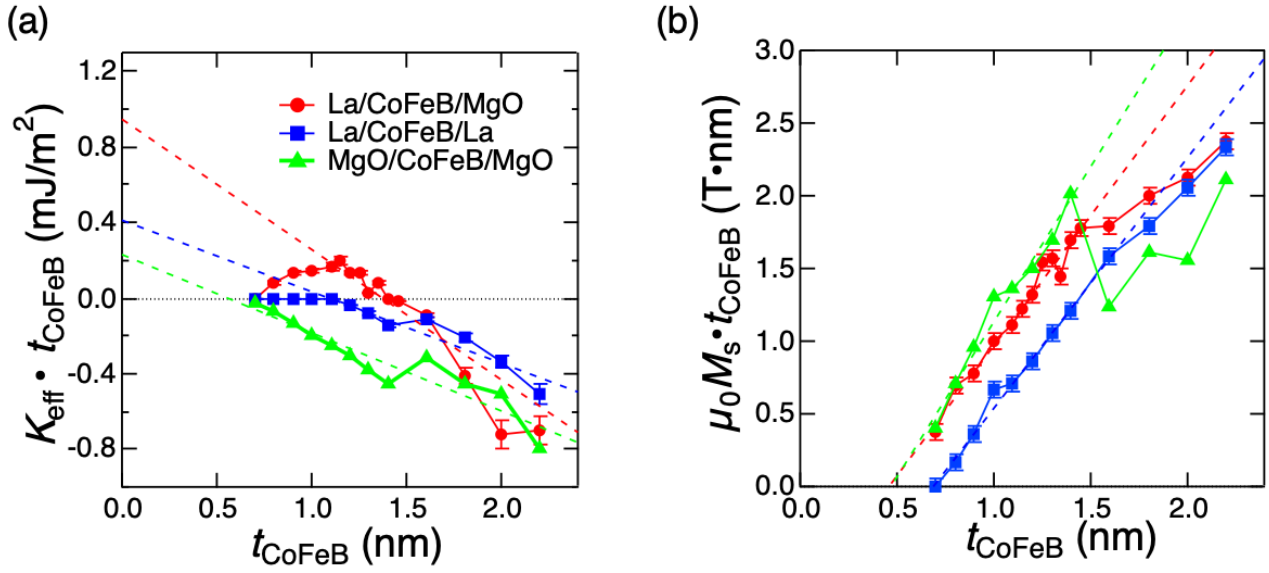

Figure 5.3 t_{CoFeB} dependence of (a) $K_{eff} \cdot t_{CoFeB}$ and (b) $\mu_0 M_s \cdot t_{CoFeB}$.

Table 5.1 t_{dead} and K_i in La/CoFeB/MgO, La/CoFeB/La, MgO/CoFeB/MgO

	t_{dead} (nm)	K_i (mJ/m^2)
La(2 nm)/CoFeB(t_{CoFeB} nm)/MgO(2 nm)	0.45	0.64
La(2 nm)/CoFeB(t_{CoFeB} nm)/La(2 nm)	0.69	0.15
MgO(2 nm)/CoFeB(t_{CoFeB} nm)/MgO(2 nm)	0.47	0.01

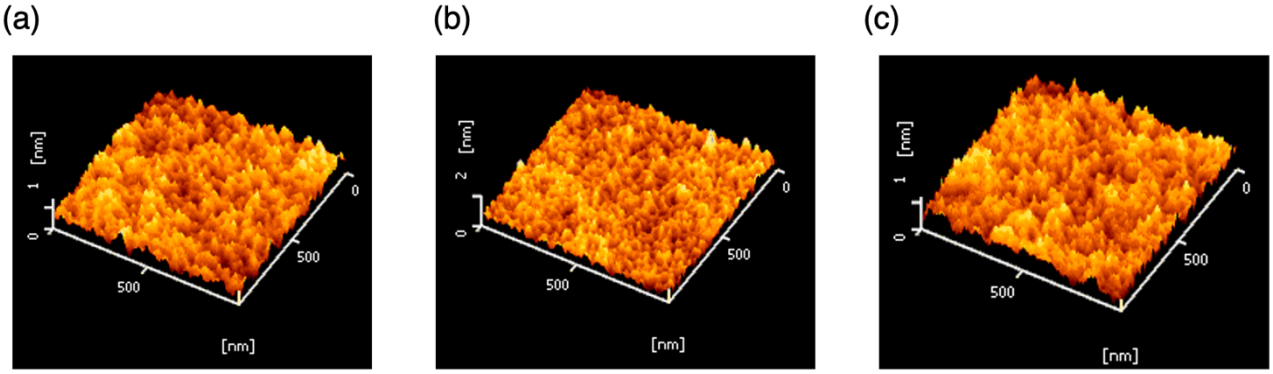

Figure 5.4 Surface morphology by AFM. (a) La(2 nm)/CoFeB(1 nm)/MgO(2 nm), *Ra* = 0.08nm, *P-V* = 0.66nm, (b) La(2 nm)/CoFeB(1 nm)/La(2 nm), *Ra* = 0.09nm, *P-V* = 0.78nm, (c) MgO(2 nm)/CoFeB(1 nm)/MgO(2 nm), *Ra* = 0.05nm, *P-V* = 0.52nm.

The t_{dead} and K_i were derived from Figure 5.3 and summarized in Table 5.1. Importantly, the K_i of La/CoFeB/MgO is clearly larger than that of La/CoFeB/La. This means that the contribution of the La/CoFeB interface for PMA is small. Figure 5.4 shows the surface morphology by AFM. All structures have low roughness, which means that the shape magnetic anisotropy which contributes to the negative magnetic anisotropy is not eliminated due to the severe roughness. Hence, it is not the disappearance of the shape magnetic anisotropy that makes it PMA.

XMCD measurements were performed to investigate more detailed interface conditions.

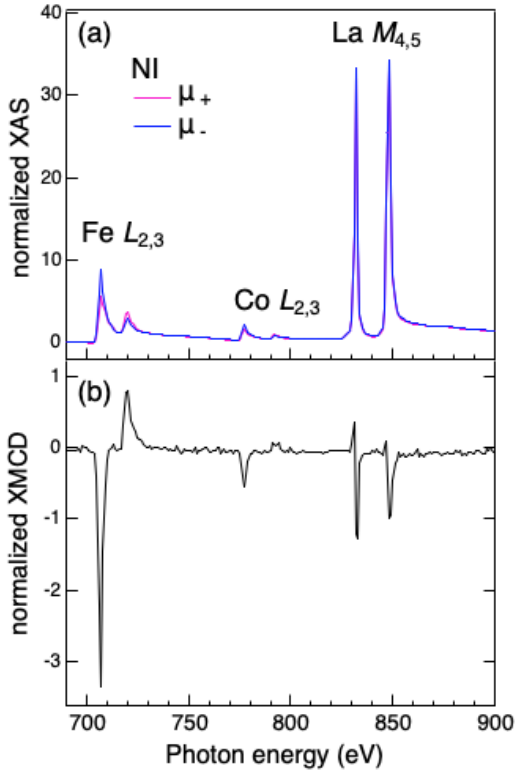

Figure 5.5 (a) XAS and (b) XMCD spectra for Fe $L_{2,3}$, Co $L_{2,3}$ and La $M_{4,5}$ edges in La(2 nm)/CoFeB(1 nm)/MgO(2 nm) taken at NI configuration.

Figure 5.5 shows the results of XAS and XMCD measurements taken in the NI configuration. Fe $L_{2,3}$, Co $L_{2,3}$, and La $M_{4,5}$ edges in La(2 nm)/CoFeB(1 nm)/MgO(2 nm) were observed. Since the ratio of peak intensities of Fe and Co is about 3: 1, it can be confirmed that it is as designed structure. The reason of large peak intensity of La is considered to be the transition from 3d to 4f. XMCD is observed in Fe and Co, which means both Fe and Co are magnetized. XMCD is also observed in La, but this is considered to be noise because the original signal is large. Fe $L_{2,3}$ edges were evaluated in the NI and GI configurations, and ΔM_{orb} was derived.

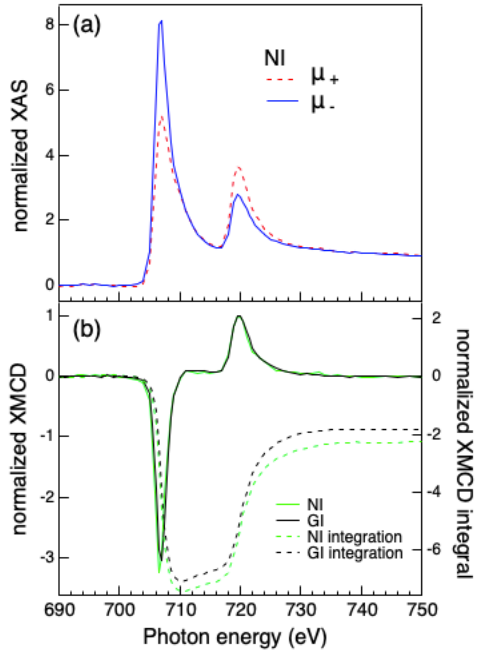

Figure 5.6 XAS and XMCD spectra for Fe $L_{2,3}$ edges taken at NI and GI configuration.

Figure 5.6 (b) shows XMCD at the Fe $L_{2,3}$ edges in the NI and GI directions. As can be seen at the residuals of the integration, there is a difference between the NI direction and the GI direction. This indicates that there is anisotropy of M_{orb}. M_{spin} and M_{orb} in the NI and GI directions were derived using the XMCD sum rule. The values are summarized in Table 5.2.

Table 5.2 M_{spin} and M_{orb} of Fe in La(2 nm)/CoFeB(1 nm)/MgO(2 nm).

	NI	GI
M_{spin} (μ_B)	1.19	1.15
M_{orb} (μ_B)	0.11	0.09

The anisotropy of the orbital magnetic moments in the NI and GI configurations is ΔM_{orb} = 0.02 (μ_B). In Bruno relation, this value is reasonable with the interface magnetic anisotropy.

5.3 Discussion

PMA in as deposited CoFeB/MgO is discussed. CoFeB is crystallized by annealing, but it is considered that the Fe-O bond contributes to PMA even in amorphous CoFeB/MgO. Since buffer layers with low electronegativity such as Tb and La are considered to easily absorb boron, it is presumed that the amount of boron in CoFeB was adjusted without annealing. Another

suggestion is that the local electric field due to the difference in electronegativity may change the occupancy of the d orbital of CoFeB. The electric field decays quickly in metal, but the thickness of CoFeB is 1 nm, and it is calculated that the electric field reaches several atomic layers.[127] From this experiment, it is unlikely that the 4f orbitals of Tb and the 5d orbitals of La may contribute to PMA. In any case, it is considered that it is the bonding of Fe-O that actually contributes to PMA. In Bruno relation,[67] the magnetic anisotropy of the interface between bcc Fe and MgO is calculated from this ΔM_{orb} and is derived to be 0.245 mJ/m^2. This value is underestimated because the M_{orb} in the GI configuration is not completely in-plane. However, since it matches well with the value derived from the VSM measurement, it is certain that it is the anisotropy discussed in Bruno's relation.

5.4 Summary

In this study, the magnetic anisotropy of CoFeB/MgO without annealing was investigated using Tb and La as buffer layers. K_{eff} of 0.2 MJ/m^3 was obtained in as deposited sample. Since K_i of La/CoFeB/MgO is larger than La/CoFeB/La, it was clarified that this PMA occurs at the CoFeB/MgO interface and the contribution of the La/CoFeB interface for PMA is small. In La/CoFeB/MgO, ΔM_{orb} was 0.02 μ_B, which was a reasonable value compared with K_i in Bruno's relation. From these facts, it was concluded that the La buffer plays an indirect role in adjusting the CoFeB/MgO interface.

Chapter 6 Summary

This study is the new material developments for perpendicular MTJs. In particular, the magnetic anisotropy at the ferromagnetic layer/oxide interface was investigated.

Large PMA and VCMA effects can be obtained at singlecrystalline Fe/MgO interfaces grown by EB or MBE. On the other hand, the sputter-deposition is necessary from the viewpoint of the practical use. In this study, polycrystalline and singlecrystalline Fe/MgO were prepared by rf-sputtering, aiming to investigate and obtain PMA. Polycrystalline Fe/MgO was deposited on Si/SiO_2 substrate/amorphous W buffer. The oxidation state at Fe/MgO interfaces, which is important for interface PMA, was tuned by the Tb capping layer. As the result, effective PMA was achieved at polycrystalline Fe/MgO interface. Singlecrystalline Fe/MgO was prepared on MgO substrate and Cr buffer. In the stacks without annealing, the mixing of Cr and Fe and the oxidation of Fe layer were confirmed. After the annealing, Fe-oxide was reduced by Cr, and rock-salt type CrO segregated between Fe/MgO interface. The valence of CrO was deduced to be 2+ or less. These results were revealed by the structural analyses with STEM and XAS measurements. Large interface PMA energies of 1.55 mJ/m^2 was achieved at Fe/CrO interface, which means that the diffusion process provides the well-controlled interface. Moreover, the segregation to the interface stabilizes rock-salt type CrO, although it is known as an unstable compound.

Theoretical studies predicted large interface PMA by the insertion of distorted W to the Fe/MgO interfaces. In this study, the effects of W insertion to the EB-grown Fe/MgO were investigated. Structural analyses revealed the mixing of Fe and W, meaning that the structure is different with that in the theory. FeW/MgO interface showed PMA, but its value was smaller than that of pure Fe/MgO interfaces. Therefore, W doping to Fe layer is an effective way for polycrystalline FeB/MgO where PMA energy is small, but it seems to be necessary to fabricate Fe/W layered structure to obtain larger PMA than Fe/MgO interface as predicted in the theory.

Various buffer layers have been studied for CoFeB/MgO, and PMA is observed even in as-deposited samples depending on buffer layers. In this study, PMA was confirmed in as-deposited (Tb, La)/CoFeB/MgO. In order to elucidate which interface contribute to PMA, La/CoFeB/La, La/CoFeB/MgO and MgO/CoFeB/MgO were evaluated. Among them, interface PMA in La/CoFeB/MgO was the largest, suggesting that PMA occurs at CoFeB/MgO interface and La adjust the interface states by absorbing boron and oxygen even without post-annealing. These are considered to be due to the electronegativity of the buffer layer.

In these efforts, interface PMA was demonstrated in the practical deposition method and novel ferromagnetic/oxide interfaces, and the effects of some heavy metals to the interface were investigated. These results provide meaningful knowledge for the development of perpendicular MTJs.

Reference

[1] 宮崎照宣, 土浦宏紀 “スピントロニクスの基礎”, 森北出版株式会社, 第 1 版第 1 刷 2013 年

[2] G. Binasch, P. Grünberg, F. Saurenbach and W. Zinn, Phys. Rev. B **39**, 4828 (1989).

[3] M. N. Baibich, J. M. Broto, A. Fert, F. Nguyen Van Dau, F. Petroff, P. Etienne, G. Creuzet, A. Friederich, and J. Chazelas, Phys. Rev. Lett. **61**, 2472 (1988).

[4] M. Julliere, Phys. Lett. A **54**, 225 (1975).

[5] J. S. Moodera, L. R. Kider, T. M. Wong, R. Meservey, Phys. Rev. Lett. **74**, 3273 (1995).

[6] T. Miyazaki and N. Tezuka, J. Magn. Magn. Mater. **139**, L231 (1995).

[7] S. Bhatti, R. Sbiaa, A. Hirohata, H. Ohno, S. Fukami and S.N. Piramanayagam, Materials Today **20**, 530 (2017).

[8] H. Cai, W. Kang, Y. Wang, L. A. D. B. Naviner, J. Yang and W. Zhao, Appl. Sci. **7**, 929 (2017).

[9] J. A. Katine, F. J. Albert, R. A. Buhrman, E. B. Myers and D. C. Ralph, Phys. Rev. Lett. **84** 3149 (2000).

[10] S. Z. Peng, Y. Zhang, M. X. Wang, Y. G. Zhang, W. S. Zhao, “Magnetic Tunnel Junctions for Spintronics: Principles and Applications” Wiley Encyclopedia of Electrical and Electronics Engineering, 1-16, (2014).

[11] J. Z. Sun, Phys. Rev. B **62**, 570 (2000).

[12] M. I. Dyakonov and V. I. Perel, Physics Letters A, **35(6)**, 459 (1971).

[13] T. Maruyama, Y. Shiota, T. Nozaki, K. Ohta, N. Toda, M. Mizuguchi, A. A. Tulapurkar, T. Shinjo, M. Shiraishi, S. Mizukami, Y. Ando and Y. Suzuki, Nat. Nanotechnol. **4**, 158 (2009).

[14] M. Sharma, S.X. Wang, and J.H. Nickel, J. Appl. Phys. **85**, 7803 (1999).

[15] H. Kyung, H.S. Ahn, C.S. Yoon, C.K. Kim, O. Song, T. Miyazaki, Y. Ando, and H. Kubota, J. Appl. Phys. **89**, 2752 (2001).

[16] P. Rottlaẗnder, M. Hehn, O. Lenoble, and A. Schuhl, Appl. Phys. Lett. **78**, 3274 (2001).

[17] C.L. Platt, B. Dieny, and A.E. Berkowitz, Appl. Phys. Lett. **69**, 2291 (1996).

[18] B.G. Park and T.D. Lee, Appl. Phys. Lett. **81**, 2214 (2002).

[19] B.G. Park, T.D. Lee, T.H. Lee, C.G. Kim, and C.O. Kim, J. Appl. Phys. **93**, 6423 (2003).

[20] S. Mitani, T. Moriyama, and K. Takanashi, J. Appl. Phys. **91**, 7200 (2002).

[21] Z.H. Xiong, D. Wu, Z.V. Vardeny, and J. Shi, Nature **427**, 821 (2004).

[22] T.S. Santos, J.S. Lee, P. Migdal, I.C. Lekshmi, B. Satpati, and J.S. Moodera, Phys. Rev. Lett. **98**, 016601 (2007).

[23] G. Szulczewski, H. Tokuc, K. Oguz, and J.M.D. Coey, Appl. Phys. Lett. **95**, 202506 (2009).

[24] C.L. Platt, B. Dieny, and A.E. Berkowitz, J. Appl. Phys. **81**, 5523 (1997).

[25] X.W. Li, A. Gupta, G. Xiao, W. Qian, and V.P. Dravid, Appl. Phys. Lett. **73**, 3282 (1998).

[26] M. Bowen, V. Cros, F. Petroff, A. Fert, C. Martínez Boubeta, J.L. Costa-Kraẗmer, J. V. Anguita, A. Cebollada, F. Briones, J.M. De Teresa, L. Morellón, M.R. Ibarra, F. Güell, F. Peiró, and A. Cornet, Appl. Phys. Lett. **79**, 1655 (2001).

[27] E. Popova, J. Faure-Vincent, C. Tiusan, C. Bellouard, H. Fischer, M. Hehn, F. Montaigne, M. Alnot, S. Andrieu, A. Schuhl, E. Snoeck, and V. Da Costa, Appl. Phys. Lett. **81**, 1035 (2002).

[28] S. Mitani, T. Moriyama, and K. Takanashi, J. Appl. Phys. **93**, 8041 (2003).

[29] J. Faure-Vincent, C. Tiusan, E. Jouguelet, F. Canet, M. Sajieddine, C. Bellouard, E. Popova, M. Hehn, F. Montaigne, and A. Schuhl, Appl. Phys. Lett. **82**, 4507 (2003).

[30] S.S.P. Parkin, C. Kaiser, A. Panchula, P.M. Rice, B. Hughes, M. Samant, and S.H. Yang, Nat. Mater. **3**, 862 (2004).

[31] S. Yuasa, T. Nagahama, A. Fukushima, Y. Suzuki, and K. Ando, Nat. Mater. **3**, 868 (2004).

[32] W. H. Butler, X, -G. Zhang and T. C. Schulthess, Phys. Rev. B **63**, 054416 (2001).

[33] A.T.A. Wee, K. Sin, and S.X. Wang, Appl. Phys. Lett. **74**, 2528 (1999).

[34] K. Matsuda, A. Kamijo, T. Mitsuzuka, and H. Tsuge, J. Appl. Phys. **85**, 5261 (1999).

[35] D. Wang, M. Tondra, C. Nordman, and J.M. Daughton, IEEE Trans. Magn. **35**, 2886 (1999).

[36] H. Kikuchi, M. Sato, and K. Kobayashi, J. Appl. Phys. **87**, 6055 (2000).

[37] D.D. Djayaprawira, K. Tsunekawa, M. Nagai, H. Maehara, S. Yamagata, N. Watanabe, S. Yuasa, Y. Suzuki, and K. Ando, Appl. Phys. Lett. **86**, 092502 (2005).

[38] Y. Lu, X. Li, G. Gong, G. Xiao, A. Gupta, P. Lecoeur, and J. Sun, Phys. Rev. B **54**, R8357 (1996).

[39] M. Bowen, M. Bibes, A. Barthélémy, J.P. Contour, A. Anane, Y. Lemaître, and A. Fert, Appl. Phys. Lett. **82**, 233 (2003).

[40] H.X. Liu, T. Kawami, K. Moges, T. Uemura, M. Yamamoto, F. Shi, and P.M. Voyles, J. Phys. D. Appl. Phys. **48**, 164001 (2015).

[41] N. Nishimura, T. Hirai, A. Koganei, T. Ikeda, K. Okano, Y. Sekiguchi, and Y. Osada, J. Appl. Phys. **91**, 5246 (2002).

[42] S. Yakata, H. Kubota, Y. Suzuki, K. Yakushiji, A. Fukushima, S. Yuasa and K. Ando, J. Appl. Phys. **105**, 07D131 (2009).

[43] S. Ikeda, K. Miura, H. Yamamoto, K. Mizunuma, H. D. Gan, M. Endo, S. Kanai, J. Hayakawa, F. Matsukura and H. Ohno, Nat. Mater. **9**, 721 (2010).

[44] J.M. De Teresa, A. Barthélémy, A. Fert, J.P. Contour, F. Montaigne, and P. Seneor, Science (80-.). **286**, 507 (1999).

[45] J.Z. Sun, P.L. Trouilloud, M.J. Gajek, J. Nowak, R.P. Robertazzi, G. Hu, D.W. Abraham, M.C. Gaidis, S.L. Brown, E.J. O'Sullivan, W.J. Gallagher, and D.C. Worledge, J. Appl. Phys. **111**, 07C711 (2012).

[46] K. Yakushiji, K. Noma, T. Saruya, H. Kubota, A. Fukushima, T. Nagahama, S. Yuasa, and K. Ando, Appl. Phys. Express **3**, 053003 (2010).

[47] Q.L. Ma, T. Kubota, S. Mizukami, X.M. Zhang, M. Oogane, H. Naganuma, Y. Ando, and T. Miyazaki, IEEE Trans. Magn. **48**, 2808 (2012).

[48] G. Kim, Y. Sakuraba, M. Oogane, Y. Ando, and T. Miyazaki, Appl. Phys. Lett. **92**, 172502

(2008).
[49] M. Yoshikawa, E. Kitagawa, T. Nagase, T. Daibou, M. Nagamine, K. Nishiyama, T. Kishi, and H. Yoda, IEEE Trans. Magn. **44**, 2573 (2008).
[50] D.L. Zhang, K.B. Schliep, R.J. Wu, P. Quarterman, D. Reifsnyder Hickey, Y. Lv, X. Chao, H. Li, J.Y. Chen, Z. Zhao, M. Jamali, K.A. Mkhoyan, and J.P. Wang, Appl. Phys. Lett. **112**, 152401 (2018).
[51] T. Kubota, S. Mizukami, D. Watanabe, F. Wu, X. Zhang, H. Naganuma, M. Oogane, Y. Ando, and T. Miyazaki, J. Appl. Phys. **110**, 013915 (2011).
[52] T. Kubota, S. Mizukami, Q.L. Ma, H. Naganuma, M. Oogane, Y. Ando, and T. Miyazaki, J. Appl. Phys. **115**, 17C704 (2014).
[53] H. Kinjo, K. Machida, K. Matsui, K.I. Aoshima, D. Kato, K. Kuga, H. Kikuchi, and N. Shimidzu, J. Appl. Phys. **115**, 203903 (2014).
[54] A. Sugihara, K. Suzuki, T. Miyazaki, and S. Mizukami, Jpn. J. Appl. Phys. **54**, 078002 (2015).
[55] K. Borisov, D. Betto, Y.C. Lau, C. Fowley, A. Titova, N. Thiyagarajah, G. Atcheson, J. Lindner, A.M. Deac, J.M.D. Coey, P. Stamenov, and K. Rode, Appl. Phys. Lett. **108**, 192407 (2016).
[56] K.Z. Suzuki, R. Ranjbar, J. Okabayashi, Y. Miura, A. Sugihara, H. Tsuchiura, and S. Mizukami, Sci. Rep. **6**, 30249 (2016).
[57] H. Lee, H. Sukegawa, J. Liu, Z. Wen, S. Mitani, and K. Hono, IEEE Trans. Magn. **52**, 4400204 (2016).
[58] K. Mizunuma, S. Ikeda, H. Yamamoto, H.D. Gan, K. Miura, H. Hasegawa, J. Hayakawa, K. Ito, F. Matsukura, and H. Ohno, Jpn. J. Appl. Phys. **49**, 04DM04 (2010).
[59] I. Lytvynenko, C. Deranlot, S. Andrieu, and T. Hauet, J. Appl. Phys. 117, 053906 (2015).
[60] J.W. Koo, H. Sukegawa, S. Kasai, Z.C. Wen, and S. Mitani, J. Phys. D. Appl. Phys. **47**, 322001 (2014).
[61] B.S. Tao, D.L. Li, Z.H. Yuan, H.F. Liu, S.S. Ali, J.F. Feng, H.X. Wei, X.F. Han, Y. Liu, Y.G. Zhao, Q. Zhang, Z.B. Guo, and X.X. Zhang, Appl. Phys. Lett. **105**, 102407 (2014).
[62] Y.P. Wang, S. Ter Lim, G.C. Han, and K.L. Teo, J. Appl. Phys. **118**, 233906 (2015).
[63] Q. Xiang, H. Sukegawa, M. Belmoubarik, M. Al-Mahdawi, T. Scheike, S. Kasai, Y. Miura, and S. Mitani, Adv. Sci. **6**, 1901438 (2019).
[64] Z. Wen, H. Sukegawa, T. Furubayashi, J. Koo, K. Inomata, S. Mitani, J.P. Hadorn, T. Ohkubo and K. Hono, Adv. Mater. **26**, 6483 (2014).
[65] 太田恵造 "磁気工学の基礎 II -磁気の応用",共立出版株式会社 2009 年 9 月 15 日初版 19 刷
[66] Y. Miura, S. Ozaki, Y. Kuwahara, M. Tsujikawa, K. Abe and M. Shirai, J. Phys.: Condens. Matter **25**, 106005 (2013).
[67] P. Bruno, Phys. Rev. B **39**, 865 (1989).
[68] J. Stöhr, J. Magn. Magn. Mater. **200**, 470 (1999).

[69] G.H.O. Daalderop, P.J. Kelly, M.F.H. Schuurmans, Phys.Rev. B **50**. 9989 (1994).
[70] B. Újfalussy, L. Szunyogh, P. Bruno, P. Weinberger, Phys. Rev. Lett. **77** 1805 (1996).
[71] K. Nakajima, R. Shimabukuro, Y. Fujiwara, T. Akiyama, T, Ito, A. J. Freeman, Phys. Rev. Lett. **102**, 187201 (2009).
[72] Y. Miura, M. Tsujikawa, M. Shirai, J. Appl. Phys. **113**, 233908 (2013).
[73] H. X. Yang, M. Chshiev, B. Dieny, J. H. Lee, A. Manchon and K. H. Shin, Phys. Rev. B **84**, 054401 (2011).
[74] J. W. Koo, S. Mitani, T. Sasaki, H. Sukegawa, Z. C. Wen, T. Ohkubo, T. Niizeki, K. Inomata and K. Hono, Appl. Phys. Lett. **103**, 192401 (2013).
[75] H. Sukegawa, H. Xiu, T. Ohkubo, T. Furubayashi, T. Niizeki, W. Wang, S. Kasai, S. Mitani, K. Inomata, K. Hono Appl. Phys. Lett. **96**, 212505 (2010).
[76] Q. Xiang, R. Mandal, H. Sukegawa, Y. K. Takahashi and Seiji Mitani, Appl. Phys. Express **11**, 063008 (2018).
[77] K. Masuda and Y. Miura, Phys. Rev. B 98, 224421 (2018).
[78] J. Okabayashi, J. W. Koo, H. Sukegawa, S. Mitani, Y. Takagi, and T. Yokoyama, Appl. Phys. Lett. 105, 122408 (2014).
[79] J. Okabayashi, Y. Iida, Q. Xiang, H. Sukegawa and S. Mitani, Appl. Phys. Lett. **115**, 252402 (2019).
[80] D. E. Nikonov and I. A. Young, J. Mater. Res. **29**, 2109 (2014).
[81] Y. Shiota, T. Nozaki, F. Bonell, S. Murakami, T. Shinjo and Y. Suzuki, Nat. Mater. **11**, 39 (2011).
[82] Y. Shiota, F. Bonell, S. Miwa, N. Mizuochi, T. Shinjo and Y. Suzuki, Appl. Phys. Lett. **103**, 082410 (2013).
[83] W. Skowroński, T. Nozaki, D. D. Lam, Y. Shiota, K. Yakushiji, H. Kubota, A. Fukushima, S. Yuasa and Y. Suzuki, Phys. Rev. B **91**, 184410 (2015).
[84] W. Skowroński, T. Nozaki, Y. Shiota, S. Tamaru, K. Yakushiji, H. Kubota, A. Fukushima, S. Yuasa and Y. Suzuki, Appl. Phys. Express **8**, 053003 (2015).
[85] T. Nozaki, A. Kozioł-Rachwał, W. Skowroński, V. Zayets, Y. Shiota, S. Tamaru, H. Kubota, A. Fukushima, S. Yuasa and Y. Suzuki, Phys. Rev. Appl. **5**, 044006 (2016).
[86] A. Kozioł-Rachwał, T. Nozaki, K. Freindl, J. Korecki, S. Yuasa and Y. Suzuki, Sci. Rep. **7**, 5993 (2017).
[87] A. Rajanikanth, T. Hauet, F. Montaigne, S. Mangin, and S. Andrieu, Appl. Phys. Lett. **103**, 062402 (2013)
[88] U. Bauer, L. Yao, A. J. Tan, P. Agrawal, S. Emori, H. L. Tuller, S. Dijken and G. S. D. Beach Nat. Mater. **14**, 174–81 (2015).
[89] T. Scheike, Q. Xiang, Z. Wen, H. Sukegawa, T. Ohkubo, K. Hono, S. Mitani, arXiv preprint arXiv:2011.08739
[90] R. Suzuki, Y. Tadano, M. Tanaka, S. Ohya, AIP Adv. **10**, 085115 (2020).
[91] A. Sugihara, A. Spiesser, T. Nozaki, H. Kubota, H. Imamura, A. Fukushima, K. Yakushiji,

S. Yuasa, Jpn. J. Appl. Phys. **59**, 010901 (2020)

[92] T. Nozaki, T. Yamamoto, S. Tamaru, H. Kubota, A. Fukushima, Y. Suzuki and S. Yuasa, APL Mater. **6**, 026101 (2018).

[93] Y. Matsumoto, S. Okamoto, N. Kikuchi, O. Kitakami, Y. Miura, M. Suzuki, M. Mizumaki and N. Kawamura, IEEE Trans. Magn. **51**, 2100704 (2015).

[94] Y. Matsumoto, Y. Miura, S. Okamoto, N. Kikuchi and O. Kitakami, Appl. Phys. Express **10**, 063005 (2017).

[95] Y. W. Oh, K. D. Lee, J. R. Jeong and B. G. Park, J. Appl. Phys. **115**, 17C724 (2014).

[96] P. J. Chen, Y. L. Iunin, S. F. Cheng and R. D. Shull IEEE Trans. Magn. **52**, 4400504 (2016).

[97] M. Yamanouchi, R. Koizumi, S. Ikeda, H. Sato, K. Mizunuma, K. Miura, H. D. Gan, F. Matsukura and H. Ohno, J. Appl. Phys. **109**, 07C712 (2011).

[98] W. X. Wang, Y. Yang, H. Naganuma, Y. Ando, R. C. Yu and X. F. Han Appl. Phys. Lett. **99**, 012502 (2011).

[99] C. T. Chen, Y. U. Idzerda, H. -J. Lin, N. V. Smith, G. Meigs, E. Chaban, G. H. Ho, E. Pellegrin and F. Sette, Phys. Rev. Lett. **75**, 152 (1995).

[100] Q. Xiang, Z. Wen, H. Sukegawa, S. Kasai, T. Seki, T. Kubota, K. Takanashi and Seiji Mitani, J. Phys. D: Appl. Phys. **50** 40LT04 (2017).

[101] J. Liu, T. Ohkubo, S. Mitani, K. Hono and M. Hayashi, Appl. Phys. Lett. **107**, 232408 (2015).

[102] K. Hirota, T. H. Okabe, F. Saito, Y. Waseda and K. T. Jacob, J. Alloys Compd. **282**, 101 (1999).

[103] H. Wende, Z. Li, A. Scherz, G. Ceballos, K. Baberschke, A. Ankudinov, J. J. Rehr, F. Wilhelm, A. Rogalev, D. L. Schlagel, and T. A. Lograsso, J. Appl. Phys. **91**, 7361 (2002).

[104] G. Xiao and C. L. Chien, Phys. Rev. B **35**, 8763 (1987).

[105] S. Seong, E. Lee, H. W. Kim, B. I. Min, S. Lee, J. Dho, Y. Kim, J. Y. Kim, J. S. Kang, J. Magn. Magn. Mater. **452**, 447 (2018).

[106] M. Asa, G. Vinai, J. L. Hart, C. Autieri, C. Rinaldi, P. Torelli, G. Panaccione, M. L. Taheri, S. Picozzi, M. Cantoni, Phys. Rev. Mater. **2**, 033401 (2018).

[107] M. C. Biesinger, C. Brown, J. R. Mycroft, R. D. Davidson, N. S. Mclntyre, Surf. interface Anal. 36, 1550 (2004).

[108] C. Xu, M. Hassel, H. Kuhlenbeck, H. J. Freund, Surf. Sci. **258**, 23 (1991).

[109] D. Alontseva, E. Ghassemieh, A. Russakova, A. Krassavin, N. Prokhorenkova, Acta Phys. Pol. A **134**, 374 (2018).

[110] J. Liu, T. Yang, A. Xu, R. L. Martin, Y. Yang, H. Jiao, Y. Li, X. D. Wen, J. Alloys Compd. **808**, 151707 (2019).

[111] K. Toyoki, Y. Shiratsuchi, T. Nakamura, C. Mitsumata, S. Harimoto, Y. Takechi, T. Nishimura, H. Nomura, R. Nakatani, Appl. Phys. Express **7**, 114201 (2014).

[112] A. Brambilla, G. Berti, A. Calloni, A. Picone, M. Riva, G. Bussetti, S. Nappini, E.

Magnano, M. Finazzi, L. Duò, F. Ciccacci, J. Appl. Phys. **114**, 123905 (2013).
[113] M. Yoshitake, Y.-R. Aparna, K. Yoshihara, J. Vac. Sci. Technol. A Vacuum, Surfaces, Film. **19**, 1432 (2001).
[114] M. Yoshitake, Jpn. J. Appl. Phys. **51**, 085601 (2012).
[115] https://surfseg.nims.go.jp/
[116] O. Nast, T. Puzzer, L. M. Koschier, A. B. Sproul, S. R. Wenham, Appl. Phys. Lett. **73**, 3214 (1998).
[117] M. Scholz, M. Gjukic, M. Stutzmann, Appl. Phys. Lett. **94**, 012108 (2009).
[118] K. Toko, M. Kurosawa, N. Saitoh, N. Yoshizawa, N. Usami, M. Miyao, T. Suemasu, Appl. Phys. Lett. **101**, 072106 (2012).
[119] K. Toko and T. Suemasu, J. Phys. D: Appl. Phys. **53**, 373002 (2020).
[120] K. Nakamura, T. Akiyama, T. Ito, M. Weinert and A. J. Freeman, Phys. Rev. B **81**, 220409(R) (2010).
[121] M. Akimitsu, T. Mizoguchi, J. Akimitsu, S. Kimura, J. Phys. Chem. Solids **44**, 497 (1983).
[122] F. F. Ferreira, M. H. Tabacniks, M. C. A. Fantini, I. C. Faria, A. Gorenstein, Solid State Ionics **86–88**, 971 (1996).
[123] O. Banakh, P. E. Schmid, R. Sanjinés, F. Lévy, Surf. Coatings Technol. **151–152**, 272 (2002).
[124] M. Saeki, M. Nakahira, Mater. Res. Bull. **6**, 603 (1971).
[125] M. Wang, W. Cai, K. Cao, J. Zhou, J. Wrona, S. Peng, H. Yang, J. Wei, W. Kang, Y. Zhang, J. Langer, B. Ocker, A. Fert, and W. Zhao, Nat. Commun. **9**, 671 (2018).
[126] T. Nozaki, A. Kozioł-Rachwał, M. Tsujikawa, Y. Shiota, X. Xu, T. Ohkubo, T. Tsukahara, S. Miwa, M. Suzuki, S. Tamaru, H. Kubota, A. Fukushima, K. Hono, M. Shirai, Y. Suzuki and Shinji Yuasa, NPG Asia Materials **9**, e451 (2017).
[127] S. Miwa, M. Suzuki, M. Tsujikawa, K. Matsuda, T. Nozaki, K. Tanaka, T. Tsukahara, K. Nawaoka, M. Goto, Y. Kotani, T. Ohkubo, F. Bonell, E. Tamura, K. Hono, T. Nakamura, M. Shirai, S. Yuasa and Y. Suzuki, Nat. Commun. **8**, 15848 (2017).

Acknowledgement

Firstly, I would like to express my sincere gratitude supervisor Prof. S. Mitani for teaching me in the 2 years master's and 3 years doctoral program. Through research activity with him, I learned everything from how to start a research to writing a paper. Thanks to his careful guidance, I was able to complete this doctoral program.

I would like to thank the committee members, Prof. H. Yanagihara, Prof. T. Suemasu, Prof. K. Uchida for the examination of my Ph.D studies. Thanks to their insightful comments, I was able to improve my Ph.D thesis.

I would like to thank Dr. H. Sukegawa, Dr. Z. Wen for teaching me the experimental knowledge. I learned a lot of knowledges about spintronics from them that I could not have known from just reading papers. I would like to thank Dr. S. Hirayama, Dr T. Scheike, Dr. Q. Xiang. They always helped me in the activity at NIMS.

I would like to thank Prof. J. Okabayashi for the collaborative research. Thanks to his educational guidance, I have a better understanding of x-ray absorption spectroscopy measurements and can improve my research.

I would like to thank director of Research Center for Magnetic and Spintronic Materials, Prof. K. Hono for providing me the great research circumstance. And I also would like to thank Prof. K. Hono, Dr. T. Ohkubo, Mr. J. Uzuhashi, Dr. X. Xu for the structural analyses by TEM.

I would like to thank Dr. S. Kasai, Ms. H. Ikeda for teaching me about microfabrication and measurement of MTJs.

I would like to thank Ms. A. Tomaru for helping me with administrative procedures.

I would like to thank Prof. M. Hayashi, Dr. P. Sheng, Dr. S. Isogami, Dr. Y. Miura, Dr. K. Masuda, Dr. K. Nawa, Dr. Y. Sakuraba, Dr. T. Nakatani, Dr. W. Zhou, Mr. H. Shimazu, K. Goto, Z. Li, K. Tang, J. Song and the member of Research Center for Magnetic and Spintronic Materials.

I acknowledge National Institute for Materials Science for provision of a NIMS Junior Research Assistantship.

Finally, I would like to thank my parents for their support throughout my life.

Appendix

List of magnetic tunnel junction

TMR of MTJs was investigated from 1995 to 2019 using Google Scholar. Keywords are "tunnel magnetoresistance" and "tunneling magnetoresistance". Around 100 papers were checked per a year. Finally, I was able to collect 733 papers that experimentally evaluated TMR.

Measurement temperature: T_m

Perpendicular to plane: perp.

TMR_1995

References	**Structures**	**TMR (%)**	**T_m**	**in-plane or perp.**
T. Miyazaki and N. Tezuka, J. Magn. Magn. Mater. **151**, 403 (1995).	Fe/Al_2O_3/Fe	18	300K	in-plane
K. Matsuyama, H. Asada, H. Miyoshi, and K. Taniguchi, IEEE Trans. Magn. **31**, 3176 (1995).	NiFe/Al_2O_3/Co	0.2	300K	in-plane
J.S. Moodera, L.R. Kinder, T.M. Wong, and R. Meservey, Phys. Rev. Lett. **74**, 3273 (1995).	CoFe/Al_2O_3/Co	11.8	295K	in-plane
		24	4.2K	in-plane
T. Miyazaki and N. Tezuka, J. Magn. Magn. Mater. **139**, L231 (1995).	Fe/Al_2O_3/Fe	30	4.2K	in-plane
		18	300K	in-plane

TMR_1996

References	**Structures**	**TMR (%)**	**T_m**	**in-plane or perp.**
C.L. Platt, B. Dieny, and A.E. Berkowitz, Appl. Phys. Lett. **69**, 2291 (1996).	Fe/HfO_2/Co	31	30K	in-plane
J.S. Moodera, L.R. Kinder, J. Nowak, P. LeClair, and R. Meservey, Appl. Phys. Lett. **69**, 708 (1996).	Co/Al_2O_3/CoFe	32	77K	in-plane
K. Matsuyama, H. Asada, I. Matsuguma, T. Saeki, and K. Taniguchi, J. Appl. Phys. **79**, 5318 (1996).	Co/Cu-Cu oxide/Co	0.85	RT	in-plane
N. Tezuka and T. Miyazaki, J. Appl. Phys. **79**, 6262 (1996).	Fe/Al_2O_3/NiFe	35	4.2K	in-plane
R.S. Beech, J. Anderson, J. Daughton, B.A. Everitt, and D. Wang, IEEE Trans. Magn. **32**, 4713 (1996).	NiFeCo/Al_2O_3/CoFe	4	RT	in-plane
Y. Lu, X. Li, G. Gong, G. Xiao, A. Gupta, P. Lecoeur, and J. Sun, Phys. Rev. B - Condens. Matter Mater. Phys. **54**, R8357 (1996).	LaSrMnO/SrTiO/LaSrMnO	83	4.2K	in-plane

TMR_1997

References	**Structures**	**TMR (%)**	T_m	**in-plane or perp.**
T. Miyazaki, S. Kumagai, and T. Yaoi, J. Appl. Phys. **81**, 3753 (1997).	NiFe/Al-oxide/Co	0.1	RT	in-plane
S.A. Rishton, Y. Lu, R.A. Altman, A.C. Marley, X.P. Bian, C. Jahnes, R. Viswanathan, G. Xiao, W.J. Gallagher, and S.S.P. Parkin, Microelectron. Eng. **35**, 249 (1997).	FeNi/Al_2O_3/Co	22	RT	in-plane
J.S. Moodera, E.F. Gallagher, K. Robinson, J. Nowak, J.S. Moodera, E.F. Gallagher, K. Robinson, and J. Nowak, Appl. Phys. Lett. **70**, 3050 (1997).	Co/Al_2O_3/NiFe	15.3	RT	in-plane
		23	77K	in-plane
	Co/Al_2O_3/CoFe	17	RT	in-plane
		24	77K	in-plane
Y. Lu, R.A. Altman, A. Marley, S.A. Rishton, P.L. Trouilloud, G. Xiao, W.J. Gallagher, and S.S.P. Parkin, Appl. Phys. Lett. **70**, 2610 (1997).	Co/Al-O/Co	20	RT	in-plane
H. Tsuge and T. Mitsuzuka, Appl. Phys. Lett. **71**, 3296 (1997).	Fe/Al_2O_3/CoFe	5	RT	in-plane
X.W. Li, Y. Lu, G.Q. Gong, G. Xiao, A. Gupta, P. Lecoeur, J.Z. Sun, Y.Y. Wang, and V.P. Dravid, J. Appl. Phys. **81**, 5509 (1997).	LaSrMnO_3/SrTiO_3/LaSrMnO_3	83	4.2K	in-plane
C.T. Tanaka, J. Nowak, and J.S. Moodera, J. Appl. Phys. **81**, 5515 (1997).	NIMnSb/Al_2O_3/$Ni_{0.8}Fe_{0.2}$	8.1	77K	in-plane
	NIMnSb/Al_2O_3/$Co_{0.5}Fe_{0.5}$	5.7	77K	in-plane
C.L. Platt, B. Dieny, and A.E. Berkowitz, J. Appl. Phys. **81**, 5523 (1997).	Fe/MgO/Co	20	77K	in-plane
W.J. Gallagher, Y. Lu, X.P. Bian, A. Marley, K.P. Roche, R.A. Altman, S.A. Rishton, C. Jahnes, T.M. Shaw, and G. Xiao, J. Appl. Phys. **81**, 3741 (1997).	Py/Al_2O_3/Co	22	RT	in-plane
M. Sato and K. Kobayashi, Jpn. J. Appl. Phys. **36**, L200 (1997).	NiFe/Co/Al-oxide/Co/Ni-Fe	10	RT	in-plane

TMR_1998

References	**Structures**	**TMR (%)**	T_m	**in-plane or perp.**
C. Kwon, Q.X. Jia, M.F. Hundley, D.W. Reagor, J.Y. Coulter, and D.E. Peterson, **72**, 486 (1998).	LSMO/STO/LSMO	23	99.6K	in-plane
C.H. Shang, G.P. Berera, and J.S. Moodera, Appl. Phys. Lett. **72**, 605 (1998).	Co/Al_2O_3/Co/NiO	17	295K	in-plane
		22	77K	in-plane
P.K. Wong, J.E. Evetts, and M.G. Blamire, Appl. Phys. Lett. **73**, 384 (1998).	Fe/Al_2O_3/CoFe	6.2	RT	in-plane
		9.2	77K	in-plane
J. Nassar, M. Hehn, A. Vaurès, F. Petroff, and	Co/Al_2O_3/$Ni_{80}Fe_{20}$	16	4.2K	in-plane

A. Fert, Appl. Phys. Lett. **73**, 698 (1998).		6	RT	in-plane
W. Oepts, H.J. Verhagen, W.J.M. De Jonge, and R. Coehoorn, Appl. Phys. Lett. **73**, 2363 (1998).	$Co/Al_2O_3/Co_{50}Fe_{50}$	18	RT	in-plane
F. Montaigne, J. Nassar, A. Vaurès, F.N. Van Dau, F. Petroff, A. Schuhl, and A. Fert, Appl. Phys. Lett. **73**, 2829 (1998).	$Co/Al_2O_3/Ni_{80}Fe_{20}$	16.5	RT	in-plane
		25	30K	in-plane
X.W. Li, A. Gupta, G. Xiao, W. Qian, and V.P. Dravid, Appl. Phys. Lett. **73**, 3282 (1998).	$Fe_3O_4/MgO/Fe_3O_4$	0.5	300K	in-plane
		1.5	150K	in-plane
R.C. Sousa, J.J. Sun, V. Soares, P.P. Freitas, A. Kling, M.F. Da Silva, and J.C. Soares, Appl. Phys. Lett. **73**, 3288 (1998).	$CoFe/Al_2O_3/CoFe$	36.5	300K	in-plane
C. Kwon, Q.X. Jia, Y. Fan, M.F. Hundley, and D.W. Reagor, J. Appl. Phys. **83**, 7052 (1998).	LSMO/STO/LSMO	30	15.7K	in-plane
J.J. Sun, R.C. Sousa, T.T.P. Galvão, V. Soares, T.S. Plaskett, and P.P. Freitas, J. Appl. Phys. **83**, 6694 (1998).	$NiFe/Al_2O_3/CoFe$	13.5	RT	in-plane
Y. Lu, X.W. Li, G. Xiao, R.A. Altman, W.J. Gallagher, A. Marley, K. Roche, and S. Parkin, J. Appl. Phys. **83**, 6515 (1998).	$Co/Al_2O_3/NiFe$	27	RT	in-plane
J.F. Bobo, F.B. Mancoff, K. Bessho, M. Sharma, K. Sin, D. Guarisco, S.X. Wang, and B.M. Clemens, J. Appl. Phys. **83**, 6685 (1998).	$Co/Al_2O_3/NiFe$	13	RT	in-plane
H. Boeve, R.J.M. Van De Veerdonk, B. Dutta, J. De Boeck, J.S. Moodera, and G. Borghs, J. Appl. Phys. **83**, 6700 (1998).	$Co/Al_2O_3/NiFe$	15	RT	in-plane
P.K. Wong, J.E. Evetts, and M.G. Blamire, J. Appl. Phys. **83**, 6697 (1998).	$Nb/Fe/Al_2O_3/Al/CoFe/Nb$	6.2	RT	in-plane
		9.2	77K	in-plane
M. Sato, H. Kikuchi, and K. Kobayashi, J. Appl. Phys. **83**, 6691 (1998).	NiFe/Co/Al-AlO/Co/NiFe/Fe-Mn/Ni-Fe	24	RT	in-plane
E.R. Nowak, R.D. Merithew, M.B. Weissman, I. Bloom, and S.S.P. Parkin, J. Appl. Phys. **84**, 6195 (1998).	$MnFe/Co/Al_2O_3/NiFe/Pd$	34	4.2K	in-plane
		22	RT	in-plane
C.H. Shang, J. Nowak, R. Jansen, and J.S. Moodera, Phys. Rev. B - Condens. Matter Mater. Phys. **58**, R2917 (1998).	$Co/Al_2O_3/NiFe/NiO$	14	RT	in-plane
		27	77K	in-plane
J.S. Moodera, J. Nowak, and R.J.M. Van De Veerdonk, Phys. Rev. Lett. **80**, 2941 (1998).	$Co/Al_2O_3/Ni_{80}Fe_{20}$	20.2	295K	in-plane
		27.1	77K	in-plane

TMR_1999

References	**Structures**	**TMR (%)**	T_m	**in-plane or perp.**
T. Hayashi, H. Shimada, H. Shimizu, and M. Tanaka, J. Cryst. Growth **201**, 689 (1999).	GaMnAs/AlAs/GaMnAs	44.4	4.2K	in-plane
Y. Shimazu, I. Yamamoto, and M. Yamaguchi, J. Magn. Magn. Mater. **198**, 76 (1999).	$Ni/Al\text{-}Al_2O_3/Co$	14	1.4K	in-plane

H. Kubota, T. Watabe, and T. Miyazaki, J. Magn. Magn. Mater. **198**, 173 (1999).	$Ni_{80}Fe_{20}/Al_2O_3/Co/Al_2O_3/Co$	2	RT	in-plane
Y. Ando, M. Yokota, N. Tezuka, and T. Miyazaki, J. Magn. Magn. Mater. **198**, 155 (1999).	NiFe/Co/Al-oxide/Co	12	RT	in-plane
T. Obata, T. Manako, Y. Shimakawa, and Y. Kubo, Appl. Phys. Lett. **74**, 290 (1999).	$La_{0.8}Sr_{0.2}MnO_3/SrTiO_3/La_{0.8}Sr0_{.2}MnO_3$	150	5K	in-plane
J.J. Sun, V. Soares, and P.P. Freitas, Appl. Phys. Lett. **74**, 448 (1999).	$NiFe/CoFe/Al_2O_3/CoFe$	27	RT	in-plane
E.R. Nowak, M.B. Weissman, and S.S.P. Parkin, Appl. Phys. Lett. **74**, 600 (1999).	$Mn_{46}Fe_{54}/Co_{84}Fe_{16}/Al_2O_3/Co_{84}Fe_{16}$	35	295K	in-plane
K.S. Moon, R.E. Fontana, and S.S.P. Parkin, Appl. Phys. Lett. **74**, 3690 (1999).	$Ni_{81}Fe_{19}/Mn_{54}Fe_{46}/Ni_{81}Fe_{19}/Co/Al_2O_3/Ni_{81}Fe_{19}$	22	RT	in-plane
P. Seneor, A. Fert, J.L. Maurice, F. Montaigne, F. Petroff, and A. Vaurès, Appl. Phys. Lett. **74**, 4017 (1999).	$Co/Al_2O_3/Fe_3O_4$	43	4.2K	in-plane
		13	RT	in-plane
A.T.A. Wee, K. Sin, and S.X. Wang, Appl. Phys. Lett. **74**, 2528 (1999).	$Fe_{55}Ni_{45}/FeMn/Fe_{55}Ni_{45}/Al_2O_3/Fe_{55}Ni_{45}$	16.5	RT	in-plane
R.C. Sousa, P.P. Freitas, and J.P. Conde, Appl. Phys. Lett. **74**, 3893 (1999).	$NiFe/CoFe/Al_2O_3/CoFe$	25.3	RT	in-plane
R. Jansen and J.S. Moodera, Appl. Phys. Lett. **75**, 400 (1999).	$Co/Fe\text{-}doped\_Al_2O_3/Ni_{80}Fe_{20}$	23.4	77K	in-plane
S.S.P. Parkin, K.S. Moon, K.E. Pettit, D.J. Smith, R.E. Dunin-Borkowski, and M.R. McCartney, Appl. Phys. Lett. **75**, 543 (1999).	$Co_{75}Pt_{12}Cr_{13}/Al_2O_3/Co_{88}Pt_{12}$	13	RT	in-plane
J.J. Sun and P.P. Freitas, J. Appl. Phys. **85**, 5264 (1999).	$Ni_{81}Fe_{19}/Mn_{78}Rh_{22}/Ni_{81}Fe_{19}/Co_{90}Fe_{10}/Al_2O_3/Co_{90}Fe_{10}$	22	RT	in-plane
H. Chen, Q.Y. xu, G. ni, J. lu, H. Sang, S.Y. Zhang, and Y.W. du, J. Appl. Phys. **85**, 5798 (1999).	$Fe/Al_2O_3/Fe$	5.89	RT	in-plane
D. Wang, M. Tondra, J.M. Daughton, C. Nordman, and A. V. Pohm, J. Appl. Phys. **85**, 5255 (1999).	$NiFeCo/Al_2O_3/CoFe$	24.4	RT	in-plane
R.C. Sousa, J.J. Sun, V. Soares, P.P. Freitas, A. Kling, M.F. da Silva, and J.C. Soares, J. Appl. Phys. **85**, 5258 (1999).	$NiFe/CoFe/Al_2O_3/CoFe$	37	RT	in-plane
K. Matsuda, A. Kamijo, T. Mitsuzuka, and H. Tsuge, J. Appl. Phys. **85**, 5261 (1999).	NiFe/FeMn/NiFe/Al-oxide/NiFe	13	RT	in-plane
M. Sharma, S.X. Wang, and J.H. Nickel, J. Appl. Phys. **85**, 7803 (1999).	NiFe/Ta-oxide/NiFe	1.4	RT	in-plane
W. Oepts, H.J. Verhagen, R. Coehoorn, and W.J.M. De Jonge, J. Appl. Phys. **86**, 3863 (1999).	$Co/Al_2O_3/Co_{50}Fe_{50}$	8.2	RT	in-plane
C.T. Tanaka, J. Nowak, and J.S. Moodera, J. Appl. Phys. **86**, 6239 (1999).	$NiMnSb/Al_2O_3/Ni_{80}Fe_{20}$	9	RT	in-plane
		19.5	4.2K	in-plane
J.J. Sun, R.C. Sousa, T.T.P. Galvão, V. Soares, and P.P. Freitas, J. Magn. Soc. Japan **23**, 55 (1999).	$CoFe/Al_2O_3/CoFe$	23.1	RT	in-plane
H. Kubota, T. Watabe, Y. Fukumoto, and T. Miyazaki, J. Magn. Soc. Japan **23**, 67 (1999).	$NiFe/Al_2O_3/Co/Al_2O_3/Co$	2	RT	in-plane
H. Yamanaka, K. Saito, K. Takanashi, and H. Fujimori, J. Magn. Soc. Japan **23**, 70 (1999).	Fe/Al-O/Co/NiFe/FeMn	18	4.2K	in-plane

C.-H. Lee, Y. Sato, T. Sato, M. Doi, and M. Matsui, J. Magn. Soc. Japan **23**, 1321 (1999).	$FeCo/Al_2O_3/Fe$	35	RT	in-plane
J.M. De Teresa, A. Barthélémy, A. Fert, J.P. Contour, F. Montaigne, and P. Seneor, Science (80-.). **286**, 507 (1999).	Co/STO/LSMO	-32	40K	in-plane
H. Boeve, C. Bruynseraede, J. Das, K. Dessein, G. Borghs, and J. De Boeck, IEEE Trans. Magn. **35**, 2820 (1999).	$Co/Al_2O_3/Co$	25	RT	in-plane
R.C. Sousa, P.P. Freitas, V. Chu, and J.P. Conde, IEEE Trans. Magn. **35**, 2832 (1999).	$CoFe/Al_2O_3/CoFe$	25.3	RT	in-plane
H. Yamanaka, K. Saito, K. Takanashi, and H. Fujimori, IEEE Trans. Magn. **35**, 2883 (1999).	Fe/Al-O/Co/NiFe/FeMn	18.8	77K	in-plane
D. Wang, M. Tondra, C. Nordman, and J.M. Daughton, IEEE Trans. Magn. **35**, 2886 (1999).	$NiFeCo/Al_2O_3/CoFe/IrMn$	22	RT	in-plane
A.T.A. Wee, S.X. Wang, and K. Sin, IEEE Trans. Magn. **35**, 2949 (1999).	$Ni_{45}Fe_{55}/Al_2O_3/Ni_{45}Fe_{55}$	16.5	RT	in-plane
S. Cardoso, V. Gehanno, R. Ferreira, and P.P. Freitas, IEEE Trans. Magn. **35**, 2952 (1999).	$Co_{82}Fe_{18}/Al_2O_3/Co_{82}Fe_{18}$	41	RT	in-plane
J. Murai, Y. Ando, M. Kamijo, H. Kubota, and T. Miyazaki, Japanese J. Appl. Physics, Part 2 Lett. **38**, L1106 (1999).	$Ni_{80}Fe_{20}$/Al-oxide/Co	12	4.2K	in-plane
J.M. De Teresa, A. Barthélémy, A. Fert, J.P. Contour, R. Lyonnet, F. Montaigne, P. Seneor, and A. Vaurès, Phys. Rev. Lett. **82**, 4288 (1999).	Co/STO/LSMO	-50	5K	in-plane

TMR_2000

References	**Structures**	**TMR (%)**	T_m	**in-plane or perp.**
E.R. Nowak, P. Spradling, M.B. Weissman, and S.S.P. Parkin, Thin Solid Films **377**–**378**, 699 (2000).	$Co_{84}Fe_{16}/Al_2O_3/Co_{84}Fe_{16}$	38	RT	in-plane
E. Girgis, H. Boeve, J. De Boeck, J. Schelten, P. Rottländer, H. Kohlstedt, and P. Grünberg, J. Magn. Magn. Mater. **222**, 133 (2000).	$Co/Al_2O_3/Ni_{80}Fe_{20}$	14	RT	in-plane
P. Rottländer, H. Kohlstedt, H.A.M. De Gronckel, E. Girgis, J. Schelten, and P. Grünberg, J. Magn. Magn. Mater. **210**, 251 (2000).	$Co/Al\text{-}Al_2O_3/Ni_{80}Fe_{20}$	22	RT	in-plane
J.M. De Teresa, A. Barthélémy, J.P. Contour, and A. Fert, J. Magn. Magn. Mater. **211**, 160 (2000).	$La0.7Sr_{0.3}MnO_3/SrTiO_3/Co$	5	RT	in-plane
S. Cardoso, P.P. Freitas, C. De Jesus, P. Wei, and J.C. Soares, Appl. Phys. Lett. **76**, 610 (2000).	$CoFe/Al_2O_3/CoFe/MnIr$	41	RT	in-plane
H. Boeve, E. Girgis, J. Schelten, J. De Boeck, and G. Borghs, Appl. Phys. Lett. **76**, 1048 (2000).	$Co/Al_2O_3/Ni_{80}Fe_{20}$	20	RT	in-plane
J. O'Donnell, A.E. Andrus, S. Oh, E. V. Colla, and J.N. Eckstein, Appl. Phys. Lett. **76**, 1914 (2000).	$(La_{0.75}Sr_{0.25})_{0.97}MnO_3/CaTiO_3/(La_{0.75}Sr_{0.25})_{0.97}MnO_3$	450	4.2K	in-plane
J.J. Sun, K. Shimazawa, N. Kasahara, K.	$CoFe/Al_2O_3/CoFe$	31.6	RT	in-plane

Sato, S. Saruki, T. Kagami, O. Redon, S. Araki, H. Morita, and M. Matsuzaki, Appl. Phys. Lett. **76**, 2424 (2000).				
F. Montaigne, P. Gogol, J. Briatico, J.L. Maurice, F. Nguyen Van Dau, F. Petroff, A. Fert, and A. Schuhl, Appl. Phys. Lett. **76**, 3286 (2000).	$Co/Al_2O_3/NiFe$	14	RT	in-plane
S. Cardoso, R. Ferreira, P.P. Freitas, P. Wei, and J.C. Soares, Appl. Phys. Lett. **76**, 3792 (2000).	$CoFe/Al_2O_3/CoFe$	40	RT	in-plane
M. Covington, J. Nowak, and D. Song, Appl. Phys. Lett. **76**, 3965 (2000).	NiFe/Al-oxide/NiFe	21	RT	in-plane
X.F. Han, M. Oogane, H. Kubota, Y. Ando, and T. Miyazaki, Appl. Phys. Lett. **77**, 283 (2000).	$Ni_{79}Fe_{21}/Cu/Ni_{79}Fe_{21}/Ir_{22}Mn_{78}/Co_{75}Fe_{25}$/Al-oxide/$Co_{75}Fe_{25}/Ni_{79}Fe_{21}$	49.7	RT	in-plane
		69.1	4.2K	in-plane
H. Kikuchi, M. Sato, and K. Kobayashi, J. Appl. Phys. **87**, 6055 (2000).	NiFe/$Co_{74}Fe_{26}$/Al-O/$Co_{74}Fe_{26}$/NiFe/IrMn	42	RT	in-plane
S. Cardoso, P.P. Freitas, C. de Jesus, and J.C. Soares, J. Appl. Phys. **87**, 6058 (2000).	$CoFe/Al_2O_3/CoFe$	40	RT	in-plane
E.Y. Chen, R. Whig, J.M. Slaughter, D. Cronk, J. Goggin, G. Steiner, and S. Tehrani, J. Appl. Phys. **87**, 6061 (2000).	$NiFe/Al_2O_3/NiFe$	16	RT	in-plane
K. Inomata, Y. Saito, K. Nakajima, and M. Sagoi, J. Appl. Phys. **87**, 6064 (2000).	$Co_{80}Pt_{20}/Al_2O_3/Co_{80}Pt_{20}/Al_2O_3/Co_9Fe$	15.6	RT	in-plane
P. Rottländer, H. Kohlstedt, P. Grünberg, and E. Girgis, J. Appl. Phys. **87**, 6067 (2000).	$Ni_{80}Fe_{20}$/Al-oxide/Co	22.5	RT	in-plane
T. Hayashi, M. Tanaka, and A. Asamitsu, J. Appl. Phys. **87**, 4673 (2000).	GaMnAs/AlAs/GaMnAs/AlAs/GaMnAs	170	4.2K	in-plane
O. Redon, N. Kasahara, K. Shimazawa, S. Araki, H. Morita, and M. Matsuzaki, J. Appl. Phys. **87**, 4688 (2000).	$Co/Al_2O_3/Co$	17.47	RT	in-plane
K. Shimazawa, N. Kasahara, J.J. Sun, S. Araki, H. Morita, and M. Matsuzaki, J. Appl. Phys. **87**, 5194 (2000).	Co/Al-oxide/Co	17.2	RT	in-plane
D. Song, J. Nowak, and M. Covington, J. Appl. Phys. **87**, 5197 (2000).	Co/Al-oxide/Co	38	RT	in-plane
D. Ozkaya, R.E. Dunin-Borkowski, A.K. Petford-Long, P.K. Wong, and M.G. Blamire, J. Appl. Phys. **87**, 5200 (2000).	$Fe/Al_2O_3/CoFe$	6.2	RT	in-plane
J. Nowak, D. Song, and E. Murdock, J. Appl. Phys. **87**, 5203 (2000).	$Ni_{80}Fe_{20}$/Al-Oxide/$Ni_{80}Fe_{20}$	26.6	RT	in-plane
Y. Ando, J. Murai, H. Kubota, and T. Miyazaki, J. Appl. Phys. **87**, 5209 (2000).	Co/Al-oxide/Co	15	RT	in-plane
S. Tanoue and A. Yamasaki, J. Appl. Phys. **88**, 4764 (2000).	$CoFe/Al_2O_3/Co/Al_2O_3/NiFe$	14.6	50K	in-plane
D. Chiba, N. Akiba, F. Matsukura, Y. Ohno, and H. Ohno, Appl. Phys. Lett. **77**, 1873 (2000).	GaMnAs/AlGaAs/GaMnAs	0.28	30K	in-plane
M. Sharma, J.H. Nickel, T.C. Anthony, and S.X. Wang, Appl. Phys. Lett. **77**, 2219 (2000).	NiFe/AlON/NiFe	18	RT	in-plane
K. Matsuda, N. Watari, A. Kamijo, and H. Tsuge, Appl. Phys. Lett. **77**, 3060 (2000).	NiFe/Al-oxide/CoFe	20	RT	in-plane
T. Dimopoulos, C. Tiusan, V. Da Costa, K.	$Co/Al_2O_3/CoFe$	30	RT	in-plane

Ounadjela, and H.A.M. Van Den Berg, Appl. Phys. Lett. **77**, 3624 (2000).				
Z. Li, C. De Groot, and J.H. Moodera, Appl. Phys. Lett. **77**, 3630 (2000).	$Co/Ga_2O_3/Ni_{80}Fe_{20}$	18.2	RT	in-plane
		27.6	77K	in-plane
M.H. Jo, N.D. Mathur, J.E. Evetts, and M.G. Blamire, Appl. Phys. Lett. **77**, 3803 (2000).	$La_{0.7}Ca_{0.3}MnO_3/NdGaO_3/La_{0.7}Ca_{0.3}MnO_3$	86	77K	in-plane
H. Kubota, S. Otsuka, M. Kamijo, N. Tezuka, Y. Ando, C.C. Yu, and T. Miyazaki, J. Magn. Soc. Japan **24**, 595 (2000).	NiFe/Co/Al-O/Co	35	RT	in-plane
E. Girgis, J. Schelten, P. Gruenberg, P. Rottlaender, and H. Kohlstedt, IEEE Trans. Electron Devices **47**, 697 (2000).	$Co/Al_2O_3/NiFe$	20	RT	in-plane
S. Tehrani, B. Engel, J.M. Slaughter, E. Chen, M. DeHerrera, M. Durlam, P. Naji, R. Whig, J. Janesky, and J. Calder, IEEE Trans. Magn. **36**, 2752 (2000).	NiFe/Al-oxide/NiFe	45	RT	in-plane
P.P. Freitas, S. Cardoso, R. Sousa, W. Ku, R. Ferreira, V. Chu, and J.P. Conde, IEEE Trans. Magn. **36**, 2796 (2000).	CoFe/Al-oxide/CoFe	40	RT	in-plane
D. Wang, J.M. Daughton, W.D. Wang, and J.Q. Wang, IEEE Trans. Magn. **36**, 2802 (2000).	$NiFeCo/Al_2O_3/CoFe/IrMn$	20	RT	in-plane
A. Wallash, J. Hillman, M. Sharma, and S.X. Wang, IEEE Trans. Magn. **36**, 2809 (2000).	$Co/Al_2O_3/NiFe$	13	RT	in-plane
E. Nakashio, J. Sugawara, S. Onoe, and S. Kumagai, IEEE Trans. Magn. **36**, 2812 (2000).	$Co_{75}Fe_{25}/Al_2O_3/Co_{75}Fe_{25}$	49	RT	in-plane
K. Sin, C. Chien, L. Miloslavsky, S. Funada, M. Miller, H.C. Tong, and S. Gupta, IEEE Trans. Magn. **36**, 2818 (2000).	$Co_{90}Fe_{10}/Al_2O_3/Co_{90}Fe_{10}$	28.7	RT	in-plane
Y. Ando, H. Kubota, M. Hayashi, M. Kamijo, K. Yaoita, A.C.C. Yu, X.F. Han, and T. Miyazaki, Japanese J. Appl. Physics, Part 1 Regul. Pap. Short Notes Rev. Pap. **39**, 5832 (2000).	$Co_{75}Fe_{25}/Al$-oxide/$Co_{75}Fe_{25}$	49	RT	in-plane
T. Obata, T. Manako, Y. Shimakawa, and Y. Kubo, J. Electroceramics **4**, 427 (2000).	$La_{0.8}Sr_{0.2}MnO_3/SrTiO_3/La_{0.8}Sr_{0.2}MnO_3$	150	5K	in-plane
C. Platt and A. Katz, Phys. Rev. B - Condens. Matter Mater. Phys. **61**, 68 (2000).	Co/CoFe-oxide/CoFe	6	77K	in-plane
M.H. Jo, N. Mathur, N. Todd, and M. Blamire, Phys. Rev. B - Condens. Matter Mater. Phys. **61**, R14905 (2000).	$La_{0.7}Ca_{0.3}MnO_3/NdGaO_3/La_{0.7}Ca_{0.3}MnO_3$	86	77K	in-plane
P. LeClair, H.J.M. Swagten, J.T. Kohlhepp, R.J.M. Van De Veerdonk, and W.J.M. De Jonge, Phys. Rev. Lett. **84**, 2933 (2000).	$Co/Al_2O_3/Co$	27	RT	in-plane
Y. Saito, M. Amano, K. Nakajima, S. Takahashi, M. Sagoi, and K. Inomata, Jpn. J. Appl. Phys. **39**, L1035 (2000).	CoFe/Al-oxide/$Co_{90}Fe_{10}$/Al-oxide/CoFe	42.4	RT	in-plane
X.F. Han, T. Daibou, M. Kamijo, K. Yaoita, H. Kubota, Y. Ando, and T. Miyazaki, Jpn. J. Appl. Phys. **39**, L439 (2000).	$Co_{75}Fe_{25}/Al$-oxide/$Co_{75}Fe_{25}$	49.7	RT	in-plane
		69.1	4.2K	in-plane

TMR_2001

References	**Structures**	**TMR (%)**	T_m	**in-plane or perp.**
H. Ohno, F. Matsukura, and Y. Ohno, Solid State Commun. **119**, 281 (2001).	GaMnAs/AlGaAs/GaMnAs	5.5	30K	in-plane
H. Boeve, J. De Boeckt, and G. Borghs, J. Magn. Magn. Mater. **226**–**230**, 939 (2001).	CoFe/Al_2O_3/CoFe	20	RT	in-plane
Y. Saito, M. Amano, K. Nakajima, S. Takahashi, and M. Sagoi, J. Magn. Magn. Mater. **223**, 293 (2001).	CoFe/Al-oxide/$Co_{90}Fe_{10}$/Al-oxide/CoFe	42.4	RT	in-plane
B. Park and T.D. Lee, J. Magn. Magn. Mater. **226**–**230**, 926 (2001).	NiFe/FeMn/NiFe/CoFe/Al_2O_3/CoFe /NiFe	32	RT	in-plane
P.J. Chang, J.H. Lee, S.G. Youn, C.S. Yoon, C.K. Kim, and O. Song, Mater. Sci. Eng. B Solid-State Mater. Adv. Technol. **86**, 48 (2001).	CoFe/Al-oxide/CoFe	32	RT	in-plane
Y. Higo, H. Shimizu, and M. Tanaka, Phys. E **10**, 292 (2001).	GaMnAs/AlAs/GaMnAs	72	8K	in-plane
H. Boeve, J. De Boeck, and G. Borghs, J. Appl. Phys. **89**, 482 (2001).	CoFe/Al_2O_3/CoFe/NiFe	20	RT	in-plane
A.E.T. Kuiper, M.F. Gillies, V. Kottler, G.W. 'T Hooft, J.G.M. Van Berkum, C. Van Der Marel, Y. Tamminga, and J.H.M. Snijders, J. Appl. Phys. **89**, 1965 (2001).	Co/Al-oxide/Co	25	RT	in-plane
V. Kottler, M.F. Gillies, and A.E.T. Kuiper, J. Appl. Phys. **89**, 3301 (2001).	Co-oxide/Al-oxide/Co	35	RT	in-plane
H. Kyung, H.S. Ahn, C.S. Yoon, C.K. Kim, O. Song, T. Miyazaki, Y. Ando, and H. Kubota, J. Appl. Phys. **89**, 2752 (2001).	Co/Ta-oxide/Co	9	RT	in-plane
H. Brückl, J. Schmalhorst, G. Reiss, G. Gieres, and J. Wecker, Appl. Phys. Lett. **78**, 1113 (2001).	Co/Al-oxide/Co	18	RT	in-plane
Z. Zhang, S. Cardoso, P.P. Freitas, X. Batlle, P. Wei, N. Barradas, and J.C. Soares, J. Appl. Phys. **89**, 6665 (2001).	CoFe/Al-oxide/Fe-oxide	40	RT	in-plane
J. Wang, S. Cardoso, P.P. Freitas, P. Wei, N.P. Barradas, and J.C. Soares, J. Appl. Phys. **89**, 6868 (2001).	CoFe/AlN/CoFe	33	RT	in-plane
A. Gupta, X.W. Li, and G. Xiao, Appl. Phys. Lett. **78**, 1894 (2001).	CrO_2/Co	-8	4.2K	in-plane
E. Nakashio, J. Sugawara, S. Onoe, and S. Kumagai, J. Appl. Phys. **89**, 7356 (2001).	$Co_{75}Fe_{25}$/Al-oxide/$Co_{75}Fe_{25}$	15	RT	in-plane
Y. Higo, H. Shimizu, and M. Tanaka, J. Appl. Phys. **89**, 6745 (2001).	GaMnAs/AlAs/GaMnAs	77	8K	in-plane
D. Wang, Z. Qian, J.M. Daughton, C. Nordman, M. Tondra, D. Reed, and D. Brownell, J. Appl. Phys. **89**, 6754 (2001).	CoFeHfO/Al_2O_3/FeCo	34	RT	in-plane
D. Ozkaya, A.K. Petford-Long, M.H. Jo, and M.G. Blamire, J. Appl. Phys. **89**, 6757 (2001).	$La_{0.7}Ca_{0.3}MnO_3$/$NdGaO_3$/$La_{0.7}Ca_{0.3}MnO_3$	85	77K	in-plane
S. Cardoso, P.P. Freitas, Z.G. Zhang, P. Wei, N. Barradas, and J.C. Soares, J. Appl. Phys. **89**, 6650 (2001).	CoFe/Al-oxide/CoFe	25	RT	in-plane

J.J. Sun, K. Shimazawa, N. Kasahara, K. Sato, T. Kagami, S. Saruki, S. Araki, and M. Matsuzaki, J. Appl. Phys. **89**, 6653 (2001).	CoFe/Al-oxide/CoFe	18	RT	in-plane
C. Tiusan, M. Hehn, T. Dimopoulos, and K. Ounadjela, J. Appl. Phys. **89**, 6668 (2001).	CoFe/Al-oxide/Co/Fe	28.8	RT	in-plane
J.R. Childress, M.M. Schwickert, R.E. Fontana, M.K. Ho, P.M. Rice, and B.A. Gurney, J. Appl. Phys. **89**, 7353 (2001).	CoFe/Al_2O_3/CoFe	26	RT	in-plane
T. Dimopoulos, V. Da Costa, C. Tiusan, K. Ounadjela, and H.A.M. Van Den Berg, J. Appl. Phys. **89**, 7371 (2001).	CoFe/Al-oxide/CoFe/Fe	25.5	RT	in-plane
J. Fujikata, T. Ishi, S. Mori, K. Matsuda, K. Mori, H. Yokota, K. Hayashi, M. Nakada, A. Kamijo, and K. Ohashi, J. Appl. Phys. **89**, 7558 (2001).	$Ni_{81}Fe_{19}$/Al-oxide/$Ni_{81}Fe_{19}$	17	RT	in-plane
U. Rüdiger, R. Calarco, U. May, K. Samm, J. Hauch, H. Kittur, M. Sperlich, and G. Güntherodt, J. Appl. Phys. **89**, 7573 (2001).	Co/Al-oxide/Co	36	100K	in-plane
U. May, K. Samm, H. Kittur, J. Hauch, R. Calarco, U. Rüdiger, and G. Güntherodt, Appl. Phys. Lett. **78**, 2026 (2001).	Co/Al-oxide/Co	38	100K	in-plane
Z. Zhang, S. Cardoso, P.P. Freitas, P. Wei, N. Barradas, and J.C. Soares, Appl. Phys. Lett. **78**, 2911 (2001).	CoFe/Al-oxide/Fe-oxide/CoFe	39	RT	in-plane
M. Guth, A. Dinia, G. Schmerber, and H.A.M. Van Den Berg, Appl. Phys. Lett. **78**, 3487 (2001).	CoFe/ZnS/CoFe	5	RT	in-plane
M.F. Gillies, A.E.T. Kuiper, J.B.A. Van Zon, and J.M. Sturm, Appl. Phys. Lett. **78**, 3496 (2001).	$Ni_{80}Fe_{20}$/Co/Ta_2O_5/Co/$Ni_{80}Fe_{20}$	10	RT	in-plane
P. Rottländer, M. Hehn, O. Lenoble, and A. Schuhl, Appl. Phys. Lett. **78**, 3274 (2001).	Co/Ta-oxide/Co	2.5	RT	in-plane
W. Oepts, M.F. Gillies, R. Coehoorn, R.J.M. Van De Veerdonk, and W.J.M. De Jonge, J. Appl. Phys. **89**, 8038 (2001).	Co/Al_2O_3/Co	20	RT	in-plane
K.S. Yoon, J.H. Park, J.H. Choi, J.Y. Yang, C.H. Lee, C.O. Kim, J.P. Hong, and T.W. Kang, Appl. Phys. Lett. **79**, 1160 (2001).	Co/Al-oxide/NiFe	4.7	RT	in-plane
M. Bowen, V. Cros, F. Petroff, A. Fert, C. Martínez Boubeta, J.L. Costa-Krämer, J. V. Anguita, A. Cebollada, F. Briones, J.M. De Teresa, L. Morellón, M.R. Ibarra, F. Güell, F. Peiró, and A. Cornet, Appl. Phys. Lett. **79**, 1655 (2001).	Fe/MgO/FeCo	27	RT	in-plane
		60	30K	in-plane
Z.G. Zhang, P.P. Freitas, A.R. Ramos, N.P. Barradas, and J.C. Soares, Appl. Phys. Lett. **79**, 2219 (2001).	$Co_{90}Fe_{10}$/Al-oxide/$Co_{90}Fe_{10}$	30	RT	in-plane
C.H. Ho, M.T. Lin, Y.D. Yao, S.F. Lee, C.C. Liao, F.R. Chen, and J.J. Kai, J. Appl. Phys. **90**, 6222 (2001).	Co/Al_2O_3/CoFe/NiFe	18.7	RT	in-plane
K. Li, Y. Wu, J. Qiu, G. Han, Z. Guo, H. Xie, and T. Chong, Appl. Phys. Lett. **79**, 3663 (2001).	CoFe-oxide/CoFe/Cu/CoFe-oxide	15.3	RT	in-plane
J. Wang, P.P. Freitas, E. Snoeck, P. Wei, and J.C. Soares, Appl. Phys. Lett. **79**, 4387 (2001).	CoFe/Zr-oxide/CoFe	20	RT	in-plane
J. Wang, P.P. Freitas, and E. Snoeck, Appl. Phys. Lett. **79**, 4553 (2001).	CoFe/ZrAl-oxide/CoFe	15.3	RT	in-plane

C.H. Ho, M.-T. Lin, Y.D. Yao, S.F. Lee, Y. Liou, F.R. Chen, J.J. Kai, and C.C. Liao, J. Magn. Soc. Japan **25**, 210 (2001).	Co/Al-oxide/CoFe	14	RT	in-plane
X.F. Han, M. Oogane, T. Daibou, K. Yaoita, Y. Ando, H. Kubota, and T. Miyazaki, J. Magn. Soc. Japan **25**, 707 (2001).	$Co_{75}Fe_{25}$/Al-oxide/$Co_{75}Fe_{25}$	49.7	RT	in-plane
K. Shimazawa, J.J. Sun, N. Kasahara, K. Sato, T. Kagami, S. Saruki, O. Redon, Y. Fujita, T. Umehara, J. Syoji, S. Araki, and M. Matsuzaki, IEEE Trans. Magn. **37**, 1684 (2001).	CoFe/Al-oxide/CoFe/Ru/CoFe	14	RT	in-plane
Y. Saito, M. Amano, K. Nakajima, S. Takahashi, M. Sagoi, and K. Inomata, IEEE Trans. Magn. **37**, 1979 (2001).	CoFe/Al-oxide/$Co_{90}Fe_{10}$/Al-oxide/CoFe	42.4	RT	in-plane
H.S. Lym, D.M. Jeon, H.K. Baek, S.Y. Yoon, D.H. Lee, D.H. Yoon, and S.J. Suh, Japanese J. Appl. Physics, Part 1 Regul. Pap. Short Notes Rev. Pap. **40**, 6360 (2001).	Co/Al_2O_3/Co/NiFe	16.5	RT	in-plane
X.F. Han, A.C.C. Yu, M. Oogane, J. Murai, T. Daibou, and T. Miyazaki, Phys. Rev. B - Condens. Matter Mater. Phys. **63**, 224404 (2001).	$Co_{75}Fe_{25}$/Al-oxide/$Co_{75}Fe_{25}$	44.2	RT	in-plane
		64.7	4.2K	in-plane
P. LeClair, B. Hoex, H. Wieldraaijer, J.T. Kohlhepp, H.J.M. Swagten, and W.J.M. de Jonge, Phys. Rev. B - Condens. Matter Mater. Phys. **64**, 100406(R) (2001).	Co/Ru/Al_2O_3/Co	-3	RT	in-plane
M. Tanaka and Y. Higo, Phys. Rev. Lett. **87**, 026602 (2001).	GaMnAs/AlAs/GaMnAs	75	8K	in-plane

TMR_2002

References	**Structures**	**TMR (%)**	T_m	**in-plane or perp.**
T. Manago, M. Mizuguchi, and H. Akinaga, J. Cryst. Growth **237**–**239**, 1378 (2002).	Fe/Al_2O_3/Co	11	RT	in-plane
A.C.C. Yu, X.F. Han, J. Murai, Y. Ando, T. Miyazaki, and K. Hiraga, J. Magn. Magn. Mater. **240**, 130 (2002).	CoFe/Al-oxide/CoFe	46	RT	in-plane
X.F. Han, W.Y. Lai, J.Q. Wang, C.J. O'Connor, and T. Miyazaki, J. Magn. Magn. Mater. **239**, 167 (2002).	CoFe/Al-oxide/CoFe	58.7	4.2K	in-plane
K.I. Lee, J.H. Lee, W.Y. Lee, K.W. Rhie, J.G. Ha, C.S. Kim, and K.H. Shin, J. Magn. Magn. Mater. **239**, 120 (2002).	$Co_{84}Fe_{16}$/Al_2O_3/$Co_{84}Fe_{16}$	46	RT	in-plane
Y. Aoki, H. Kinoshita, T. Mizuno, H. Sugawara, H. Sato, K. Matsuda, A. Kamijo, and H. Tsuge, J. Magn. Magn. Mater. **240**, 134 (2002).	NiFe/Al-oxide/NiFe	8	300K	in-plane
		13	4.2K	in-plane
J.H. Lee, I.W. Chang, S.J. Byun, T.K. Hong, K. Rhie, W.Y. Lee, K.H. Shin, C. Hwang, S.S. Lee, and B.C. Lee, J. Magn. Magn. Mater. **240**, 137 (2002).	CoFe/Al_2O_3/NiFe/Al_2O_3/CoFe	16	300K	in-plane
		26	77K	in-plane
M. Justus, H. Brückl, and G. Reiss, J. Magn. Magn. Mater. **240**, 212 (2002).	CoCr/Co/Al-oxide/Co/Py	12	RT	in-plane
J.H. Lee, I.W. Chang, S.J. Byun, K. Rhie, K.H. Shin, K. Il Lee, J.G. Ha, and B.C. Lee,	CoFe/Al_2O_3/CoFe	59	100K	in-plane

J. Magn. Magn. Mater. **240**, 149 (2002).				
M. Guth, G. Schmerber, Y. Henry, and A. Dinia, J. Magn. Magn. Mater. **240**, 152 (2002).	CoFe/ZnS/CoFe	5	290K	in-plane
H. Kyung, C.S. Yoon, and C.K. Kim, Mater. Sci. Eng. B Solid-State Mater. Adv. Technol. **90**, 55 (2002).	CoFe/Al-oxide/CoFe	48	RT	in-plane
S. Sugahara and M. Tanaka, Phys. E Low-Dimensional Syst. Nanostructures **13**, 582 (2002).	MnAs/AlAs/MnAs	1.2	10K	in-plane
A. Käufler, Y. Luo, K. Samwer, G. Gieres, M. Vieth, and J. Wecker, J. Appl. Phys. **91**, 1701 (2002).	Co/Al-oxide/CoFeNiSiB	22	RT	in-plane
J. Wang, P.P. Freitas, E. Snoeck, X. Battle, and J. Cuadra, J. Appl. Phys. **91**, 7463 (2002).	CoFe/ZrAl-oxide/CoFe	15.2	RT	in-plane
Z.G. Zhang, P.P. Freitas, A.R. Ramos, N.P. Barradas, and J.C. Soares, J. Appl. Phys. **91**, 8786 (2002).	$Co_{90}Fe_{10}$/Al-oxide/$Co_{90}Fe_{10}$	29	RT	in-plane
K.S. Kim, H.J. Shim, I.J. Hwang, B.K. Cho, J.H. Seok, and J.T. Kim, J. Appl. Phys. **91**, 8804 (2002).	NiFe/Al_2O_3/CoFe	13.5	RT	in-plane
R.C. Sousa, Z. Zhang, and P.P. Freitas, J. Appl. Phys. **91**, 7700 (2002).	CoFe/Al-oxide/CoFe	17.8	RT	in-plane
H. Boeve, L. Esparbe, G. Gieres, L. Bär, J. Wecker, and H. Brückl, J. Appl. Phys. **91**, 7962 (2002).	CoFe/Al-oxide/NiFe	40	RT	in-plane
S. Mitani, T. Moriyama, and K. Takanashi, J. Appl. Phys. **91**, 7200 (2002).	Fe/MgF_2/Co	10	4.2K	in-plane
J.H. Lee, K.I. Lee, W.L. Lee, K.H. Shin, J.S. Lee, K. Rhie, and B.C. Lee, J. Appl. Phys. **91**, 7956 (2002).	CoFe/Al_2O_3/NiFe/Al_2O_3/CoFe	30	300K	in-plane
		45	80K	in-plane
K.I. Lee, J.H. Lee, W.L. Lee, K.H. Shin, Y.B. Sung, J.G. Ha, K. Rhie, and B.C. Lee, J. Appl. Phys. **91**, 7959 (2002).	CoFe/Al-oxide/CoFe	48	RT	in-plane
		59	80K	in-plane
L.S. Dorneles, R.L. Sommer, and L.F. Schelp, J. Appl. Phys. **91**, 7971 (2002).	NiFe/Ta-oxide/Al_2O_3/Co	2	RT	in-plane
J. Hayakawa, K. Ito, S. Kokado, M. Ichimura, A. Sakuma, M. Sugiyama, H. Asano, and M. Matsui, J. Appl. Phys. **91**, 8792 (2002).	Co/$SrTiO_3$/$La_{0.7}Sr_{0.3}MnO_3$	-22	4.2K	in-plane
K.S. Yoon, J.H. Park, J.Y. Yang, C.O. Kim, and J.P. Hong, J. Appl. Phys. **91**, 7953 (2002).	CoFe/Al-oxide/CoFe	33.6	RT	in-plane
N. Nishimura, T. Hirai, A. Koganei, T. Ikeda, K. Okano, Y. Sekiguchi, and Y. Osada, J. Appl. Phys. **91**, 5246 (2002).	GdFeCo/CoFe/Al_2O_3/CoFe/TbFeCo	55	RT	perp.
B. Oliver, Q. He, X. Tang, and J. Nowak, J. Appl. Phys. **91**, 4348 (2002).	CoFe/Al-oxide/CoFe	22	RT	in-plane
S. Sugahara and M. Tanaka, Appl. Phys. Lett. **80**, 1969 (2002).	MnAs/AlAs/MnAs	1.4	4.2K	in-plane
J. Schmalhorst, H. Brückl, G. Reiss, G. Gieres, and J. Wecker, J. Appl. Phys. **91**, 6617 (2002).	CoFe/Al_2O_3/$Ni_{81}Fe_{19}$	37	RT	in-plane
M. Tsunoda, K. Nishikawa, S. Ogata, and M. Takahashi, Appl. Phys. Lett. **80**, 3135 (2002).	$Co_{70}Fe_{30}$/Al-oxide/$Co_{70}Fe_{30}$	58.8	RT	in-plane
S. Kreuzer, J. Moser, W. Wegscheider, D. Weiss, M. Bichler, and D. Schuh, Appl. Phys. Lett. **80**, 4582 (2002).	Fe/GaAs/Fe	0.21	4.2K	in-plane

H.J. Shim, I.J. Hwang, K.S. Kim, B.K. Cho, J.T. Kim, and J.H. Sok, J. Appl. Phys. **92**, 1095 (2002).	NiFe/AlN/NiFe	12.7	RT	in-plane
E. Popova, J. Faure-Vincent, C. Tiusan, C. Bellouard, H. Fischer, M. Hehn, F. Montaigne, M. Alnot, S. Andrieu, A. Schuhl, E. Snoeck, and V. Da Costa, Appl. Phys. Lett. **81**, 1035 (2002).	Fe/MgO/Fe/Co/Pd	17	RT	in-plane
X. Liu, C. Ren, and G. Xiao, J. Appl. Phys. **92**, 4722 (2002).	$Ni_{81}Fe_{19}/Al_2O_3/Ni_{81}Fe_{19}$	35	RT	in-plane
B.G. Park and T.D. Lee, Appl. Phys. Lett. **81**, 2214 (2002).	CoFe/Al-Hf-Al-oxide/CoFe	36	300K	in-plane
		45	30K	in-plane
J.H. Lee, S.J. Kim, C.S. Yoon, C.K. Kim, B.G. Park, and T.D. Lee, J. Appl. Phys. **92**, 6241 (2002).	CoFe/Al-oxide/CoFe	30	RT	in-plane
J. Wingbermühle, S. Stein, and H. Kohlstedt, J. Appl. Phys. **92**, 7261 (2002).	$Co_{75}Fe_{25}/Al_2O_3/Co_{75}Fe_{25}$	20	RT	in-plane
N. Matsukawa, A. Odagawa, Y. Sugita, Y. Kawashima, Y. Morinaga, M. Satomi, M. Hiramoto, and J. Kuwata, Appl. Phys. Lett. **81**, 4784 (2003).	FePt/Al-oxide/FePt	40	RT	in-plane
S. Yuasa, T. Nagahama, and Y. Suzuki, Science (80-.). **297**, 234 (2002).	Co/Cu/Al-oxide/NiFe	-1	RT	in-plane
J.R. Childress, M.K. Ho, R.E. Fontana, M.J. Carey, P.M. Rice, B.A. Gurney, and C.H. Tsang, IEEE Trans. Magn. **38**, 2286 (2002).	$CoFe/Al_2O_3/CoFe$	25	RT	in-plane
J. Wang, P.P. Freitas, E. Snoeck, X. Batlle, and J. Cuadra, IEEE Trans. Magn. **38**, 2703 (2002).	CoFe/HfAl-oxide/CoFe	13.5	RT	in-plane
B.G. Park and T.D. Lee, IEEE Trans. Magn. **38**, 2706 (2002).	CoFe/Al-Hf-Al-oxide/CoFe	35	RT	in-plane
K. Nishikawa, M. Tsunoda, S. Ogata, and M. Takahashi, IEEE Trans. Magn. **38**, 2718 (2002).	$Co_{70}Fe_{30}$/Al-oxide/$Co_{70}Fe_{30}$	48.4	RT	in-plane
		76	4.2K	in-plane
S.Y. Bae and S.X. Wang, IEEE Trans. Magn. **38**, 2721 (2002).	$Co_{84}Fe_{16}/Al_2O_3/Co_{84}Fe_{16}$	43	RT	in-plane
J. Hayakawa, S. Kokado, K. Ito, M. Sugiyama, H. Asano, M. Matsui, A. Sakuma, and M. Ichimura, Jpn. J. Appl. Phys. **41**, 1340 (2002).	$Co_{90}Fe_{10}/SrTiO_3/La_{0.7}Sr_{0.3}MnO_3$	-22	4.2K	in-plane
H. Matsuda, M. Takeuchi, H. Adachi, M. Hiramoto, N. Matsukawa, A. Odagawa, K. Setsune, and H. Sakakima, Japanese J. Appl. Physics, Part 2 Lett. **41**, L387 (2002).	Fe_3O_4/Al-oxide/CoFe	13	RT	in-plane
T. Zhu, X. Xiang, F. Shen, Z. Zhang, G. Landry, D. V. Dimitrov, N. García, and J.Q. Xiao, Phys. Rev. B - Condens. Matter Mater. Phys. **66**, 094423 (2002).	$CoFe/Al_2O_3$/PY	26.5	RT	in-plane
S.H. Chun, S.J. Potashnik, K.C. Ku, P. Schiffer, and N. Samarth, Phys. Rev. B - Condens. Matter Mater. Phys. **66**, 100408(R) (2002).	GaMnAs/GaAs/AlAs/GaAs/MnAs	30	4.2K	in-plane
Y. Sugita, A. Odagawa, N. Matsukawa, Y. Kawashima, M. Satomi, Y. Morinaga, H. Adachi, and M. Hiramoto, Japanese J. Appl. Physics, Part 2 Lett. **41**, L1072 (2002).	CoFePt/Al-oxide/CoFePt	58	RT	in-plane
		81	5K	in-plane

TMR_2003

References	Structures	TMR (%)	T_m	in-plane or perp.
C. Lü, M.W. Wu, and X.F. Han, Phys. Lett. Sect. A Gen. At. Solid State Phys. **319**, 205 (2003).	$Co_{75}Fe_{25}$/Al-oxide/$Co_{75}Fe_{25}$	58.7	4.2K	in-plane
		41	RT	in-plane
D.M. Jeon, J.W. Park, Y.S. Kim, D.H. Yoon, and S.J. Suh, Thin Solid Films **435**, 135 (2003).	Co/Al-oxide/Co	16	RT	in-plane
K.I. Lee, K.H. Chae, J.H. Lee, J.G. Ha, K. Rhie, W.Y. Lee, and K.H. Shin, Microelectron. Eng. **69**, 305 (2003).	$Co_{86}Fe_{16}/Al_2O_3/Co_{86}Fe_{16}$	46	RT	in-plane
X. Batlle, P.J. Cuadra, Z. Zhang, S. Cardoso, and P.P. Freitas, J. Magn. Magn. Mater. **261**, 305 (2003).	$Co_{80}Fe_{20}$/Al-oxide/Fe-oxide/$Co_{80}Fe_{20}$	39	RT	in-plane
O. Song, Y.M. Lee, C.S. Yoon, and C.K. Kim, J. Appl. Phys. **93**, 1146 (2003).	CoFe/Al-oxide/CoFe	30.3	RT	in-plane
M. Bowen, M. Bibes, A. Barthélémy, J.P. Contour, A. Anane, Y. Lemaître, and A. Fert, Appl. Phys. Lett. **82**, 233 (2003).	$La_{2/3}Sr_{1/3}MnO_3/SrTiO_3/La_{2/3}Sr_{1/3}MnO_3$	1850	4.2K	in-plane
B.G. Park, T.D. Lee, T.H. Lee, C.G. Kim, and C.O. Kim, J. Appl. Phys. **93**, 6423 (2003).	$Co_{80}Fe_{20}$/Hf-oxide/$Co_{80}Fe_{20}$	13	RT	in-plane
		21	77K	in-plane
Y. Liu, Z. Zhang, J. Wang, P.P. Freitas, and J.L. Martins, J. Appl. Phys. **93**, 8385 (2003).	CoFe/ZrAl-oxide/CoFe	21	RT	in-plane
H. Shim, B.K. Cho, and J.T. Kim, J. Appl. Phys. **93**, 2812 (2003).	Co/Au/Al-oxide/NiFe	9	RT	in-plane
J.H. Yu, H.M. Lee, M. Hayashi, M. Oogane, T. Daibou, H. Nakamura, H. Kubota, Y. Ando, and T. Miyazaki, J. Appl. Phys. **93**, 8555 (2003).	NiFe/Al-oxide/$Co_{75}Fe_{25}$	51	RT	in-plane
J. Wang, Y. Liu, P.P. Freitas, E. Snoeck, and J.L. Martins, J. Appl. Phys. **93**, 8367 (2003).	CoFe/HfAl-oxide/CoFe	15	RT	in-plane
J.R. Childress, J.S. Py, M.K. Ho, R.E. Fontana, and B.A. Gurney, J. Appl. Phys. **93**, 6426 (2003).	$Co_{75}Fe_{25}/Al_{90}B_{10}/Co_{75}Fe_{25}$	23	RT	in-plane
S. Mitani, T. Moriyama, and K. Takanashi, J. Appl. Phys. **93**, 8041 (2003).	Fe/MgO/Fe	23	4.2K	in-plane
B.S. Chun, S.R. Lee, and Y.K. Kim, J. Appl. Phys. **93**, 8361 (2003).	CoFe/Al-oxide/CoFe	32	RT	in-plane
K.I. Aoshima and S.X. Wang, J. Appl. Phys. **93**, 7954 (2003).	Fe_3O_4/Al-oxide/CoFe	14	RT	in-plane
W.K. Park, J.S. Moodera, J. Taylor, M. Tondra, J.M. Daughton, A. Thomas, and H. Brückl, J. Appl. Phys. **93**, 7020 (2003).	$Co_{70}Fe_{30}$/Al-oxide/$Ni_{80}Fe_{20}$	50	RT	in-plane
Z.G. Zhang, Z.Z. Zhang, and P.P. Freitas, J. Appl. Phys. **93**, 8552 (2003).	CoFe/Al-oxide/CoFe	25	RT	in-plane
G. Hu, R. Chopdekar, and Y. Suzuki, J. Appl. Phys. **93**, 7516 (2003).	$Fe_3O_4/CoCr_2O_4/La_{0.7}Sr_{0.3}MnO_3$	-25	60K	in-plane
M. Bibes, M. Bowen, A. Barthélémy, A. Anane, K. Bouzehouane, C. Carrétéro, E. Jacquet, J.P. Contour, and O. Durand, Appl. Phys. Lett. **82**, 3269 (2003).	LSMO/TiO_2/LSMO	165	4.2K	in-plane
	LSMO/TiO_2/Co	-3	4.2K	in-plane

T. Zhu, X. Xiang, and J.Q. Xiao, Appl. Phys. Lett. **82**, 2676 (2003).	CoFe/Al-oxide/Py	26.5	RT	in-plane
J. Faure-Vincent, C. Tiusan, E. Jouguelet, F. Canet, M. Sajieddine, C. Bellouard, E. Popova, M. Hehn, F. Montaigne, and A. Schuhl, Appl. Phys. Lett. **82**, 4507 (2003).	Fe/MgO/Fe	67	RT	in-plane
		100	80K	in-plane
J.H. Yu, H.M. Lee, Y. Ando, and T. Miyazaki, Appl. Phys. Lett. **82**, 4735 (2003).	$Ni_{80}Fe_{20}$/Al-oxide/$Co_{75}Fe_{25}$	50.7	RT	in-plane
B. Oliver, Q. He, X. Tang, and J. Nowak, J. Appl. Phys. **94**, 1783 (2003).	CoFe/Al-oxide/CoFe	24.5	RT	in-plane
S.R. Lee, C.M. Choi, and Y.K. Kim, Appl. Phys. Lett. **83**, 317 (2003).	CoFe/ZrAl-oxide/CoFe	39.5	RT	in-plane
S. Colis, G. Gieres, L. Bär, and J. Wecker, Appl. Phys. Lett. **83**, 948 (2003).	CoFe/Al-oxide/CoFe/NiFe/CoFe/Al-oxide/CoFe	49.5	RT	in-plane
J. Schmalhorst, H. Brückl, G. Reiss, G. Gieres, and J. Wecker, J. Appl. Phys. **94**, 3268 (2003).	CoFe/Al-oxide/NiFe	43.9	RT	in-plane
M. Bibes, K. Bouzehouane, A. Barthélémy, M. Besse, S. Fusil, M. Bowen, P. Seneor, J. Carrey, V. Cros, A. Vaurès, J.P. Contour, and A. Fert, Appl. Phys. Lett. **83**, 2629 (2003).	Sr_2FeMoO_6/$SrTiO_3$/Co	50	4K	in-plane
X. Liu and G. Xiao, J. Appl. Phys. **94**, 6218 (2003).	NiFe/Al-oxide/NiFe	35	RT	in-plane
L. Bernard, J. Monson, A. Sokolov, Z.Y. Liu, C.S. Yang, P.A. Dowben, B. Doudin, A. Harken, P. Welsch, and B.W. Robertson, Appl. Phys. Lett. **83**, 3743 (2003).	Co/B_5C/Co	1	1.6K	in-plane
T. Dimopoulos, G. Gieres, S. Colis, J. Wecker, Y. Luo, and K. Samwer, Appl. Phys. Lett. **83**, 3338 (2003).	$Co_{50}Fe_{50}$/Y-oxide/$Co_{50}Fe_{50}$	25	RT	in-plane
		44	5K	in-plane
X. Jiang, A.F. Panchula, and S.S.P. Parkin, Appl. Phys. Lett. **83**, 5244 (2003).	Fe/ZnSe/$Co_{70}Fe_{30}$	10.2	295K	in-plane
H. Shim, J.M. Park, K.P. Kim, B.K. Cho, J.T. Kim, and Y. Park, Appl. Phys. Lett. **83**, 4583 (2003).	CoFe/AlON/CoFe	34	RT	in-plane
X.H. Xiang, T. Zhu, F. Sheng, Z. Zhang, and J.Q. Xiao, IEEE Trans. Magn. **39**, 2770 (2003).	CoFe/Al_2O_3/Py	26.5	RT	in-plane
X.F. Han, F.F. Li, W.N. Wang, S.F. Zhao, Z.L. Peng, W.S. Zhan, and B.S. Han, IEEE Trans. Magn. **39**, 2794 (2003).	$Co_{75}Fe_{25}$/Al-oxide/$Co_{75}Fe_{25}$	45	RT	in-plane
T. Ochiai, N. Tezuka, K. Inomata, S. Sugimoto, and Y. Saito, IEEE Trans. Magn. **39**, 2797 (2003).	CoFe/Al-oxide/CoFe/CoFe-oxide/CoFe	46.5	RT	in-plane
C. Park, Y. Shi, Y. Peng, K. Barmak, J.G. Zhu, D.E. Laughlin, and R.M. White, IEEE Trans. Magn. **39**, 2806 (2003).	NiFe/Al-oxide/Fe_3O_4	7	RT	in-plane
K. Inomata, S. Okamura, R. Goto, and N. Tezuka, Japanese J. Appl. Physics, Part 2 Lett. **42**, L419 (2003).	$Co_2Cr_{0.6}Fe_{0.4}$Al/Al-oxide/CoFe	16	RT	in-plane
		26.5	5K	in-plane
D. Kim, T. Kim, S. Kim, J.H. Kong, Y. Yu, and K. Char, Japanese J. Appl. Physics, Part 1 Regul. Pap. Short Notes Rev. Pap. **42**, 1242 (2003).	CoFe/Al-oxide/CoFe	22.74	RT	in-plane

K. Nagahara, T. Mukai, N. Ishiwata, H. Hada, and S. Tahara, Japanese J. Appl. Physics, Part 2 Lett. **42**, L499 (2003).	NiFe/Al-oxide/CoFe	35	RT	in-plane
J. Schmalhorst and G. Reiss, Phys. Rev. B - Condens. Matter Mater. Phys. **68**, 224437 (2003).	$Co_{70}Fe_{30}$/Al-oxide/$Ni_{80}Fe_{20}$	71	10K	in-plane

TMR_2004

References	**Structures**	**TMR (%)**	T_m	**in-plane or perp.**
L. Gabillet, B. Diouf, J.F. Bobo, D. Serrate, and J.M. De Teresa, J. Magn. Magn. Mater. **272**, e1525 (2004).	Co/Al_2O_3/MgO/Al_2O_3/Co	10.4	RT	in-plane
K. Yamane, K. Yakushiji, F. Ernult, M. Matsuura, S. Mitani, K. Takanashi, and H. Fujimori, J. Magn. Magn. Mater. **272**–**276**, e1091 (2004).	Co/Al-oxide/CoAl-oxide/Co	30	4.2K	in-plane
T. Niizeki, H. Kubota, Y. Ando, and T. Miyazaki, J. Magn. Magn. Mater. **272**, 1947 (2004).	$Co_{75}Fe_{25}$/Al-oxide/$Co_{75}Fe_{25}$	38	RT	in-plane
J. Schmalhorst and G. Reiss, J. Magn. Magn. Mater. **272**, e1485 (2004).	CoFe/Al-oxide/NiFe	48	RT	in-plane
K. Inomata, S. Okamura, and N. Tezuka, J. Magn. Magn. Mater. **282**, 269 (2004).	$Co_2Cr_{0.6}Fe_{0.4}$Al/Al-oxide/CoFe	19	RT	in-plane
D. Chiba, F. Matsukura, and H. Ohno, Phys. E Low-Dimensional Syst. Nanostructures **21**, 966 (2004).	$(Ga_{0.956}Mn_{0.044})$As/GaAs/$(Ga_{0.926}Mn_{0.074})$As	290	0.39K	in-plane
X.F. Han and A.C.C. Yu, J. Appl. Phys. **95**, 764 (2004).	$Co_{75}Fe_{25}$/Al-oxide/$Co_{75}Fe_{25}$	43	RT	in-plane
Y. Fukumoto, K.I. Shimura, A. Kamijo, S. Tahara, and H. Yoda, Appl. Phys. Lett. **84**, 233 (2004).	CoFeTa-oxide/$Co_{90}Fe_{10}$/Al-oxide/$Co_{90}Fe_{10}$/Al-oxide	45	RT	in-plane
K. Inomata, N. Tezuka, S. Okamura, H. Kurebayashi, and A. Hirohata, J. Appl. Phys. **95**, 7234 (2004).	$Co_2Cr_{0.6}Fe_{0.4}$Al/Al-oxide/CoFe	19	RT	in-plane
T. Moriyama, S. Mitani, T. Seki, T. Shima, K. Takanashi, and A. Sakuma, J. Appl. Phys. **95**, 6789 (2004).	$Fe_{52}Pt_{48}$/Al-oxide/$Fe_{50}Co_{50}$	3.6	RT	in-plane
		34	77K	in-plane
Y. Huai, F. Albert, P. Nguyen, M. Pakala, and T. Valet, Appl. Phys. Lett. **84**, 3118 (2004).	CoFe/Al-oxide/CoFe	20	RT	in-plane
T.S. Yoon, C.O. Kim, T. Shoyama, M. Tsunoda, and M. Takahashi, Appl. Phys. Lett. **85**, 82 (2004).	$Co_{71}Fe_{29}$/Al-nitride/$Co_{71}Fe_{29}$	49	RT	in-plane
S. Kämmerer, A. Thomas, A. Hütten, and G. Reiss, Appl. Phys. Lett. **85**, 79 (2004).	Co_2MnSi/Al-oxide/$Co_{70}Fe_{30}$	33	RT	in-plane
		86	10K	in-plane
D.S. Kim, Y.Y. Yu, and K. Char, J. Appl. Phys. **96**, 2278 (2004).	$Co_{60}Fe_{40}$/AlOF/$Co_{60}Fe_{40}$	35	RT	in-plane
M. Zenger, J. Moser, W. Wegscheider, D. Weiss, and T. Dietl, J. Appl. Phys. **96**, 2400 (2004).	Fe/GaAs/Fe	1.7	4.2K	in-plane
G.D. Fuchs, N.C. Emley, I.N. Krivorotov, P.M. Braganca, E.M. Ryan, S.I. Kiselev, J.C. Sankey, D.C. Ralph, R.A. Buhrman, and J.A.	CoFeB/Al-oxide/CoFeB	11	77K	in-plane

Katine, Appl. Phys. Lett. **85**, 1205 (2004).				
E. Snoeck, V. Serin, R. Fourmeaux, Z. Zhang, and P.P. Freitas, J. Appl. Phys. **96**, 3307 (2004).	$Co_{80}Fe_{20}$/Al-oxide/Fe-oxide/$Co_{80}Fe_{20}$	38	RT	in-plane
N. Wiese, T. Dimopoulos, M. Rührig, J. Wecker, M. Brückl, and G. Reiss, Appl. Phys. Lett. **85**, 2020 (2004).	$Co_{90}Fe_{10}$/Ru/$Co_{90}Fe_{10}$/Al-oxide/CoFeB/Ru/CoFeB	50	RT	in-plane
T. Dimopoulos, G. Gieres, J. Wecker, N. Wiese, and M.D. Sacher, J. Appl. Phys. **96**, 6382 (2004).	CoFeB/Al-oxide/CoFeB	40	RT	in-plane
S. Okamura, R. Goto, S. Sugimoto, N. Tezuka, and K. Inomata, J. Appl. Phys. **96**, 6561 (2004).	$Co_{90}Fe_{10}$/Al-oxide/$Co_2(Cr_{0.6}Fe_{0.4})Al$	19.1	RT	in-plane
Y.Y. Yu, D.S. Kim, and K. Char, J. Appl. Phys. **96**, 6393 (2004).	$Co_{60}Fe_{40}$/AlOF/$Co_{60}Fe_{40}$	8.3	RT	in-plane
D. Wang, C. Nordman, J.M. Daughton, Z. Qian, and J. Fink, IEEE Trans. Magn. **40**, 2269 (2004).	CoFeB/Al-oxide/CoFeB	70.4	RT	in-plane
S. Cardoso, R. Ferreira, P.P. Freitas, M. MacKenzie, J. Chapman, J.O. Ventura, J.B. Sousa, and U. Kreissig, IEEE Trans. Magn. **40**, 2272 (2004).	CoFeB/Al-oxide/CoFe	47.6	RT	in-plane
S.J. Kim, S.J. Kim, D.H. Im, C.K. Kim, and C.S. Yoon, IEEE Trans. Magn. **40**, 2284 (2004).	Fe/Al-oxide/Fe-oxide/Al-oxide/Fe	24	RT	in-plane
S. Colis, G. Gieres, T. Dimopoulos, L. Bär, and J. Wecker, IEEE Trans. Magn. **40**, 2287 (2004).	CoFe/Al-oxide/CoFe/NiFe/CoFe/Al-oxide/CoFe	49	RT	in-plane
S. Yoshimura, T. Shoyama, T. Nozawa, M. Tsunoda, and M. Takahashi, IEEE Trans. Magn. **40**, 2290 (2004).	CoFe/AlN/CoFe	49	RT	in-plane
T. Dimopoulos, G. Gieres, S. Colis, R. Lopez, M. Vieth, J. Wecker, Y. Luo, and K. Samwer, IEEE Trans. Magn. **40**, 2296 (2004).	CoFe/Y-oxide/CoFe	25	RT	in-plane
		40	5K	in-plane
A. Hütten, S. Kämmerer, J. Schmalhorst, A. Thomas, and G. Reiss, Phys. Status Solidi Appl. Res. **201**, 3271 (2004).	Co_2MnSi/Al-oxide/$Co_{70}Fe_{30}$	94.6	20K	in-plane
M. Hayashi, Y. Ando, M. Oogane, H. Kubota, and T. Miyazaki, Japanese J. Appl. Physics, Part 1 Regul. Pap. Short Notes Rev. Pap. **43**, 7472 (2004).	$Co_{75}Fe_{25}$/Al-oxide/Al/$Co_{75}Fe_{25}$	40	4.2K	in-plane
H. Kubota, J. Nakata, M. Oogane, Y. Ando, A. Sakuma, and T. Miyazaki, Japanese J. Appl. Physics, Part 2 Lett. **43**, L984 (2004).	CoMnAl/Al-oxide/CoFe	40	RT	in-plane
Z.H. Xiong, D. Wu, Z.V. Vardeny, and J. Shi, Nature **427**, 821 (2004).	$La_{0.67}Sr_{0.33}MnO_3$/Alq_3/Co	-40	11K	in-plane
S.S.P. Parkin, C. Kaiser, A. Panchula, P.M. Rice, B. Hughes, M. Samant, and S.H. Yang, Nat. Mater. **3**, 862 (2004).	$Co_{70}Fe_{30}$/MgO/$(Co_{70}Fe_{30})_{80}B_{20}$	220	RT	in-plane
		300	4K	in-plane
S. Yuasa, T. Nagahama, A. Fukushima, Y. Suzuki, and K. Ando, Nat. Mater. **3**, 868 (2004).	Fe/MgO/Fe	180	RT	in-plane
		247	20K	in-plane
S.Y. Park, J.H. Lee, I.J. Shin, J.P. Hong, K.H. Shin, K. Rhie, and B.C. Lee, Phys. Status	CoFe/Al-oxide/CoFe	31	RT	in-plane

Solidi Appl. Res. **201**, 1692 (2004).				
C. Ren, X. Liu, B.D. Schrag, and G. Xiao, Phys. Rev. B - Condens. Matter Mater. Phys. **69**, 104405 (2004).	$Ni_{79}Fe_{21}/Al_2O_3/Ni_{79}Fe_{21}$	31	RT	in-plane
J.S. Parker, P.G. Ivanov, D.M. Lind, P. Xiong, and Y. Xin, Phys. Rev. B - Condens. Matter Mater. Phys. **69**, 220413(R) (2004).	CrO_2/Cr-oxide-Al-oxide/Co	-24	5K	in-plane
		-1	RT	in-plane
J. Schmalhorst, S. Kämmerer, M. Sacher, G. Reiss, A. Hütten, and A. Scholl, Phys. Rev. B - Condens. Matter Mater. Phys. **70**, 024426 (2004).	Co_2MnSi/Al-oxide/$Co_{70}Fe_{30}$	86	10K	in-plane
T. Nozaki, Y. Jiang, Y. Kaneko, A. Hirohata, N. Tezuka, S. Sugimoto, and K. Inomata, Phys. Rev. B - Condens. Matter Mater. Phys. **70**, 172401 (2004).	$Co_{90}Fe_{10}$/Ru/Al-oxide/$Co_{90}Fe_{10}$	-1.2	RT	in-plane
D. Chiba, Y. Sato, T. Kita, F. Matsukura, and H. Ohno, Phys. Rev. Lett. **93**, 216602 (2004).	GaMnAs/GaAs/GaMnAs	60	5K	in-plane
S. Yuasa, A. Fukushima, T. Nagahama, K. Ando, and Y. Suzuki, Japanese J. Appl. Physics, Part 2 Lett. **43**, L588 (2004).	Fe/MgO/Fe	88	293K	in-plane
		146	20K	in-plane

TMR_2005

References	**Structures**	**TMR (%)**	T_m	**in-plane or perp.**
J. Androulakis, S. Gardelis, J. Giapintzakis, E. Gagaoudakis, and G. Kiriakidis, Thin Solid Films **471**, 293 (2005).	$Ni_{80}Fe_{20}$/In-oxide/Co	15	100K	in-plane
D. Lim, S. Kim, and S.R. Lee, J. Appl. Phys. **97**, 10C902 (2005).	[Co/Pd]/Co/Al-oxide/Co/[Pd/Co]	1	300K	perp.
		12.6	10K	perp.
K. Nakajima, G. Fen, C. Caillol, L.S. Dorneles, M. Venkatesan, and J.M.D. Coey, J. Appl. Phys. **97**, 10C904 (2005).	CoMnSi/Al-oxide/Co	10	RT	in-plane
		22.7	50K	in-plane
H. Saito, S. Yuasa, and K. Ando, J. Appl. Phys. **97**, 10D305 (2005).	CrTe/AlAs/GaMnAs	14.5	5K	perp.
M. Kerekes, R.C. Sousa, I.L. Prejbeanu, O. Redon, U. Ebels, C. Baraduc, B. Dieny, J.P. Nozìres, P.P. Freitas, and P. Xavier, J. Appl. Phys. **97**, 10P501 (2005).	NiFe/Al-oxide/CoFe	10	RT	in-plane
T. Nozaki, A. Hirohata, N. Tezuka, S. Sugimoto, and K. Inomata, Appl. Phys. Lett. **86**, 082501 (2005).	Fe/MgO/Fe/MgO/Fe	110	RT	in-plane
S.J. Ahn, T. Kato, H. Kubota, Y. Ando, and T. Miyazaki, Appl. Phys. Lett. **86**, 102506 (2005).	$Ni_{80}Fe_{20}$/Al-oxide/$Co_{75}Fe_{25}$	43	RT	in-plane
D.D. Djayaprawira, K. Tsunekawa, M. Nagai, H. Maehara, S. Yamagata, N. Watanabe, S. Yuasa, Y. Suzuki, and K. Ando, Appl. Phys. Lett. **86**, 092502 (2005).	CoFeB/MgO/CoFeB	230	RT	in-plane
		294	20K	in-plane
L. Le Brizoual, P. Alnot, M. Hehn, F. Montaigne, M. Alnot, A. Schuhl, and E. Snoeck, Appl. Phys. Lett. **86**, 112505 (2005).	Co/ZnO/Co	8	77K	in-plane

S. Okamura, A. Miyazaki, S. Sugimoto, N. Tezuka, and K. Inomata, Appl. Phys. Lett. **86**, 232503 (2005).	Co_2FeAl/Al-oxide/$Co_{75}Fe_{25}$	47	RT	in-plane
J.O. Song, S.R. Lee, and H.J. Shin, Appl. Phys. Lett. **86**, 252501 (2005).	$Co_{90}Fe_{10}$/TiAl-oxide/$Co_{90}Fe_{10}$	49	RT	in-plane
Y. Ishii, H. Yamada, H. Sato, H. Akoh, M. Kawasaki, and Y. Tokura, Appl. Phys. Lett. **87**, 022509 (2005).	$La_{0.6}Sr_{0.4}MnO_3$/$LaAlO_3$/$La_{0.6}Sr_{0.4}MnO_3$	150	10K	in-plane
R. Guerrero, F.G. Aliev, R. Villar, J. Hauch, M. Fraune, G. Güntherodt, K. Rott, H. Brückl, and G. Reiss, Appl. Phys. Lett. **87**, 042501 (2005).	Fe(110)/MgO(111)/Fe(110)	32	RT	in-plane
Y. Higo, K. Yamane, K. Ohba, H. Narisawa, K. Bessho, M. Hosomi, and H. Kano, Appl. Phys. Lett. **87**, 082502 (2005).	CoFeB/Al-oxide/NiFe	29.4	RT	in-plane
K. Tsunekawa, D.D. Djayaprawira, M. Nagai, H. Maehara, S. Yamagata, N. Watanabe, S. Yuasa, Y. Suzuki, and K. Ando, Appl. Phys. Lett. **87**, 072503 (2005).	CoFeB/MgO/CoFeB	234	RT	in-plane
T. Dimopoulos, G. Gieres, J. Wecker, N. Wiese, Y. Luo, and K. Samwer, J. Appl. Phys. **98**, 073705 (2005).	$Co_{50}Fe_{50}$/MgO/$Co_{50}Fe_{50}$	60	RT	in-plane
Y. Ando, T. Miyakoshi, M. Oogane, T. Miyazaki, H. Kubota, K. Ando, and S. Yuasa, Appl. Phys. Lett. **87**, 142502 (2005).	Fe/MgO/Fe	270	6K	in-plane
J.C.A. Huang, C.Y. Hsu, Y.F. Liao, M.Z. Lin, and C.H. Lee, J. Appl. Phys. **98**, 103504 (2005).	CoFe/Al-oxide/CoFe	7.5	RT	in-plane
F.F. Li, R. Sharif, L.X. Jiang, X.Q. Zhang, X.F. Han, Y. Wang, and Z. Zhang, J. Appl. Phys. **98**, 113710 (2005).	$Co_{62}Fe_{20}B_{18}$/Al-oxide/$Co_{62}Fe_{20}B_{18}$	54.4	RT	in-plane
S. Yuasa, T. Katayama, T. Nagahama, A. Fukushima, H. Kubota, Y. Suzuki, and K. Ando, Appl. Phys. Lett. **87**, 222508 (2005).	Fe/Co/MgO/Co	271	RT	in-plane
		353	20K	in-plane
T. Marukame, T. Kasahara, K.I. Matsuda, T. Uemura, and M. Yamamoto, IEEE Trans. Magn. **41**, 2603 (2005).	$Co_2Cr_{0.6}Fe_{0.4}Al$/MgO/CoFe	42	RT	in-plane
		74	55K	in-plane
S. Mitani, K. Tsukamoto, T. Seki, T. Shima, and K. Takanashi, IEEE Trans. Magn. **41**, 2606 (2005).	FePt/Al-oxide/FeCo	18	RT	in-plane
		40	4.2K	in-plane
C.M. Choi, J.O. Song, and S.R. Lee, IEEE Trans. Magn. **41**, 2667 (2005).	CoFe/ZrAl-oxide/CoFe	21	RT	in-plane
J. Hayakawa, S. Ikeda, F. Matsukura, H. Takahashi, and H. Ohno, Japanese J. Appl. Physics, Part 2 Lett. **44**, L587 (2005).	CoFeB/MgO/CoFeB	260	RT	in-plane
		403	5K	in-plane
J. Hayakawa, S. Ikeda, Y.M. Lee, R. Sasaki, T. Meguro, F. Matsukura, H. Takahashi, and H. Ohno, Japanese J. Appl. Physics, Part 2 Lett. **44**, L1267 (2005).	$Co_{40}Fe_{40}B_{20}$/MgO/$Co_{40}Fe_{40}B_{20}$	160	RT	in-plane
S. Ikeda, J. Hayakawa, Y.M. Lee, R. Sasaki, T. Meguro, F. Matsukura, and H. Ohno, Japanese J. Appl. Physics, Part 2 Lett. **44**, L1442 (2005).	$Co_{40}Fe_{40}B_{20}$/MgO/$Co_{40}Fe_{40}B_{20}$	355	RT	in-plane
		578	5K	in-plane
H. Kubota, A. Fukushima, Y. Ootani, S. Yuasa, K. Ando, H. Maehara, K. Tsunekawa, D.D. Djayaprawira, N. Watanabe, and Y.	$Co_{60}Fe_{20}B_{20}$/MgO/$Co_{60}Fe_{20}B_{20}$	100	RT	in-plane

Suzuki, Japanese J. Appl. Physics, Part 2 Lett. **44**, L1237 (2005).				
M. Oogane, J. Nakata, H. Kubota, Y. Ando, A. Sakuma, and T. Miyazaki, Japanese J. Appl. Physics, Part 2 Lett. **44**, L760 (2005).	CoMnAl/Al-oxide/CoFe	40	RT	in-plane
		65	10K	in-plane
Z.M. Zeng, X.F. Han, W.S. Zhan, Y. Wang, Z. Zhang, and S. Zhang, Phys. Rev. B - Condens. Matter Mater. Phys. **72**, 054419 (2005).	CoFe/Ru/CoFe/Al-oxide/CoFe/NiFe/CoFe/Al-oxide/CoFe/Ru/CoFe	29.4	300K	in-plane
		41	4.2K	in-plane
T. Nagahama, S. Yuasa, E. Tamura, and Y. Suzuki, Phys. Rev. Lett. **95**, 086602 (2005).	Fe/Cr/Al-oxide/FeCo	-1	RT	in-plane
H. Saito, S. Yuasa, and K. Ando, Phys. Rev. Lett. **95**, 086604 (2005).	GaMnAs/ZnSe/GaMnAs	100	2K	in-plane

TMR_2006

References	**Structures**	**TMR (%)**	T_m	**in-plane or perp.**
Y. Sakuraba, M. Hattori, M. Oogane, Y. Ando, H. Kato, A. Sakuma, T. Miyazaki, and H. Kubota, Appl. Phys. Lett. **88**, 192508 (2006).	Co_2MnSi/Al-oxide/Co_2MnSi	67	RT	in-plane
		570	2K	in-plane
Y.M. Lee, J. Hayakawa, S. Ikeda, F. Matsukura, and H. Ohno, Appl. Phys. Lett. **89**, 042506 (2006).	CoFe/Ru/CoFeB/MgO/CoFeB	361	RT	in-plane
N. Tezuka, N. Ikeda, A. Miyazaki, S. Sugimoto, M. Kikuchi, and K. Inomata, Appl. Phys. Lett. **89**, 112514 (2006).	$Co_2FeAl_{0.5}Si_{0.5}$/Al-oxide/$Co_{75}Fe_{25}$	76	RT	in-plane
		106	5K	in-plane
H. Béa, M. Bibes, S. Cherifi, F. Nolting, B. Warot-Fonrose, S. Fusil, G. Herranz, C. Deranlot, E. Jacquet, K. Bouzehouane, and A. Barthélémy, Appl. Phys. Lett. **89**, 242114 (2006).	LSMO/$BiFeO_3$/Co/CoO	30	3K	in-plane
J. Hayakawa, S. Ikeda, Y.M. Lee, F. Matsukura, and H. Ohno, Appl. Phys. Lett. **89**, 232510 (2006).	CoFeB/MgO/CoFeB	472	RT	in-plane
		804	5K	in-plane
N. Tezuka, N. Ikeda, S. Sugimoto, and K. Inomata, Appl. Phys. Lett. **89**, 252508 (2006).	$Co_2FeAl_{0.5}Si_{0.5}$/MgO/$Co_2FeAl_{0.5}Si_{0.5}$	175	RT	in-plane
T. Marukame, T. Ishikawa, K.I. Matsuda, T. Uemura, and M. Yamamoto, J. Appl. Phys. **99**, 08A904 (2006).	Co_2MnFe/MgO/$Co_{50}Fe_{50}$	14	RT	in-plane
		70	7K	in-plane
N. Tezuka, S. Okamura, A. Miyazaki, M. Kikuchi, and K. Inomata, J. Appl. Phys. **99**, 08T314 (2006).	Co_2FeAl/Al-oxide/$Co_{75}Fe_{25}$	50	RT	in-plane
S. Ikeda, J. Hayakawa, Y.M. Lee, T. Tanikawa, F. Matsukura, and H. Ohno, J. Appl. Phys. **99**, 08A907 (2006).	$Co_{40}Fe_{40}B_{20}$/MgO/$Co_{40}Fe_{40}B_{20}$	355	RT	in-plane
T. Marukame, T. Ishikawa, K.I. Matsuda, T. Uemura, and M. Yamamoto, Appl. Phys. Lett. **88**, 262503 (2006).	$Co_2Cr_{0.6}Fe_{0.4}Al$/MgO/$Co_{50}Fe_{50}$	90	RT	in-plane
		240	4.2K	in-plane
S. Yuasa, A. Fukushima, H. Kubota, Y.	Co(001)/MgO(001)/Co(001)	410	290K	in-plane

Suzuki, and K. Ando, Appl. Phys. Lett. **89**, 042505 (2006).		507	20K	in-plane
Y. Nagamine, H. Maehara, K. Tsunekawa, D.D. Djayaprawira, N. Watanabe, S. Yuasa, and K. Ando, Appl. Phys. Lett. **89**, 162507 (2006).	CoFe/Ru/CoFeB/MgO/CoFeB	57	RT	in-plane
D. Ebke, J. Schmalhorst, N.N. Liu, A. Thomas, G. Reiss, and A. Hütten, Appl. Phys. Lett. **89**, 162506 (2006).	$[Co_2MnSi/Co_2FeSi]$*10/Al-oxide/CoFe	39	RT	in-plane
		114	17K	in-plane
M.S. Kim, Y.K. Zhou, M. Funakoshi, S. Emura, S. Hasegawa, and H. Asahi, Appl. Phys. Lett. **89**, 232511 (2006).	GaCrN/AlN/GaCrN	0.1	77K	in-plane
G.D. Fuchs, J.A. Katine, S.I. Kiselev, D. Mauri, K.S. Wooley, D.C. Ralph, and R.A. Buhrman, Phys. Rev. Lett. **96**, 186603 (2006).	$Co_{90}Fe_{10}/MgO/Co_{90}Fe_{10}$	33	RT	in-plane
Z. Sefrioui, V. Cros, A. Barthélémy, V. Pẽa, C. León, J. Santamaria, M. Varela, and S.J. Pennycook, Appl. Phys. Lett. **88**, 022512 (2006).	$La_{0.7}Ca_{0.3}MnO_3/PrBa_2Cu_3O_7/La_{0.7}Ca_{0.3}MnO_3$	110	80K	in-plane
Y. Tomoda, Y. Shibata, J.I. Shirakashi, and Y. Takemura, J. Appl. Phys. **99**, 08T312 (2006).	Ni/Ni-oxide/Ni	103	16.3K	in-plane
U. Lüders, M. Bibes, K. Bouzehouane, E. Jacquet, J.P. Contour, S. Fusil, J.F. Bobo, J. Fontcuberta, A. BarthÍmy, and A. Fert, Appl. Phys. Lett. **88**, 082505 (2006).	$La_{2/3}Sr_{1/3}MnO_3/SrTiO_3/NiFe_2O_4$	50	10K	in-plane
W. Shen, D. Mazumdar, X. Zou, X. Liu, B.D. Schrag, and G. Xiao, Appl. Phys. Lett. **88**, 182508 (2006).	$Co_{40}Fe_{40}B_{20}/MgO/Co_{40}Fe_{40}B_{20}$	236	RT	in-plane
G. Feng, S. Van Dijken, and J.M.D. Coey, Appl. Phys. Lett. **89**, 162501 (2006).	CoFeB/MgO/CoFeB/MgO/CoFeB	105	RT	in-plane
J. Moser, M. Zenger, C. Gerl, D. Schuh, R. Meier, P. Chen, G. Bayreuther, W. Wegscheider, D. Weiss, C.H. Lai, R.T. Huang, M. Kosuth, and H. Ebert, Appl. Phys. Lett. **89**, 162106 (2006).	Fe/GaAs-oxide/Fe	5.6	4.2K	in-plane
T. Ishikawa, T. Marukame, H. Kijima, K.I. Matsuda, T. Uemura, M. Arita, and M. Yamamoto, Appl. Phys. Lett. **89**, 192505 (2006).	$Co_2MnSi/MgO/Co_{50}Fe_{50}$	90	RT	in-plane
		192	4.2K	in-plane
T. Daibou, M. Shinano, M. Hattori, Y. Sakuraba, M. Oogane, Y. Ando, and T. Miyazaki, IEEE Trans. Magn. **42**, 2655 (2006).	$Co_{40}Fe_{40}B_{20}/MgO/Co_2FeSi$	90	RT	in-plane
		189	2K	in-plane
	$Co_{40}Fe_{40}B_{20}/MgO/Co_2MnSi$	30	RT	in-plane
		113	2K	in-plane
S. Mukhopadhyay and I. Das, Phys. Rev. Lett. **96**, 026601 (2006).	$La_{0.67}Sr_{0.33}MnO_3/Ba_2LaNbO_6/LSMO$	-4.6	10K	in-plane
Y. Sakuraba, J. Nakata, M. Oogane, Y. Ando, H. Kato, A. Sakuma, T. Miyazaki, and H. Kubota, Appl. Phys. Lett. **88**, 022503 (2006).	Co_2MnSi/Al-oxide/CoFe	65	RT	in-plane
		83	10K	in-plane
J.M. Almeida, R. Ferreira, P.P. Freitas, J. Langer, B. Ocker, and W. Maass, J. Appl. Phys. **99**, 08B314 (2006).	CoFeB/MgO/CoFeB	130	RT	in-plane
C. Kaiser and S.S.P. Parkin, Appl. Phys. Lett.	CoFe/MgO/CoFe/CoFeGd	-90	RT	in-plane

88, 112511 (2006).				
T.X. Wang, H.X. Wei, Z.M. Zeng, X.F. Han, Z.M. Hong, and G.Q. Shi, Appl. Phys. Lett. **88**, 242505 (2006).	$Co_{60}Fe_{20}B_{20}$/3HDP/$Co_{60}Fe_{20}B_{20}$	20	RT	in-plane
Y. Ishii, H. Yamada, H. Sato, H. Akoh, Y. Ogawa, M. Kawasaki, and Y. Tokura, Appl. Phys. Lett. **89**, 042509 (2006).	LSMO/$LaAlO_3$/LSMO	230	10K	in-plane
Z. Gercsi, A. Rajanikanth, Y.K. Takahashi, K. Hono, M. Kikuchi, N. Tezuka, and K. Inomata, Appl. Phys. Lett. **89**, 082512 (2006).	Co_2FeAl/Al-oxide/$Co_{75}Fe_{25}$	43.6	RT	in-plane
		67.5	5K	in-plane
J.J. Yang, C. Ji, Y.A. Chang, X. Ke, and M.S. Rzchowski, Appl. Phys. Lett. **89**, 202502 (2006).	$Co_{84}Fe_{16}$/Al-oxide/$Co_{84}Fe_{16}$	71.5	RT	in-plane
C. Park, J.G. Zhu, M.T. Moneck, Y. Peng, and D.E. Laughlin, J. Appl. Phys. **99**, 08A901 (2006).	CoFeB/MgO/CoFeB	102	RT	in-plane
X. Kou, J. Schmalhorst, A. Thomas, and G. Reiss, Appl. Phys. Lett. **88**, 212115 (2006).	CoFeB/Mg/MgO/CoFeB	90	RT	in-plane
		139	15K	in-plane
T. Moriyama, C. Ni, W.G. Wang, X. Zhang, and J.Q. Xiao, Appl. Phys. Lett. **88**, 222503 (2006).	FeCo/MgO/FeCo	84	RT	in-plane

TMR_2007

References	**Structures**	**TMR (%)**	T_m	**in-plane or perp.**
T. Marukame and M. Yamamoto, J. Appl. Phys. **101**, 083906 (2007).	$Co_2Cr_{0.6}Fe_{0.4}Al$/MgO/$Co_{50}Fe_{50}$	109	RT	in-plane
		317	4.2K	in-plane
Y.M. Lee, J. Hayakawa, S. Ikeda, F. Matsukura, and H. Ohno, Appl. Phys. Lett. **90**, 212507 (2007).	$(Co_{25}Fe_{75})_{80}B_{20}$/MgO/$(Co_{25}Fe_{75})_{80}B_{20}$	500	RT	in-plane
		1010	5K	in-plane
K. Sunaga, M. Tsunoda, K. Komagaki, Y. Uehara, and M. Takahashi, J. Appl. Phys. **102**, 013917 (2007).	Fe_4N/MgO/CoFeB	-18.5	RT	in-plane
C. Song, X.J. Liu, F. Zeng, and F. Pan, Appl. Phys. Lett. **91**, 042106 (2007).	$Zn_{0.94}Co_{0.06}O$/ZnO/$Zn_{0.94}Co_{0.6}O$	20.8	4K	in-plane
T.S. Santos, J.S. Lee, P. Migdal, I.C. Lekshmi, B. Satpati, and J.S. Moodera, Phys. Rev. Lett. **98**, 016601 (2007).	Co/Al_2O_3/Alq_3/NiFe	4.6	300K	in-plane
		7.5	4.2K	in-plane
N. Tezuka, N. Ikeda, S. Sugimoto, and K. Inomata, Japanese J. Appl. Physics, Part 2 Lett. **46**, L454 (2007).	$Co_2FeAl_{0.5}Si_{0.5}$/MgO/$Co_2FeAl_{0.5}Si_{0.5}$	220	RT	in-plane
		390	5K	in-plane
Y.S. Choi, K. Tsunekawa, Y. Nagamine, and D. Djayaprawira, J. Appl. Phys. **101**, 013907 (2007).	CoFeB/MgO/CoFeB	200	RT	in-plane
H.X. Wei, Q.H. Qin, M. Ma, R. Sharif, and X.F. Han, J. Appl. Phys. **101**, 09B501 (2007).	$Co_{40}Fe_{40}B_{20}$/Al-oxide/$Co_{40}Fe_{40}B_{20}$	81	RT	in-plane
		107	4.2K	in-plane

S. Hakamata, T. Ishikawa, T. Marukame, K.I. Matsuda, T. Uemura, M. Arita, and M. Yamamoto, J. Appl. Phys. **101**, 09J513 (2007).	$Co_2MnGe/MgO/Co_{50}Fe_{50}$	83	RT	in-plane
		185	4.2K	in-plane
P. Padhan, P. Leclair, A. Gupta, K. Tsunekawa, and D.D. Djayaprawira, Appl. Phys. Lett. **90**, 142105 (2007).	$Co_{60}Fe_{20}B_{20}/MgO/Co_{60}Fe_{20}B_{20}$	247	RT	in-plane
Y. Lu, C. Deranlot, A. Vaurs, F. Petroff, J.M. George, Y. Zheng, and D. Demailles, Appl. Phys. Lett. **91**, 222504 (2007).	$Co_{40}Fe_{40}B_{20}/Mg/MgO/Co_{40}Fe_{40}B_{20}$	120	RT	in-plane
		210	3K	in-plane
S. Ikeda, J. Hayakawa, Y.M. Lee, F. Matsukura, and H. Ohno, J. Magn. Magn. Mater. **310**, 1937 (2007).	$Co_{40}Fe_{40}B_{20}/MgO/Co_{40}Fe_{40}B_{20}$	355	RT	in-plane
N. Tezuka, N. Ikeda, A. Miyazaki, S. Okamura, M. Kikuchi, S. Sugimoto, and K. Inomata, J. Magn. Magn. Mater. **310**, 1940 (2007).	$Co_2FeAl_{0.5}Si_{0.5}$/Al-oxide/$Co_{75}Fe_{25}$	76	RT	in-plane
		106	5K	in-plane
Y.S. Choi, Y. Nagamine, K. Tsunekawa, H. Maehara, D.D. Djayaprawira, S. Yuasa, and K. Ando, Appl. Phys. Lett. **90**, 012505 (2007).	CoFeB/MgO/CoFeB	205	RT	in-plane
T. Marukame, T. Ishikawa, S. Hakamata, K.I. Matsuda, T. Uemura, and M. Yamamoto, Appl. Phys. Lett. **90**, 012508 (2007).	$Co_2Cr_{0.6}Fe_{0.4}Al/MgO/Co_{50}Fe_{50}$	109	RT	in-plane
		317	4.2K	in-plane
R. Matsumoto, A. Fukushima, T. Nagahama, Y. Suzuki, K. Ando, and S. Yuasa, Appl. Phys. Lett. **90**, 252506 (2007).	Fe/MgO/Fe	304	20K	in-plane
J. Schmalhorst, A. Thomas, G. Reiss, X. Kou, and E. Arenholz, J. Appl. Phys. **102**, 053907 (2007).	$Co_{40}Fe_{40}B_{20}/Mg/MgO/Co_{40}Fe_{40}B_{20}$	112	RT	in-plane
Z.C. Wen, H.X. Wei, and X.F. Han, Appl. Phys. Lett. **91**, 122511 (2007).	$Co_{60}Fe_{20}B_{20}$/Al-oxide/$Co_{60}Fe_{20}B_{20}$	44	300K	in-plane
A. V. Ramos, M.J. Guittet, J.B. Moussy, R. Mattana, C. Deranlot, F. Petroff, and C. Gatel, Appl. Phys. Lett. **91**, 122107 (2007).	$CoFe_2O_4/Al_2O_3$/Co	-3	RT	in-plane
		-18	2K	in-plane
C. Song, Y.C. Yang, X.W. Li, X.J. Liu, F. Zeng, and F. Pan, Appl. Phys. Lett. **91**, 172109 (2007).	(Zn, Co)O/ZnO/(Zn, Co)O/ZnO/(Zn,Co)O	27.8	5K	in-plane
T. Kado, H. Saito, and K. Ando, J. Appl. Phys. **101**, 09J511 (2007).	$Fe_3O_4/MgO/Co_{75}Fe_{25}$	-14	RT	in-plane
Z. Diao, A. Panchula, Y. Ding, M. Pakala, S. Wang, Z. Li, D. Apalkov, H. Nagai, A. Driskill-Smith, L.C. Wang, E. Chen, and Y. Huai, Appl. Phys. Lett. **90**, 132508 (2007).	CoFeB/MgO/CoFeB/MgO/CoFeB	70	RT	in-plane
D. Mazumdar, X. Liu, B.D. Schrag, M. Carter, W. Shen, and G. Xiao, Appl. Phys. Lett. **91**, 033507 (2007).	$Co_{40}Fe_{40}B_{20}/MgO/Ni_{79}Fe_{21}$	120	RT	in-plane
T. Uemura, T. Marukame, K.I. Matsuda, and M. Yamamoto, IEEE Trans. Magn. **43**, 2791 (2007).	$Co_{50}Fe_{50}/MgO/Co_{50}Fe_{50}$	145	RT	in-plane
H. Kijima, T. Ishikawa, T. Marukame, K.I. Matsuda, T. Uemura, and M. Yamamoto, J. Magn. Magn. Mater. **310**, 2006 (2007).	$Co_2MnSi/MgO/Co_{50}Fe_{50}$	90	RT	in-plane
		192	4.2K	in-plane
D. Mazumdar, X. Liu, B.D. Schrag, W. Shen, M. Carter, and G. Xiao, J. Appl. Phys. **101**, 09B502 (2007).	$Co_{40}Fe_{40}B_{20}/MgO/Co_{40}Fe_{40}B_{20}$	260	RT	in-plane

J.F. Feng, G. Feng, J.M.D. Coey, X.F. Han, and W.S. Zhan, Appl. Phys. Lett. **91**, 102505 (2007).	Ru/CoFeB/MgO/CoFeB	-55	RT	in-plane
R. Guerrero, D. Herranz, F.G. Aliev, F. Greullet, C. Tiusan, M. Hehn, and F. Montaigne, Appl. Phys. Lett. **91**, 132504 (2007).	Fe/Fe-C/MgO/Fe/Co	185	RT	in-plane
		330	4K	in-plane
J. Schmalhorst, A. Thomas, S. Kämmerer, O. Schebaum, D. Ebke, M.D. Sacher, G. Reiss, A. Hütten, A. Turchanin, A. Gölzhäuser, and E. Arenholz, Phys. Rev. B - Condens. Matter Mater. Phys. **75**, 014403 (2007).	Co_2MnSi/Al-oxide/$Co_{70}Fe_{30}$	95	20K	in-plane
A.D. Rata, H. Braak, D.E. Bürgler, and C.M. Schneider, Appl. Phys. Lett. **90**, 162512 (2007).	$Co_2Cr_{0.6}Fe_{0.4}Al$/MgO/$Co_{80}Fe_{20}$	-66	RT	in-plane
		-84	20K	in-plane

TMR_2008

References	**Structures**	**TMR (%)**	T_m	**in-plane or perp.**
G. Kim, Y. Sakuraba, M. Oogane, Y. Ando, and T. Miyazaki, Appl. Phys. Lett. **92**, 172502 (2008).	CoPt/MgO/CoPt	6	RT	perp.
		13	10K	perp.
S. Ikeda, J. Hayakawa, Y. Ashizawa, Y.M. Lee, K. Miura, H. Hasegawa, M. Tsunoda, F. Matsukura, and H. Ohno, Appl. Phys. Lett. **93**, 082508 (2008).	$Co_{20}Fe_{60}B_{20}$/MgO/$Co_{20}Fe_{60}B_{20}$	604	RT	in-plane
		1144	5K	in-plane
S. Tsunegi, Y. Sakuraba, M. Oogane, K. Takanashi, and Y. Ando, Appl. Phys. Lett. **93**, 112506 (2008).	Co_2MnSi/MgO/$Co_{50}Fe_{50}$	217	RT	in-plane
		753	2K	in-plane
M. Yoshikawa, E. Kitagawa, T. Nagase, T. Daibou, M. Nagamine, K. Nishiyama, T. Kishi, and H. Yoda, IEEE Trans. Magn. **44**, 2573 (2008).	FePt/MgO/FePt	120	RT	perp.
A.M. Deac, A. Fukushima, H. Kubota, H. Maehara, Y. Suzuki, S. Yuasa, Y. Nagamine, K. Tsunekawa, D.D. Djayaprawira, and N. Watanabe, Nat. Phys. **4**, 803 (2008).	CoFeB/Mg/MgO/CoFeB	110	RT	in-plane
K. Inomata, M. Wojcik, E. Jedryka, N. Ikeda, and N. Tezuka, Phys. Rev. B - Condens. Matter Mater. Phys. **77**, 214425 (2008).	$Co_2FeSi_{0.5}Al_{0.5}$/MgO/$Co_2FeSi_{0.5}Al_{0.5}$	220	RT	in-plane
S.G. Wang, R.C.C. Ward, G.X. Du, X.F. Han, C. Wang, and A. Kohn, Phys. Rev. B - Condens. Matter Mater. Phys. **78**, 180411(R) (2008).	Fe/MgO/Fe	170	RT	in-plane
		318	10K	in-plane
H. Ohmori, T. Hatori, and S. Nakagawa, J. Appl. Phys. **103**, 07A911 (2008).	GdFeCo/Fe/MgO/Fe/TbFeCo	64	RT	perp.
T. Kado, Appl. Phys. Lett. **92**, 092502 (2008).	Fe_3O_4/MgO/Al_2O_3/CoFe	-26	RT	in-plane
B. Carvello, C. Ducruet, B. Rodmacq, S. Auffret, E. Gautier, G. Gaudin, and B. Dieny, Appl. Phys. Lett. **92**, 102508 (2008).	[Co/Pt]/$Co_{90}Fe_{10}$/Al-oxide/[Co/Pt]	8	RT	perp.
W.G. Wang, C. Ni, A. Rumaiz, Y. Wang, X. Fan, T. Moriyama, R. Cao, Q.Y. Wen, H.W.	CoFeB/MgO/CoFeB	230	RT	in-plane

Zhang, and J.Q. Xiao, Appl. Phys. Lett. **92**, 152501 (2008).				
W. Wang, H. Sukegawa, R. Shan, and K. Inomata, Appl. Phys. Lett. **93**, 182504 (2008).	$Co_2FeAl_{0.5}Si_{0.5}$/MgO/$Co_2FeAl_{0.5}Si_{0.5}$	125	RT	in-plane
		196	7K	in-plane
S. Isogami, M. Tsunoda, K. Komagaki, K. Sunaga, Y. Uehara, M. Sato, T. Miyajima, and M. Takahashi, Appl. Phys. Lett. **93**, 192109 (2008).	CoFeB/MgO/CoFeB	206	RT	in-plane
T. Niizeki, N. Tezuka, and K. Inomata, Phys. Rev. Lett. **100**, 047207 (2008).	Fe/MgO/Fe	190	RT	in-plane
X.J. Bai, J. Du, J. Zhang, B. You, L. Sun, W. Zhang, X.S. Wu, S.L. Tang, A. Hu, H.N. Hu, and S.M. Zhou, J. Appl. Phys. **103**, 07F305 (2008).	FeCoGd/Al-oxide/FeCo	-6	RT	in-plane
C. Ducruet, B. Carvello, B. Rodmacq, S. Auffret, G. Gaudin, and B. Dieny, J. Appl. Phys. **103**, 07A918 (2008).	[Co/Pt]*3/Co/Al-oxide/CoFe/Pt/Co/Pt	8	RT	perp.
J.H. Park, C. Park, T. Jeong, M.T. Moneck, N.T. Nufer, and J.G. Zhu, J. Appl. Phys. **103**, 07A917 (2008).	[Co/Pt]*4/Co/Al-oxide/[Co/Pt]*2	15	RT	perp.
F. Greullet, E. Snoeck, C. Tiusan, M. Hehn, D. Lacour, O. Lenoble, C. Magen, and L. Calmels, Appl. Phys. Lett. **92**, 053508 (2008).	Fe/Fe_3O_4/MgO/Co	-8.5	300K	in-plane
		-22	80K	in-plane
T. Ishikawa, S. Hakamata, K.I. Matsuda, T. Uemura, and M. Yamamoto, J. Appl. Phys. **103**, 07A919 (2008).	Co_2MnSi/MgO/Co_2MnSi	179	RT	in-plane
		683	4.2K	in-plane
W. Wang, H. Sukegawa, R. Shan, and K. Inomata, Appl. Phys. Lett. **93**, 122506 (2008).	$Co_2FeAl_{0.5}Si_{0.5}$/MgO/$Co_2FeAl_{0.5}Si_{0.5}$	150	RT	in-plane
		312	7K	in-plane
M. Hattori, Y. Sakuraba, M. Oogane, Y. Ando, and T. Miyazaki, Appl. Phys. Express **1**, 021301 (2008).	Co_2MnSi(110)/Mg/Al-oxide/$Co_{75}Fe_{25}$	40	RT	in-plane
		120	2K	in-plane
S. Matsunaga, J. Hayakawa, S. Ikeda, K. Miura, H. Hasegawa, T. Endoh, H. Ohno, and T. Hanyu, Appl. Phys. Express **1**, 091301 (2008).	$Co_{40}Fe_{40}B_{20}$/MgO/$Co_{40}Fe_{40}B_{20}$	70	RT	in-plane
M. Nakayama, T. Kai, N. Shimomura, M. Amano, E. Kitagawa, T. Nagase, M. Yoshikawa, T. Kishi, S. Ikegawa, and H. Yoda, J. Appl. Phys. **103**, 07A710 (2008).	TbCoFe/CoFeB/MgO/CoFeB/TbCoFe	15	RT	perp.
D. Halley, H. Majjad, M. Bowen, N. Najjari, Y. Henry, C. Ulhaq-Bouillet, W. Weber, G. Bertoni, J. Verbeeck, and G. Van Tendeloo, Appl. Phys. Lett. **92**, 212115 (2008).	Fe/Cr/MgO/Fe	6	RT	in-plane
G.X. Miao, Y.J. Park, J.S. Moodera, M. Seibt, G. Eilers, and M. Münzenberg, Phys. Rev. Lett. **100**, 246803 (2008).	Fe/MgO/Fe	130	RT	in-plane
		195	1K	in-plane
W. Shen, B.D. Schrag, M.J. Carter, J. Xie, C. Xu, S. Sun, and G. Xiao, J. Appl. Phys. **103**, 07A306 (2008).	$Co_{40}Fe_{40}B_{20}$/MgO/$Co_{40}Fe_{40}B_{20}$	97	RT	in-plane
J.M. Almeida, P. Wisniowski, and P.P. Freitas, J. Appl. Phys. **103**, 07E922 (2008).	CoFeB/MgO/CoFeB	160	RT	in-plane

X. Yao, H. Meng, Y. Zhang, and J.P. Wang, J. Appl. Phys. **103**, 07A717 (2008).	CoFe/Al-oxide/CoFe	16.5	RT	in-plane
J.J. Yang, A.K. Bengtson, C.X. Ji, D. Morgan, and Y.A. Chang, J. Appl. Phys. **103**, 056102 (2008).	CoFe/Al-oxide/CoFe	47.4	RT	in-plane
C. Yoshida, M. Kurasawa, Y.M. Lee, M. Aoki, and Y. Sugiyama, Appl. Phys. Lett. **92**, 113508 (2008).	CoFeB/MgO/CoFeB	110	RT	in-plane
D. Mazumdar, W. Shen, X. Liu, B.D. Schrag, M. Carter, and G. Xiao, J. Appl. Phys. **103**, 113911 (2008).	$Co_{40}Fe_{40}B_{20}$/MgO/$Ni_{79}Fe_{21}$	140	RT	in-plane
M. Zhu, M.J. Wilson, P. Mitra, P. Schiffer, and N. Samarth, Phys. Rev. B - Condens. Matter Mater. Phys. **78**, 195307 (2008).	GaMnAs/GaAs/GaMnAs	40	4.2K	in-plane
H. Saito, A. Yamamoto, S. Yuasa, and K. Ando, Appl. Phys. Lett. **93**, 172515 (2008).	Fe/Ga-oxide/$Ga_{0.95}Mn_{0.05}As$	58	6K	in-plane

TMR_2009

References	**Structures**	**TMR (%)**	T_m	**in-plane or perp.**
G. Chen, F. Zeng, and F. Pan, Appl. Phys. Lett. **95**, 232508 (2009).	CoFeB/MgO/CoFeB	230	RT	in-plane
	CoFeB/MgO/CoFeB/MgO/CoFeB	120	RT	in-plane
Y. Komasaki, M. Tsunoda, S. Isogami, and M. Takahashi, J. Appl. Phys. **105**, 07C928 (2009).	Fe_4N/MgO/CoFeB	-75.1	RT	in-plane
N. Tezuka, N. Ikeda, F. Mitsuhashi, and S. Sugimoto, Appl. Phys. Lett. **94**, 162504 (2009).	$Co_2FeAl_{0.5}Si_{0.5}$/MgO/$Co_2FeAl_{0.5}Si_{0.5}$	386	300K	in-plane
		832	9K	in-plane
W. Wang, H. Sukegawa, R. Shan, S. Mitani, and K. Inomata, Appl. Phys. Lett. **95**, 182502 (2009).	Co_2FeAl/MgO/CoFe	330	RT	in-plane
		700	10K	in-plane
G. Szulczewski, H. Tokuc, K. Oguz, and J.M.D. Coey, Appl. Phys. Lett. **95**, 202506 (2009).	CoFeB/MgO/Alq_3/Co	16	RT	in-plane
	CoFe/Al-oxide/Alq_3/CoFe	13	RT	in-plane
T. Ishikawa, H.X. Liu, T. Taira, K.I. Matsuda, T. Uemura, and M. Yamamoto, Appl. Phys. Lett. **95**, 232512 (2009).	Co_2MnSi/MgO/Co_2MnSi	236	RT	in-plane
		1135	4.2K	in-plane
M. Oogane, M. Shinano, Y. Sakuraba, and Y. Ando, J. Appl. Phys. **105**, 07C903 (2009).	Co_2FeSi/Al-oxide/CoFe	48	RT	in-plane
		80	2K	in-plane
D. Meyners, T. Von Hofe, M. Vieth, M. Rührig, S. Schmitt, and E. Quandt, J. Appl. Phys. **105**, 07C914 (2009).	CoFeB/MgO/CoFeB	160	RT	in-plane
A. Reinartz, J. Schmalhorst, and G. Reiss, J. Appl. Phys. **105**, 014510 (2009).	CoFeB/MgO/CoFeB/MgO/CoFeB/CoFe	87	RT	in-plane
	CoFeB/MgO/CoFeB	124	RT	in-plane
J.C. Read, J.J. Cha, W.F. Egelhoff, H.W. Tseng, P.Y. Huang, Y. Li, D.A. Muller, and R.A. Buhrman, Appl. Phys. Lett. **94**, 112504	$Fe_{60}Co_{20}B_{20}$/MgBO/$Ni_{65}Fe_{15}B_{20}$	155	RT	in-plane

(2009).				
T. Miyajima, T. Ibusuki, S. Umehara, M. Sato, S. Eguchi, M. Tsukada, and Y. Kataoka, Appl. Phys. Lett. **94**, 122501 (2009).	CoFeB/MgO/CoFeB	138	RT	in-plane
S. Tsunegi, Y. Sakuraba, M. Oogane, H. Naganuma, K. Takanashi, and Y. Ando, Appl. Phys. Lett. **94**, 252503 (2009).	Co_2MnSi/CoFeB/MgO/CoFe	222	310K	in-plane
		510	10K	in-plane
J. Cao, J. Kanak, T. Stobiecki, P. Wisniowski, and P.P. Freitas, IEEE Trans. Magn. **45**, 3464 (2009).	CoFeB/MgO/CoFeB	290	RT	in-plane
S. Tsunegi, Y. Sakuraba, M. Oogane, N.D. Telling, L.R. Shelford, E. Arenholz, G. Van Der Laan, R.J. Hicken, K. Takanashi, and Y. Ando, J. Phys. D. Appl. Phys. **42**, 195004 (2009).	Co_2MnSi/MgO/CoFe	217	RT	in-plane
		753	2K	in-plane
K. Oguz and J.M.D. Coey, J. Magn. Magn. Mater. **321**, 1009 (2009).	$Co_{40}Fe_{40}B_{20}/SrTiO_3/Co_{40}Fe_{40}B_{20}$	2	RT	in-plane
C. Herbort, E.A. Jorge, and M. Jourdan, Appl. Phys. Lett. **94**, 142504 (2009).	$Co_2Cr_{0.6}Fe_{0.4}$Al/Al-oxide/$Co_{70}Fe_{30}$	101	4K	in-plane
J.J. Cha, J.C. Read, W.F. Egelhoff, P.Y. Huang, H.W. Tseng, Y. Li, R.A. Buhrman, and D.A. Muller, Appl. Phys. Lett. **95**, 032506 (2009).	CoFeB/MgBO/CoFeB	200	RT	in-plane
P. Krzysteczko, G. Reiss, and A. Thomas, Appl. Phys. Lett. **95**, 112508 (2009).	$Co_{66}Fe_{22}B_{12}$/MgO/$Co_{66}Fe_{22}B_{12}$	100	RT	in-plane
Y. Ohdaira, M. Oogane, and Y. Ando, J. Appl. Phys. **105**, 07C920 (2009).	Co_2MnSi/Al-oxide/Co_2MnSi	25	RT	in-plane
		320	6K	in-plane
G.X. Miao and J.S. Moodera, Appl. Phys. Lett. **94**, 182504 (2009).	EuS/Al_2O_3/EuS	50	1K	in-plane
S. Ohya, I. Muneta, P.N. Hai, and M. Tanaka, Appl. Phys. Lett. **95**, 242593 (2009).	GaMnAs/GaAs/AlMnAs/GaAs/GaMnAs	175	2.6K	in-plane
V. Drewello, M. Schäfers, O. Schebaum, A.A. Khan, J. Münchenberger, J. Schmalhorst, G. Reiss, and A. Thomas, Phys. Rev. B - Condens. Matter Mater. Phys. **79**, 174417 (2009).	CoFeB/MgO/CoFeB	230	RT	in-plane
		345	13K	in-plane
J.M. Almeida and P.P. Freitas, J. Appl. Phys. **105**, 07E722 (2009).	CoFeB/MgO/CoFeB	210	RT	in-plane
T. Ibusuki, T. Miyajima, S. Umehara, S. Eguchi, and M. Sato, Appl. Phys. Lett. **94**, 062509 (2009).	CoFeB/MgO/CoFeB	130	RT	in-plane
G. Chen, F. Zeng, and F. Pan, Appl. Phys. Lett. **95**, 232508 (2009).	(Zn,Co)O/MgO/(Zn,Co)O	46.8	4K	in-plane
I.J. Shin, B.C. Min, J.P. Hong, and K.H. Shin, IEEE Trans. Magn. **45**, 2393 (2009).	CoFeB/MgO/CoFeB	150.9	RT	in-plane
F. Bonell, S. Andrieu, F. Bertran, P. Lefevre, A.T. Ibrahimi, E. Snoeck, C.V. Tiusan, and F. Montaigne, IEEE Trans. Magn. **45**, 3467 (2009).	$Fe_{0.8}V_{0.2}$/MgO/Fe	200	RT	in-plane
Q.L. Ma, S.G. Wang, J. Zhang, Y. Wang, R.C.C. Ward, C. Wang, A. Kohn, X.G. Zhang, and X.F. Han, Appl. Phys. Lett. **95**, 052506 (2009).	Fe/MgO/Fe	318	4.2K	in-plane

TMR_2010

References	Structures	TMR (%)	T_m	in-plane or perp.
S. Ikeda, K. Miura, H. Yamamoto, K. Mizunuma, H.D. Gan, M. Endo, S. Kanai, J. Hayakawa, F. Matsukura, and H. Ohno, Nat. Mater. **9**, 721 (2010).	CoFeB/MgO/CoFeB	120	RT	perp.
D. Ebke, P. Thomas, O. Schebaum, M. Schäfers, D. Nissen, V. Drewello, A. Hütten, and A. Thomas, J. Magn. Magn. Mater. **322**, 996 (2010).	Co_2FeAl/MgO/CoFe	147	RT	in-plane
		273	13K	in-plane
C. Barraud, C. Deranlot, P. Seneor, R. Mattana, B. Dlubak, S. Fusil, K. Bouzehouane, D. Deneuve, F. Petroff, and A. Fert, Appl. Phys. Lett. **96**, 072502 (2010).	Co/Al_2O_3/Co	12.5	RT	in-plane
H.D. Gan, S. Ikeda, W. Shiga, J. Hayakawa, K. Miura, H. Yamamoto, H. Hasegawa, F. Matsukura, T. Ohkubo, K. Hono, and H. Ohno, Appl. Phys. Lett. **96**, 192507 (2010).	$Co_{40}Fe_{40}B_{20}$/MgO/$Co_{50}Fe_{50}$/$Co_{40}Fe_{40}B_{20}$/MgO/$Co_{40}Fe_{40}B_{20}$	212	RT	in-plane
H. Sukegawa, H. Xiu, T. Ohkubo, T. Furubayashi, T. Niizeki, W. Wang, S. Kasai, S. Mitani, K. Inomata, and K. Hono, Appl. Phys. Lett. **96**, 212505 (2010).	Fe/$MgAl_2O_4$/Fe	117	RT	in-plane
		165	15K	in-plane
T. Moriyama, T.J. Gudmundsen, P.Y. Huang, L. Liu, D.A. Muller, D.C. Ralph, and R.A. Buhrman, Appl. Phys. Lett. **97**, 072513 (2010).	[Co/Ni]*2/$Fe_{60}Co_{20}B_{20}$/MgO/$Fe_{60}Co_{20}B_{20}$	106	RT	in-plane
K. Mizunuma, S. Ikeda, H. Yamamoto, H.D. Gan, K. Miura, H. Hasegawa, J. Hayakawa, K. Ito, F. Matsukura, and H. Ohno, Jpn. J. Appl. Phys. **49**, 04DM04 (2010).	[$Co_{90}Fe_{10}$/Pd]*3/$Co_{20}Fe_{60}B_{20}$/MgO/$Co_{20}Fe_{60}B_{20}$/[Pd/$Co_{90}Fe_{10}$]*10	91	RT	perp.
W. Wang, H. Sukegawa, and K. Inomata, Phys. Rev. B - Condens. Matter Mater. Phys. **82**, 092402 (2010).	Co_2FeAl/MgO/CoFe	330	RT	in-plane
		700	10K	in-plane
F. Bonell, S. Andrieu, C. Tiusan, F. Montaigne, E. Snoeck, B. Belhadji, L. Calmels, F. Bertran, P. Le Fèvre, and A. Taleb-Ibrahimi, Phys. Rev. B - Condens. Matter Mater. Phys. **82**, 092405 (2010).	FeV/MgO/Fe	240	RT	in-plane
Z.R. Tadisina, A. Natarajarathinam, B.D. Clark, A.L. Highsmith, T. Mewes, S. Gupta, E. Chen, and S. Wang, J. Appl. Phys. **107**, 09C703 (2010).	[Co/Pd]*9/CoFeB/MgO/CoFeB/[Co/Pd]*4	10	RT	perp.
		10	10K	perp.
A. Lyle, J. Harms, S. Patil, X. Yao, D.J. Lilja, and J.P. Wang, Appl. Phys. Lett. **97**, 152504 (2010).	$Co_{60}Fe_{20}B_{20}$/MgO/$Co_{60}Fe_{20}B_{20}$	50	RT	in-plane
K. Yakushiji, T. Saruya, H. Kubota, A. Fukushima, T. Nagahama, S. Yuasa, and K. Ando, Appl. Phys. Lett. **97**, 232508 (2010).	[Co/Pt]*4/$Co_{60}Fe_{20}B_{20}$/MgO/$Co_{70}Fe_{30}$/$Co_{60}Fe_{20}B_{20}$/TbFeCo	62	RT	perp.
W. Wang, E. Liu, M. Kodzuka, H. Sukegawa, M. Wojcik, E. Jedryka, G.H. Wu, K. Inomata, S. Mitani, and K. Hono, Phys. Rev. B - Condens. Matter Mater. Phys. **81**, 140402(R) (2010).	Co_2FeAl/MgO/CoFe	340	RT	in-plane

H. Kurt, K. Oguz, T. Niizeki, and J.M.D. Coey, J. Appl. Phys. **107**, 083920 (2010).	$Co_{40}Fe_{40}B_{20}$/MgO/$Co_{40}Fe_{40}B_{20}$	240	RT	in-plane
		312	25K	in-plane
W. Skowroński, T. Stobiecki, J. Wrona, K. Rott, A. Thomas, G. Reiss, and S. Van Dijken, J. Appl. Phys. **107**, 093917 (2010).	CoFeB/MgO/CoFeB	170	RT	in-plane
Z. Diao, J.F. Feng, H. Kurt, G. Feng, and J.M.D. Coey, Appl. Phys. Lett. **96**, 202506 (2010).	$Co_{40}Fe_{40}B_{20}$/MgO/$Co_{40}Fe_{40}B_{20}$	240	RT	in-plane
G.M. Choi, B.C. Min, and K.H. Shin, Appl. Phys. Lett. **97**, 202503 (2010).	$Co_{72}Pt_{28}$/$Co_{40}Fe_{40}B_{20}$/MgO/$Fe_{40}Pd_{40}B_{20}$/MgO/$Co_{40}Fe_{40}B_{20}$/Pt	6.8	RT	perp.
J.F. Feng, Z. Diao, G. Feng, E.R. Nowak, and J.M.D. Coey, Appl. Phys. Lett. **96**, 052504 (2010).	CoFeB/MgO/CoFeB	168	RT	in-plane
O. Schebaum, D. Ebke, A. Niemeyer, G. Reiss, J.S. Moodera, and A. Thomas, J. Appl. Phys. **107**, 09C717 (2010).	Co_2FeAl/MgO/CoFe	153	RT	in-plane
Y. Wang, W.X. Wang, H.X. Wei, B.S. Zhang, W.S. Zhan, and X.F. Han, J. Appl. Phys. **107**, 09C711 (2010).	[Co/Pt]*6/Co/Al-oxide/[Co/Pt]*3	14.7	RT	perp.
Y.M. Chang, K.S. Li, H. Huang, M.J. Tung, S.Y. Tong, and M.T. Lin, J. Appl. Phys. **107**, 093904 (2010).	CoFe/Al_2O_3/CoFe	30.67	RT	in-plane
J. Wrona, J. Langer, B. Ocker, W. Maass, J. Kanak, T. Stobiecki, and W. Powroźnik, J. Phys. Conf. Ser. **200**, 052032 (2010).	$Co_{40}Fe_{40}B_{20}$/MgO/$Co_{40}Fe_{40}B_{20}$	96	RT	in-plane
L.X. Jiang, H. Naganuma, M. Oogane, K. Fujiwara, T. Miyazaki, K. Sato, T.J. Konno, S. Mizukami, and Y. Ando, J. Phys. Conf. Ser. **200**, 052009 (2010).	CoFeB/MgO/CoFe/MgO/CoFeB	-30	RT	in-plane
J. Cao and P.P. Freitas, J. Appl. Phys. **107**, 09E712 (2010).	$Co_{40}Fe_{40}B_{20}$/MgO/$Co_{40}Fe_{40}B_{20}$	45	RT	in-plane
G.M. Choi, I.J. Shin, B.C. Min, and K.H. Shin, J. Appl. Phys. **108**, 073913 (2010).	CoPt/Co/Ru/Co/CoFeB/MgO/CoFeB/Pt	-2	300K	perp.
		-4	10K	perp.
	CoPt/CoFeB/MgO/CoFeB/Pt	10	300K	perp.
		22	10K	perp.
J. Bernos, M. Hehn, F. Montaigne, C. Tiusan, D. Lacour, M. Alnot, B. Negulescu, G. Lengaigne, E. Snoeck, and F.G. Aliev, Phys. Rev. B - Condens. Matter Mater. Phys. **82**, 060405(R) (2010).	CoFeB/MgO/CoFeB	150	RT	in-plane
K. Yakushiji, K. Noma, T. Saruya, H. Kubota, A. Fukushima, T. Nagahama, S. Yuasa, and K. Ando, Appl. Phys. Express **3**, 053003 (2010).	[Co/Pt]*6/CoFeB/CoFe/MgO/CoFe/CoFeB/TbFeCo	97	RT	perp.
Q.L. Ma, J.F. Feng, G. Feng, K. Oguz, X.F. Han, and J.M.D. Coey, J. Magn. Magn. Mater. **322**, 108 (2010).	$Ni_{81}Fe_{19}$/$Fe_{50}Mn_{50}$/$Co_{90}Fe_{10}$/Ru/CoFeB/MgO/CoFeB	-57	RT	in-plane
S. Bandiera, R.C. Sousa, Y. Dahmane, C. Ducruet, C. Portemont, V. Baltz, S. Auffret, I.L. Prejbeanu, and B. Dieny, IEEE Magn. Lett. **1**, 3000204 (2010).	Pt/[Co/Pt]*5/Co/Ru/[Co/Pt]*3/Co/CoFeB/Al-oxide/CoFe/[Pt/Co]*2/Pt	6	RT	perp.
W.G. Wang, C. Ni, G.X. Miao, C. Weiland,	CoFe/IrMn/CoFe/Ru/CoFeB/MgO/	290	RT	in-plane

L.R. Shah, X. Fan, P. Parson, J. Jordan-Sweet, X.M. Kou, Y.P. Zhang, R. Stearrett, E.R. Nowak, R. Opila, J.S. Moodera, and J.Q. Xiao, Phys. Rev. B - Condens. Matter Mater. Phys. **81**, 144406 (2010).	CoFeB			

TMR_2011

References	**Structures**	**TMR (%)**	T_m	**in-plane or perp.**
Z. Wen, H. Sukegawa, S. Mitani, and K. Inomata, Appl. Phys. Lett. **98**, 192595 (2011).	$Co_2FeAl/MgO/Co_{50}Fe_{50}$	166	RT	in-plane
		252	48K	in-plane
W.G. Wang, S. Hageman, M. Li, S. Huang, X. Kou, X. Fan, J.Q. Xiao, and C.L. Chien, Appl. Phys. Lett. **99**, 102502 (2011).	$Co_{40}Fe_{40}B_{20}/MgO/Co_{40}Fe_{40}B_{20}$	111	RT	in-plane
T. Kubota, M. Araidai, S. Mizukami, X. Zhang, Q. Ma, H. Naganuma, M. Oogane, Y. Ando, M. Tsukada, and T. Miyazaki, Appl. Phys. Lett. **99**, 192509 (2011).	$Mn_{62}Ga_{38}/MgO/CoFe$	23	10K	perp.
H.D. Gan, H. Sato, M. Yamanouchi, S. Ikeda, K. Miura, R. Koizumi, F. Matsukura, and H. Ohno, Appl. Phys. Lett. **99**, 252507 (2011).	$Co_{20}Fe_{60}B_{20}/MgO/Co_{20}Fe_{60}B_{20}$	149	RT	perp.
		280	10K	perp.
H. Maehara, K. Nishimura, Y. Nagamine, K. Tsunekawa, T. Seki, H. Kubota, A. Fukushima, K. Yakushiji, K. Ando, and S. Yuasa, Appl. Phys. Express **4**, 033002 (2011).	$Co_{60}Fe_{20}B_{20}/MgO/Co_{60}Fe_{20}B_{20}$	178	RT	in-plane
K. Mizunuma, M. Yamanouchi, S. Ikeda, H. Sato, H. Yamamoto, H.D. Gan, K. Miura, J. Hayakawa, F. Matsukura, and H. Ohno, Appl. Phys. Express **4**, 023002 (2011).	$Pd/[Co_{90}Fe_{10}/Pd]*4/Co_{20}Fe_{60}B_{20}/MgO/Co_{20}Fe_{60}B_{20}/[Pd/Co_{90}Fe_{10}]*10/Pd$	101	RT	perp.
O. Schebaum, V. Drewello, A. Auge, G. Reiss, M. Mnzenberg, H. Schuhmann, M. Seibt, and A. Thomas, J. Magn. Magn. Mater. **323**, 1525 (2011).	CoFeB/MgO/CoFeB	323	RT	in-plane
	$CoFeB/Al_2O_3/CoFeB/NiFe$	73	RT	in-plane
K. Mizunuma, S. Ikeda, H. Sato, M. Yamanouchi, H.D. Gan, K. Miura, H. Yamamoto, J. Hayakawa, F. Matsukura, and H. Ohno, J. Appl. Phys. **109**, 07C711 (2011).	$Pd/[Co_{90}Fe_{10}/Pd]*4/CoFeB/MgO/CoFeB/[Pd/Co_{90}Fe_{10}]*10/Pd$	120	RT	perp.
T. Kubota, S. Mizukami, D. Watanabe, F. Wu, X. Zhang, H. Naganuma, M. Oogane, Y. Ando, and T. Miyazaki, J. Appl. Phys. **110**, 013915 (2011).	$D0_{22}$-$Mn_{2.4}Ga/Mg/MgO/CoFe$	5	RT	perp.
		15	10K	perp.
		-5	RT	perp.
		-12	10K	perp.
H. Meng, W.H. Lum, R. Sbiaa, S.Y.H. Lua, and H.K. Tan, J. Appl. Phys. **110**, 033904 (2011).	$Co_{40}Fe_{40}B_{20}/MgO/Co_{40}Fe_{40}B_{20}$	72	RT	perp.
M.A. Tanaka, T. Hori, K. Mibu, K. Kondou, T. Ono, S. Kasai, T. Asaka, and J. Inoue, J. Appl. Phys. **110**, 073905 (2011).	$Fe/MgO/Co_2MnSn$	-3	RT	in-plane
		4	20K	in-plane
H. Meng, R. Sbiaa, C.C. Wang, S.Y.H. Lua, and M.A.K. Akhtar, J. Appl. Phys. **110**,	$Co_{40}Fe_{40}B_{20}/MgO/Co_{40}Fe_{40}B_{20}$	82	RT	perp.

103915 (2011).				
H. Gan, S. Ikeda, M. Yamanouchi, K. Miura, K. Mizunuma, J. Hayakawa, F. Matsukura, and H. Ohno, IEEE Trans. Magn. **47**, 1567 (2011).	CoFeB/MgO/CoFeB/MgO/CoFeB	200	RT	in-plane
T. Kubota, Y. Miura, D. Watanabe, S. Mizukami, F. Wu, H. Naganuma, X. Zhang, M. Oogane, M. Shirai, Y. Ando, and T. Miyazaki, Appl. Phys. Express **4**, 043002 (2011).	$D0_{22}$-$Mn_{2.4}Ga$/Mg/MgO/CoFe	9.8	300K	perp.
		22.1	10K	perp.
A. Lyle, A. Klemm, J. Harms, Y. Zhang, H. Zhao, and J.P. Wang, Appl. Phys. Lett. **98**, 092502 (2011).	$Co_{40}Fe_{40}B_{20}$/MgO/$Co_{60}Fe_{20}B_{20}$	100	RT	in-plane
R. Werner, A.Y. Petrov, L.A. Miño, R. Kleiner, D. Koelle, and B.A. Davidson, Appl. Phys. Lett. **98**, 162595 (2011).	$La_{0.65}Sr_{0.35}MnO_3$/$SrTiO_3$/$La_{0.65}Sr_{0.35}MnO_3$	1904	4K	in-plane
D.K. Schreiber, Y.S. Choi, Y. Liu, A.N. Chiaramonti, D.N. Seidman, and A.K. Petford-Long, Appl. Phys. Lett. **98**, 232506 (2011).	$Co_{60}Fe_{20}B_{20}$/$Co_{90}Fe_{10}$/MgO/$Co_{10}Fe_{90}$/$Co_{60}Fe_{20}B_{20}$	192	RT	in-plane
H. Sato, M. Yamanouchi, K. Miura, S. Ikeda, H.D. Gan, K. Mizunuma, R. Koizumi, F. Matsukura, and H. Ohno, Appl. Phys. Lett. **99**, 042501 (2011).	$Co_{20}Fe_{60}B_{20}$/MgO/$Co_{20}Fe_{60}B_{20}$	130	RT	perp.
E. Ozawa, S. Tsunegi, M. Oogane, H. Naganuma, and Y. Ando, J. Phys. Conf. Ser. **266**, 012104 (2011).	Co_2MnSi/Co_2MnAl/MgO/$Co_{50}Fe_{50}$	180	310K	in-plane
		600	10K	in-plane
Q.L. Ma, S.G. Wang, H.X. Wei, H.F. Liu, X.G. Zhang, and X.F. Han, Phys. Rev. B - Condens. Matter Mater. Phys. **83**, 224430 (2011).	$Co_{40}Fe_{40}B_{20}$/MgO/$Co_{40}Fe_{40}B_{20}$	140	RT	in-plane
		210	5K	in-plane
Z.M. Zeng, P. Khalili Amiri, G. Rowlands, H. Zhao, I.N. Krivorotov, J.P. Wang, J.A. Katine, J. Langer, K. Galatsis, K.L. Wang, and H.W. Jiang, Appl. Phys. Lett. **98**, 072512 (2011).	CoFeB/MgO/CoFeB	150	RT	in-plane
G.Q. Yu, Z. Diao, J.F. Feng, H. Kurt, X.F. Han, and J.M.D. Coey, Appl. Phys. Lett. **98**, 112504 (2011).	$Co_{40}Fe_{40}B_{20}$/MgO/$Co_{50}Fe_{50}$/CoFeB/MgO/CoFeB	250	RT	in-plane
D.K. Schreiber, Y.S. Choi, Y. Liu, A.N. Chiaramonti, D.N. Seidman, and A.K. Petford-Long, J. Appl. Phys. **109**, 103909 (2011).	$Co_{60}Fe_{20}B_{20}$/MgO/$Co_{60}Fe_{20}B_{20}$	100	RT	in-plane
M. Da Silva, K. Dumesnil, C. Dufour, M. Hehn, D. Pierre, D. Lacour, F. Montaigne, G. Lengaigne, and S. Robert, Appl. Phys. Lett. **98**, 232504 (2011).	$SmGdAl_2$/Al-oxide/[Co/Pt]*5	0.2	20K	perp.
G.Q. Yu, L. Chen, S. Rizwan, J.H. Zhao, K. Xu, and X.F. Han, Appl. Phys. Lett. **98**, 262501 (2011).	(Ga, Mn)As/Al-oxide/$Co_{40}Fe_{40}B_{20}$	101	2K	in-plane
W.X. Wang, Y. Yang, H. Naganuma, Y. Ando, R.C. Yu, and X.F. Han, Appl. Phys. Lett. **99**, 012502 (2011).	$Co_{40}Fe_{40}B_{20}$/MgO/$Co_{40}Fe_{40}B_{20}$	16.2	RT	perp.
		31.3	50K	perp.
S. Amara-Dababi, R.C. Sousa, M. Chshiev, H. Béa, J. Alvarez-Hérault, L. Lombard, I.L. Prejbeanu, K. MacKay, and B. Dieny, Appl. Phys. Lett. **99**, 083501 (2011).	CoFeB/MgO/CoFeB	130	RT	in-plane

Z.M. Zeng, P. Upadhyaya, P. Khalili Amiri, K.H. Cheung, J.A. Katine, J. Langer, K.L. Wang, and H.W. Jiang, Appl. Phys. Lett. **99**, 032503 (2011).	$Co_{40}Fe_{40}B_{20}$/MgO/$Co_{40}Fe_{40}B_{20}$	120	RT	in-plane
Y. Ohdaira, M. Oogane, H. Naganuma, and Y. Ando, Appl. Phys. Lett. **99**, 132513 (2011).	Co_2MnSi/MgO/Co_2MnSi	50	RT	in-plane
		193	6K	in-plane
H. Liu, S. Rizwan, D. Liu, S. Wang, and X. Han, IEEE Trans. Magn. **47**, 2716 (2011).	CoFeB/MgAlO/CoFeB	65	RT	in-plane
X. Liu, W. Zhang, M.J. Carter, and G. Xiao, J. Appl. Phys. **110**, 033910 (2011).	$Co_{50}Fe_{50}$/IrMn/$Co_{50}Fe_{50}$/Ru/$Co_{40}Fe_{40}B_{20}$/MgO/$Co_{40}Fe_{40}B_{20}$	200	RT	in-plane
H. Yang, S.H. Yang, D.C. Qi, A. Rusydi, H. Kawai, M. Saeys, T. Leo, D.J. Smith, and S.S.P. Parkin, Phys. Rev. Lett. **106**, 167201 (2011).	CoFe/MgO/NiO/CoFe	60	2.8K	in-plane
		37	RT	in-plane
Y. Shiota, S. Murakami, F. Bonell, T. Nozaki, T. Shinjo, and Y. Suzuki, Appl. Phys. Express **4**, 043005 (2011).	$Fe_{80}Co_{20}$/MgO/Fe	15.2	RT	in-plane

TMR_2012

References	**Structures**	**TMR (%)**	T_m	**in-plane or perp.**
M. Kodzuka, T. Ohkubo, K. Hono, S. Ikeda, H.D. Gan, and H. Ohno, J. Appl. Phys. **111**, 043913 (2012).	CoFeB/MgO/CoFeB	347	RT	in-plane
J.Y. Chen, J.F. Feng, and J.M.D. Coey, Appl. Phys. Lett. **100**, 142407 (2012).	$Co_{40}Fe_{40}B_{20}$/MgO/$Co_{40}Fe_{40}B_{20}$	255	RT	in-plane
Q.L. Ma, T. Kubota, S. Mizukami, X.M. Zhang, H. Naganuma, M. Oogane, Y. Ando, and T. Miyazaki, Appl. Phys. Lett. **101**, 032402 (2012).	$Mn_{62}Ga_{38}$/Co/Mg/MgO/CoFeB	40	RT	perp.
		80	5K	perp.
H.X. Liu, Y. Honda, T. Taira, K. Matsuda, M. Arita, T. Uemura, and M. Yamamoto, Appl. Phys. Lett. **101**, 132418 (2012).	Co_2MnSi/MgO/Co_2MnSi	354	290K	in-plane
		1995	4.2K	in-plane
S. Ikeda, R. Koizumi, H. Sato, M. Yamanouchi, K. Miura, K. Mizunuma, H. Gan, F. Matsukura, and H. Ohno, IEEE Trans. Magn. **48**, 3829 (2012).	CoFeB/MgO/CoFeB	136	RT	perp.
T. Kubota, Q. Ma, S. Mizukami, X. Zhang, H. Naganuma, M. Oogane, Y. Ando, and T. Miyazaki, Appl. Phys. Express **5**, 043003 (2012).	$L1_0$-$Mn_{62}Ga_{38}$/Fe/MgO/CoFe	24	RT	perp.
W.G. Wang, M. Li, S. Hageman, and C.L. Chien, Nat. Mater. **11**, 64 (2012).	CoFeB/MgO/CoFeB	118	RT	perp.
H. Sukegawa, Y. Miura, S. Muramoto, S. Mitani, T. Niizeki, T. Ohkubo, K. Abe, M. Shirai, K. Inomata, and K. Hono, Phys. Rev. B - Condens. Matter Mater. Phys. **86**, 184401 (2012).	FeCo/Mg/MgAl-oxide/FeCo	308	RT	in-plane
		479	15K	in-plane
A. Zaleski, J. Wrona, M. Czapkiewicz, W. Skowroski, J. Kanak, and T. Stobiecki, J. Appl. Phys. **111**, 033903 (2012).	$Co_{40}Fe_{40}B_{20}$/MgO/$Co_{40}Fe_{40}B_{20}$	200	RT	in-plane

M.A. Tanaka, Y. Ishikawa, Y. Wada, S. Hori, A. Murata, S. Horii, Y. Yamanishi, K. Mibu, K. Kondou, T. Ono, and S. Kasai, J. Appl. Phys. **111**, 053902 (2012).	Fe/MgO/Co_2FeSn	43.5	RT	in-plane
		72.2	2K	in-plane
S. He, H. Bai, G. Liu, Q. Li, S. Yan, Y. Chen, L. Mei, H. Liu, S. Wang, and X. Han, Appl. Phys. Lett. **100**, 132406 (2012).	ZnO:Co/ZnO:Mg/ZnO:Co	85.6	5K	in-plane
H. Sato, M. Yamanouchi, S. Ikeda, S. Fukami, F. Matsukura, and H. Ohno, Appl. Phys. Lett. **101**, 022414 (2012).	CoFeB/MgO/CoFeB/Ta/CoFeB/MgO	97	RT	perp.
S. Kanai, M. Yamanouchi, S. Ikeda, Y. Nakatani, F. Matsukura, and H. Ohno, Appl. Phys. Lett. **101**, 122403 (2012).	CoFeB/MgO/CoFeB	150	RT	perp.
T. Harada, I. Ohkubo, M. Lippmaa, Y. Sakurai, Y. Matsumoto, S. Muto, H. Koinuma, and M. Oshima, Adv. Funct. Mater. **22**, 4471 (2012).	$LaNiO_3/SrTiO_3/Pr_{0.8}Ca_{0.2}MnCoO_3/La_{0.6}Sr_{0.4}MnO_3$	120	4K	in-plane
W. Lin, M. Hehn, L. Chaput, B. Negulescu, S. Andrieu, F. Montaigne, and S. Mangin, Nat. Commun. **3**, 744 (2012).	$Co_{90}Fe_{10}/Al_2O_3/Co_{90}Fe_{10}$	40	RT	in-plane
D. Pantel, S. Goetze, D. Hesse, and M. Alexe, Nat. Mater. **11**, 289 (2012).	$Co/PbZr_{0.2}Ti_{0.8}O_3/La_{0.7}Sr_{0.3}MnO_3$	-9	10K	in-plane
N. Tezuka, F. Mitsuhashi, and S. Sugimoto, J. Appl. Phys. **111**, 07C718 (2012).	$Co_2FeAl_{0.5}Si_{0.5}$/Al-oxide/$Co_{75}Fe_{25}$	73	RT	in-plane
		103	5K	in-plane
N. Liebing, S. Serrano-Guisan, K. Rott, G. Reiss, J. Langer, B. Ocker, and H.W. Schumacher, J. Appl. Phys. **111**, 07C520 (2012).	CoFeB/MgO/CoFeB	140	RT	in-plane
H. Meng, R. Sbiaa, M.A.K. Akhtar, R.S. Liu, V.B. Naik, and C.C. Wang, Appl. Phys. Lett. **100**, 122405 (2012).	$Co_{40}Fe_{40}B_{20}/MgO/Co_{40}Fe_{40}B_{20}$	50	RT	perp.
V.B. Naik, H. Meng, and R. Sbiaa, AIP Adv. **2**, 042182 (2012).	CoFeB/MgO/CoFeB/Ta/[Co/Pd]*15	40	RT	perp.
J.Y. Chen, N. Carroll, J.F. Feng, and J.M.D. Coey, Appl. Phys. Lett. **101**, 262402 (2012).	$Co_{40}Fe_{40}B_{20}/MgO/Co_{40}Fe_{40}B_{20}$	198	RT	in-plane
S.W. Chun, D. Kim, J. Kwon, B. Kim, S. Choi, and S.B. Lee, J. Appl. Phys. **111**, 07C722 (2012).	CoFeB/MgO/CoFeB	13	RT	perp.
E.M.J. Hassen, B. Viala, M.C. Cyrille, M. Cartier, O. Redon, P. Lima, B. Belhadji, H.X. Yang, J. Velev, and M. Chshiev, J. Appl. Phys. **111**, 07C727 (2012).	CoFeB/$SrTiO_3$/CoFeB	13	RT	in-plane
S. Joo, K.Y. Jung, B.C. Lee, T.S. Kim, K.H. Shin, M.H. Jung, K.J. Rho, J.H. Park, J. Hong, and K. Rhie, Appl. Phys. Lett. **100**, 172406 (2012).	$Co_{84}Fe_{16}/Co_{84}Fe_{16}$-oxide/Al-oxide/$Co_{84}Fe_{16}$	31	300K	in-plane
H. Sato, M. Yamanouchi, K. Miura, S. Ikeda, R. Koizumi, F. Matsukura, and H. Ohno, IEEE Magn. Lett. **3**, 3000204 (2012).	$Co_{20}Fe_{60}B_{20}/MgO/Co_{20}Fe_{60}B_{20}$	100	RT	perp.
F. Ren, A. Jander, P. Dhagat, and C. Nordman, IEEE Trans. Nucl. Sci. **59**, 3034 (2012).	CoFeB/MgO/CoFeB	68	RT	in-plane
Z.Q. Lei, L. Li, G.J. Li, C.W. Leung, J. Shi, C.M. Wong, K.C. Lo, W.K. Chan, C.S.K. Mak, S.B. Chan, N.M.M. Chan, C.H. Leung,	CoFeB/MgO/CoFeB	122	RT	in-plane

P.T. Lai, and P.W.T. Pong, J. Appl. Phys. **111**, 07E505 (2012).				
J.Z. Sun, P.L. Trouilloud, M.J. Gajek, J. Nowak, R.P. Robertazzi, G. Hu, D.W. Abraham, M.C. Gaidis, S.L. Brown, E.J. O'Sullivan, W.J. Gallagher, and D.C. Worledge, J. Appl. Phys. **111**, 07C711 (2012).	CoFeB/MgO/Fe/CoFeB/Ta/Co/Pt/[Co/Pd]*4/Co/Ru/[Co/Pd]*14	60.5	RT	perp.
A. Natarajarathinam, R. Zhu, P.B. Visscher, and S. Gupta, J. Appl. Phys. **111**, 07C918 (2012).	CoFeB/MgO/CoFeB/Ta/[Co/Pd]*5/Co/Ru/[Co/Pd]*9	40	RT	perp.
H. Yang, S.H. Yang, and S. Parkin, AIP Adv. **2**, 012150 (2012).	CoFe/CoFeB/Mg/MgO/CoFe/CoFeB	500	5K	in-plane
C. Song, Y.Y. Wang, X.J. Li, G.Y. Wang, and F. Pan, Appl. Phys. Lett. **101**, 062404 (2012).	Pd/[Co/Pd]*4/Co/MgO/Co/MgO/Co/[Pd/Co]*4/Pd	9.3	RT	perp.
	Pd/[Co/Pd]*4/Co/MgO/Co/Pd	6.8	RT	perp.
Q.L. Ma, T. Kubota, S. Mizukami, X.M. Zhang, M. Oogane, H. Naganuma, Y. Ando, and T. Miyazaki, IEEE Trans. Magn. **48**, 2808 (2012).	$L1_0$-MnGa/Co/MgO/CoFeB	41	RT	perp.
F. Dahmani, Jpn. J. Appl. Phys. **51**, 043002 (2012).	NiFe/IrMn/CoFe/MgO/CoFeB	211	RT	in-plane
H. Sukegawa, Z. Wen, K. Kondou, S. Kasai, S. Mitani, and K. Inomata, Appl. Phys. Lett. **100**, 182403 (2012).	Co_2FeAl/Mg/MgO/CoFeB	25	RT	in-plane
H. Kurt, K. Rode, H. Tokuc, P. Stamenov, M. Venkatesan, and J.M.D. Coey, Appl. Phys. Lett. **101**, 232402 (2012).	ε-Mn_3Ga/$Co_{90}Fe_{10}$/Ru/CoFeB/MgO/CoFeB	150	RT	in-plane
A. Petraru, R. Soni, and H. Kohlstedt, Phys. Status Solidi - Rapid Res. Lett. **6**, 138 (2012).	$La_{0.7}Sr_{0.3}MnO_3$/$BaTiO_3$/$SrTiO_3$/$La_{0.7}Sr_{0.3}MnO_3$	110	77K	in-plane

TMR_2013

References	**Structures**	**TMR (%)**	T_m	**in-plane or perp.**
A. Tavassolizadeh, T. Meier, K. Rott, G. Reiss, E. Quandt, H. Hölscher, and D. Meyners, Appl. Phys. Lett. **102**, 153104 (2013).	CoFeB/MgO/CoFeB	121	RT	in-plane
Y.P. Wang, G.C. Han, H. Lu, J. Qiu, Q.J. Yap, R. Ji, and K.L. Teo, J. Appl. Phys. **114**, 013910 (2013).	Fe_2CrSi/Mg/MgO/CoFe	2.5	RT	in-plane
K. Yoshida, I. Hamada, S. Sakata, A. Umeno, M. Tsukada, and K. Hirakawa, Nano Lett. **13**, 481 (2013).	Ni/C_{60}/Ni	-80	0.3K	in-plane
T. Nozaki, H. Kubota, A. Fukushima, and S. Yuasa, Appl. Phys. Express **6**, 053005 (2013).	Fe/MgO/γ-Fe_2O_3/Fe	270	20K	in-plane
		120	RT	in-plane
B. Li, G.X. Miao, and J.S. Moodera, Phys. Rev. B - Condens. Matter Mater. Phys. **88**, 161105(R) (2013).	EuS/Al/Al_2O_3/Co/CoO	36	1K	in-plane

H. Saruyama, M. Oogane, Y. Kurimoto, H. Naganuma, and Y. Ando, Jpn. J. Appl. Phys. **52**, 063003 (2013).	MnAl/CoFe/MgO/CoFe/Ta	2.1	RT	in-plane
Y. Wang, X. Yin, D. Le Roy, J. Jiang, H.X. Wei, S.H. Liou, and X.F. Han, J. Appl. Phys. **113**, 133906 (2013).	[Co/Pt]*10/Co/CoFeB/Al-oxide/CoFeB/Co/[Pt/Co]*10	32	RT	perp.
M. Yamanouchi, L. Chen, J. Kim, M. Hayashi, H. Sato, S. Fukami, S. Ikeda, F. Matsukura, and H. Ohno, Appl. Phys. Lett. **102**, 212408 (2013).	CoFeB/MgO/CoFeB	31	RT	in-plane
C. Klewe, M. Meinert, J. Schmalhorst, and G. Reiss, J. Phys. Condens. Matter **25**, 076001 (2013).	Mn_2VGa/MgO/CoFe	-1.8	RT	in-plane
T. Kubota, Q.L. Ma, S. Mizukami, X.M. Zhang, H. Naganuma, M. Oogane, Y. Ando, and T. Miyazaki, J. Phys. D. Appl. Phys. **46**, 155001 (2013).	$L1_0$-$Mn_{62}Ga_{38}$/Fe/Mg/MgO/$Co_{50}Fe_{50}$	24	RT	perp.
		30	10K	perp.
X. Liu and J. Shi, Appl. Phys. Lett. **102**, 202401 (2013).	$La_{0.7}Sr_{0.3}MnO_3$/Al_2O_3/Co	30	25K	in-plane
N. Liebing, S. Serrano-Guisan, P. Krzysteczko, K. Rott, G. Reiss, J. Langer, B. Ocker, and H.W. Schumacher, Appl. Phys. Lett. **102**, 242413 (2013).	CoFeB/MgO/CoFeB	140	RT	in-plane
H. Sukegawa, S. Mitani, T. Ohkubo, K. Inomata, and K. Hono, Appl. Phys. Lett. **103**, 142409 (2013).	CoFe/MgAlO/CoFe	185	RT	in-plane
C. Sterwerf, M. Meinert, J.M. Schmalhorst, and G. Reiss, IEEE Trans. Magn. **49**, 4386 (2013).	$Fe_{1.75}Co_{1.25}Si$/MgO/$Co_{70}Fe_{30}$/$Mn_{83}Fe_{17}$	262	15K	in-plane
		159	RT	in-plane
D. Kato, M. Oogane, K. Fujiwara, T. Nishikawa, H. Naganuma, and Y. Ando, Appl. Phys. Express **6**, 103004 (2013).	CoFeSiB/Ru/CoFeB/MgO/CoFeB	234	RT	in-plane
J.P. Cascales, D. Herranz, J.L. Sambricio, U. Ebels, J.A. Katine, and F.G. Aliev, Appl. Phys. Lett. **102**, 092404 (2013).	CoFeB/MgO/CoFe/CoFeB	40	RT	in-plane
L. Cuchet, B. Rodmacq, S. Auffret, R.C. Sousa, C. Ducruet, and B. Dieny, Appl. Phys. Lett. **103**, 052402 (2013).	Pt/[Co/Pt]*5/Co/Ta/$Co_{60}Fe_{20}B_{20}$/MgO/$Fe_{72}Co_8B_{20}$	65	RT	perp.
T. Devolder, K. Garcia, G. Agnus, M. Manfrini, S. Cornelissen, and T. Min, Appl. Phys. Lett. **103**, 182402 (2013).	CoFeB/MgO/Fe/CoFeB/Ta/[Co/Pd]*5/Co/Ru/[Co/Pd]*14	64	RT	perp.
M. Arikan, S. Ingvarsson, M. Carter, and G. Xiao, IEEE Trans. Magn. **49**, 5469 (2013).	CoFeB/MgO/CoFeB	89.5	RT	in-plane
K. Yamane, Y. Higo, H. Uchida, Y. Nanba, S. Sasaki, H. Ohmori, K. Bessho, and M. Hosomi, IEEE Trans. Magn. **49**, 4335 (2013).	CoFeB-based/MgO/CoFeB-based	120	RT	perp.
S. Amara-Dababi, H. Béa, R.C. Sousa, C. Baraduc, and B. Dieny, Appl. Phys. Lett. **102**, 052404 (2013).	CoFeB/MgO/CoFeB	130	RT	in-plane
Q. Ma, S. Mizukami, T. Kubota, X. Zhang, A. Sugihara, H. Naganuma, M. Oogane, Y. Ando, and T. Miyazaki, J. Appl. Phys. **114**, 163913 (2013).	$Mn_{62}Ga_{38}$/Fe/Co/MgO/CoFeB	-50	RT	perp.
C. Kaiser, D. Maddex, M. Pakala, and Q. Leng, Appl. Phys. Lett. **103**, 232404 (2013).	CoFeB/CoFe/MgO/CoFe/CoFeB	60	RT	in-plane
W. Skowroński, P. Ogrodnik, J. Wrona, T. Stobiecki, R. Świrkowicz, J. Barnaś, G.	CoFeB/MgO/CoFeB	170	RT	in-plane

Reiss, and S. Van Dijken, J. Appl. Phys. **114**, 233905 (2013).				
Y.J. Chang, A. Canizo-Cabrera, V. Garcia-Vazquez, Y.H. Chang, and T.H. Wu, J. Appl. Phys. **113**, 17B909 (2013).	CoFeB/MgO/CoFeB/Ta/[Co/Pd]*5/Co/Ru/[Co/Pd]*12	10.2	RT	perp.
A. Rajanikanth, T. Hauet, F. Montaigne, S. Mangin, and S. Andrieu, Appl. Phys. Lett. **103**, 062402 (2013).	Fe/MgO/Fe/Co	5	RT	in-plane
D.L. Li, J.F. Feng, G.Q. Yu, P. Guo, J.Y. Chen, H.X. Wei, X.F. Han, and J.M.D. Coey, J. Appl. Phys. **114**, 213909 (2013).	CoFeB/MgO/CoFe/CoFeB/MgO/CoFeB	215	300K	in-plane
V. Sokalski, D.M. Bromberg, M.T. Moneck, E. Yang, and J.G. Zhu, IEEE Trans. Magn. **49**, 4383 (2013).	FeCoB/MgO/FeCoB	138	RT	perp.
G. Hu, T. Topuria, P.M. Rice, J. Jordan-Sweet, and D.C. Worledge, IEEE Magn. Lett. **4**, 3000104 (2013).	CoFeB/MgO/Fe/CoFeB/Ta/[Co/Pd]*4/Ru/[Co/Pd]*8	98.5	RT	perp.
Y. Fujita, S. Yamada, G. Takemoto, S. Oki, Y. Maeda, M. Miyao, and K. Hamaya, Jpn. J. Appl. Phys. **52**, 04CM02 (2013).	$Co_{60}Fe_{40}$/Al-oxide/Fe_3Si	20	RT	in-plane
A. Kalitsov, P.J. Zermatten, F. Bonell, G. Gaudin, S. Andrieu, C. Tiusan, M. Chshiev, and J.P. Velev, J. Phys. Condens. Matter **25**, 496005 (2013).	Fe/O/MgO/Fe	115	RT	in-plane

TMR_2014

References	**Structures**	**TMR (%)**	T_m	**in-plane or perp.**
T. Nagahama, Y. Matsuda, K. Tate, T. Kawai, N. Takahashi, S. Hiratani, Y. Watanabe, T. Yanase, and T. Shimada, Appl. Phys. Lett. **105**, 102410 (2014).	NiO/Fe_3O_4/Al_2O_3/Fe/Co	-12	RT	in-plane
Z. Wen, H. Sukegawa, T. Furubayashi, J. Koo, K. Inomata, S. Mitani, J.P. Hadorn, T. Ohkubo, and K. Hono, Adv. Mater. **26**, 6483 (2014).	Co_2FeAl/MgO/Fe/CoFeB	132	RT	perp.
		237	10K	perp.
Z. Wen, H. Sukegawa, S. Kasai, K. Inomata, and S. Mitani, Phys. Rev. Appl. **2**, 024009 (2014).	Co_2FeAl/MgO/CoFe	175	RT	in-plane
T. Kubota, S. Mizukami, Q.L. Ma, H. Naganuma, M. Oogane, Y. Ando, and T. Miyazaki, J. Appl. Phys. **115**, 17C704 (2014).	$Mn_{2.6}Ga_{1.4}$/MgO/CoFeB	8	RT	perp.
	$Mn_{2.3}Co_{0.4}Ga_{1.3}$/MgO/CoFeB	5	RT	perp.
	$Mn_{1.8}Co_{1.2}Ga_{1.0}$/MgO/CoFeB	11	RT	perp.
Y.P. Wang, G.C. Han, H. Lu, J. Qiu, Q.J. Yap, and K.L. Teo, J. Appl. Phys. **115**, 17C709 (2014).	$Fe_2Cr_{0.3}Co_{0.7}Si$/Mg/MgO/CoFe	28	RT	in-plane
Y.K. Liu, Y.W. Yin, S.N. Dong, S.W. Yang, T. Jiang, and X.G. Li, Appl. Phys. Lett. **104**, 043507 (2014).	$La_{0.6}Sr_{0.4}MnO_3$/BiFeO/$La_{0.6}Sr_{0.4}MnO_3$	3.4	10K	in-plane
H. Sato, E.C.I. Enobio, M. Yamanouchi, S. Ikeda, S. Fukami, S. Kanai, F. Matsukura, and H. Ohno, Appl. Phys. Lett. **105**, 062403 (2014).	CoFeB/MgO/CoFeB	125	RT	perp.

T. Hashimoto, S. Kamikawa, D. Soriano, J.G. Pedersen, S. Roche, and J. Haruyama, Appl. Phys. Lett. **105**, 183111 (2014).	ferromagnetic graphen/SiO_2/Co	20	1.5K	in-plane
E. Paz, S. Serrano-Guisan, R. Ferreira, and P.P. Freitas, J. Appl. Phys. **115**, 17E501 (2014).	CoFeB/MgO/CoFeB	170	RT	in-plane
S. Ishikawa, H. Sato, M. Yamanouchi, S. Ikeda, S. Fukami, F. Matsukura, and H. Ohno, J. Appl. Phys. **115**, 17C719 (2014).	[Co/Pt]based multi layer/MgO/CoFeB	105	RT	perp.
D.C. Worledge, G. Hu, D.W. Abraham, P.L. Trouilloud, and S. Brown, J. Appl. Phys. **115**, 172601 (2014).	CoFeB/MgO/Fe/CoFeB/Ta/[Co/Pd] *10	40	RT	perp.
T. Scheike, H. Sukegawa, T. Furubayashi, Z. Wen, K. Inomata, T. Ohkubo, K. Hono, and S. Mitani, Appl. Phys. Lett. **105**, 242407 (2014).	CoFe/Co2FeAl/CoFe/MgAlO/CoFe	228	RT	in-plane
		398	5K	in-plane
J.H. Jeong, T. Endoh, Y. Kim, W.K. Kim, and S.O. Park, J. Appl. Phys. **115**, 17C727 (2014).	CoFeB/MgO/CoFeB	103	RT	perp.
H. Kinjo, K. Machida, K. Matsui, K.I. Aoshima, D. Kato, K. Kuga, H. Kikuchi, and N. Shimidzu, J. Appl. Phys. **115**, 203903 (2014).	$Tb_{24}Fe_{62}Co_{14}$/$Co_{20}Fe_{80}$/MgO/$Co_{20}Fe_{80}$/Gd/$Gd_{22}Fe_{78}$	7	RT	perp.
A. Neggache, T. Hauet, F. Bertran, P. Le Fevre, S. Petit-Watelot, T. Devolder, P. Ohresser, P. Boulet, C. Mewes, S. Maat, J.R. Childress, and S. Andrieu, Appl. Phys. Lett. **104**, 252412 (2014).	Fe/MgO/$Co_{1.5}Fe_{1.5}Ge$	125	RT	in-plane
		220	15K	in-plane
V.B. Naik, H. Meng, J.X. Xiao, R.S. Liu, A. Kumar, K.Y. Zeng, P. Luo, and S. Yap, Appl. Phys. Lett. **105**, 052403 (2014).	CoFeB/MgO/CoFeB	108	RT	perp.
S. Kanai, M. Gajek, D.C. Worledge, F. Matsukura, and H. Ohno, Appl. Phys. Lett. **105**, 242409 (2014).	CoFeB/MgO/CoFeB	133	RT	perp.
B. Bhusan Singh and S. Chaudhary, J. Appl. Phys. **115**, 083904 (2014).	CoFe/Mg/MgO/NiFe	0.94	300K	in-plane
		6.88	25K	in-plane
B.S. Tao, D.L. Li, Z.H. Yuan, H.F. Liu, S.S. Ali, J.F. Feng, H.X. Wei, X.F. Han, Y. Liu, Y.G. Zhao, Q. Zhang, Z.B. Guo, and X.X. Zhang, Appl. Phys. Lett. **105**, 102407 (2014).	CoFeB/$MgAl_2O_4$/CoFeB	36	300K	perp.
		63	10K	perp.
P. Li, A. Chen, D. Li, Y. Zhao, S. Zhang, L. Yang, Y. Liu, M. Zhu, H. Zhang, and X. Han, Adv. Mater. **26**, 4320 (2014).	CoFeB/Al-oxide/CoFeB	45	RT	in-plane
L.M. Loong, X. Qiu, Z.P. Neo, P. Deorani, Y. Wu, C.S. Bhatia, M. Saeys, and H. Yang, Sci. Rep. **4**, 6505 (2014).	CoFeB/MgO/CoFeB	270	RT	in-plane
M. Cubukcu, O. Boulle, M. Drouard, K. Garello, C. Onur Avci, I. Mihai Miron, J. Langer, B. Ocker, P. Gambardella, and G. Gaudin, Appl. Phys. Lett. **104**, 042406 (2014).	$Fe_{60}Co_{20}B_{20}$/MgO/$Fe_{60}Co_{20}B_{20}$	90	RT	perp.
D.W. Guo, F.A. Cardoso, R. Ferreira, E. Paz, S. Cardoso, and P.P. Freitas, J. Appl. Phys. **115**, 17E513 (2014).	IrMn/$Co_{70}Fe_{30}$/Ru/$Co_{20}Fe_{40}B_{20}$/MgO/$Co_{20}Fe_{40}B_{20}$/Ta/NiFe	159	RT	in-plane
F.A. Cardoso, L. Rosado, R. Ferreira, E. Paz, S. Cardoso, P.M. Ramos, M. Piedade, and P.P. Freitas, J. Appl. Phys. **115**, 17E516 (2014).	IrMn/CoFe/Ru/CoFeB/MgO/CoFeB/Ta/NiFe	155	RT	in-plane

S. Joo, K.Y. Jung, K.I. Jun, D.S. Kim, K.H. Shin, J.K. Hong, B.C. Lee, and K. Rhie, Appl. Phys. Lett. **104**, 152407 (2014).	NiFe/IrMn/$Co_{84}Fe_{16}$/FeZr/$Co_{84}Fe_{16}$/Al_2O_3/$Co_{84}Fe_{16}$/NiFe	25	RT	in-plane
B. Tao, D. Li, H. Liu, H. Wei, J. Feng, S. Wang, and X. Han, IEEE Trans. Magn. **50**, 4401004 (2014).	CoFeB/$MgAl_2O_4$/CoFeB/CoFe	53	RT	in-plane
T. Yoo, S. Lee, X. Liu, J.K. Furdyna, D.U. Lee, and E.K. Kim, IEEE Trans. Magn. **50**, 4401104 (2014).	GaMnAs/AlGaAs/Fe	8	4K	in-plane
Z. Yang, Q. Zhan, X. Zhu, Y. Liu, H. Yang, B. Hu, J. Shang, L. Pan, B. Chen, and R.W. Li, EPL (Europhysics Lett.) **108**, 58004 (2014).	Co/ZnO/Fe	18.7	10K	in-plane
J.W. Koo, H. Sukegawa, S. Kasai, Z.C. Wen, and S. Mitani, J. Phys. D. Appl. Phys. **47**, 322001 (2014).	Fe/MgO/CoFeB	95	RT	perp.

TMR_2015

References	**Structures**	**TMR (%)**	T_m	**in-plane or perp.**
A. Tavassolizadeh, P. Hayes, K. Rott, G. Reiss, E. Quandt, and D. Meyners, J. Magn. Magn. Mater. **384**, 308 (2015).	CoFeB/MgO/CoFeB	198	RT	in-plane
L. Marnitz, K. Rott, S. Niehörster, C. Klewe, D. Meier, S. Fabretti, M. Witziok, A. Krampf, O. Kuschel, T. Schemme, K. Kuepper, J. Wollschläger, A. Thomas, G. Reiss, and T. Kuschel, AIP Adv. **5**, 047103 (2015).	Fe_3O_4/MgO/CoFeB	-12	RT	in-plane
H. Almasi, D.R. Hickey, T. Newhouse-Illige, M. Xu, M.R. Rosales, S. Nahar, J.T. Held, K.A. Mkhoyan, and W.G. Wang, Appl. Phys. Lett. **106**, 182406 (2015).	CoFeB/MgO/CoFeB	162	RT	perp.
B. Fang, X. Zhang, B.S. Zhang, Z.M. Zeng, and J.W. Cai, AIP Adv. **5**, 067116 (2015).	CoFeB/MgO/CoFeB	120	RT	perp.
J. Swerts, S. Mertens, T. Lin, S. Couet, Y. Tomczak, K. Sankaran, G. Pourtois, W. Kim, J. Meersschaut, L. Souriau, D. Radisic, S. Van Elshocht, G. Kar, and A. Furnemont, Appl. Phys. Lett. **106**, 262407 (2015).	CoFeB/MgO/CoFeB	160	RT	perp.
M.S. Jeon, K.S. Chae, D.Y. Lee, Y. Takemura, S.E. Lee, T.H. Shim, and J.G. Park, Nanoscale **7**, 8142 (2015).	CoFeB/MgO/CoFeB	104	RT	perp.
A. Dankert, M. Venkata Kamalakar, A. Wajid, R.S. Patel, and S.P. Dash, Nano Res. **8**, 1357 (2015).	$Ni_{80}Fe_{20}$/h-BN/Co	0.5	300K	in-plane
B. Prasad, W. Zhang, J. Jian, H. Wang, and M.G. Blamire, Adv. Mater. **27**, 3079 (2015).	$LaNiO_3$/$Sm_{0.75}Sr_{0.25}MnO_3$/$SrTiO_3$/$La_{0.7}Sr_{0.3}MnO_3$	115	5K	in-plane
Y.W. Yin, M. Raju, W.J. Hu, J.D. Burton, Y.M. Kim, A.Y. Borisevich, S.J. Pennycook, S.M. Yang, T.W. Noh, A. Gruverman, X.G. Li, Z.D. Zhang, E.Y. Tsymbal, and Q. Li, J. Appl. Phys. **117**, 172601 (2015).	$La_{0.7}Ca_{0.3}MnO_3$/$Ba_{0.5}Sr_{0.5}TiO_3$/$La_{0.7}Ca_{0.3}MnO_3$	300	4.2K	in-plane
H. Liu, R. Wang, P. Guo, Z. Wen, J. Feng, H.	CoFeB/MgO/CoFeB	128	RT	perp.

Wei, X. Han, Y. Ji, and S. Zhang, Sci. Rep. **5**, 18269 (2015).		293	2K	perp.
A. Sugihara, K. Suzuki, T. Miyazaki, and S. Mizukami, Jpn. J. Appl. Phys. **54**, 078002 (2015).	CoFe/Mg/MgO/CoFe/Mn_3Ge	11.3	RT	perp.
J. Ruan, X. Qiu, Z. Yuan, D. Ji, P. Wang, A. Li, and D. Wu, Appl. Phys. Lett. **107**, 232902 (2015).	$La_{0.7}Sr_{0.3}Mn_{0.8}Ru_{0.2}O_3$/$SrTiO_3$/$BaTiO_3$/$La_{0.7}Sr_{0.3}MnO_3$	30	10K	in-plane
Y.P. Wang, S. Ter Lim, G.C. Han, and K.L. Teo, J. Appl. Phys. **118**, 233906 (2015).	Fe_2CrSi/Mg/MgO/CoFe/CoFeB	51.3	RT	perp.
I. Lytvynenko, C. Deranlot, S. Andrieu, and T. Hauet, J. Appl. Phys. **117**, 053906 (2015).	Pt/Co/[Ni/Co]*3/Al_2O_3/[Co/Ni]*3/Pt/[Co/Pt]*3	8	RT	perp.
		16	20K	perp.
J. Lee, D.I. Suh, and W. Park, J. Appl. Phys. **117**, 17D717 (2015).	CoFeB/MgO/CoFeB	41	RT	in-plane
Y.S. Gui, Y. Xiao, L.H. Bai, S. Hemour, Y.P. Zhao, D. Houssameddine, K. Wu, H. Guo, and C.M. Hu, Appl. Phys. Lett. **106**, 152403 (2015).	CoFe/Ru/CoFeB/CoFe/MgO/CoFeB	62	RT	in-plane
N. Teichert, A. Boehnke, A. Behler, B. Weise, A. Waske, and A. Hütten, Appl. Phys. Lett. **106**, 192401 (2015).	$Ni_{52}Mn_{34}Sn_{14}$/CoFeB/MgO/CoFeB	30	RT	in-plane
		30	10K	in-plane
N. Takahashi, T. Kawai, T. Yanase, T. Shimada, and T. Nagahama, Jpn. J. Appl. Phys. **54**, 118003 (2015).	Fe/MgO/CoFe/Pt/$CoFe_2O_4$	74	RT	in-plane
M. Belmoubarik, M. Al-Mahdawi, H. Sato, T. Nozaki, and M. Sahashi, Appl. Phys. Lett. **106**, 252403 (2015).	$Co_{0.3}Pt_{0.7}$/$Mg_{0.23}Zn_{0.77}O$/Co	35.5	2K	in-plane
T.M. Nakatani and J.R. Childress, J. Appl. Phys. **117**, 243908 (2015).	$Co_{50}Fe_{50}$/IZO/$Co_{50}Fe_{50}$	5.5	RT	in-plane
E. Hirayama, S. Kanai, J. Ohe, H. Sato, F. Matsukura, and H. Ohno, Appl. Phys. Lett. **107**, 132404 (2015).	$Co_{18.75}Fe_{56.25}B_{25}$/MgO/$Co_{18.75}Fe_{56.25}B_{25}$	120	RT	perp.
M. Gottwald, J.J. Kan, K. Lee, X. Zhu, C. Park, and S.H. Kang, Appl. Phys. Lett. **106**, 032413 (2015).	CoFeB/MgO/CoFeB	150	RT	perp.
G. Yang, D.L. Li, S.G. Wang, Q.L. Ma, S.H. Liang, H.X. Wei, X.F. Han, T. Hesjedal, R.C.C. Ward, A. Kohn, A. Elkayam, N. Tal, and X.G. Zhang, J. Appl. Phys. **117**, 083904 (2015).	$L1_0$-FePt/MgO/FePt	21	300K	perp.
		53	10K	perp.
Y.C. Lee, C.T. Chao, L.C. Li, Y.W. Suen, L. Horng, T.H. Wu, C.R. Chang, and J.C. Wu, J. Appl. Phys. **117**, 17A320 (2015).	CoFeB/MgO/CoFeB	27	RT	perp.
K.S. Chae and J.G. Park, J. Appl. Phys. **117**, 153901 (2015).	$Co_2Fe_6B_2$/MgO/Fe/$Co_2Fe_6B_2$/Ta/Co/Pt/[Co/Pd]*7/Co/Ru/Co/[Co/Pd]*9	120	RT	perp.
T. Nakano, M. Oogane, H. Naganuma, and Y. Ando, IEEE Trans. Magn. **51**, 4005104 (2015).	IrMn/CoFe/Ru/CoFeB/MgO/CoFeB/Ta	167	RT	in-plane
K. Zhang, Y.L. Cao, Y.W. Fang, Q. Li, J. Zhang, C.G. Duan, S.S. Yan, Y.F. Tian, R. Huang, R.K. Zheng, S.S. Kang, Y.X. Chen, G.L. Liu, and L.M. Mei, Nanoscale **7**, 6334 (2015).	Co/CoO/ZnO/Co	68	5K	in-plane
R. Galceran, L. Balcells, C. Martinez-Boubeta, B. Bozzo, J. Cisneros-Fernández,	$La_{0.7}Sr_{0.3}MnO_3$/MgO/Fe	25	70K	in-plane

M. De La Mata, C. Magén, J. Arbiol, J. Tornos, F.A. Cuellar, Z. Sefrioui, A. Cebollada, F. Golmar, L.E. Hueso, F. Casanova, J. Santamaría, and B. Martinez, Phys. Rev. B - Condens. Matter Mater. Phys. **92**, 094428 (2015).				
H.M. Yau, Z.B. Yan, N.Y. Chan, K. Au, C.M. Wong, C.W. Leung, F.Y. Zhang, X.S. Gao, and J.Y. Dai, Sci. Rep. **5**, 12826 (2015).	$NiFe/BaTiO_3/La_{0.7}Sr_{0.3}MnO_3$	0.3	8K	in-plane
Y. Takemura, D.Y. Lee, S.E. Lee, K.S. Chae, T.H. Shim, G. Lian, M. Kim, and J.G. Park, Nanotechnology **26**, 195702 (2015).	CoFeB/MgO/CoFeB/Ta/Co/Pt/[Co/Pd]*7/Co/Ru/Co/[Co/Pd]*9	70	RT	perp.
H.X. Liu, T. Kawami, K. Moges, T. Uemura, M. Yamamoto, F. Shi, and P.M. Voyles, J. Phys. D. Appl. Phys. **48**, 164001 (2015).	$Co_{50}Fe_{50}/Co_2Mn_{1.24}Fe_{0.16}Si_{0.84}/MgO/Co_2Mn_{1.24}Fe_{0.16}Si_{0.84}/Co_{50}Fe_{50}/Ir_{22}Mn_{78}$	429	RT	in-plane
		2610	4.2K	in-plane

TMR_2016

References	**Structures**	**TMR (%)**	T_m	**in-plane or perp.**
C. Grezes, F. Ebrahimi, J.G. Alzate, X. Cai, J.A. Katine, J. Langer, B. Ocker, P. Khalili Amiri, and K.L. Wang, Appl. Phys. Lett. **108**, 012403 (2016).	CoFeB/MgO/CoFeB/Ta/[Co/Pd]*10	52	RT	perp.
M. Piquemal-Banci, R. Galceran, S. Caneva, M.B. Martin, R.S. Weatherup, P.R. Kidambi, K. Bouzehouane, S. Xavier, A. Anane, F. Petroff, A. Fert, J. Robertson, S. Hofmann, B. Dlubak, and P. Seneor, Appl. Phys. Lett. **108**, 102404 (2016).	Fe/h-BN/Co	6	1.4K	in-plane
K. Borisov, D. Betto, Y.C. Lau, C. Fowley, A. Titova, N. Thiyagarajah, G. Atcheson, J. Lindner, A.M. Deac, J.M.D. Coey, P. Stamenov, and K. Rode, Appl. Phys. Lett. **108**, 192407 (2016).	Mn_2RuGa/Al/MgO/CoFeB/Ta/CoFeB/MgO	5	300K	perp.
		40	10K	perp.
		-8	300K	perp.
		-16	10K	perp.
N. Tezuka, S. Oikawa, I. Abe, M. Matsuura, S. Sugimoto, K. Nishimura, and T. Seino, IEEE Magn. Lett. **7**, 3104204 (2016).	Ru/[Co/Pt]*5/Co/Ru/Co/W/CoFeB/MgO/CoFeB/W/CoFeB	248	RT	perp.
		320	10K	perp.
T. Scheike, H. Sukegawa, K. Inomata, T. Ohkubo, K. Hono, and S. Mitani, Appl. Phys. Express **9**, 053004 (2016).	$Co_2FeAl/CoFe/MgAl_2O_4/Co_2FeAl$	342	RT	in-plane
		616	4K	in-plane
M. Belmoubarik, H. Sukegawa, T. Ohkubo, S. Mitani, and K. Hono, Appl. Phys. Lett. **108**, 132404 (2016).	$Fe/MgAl/MgAl_2O_4$/Fe/IrMn	245	RT	in-plane
		436	3K	in-plane
H. Almasi, M. Xu, Y. Xu, T. Newhouse-Illige, and W.G. Wang, Appl. Phys. Lett. **109**, 032401 (2016).	Mo/CoFeB/MgO/CoFeB/	208	RT	perp.
S. Kasai, Y.K. Takahashi, P.H. Cheng, Ikhtiar, T. Ohkubo, K. Kondou, Y. Otani, S. Mitani, and K. Hono, Appl. Phys. Lett. **109**, 032409 (2016).	$Co_2Fe(Ga_{0.5}Ge_{0.5})/Cu(In_{0.8}Ga_{0.2})Se_2/Co_2Fe(Ga_{0.5}Ge_{0.5})$	40	RT	in-plane
		100	8K	in-plane

Z. Zhao, M. Jamali, N. D'Souza, D. Zhang, S. Bandyopadhyay, J. Atulasimha, and J.P. Wang, Appl. Phys. Lett. **109**, 092403 (2016).	$Pb(Mg_{1/3}/Nb_{2/3})_{0.7}Ti_{0.3}O_3$/Ta/CoFeB/MgO/CoFeB	90	RT	in-plane
Q. Xue, Y. Yang, Z. Gao, F. Liu, Q. Li, S. Li, and G.X. Miao, Appl. Phys. Lett. **109**, 192407 (2016).	FeCo/LiF/FeCo	17	RT	in-plane
		90	77K	in-plane
K.Z. Suzuki, R. Ranjbar, J. Okabayashi, Y. Miura, A. Sugihara, H. Tsuchiura, and S. Mizukami, Sci. Rep. **6**, 30249 (2016).	CoGa/MnGa/MgO/CoFeB	3.1	RT	perp.
		12.8	5K	perp.
X. Gao, Q. Li, S. Li, J. Xu, Y. Qin, X. Shi, S. Yan, and G. Miao, J. Alloys Compd. **662**, 79 (2016).	Fe/FeCo/MgO/Fe/Co	-39	77K	in-plane
S. Kanai, F. Matsukura, and H. Ohno, Appl. Phys. Lett. **108**, 192406 (2016).	Pt/[Co/Pt]*6/Co/Ru/[Co/Pt]*2/Co/Ta/CoFeB/MgO/CoFeB	40	RT	perp.
C. Grezes, A. Rojas Rozas, F. Ebrahimi, J.G. Alzate, X. Cai, J.A. Katine, J. Langer, B. Ocker, P. Khalili Amiri, and K.L. Wang, AIP Adv. **6**, 075014 (2016).	CoFeB/MgO/CoFeB	49	RT	perp.
M. Althammer, A. Vikam Singh, S. Keshavarz, M. Kenan Yurtisigi, R. Mishra, A.Y. Borisevich, P. Leclair, and A. Gupta, J. Appl. Phys. **120**, 233903 (2016).	$La_{0.67}Sr_{0.33}MnO_3/SrSnO_3/La_{0.67}Sr_{0.33}MnO_3$	350	5K	in-plane
M. Bapna, S.K. Piotrowski, S.D. Oberdick, M. Li, C.L. Chien, and S.A. Majetich, Appl. Phys. Lett. **108**, 022406 (2016).	CoFeB/MgO/CoFeB	40	RT	perp.
R. Barman and D. Kaur, Appl. Phys. Lett. **108**, 092404 (2016).	$Ni_{50.3}Mn_{36.9}Sb_{12.8}/BiFeO_3/Ni_{50.3}Mn_{36.9}Sb_{12.8}$	11.1	RT	in-plane
H. Lee, H. Sukegawa, J. Liu, Z. Wen, S. Mitani, and K. Hono, IEEE Trans. Magn. **52**, 4400204 (2016).	MaGaN/Mg/MgO/Fe/CoFeB	3.8	RT	perp.
N. Matsuo, N. Doko, T. Takada, H. Saito, and S. Yuasa, Phys. Rev. Appl. **6**, 034011 (2016).	Fe/MgO/Ga-oxide/Fe/Co	92	RT	in-plane
		125	20K	in-plane
S. Knudde, G. Farinha, D.C. Leitao, R. Ferreira, S. Cardoso, and P.P. Freitas, J. Magn. Magn. Mater. **412**, 181 (2016).	CoFeB/Al-oxide/CoFeB	40	RT	in-plane
S. Parui, M. Ribeiro, A. Atxabal, A. Bedoya-Pinto, X. Sun, R. Llopis, F. Casanova, and L.E. Hueso, Appl. Phys. Lett. **109**, 052401 (2016).	Co/Al_2O_3/NiFe	20	RT	in-plane
Z. Gao, Y. Yang, F. Liu, Q. Xue, and G.X. Miao, Mater. Res. Express **3**, 075017 (2016).	FeCo/MgO/EuS	64	4.2K	in-plane
D. Chien, X. Li, K. Wong, M.A. Zurbuchen, S. Robbennolt, G. Yu, S. Tolbert, N. Kioussis, P. Khalili Amiri, K.L. Wang, and J.P. Chang, Appl. Phys. Lett. **108**, 112402 (2016).	CoFeB/MgO/PZT/MgO/CoFeB	53.1	RT	in-plane
R. Göckeritz, N. Homonnay, A. Müller, B. Fuhrmann, and G. Schmidt, AIP Adv. **6**, 045003 (2016).	$La_{0.7}Sr_{0.3}MnO_3/Alq_3$/Co	-70	4.3K	in-plane
S.E. Lee, Y. Takemura, and J.G. Park, Appl. Phys. Lett. **109**, 182405 (2016).	CoFeB/MgO/Fe/CoFeB/W/Co/Pt/[Co/Pt]*m/Co/Ru/Co/Pt/[Co/Pt]*n	163	RT	perp.
T. Nakano, M. Oogane, T. Furuichi, K. Ao, H. Naganuma, and Y. Ando, IEEE Trans. Magn.	Pd/[Co/Pd]*10/Co/Ta/CoFeB/MgO/	45	RT	perp.

52, 4001304 (2016).	CoFeB			
J. Hong, A. Hadjikhani, M. Stone, F.I. Allen, V. Safonov, P. Liang, J. Bokor, and S. Khizroev, IEEE Trans. Magn. **52**, 1400504 (2016).	CoFeB/MgO/CoFeB	60	RT	in-plane
D.Y. Lee, H.T. Seo, and J.G. Park, J. Mater. Chem. C **4**, 135 (2015).	CoFeB/MgO/Fe/CoFeB/cap/Co/Pt/[Co/Pt]*5/Co/Ru/Co/Pt/[Co/Pt]*6	168	RT	perp.
M.Z. Iqbal, S. Siddique, G. Hussain, and M.W. Iqbal, J. Mater. Chem. C **4**, 8711 (2016).	NiFe/graphene/h-BN/Co	-0.85	300K	in-plane
		-1.88	4.2K	in-plane
D.Y. Lee, S.E. Lee, T.H. Shim, and J.G. Park, Nanoscale Res. Lett. **11**, 433 (2016).	CoFeB/MgO/Fe/CoFeB/cap/Co/Pt/[Co/Pt]*4/Co/Ru/Co/Pt/[Co/Pt]*6	160	RT	perp.
D.Y. Lee, S.H. Hong, S.E. Lee, and J.G. Park, Sci. Rep. **6**, 38125 (2016).	CoFeB/MgO/CoFeB	134	RT	perp.
Y. Takemura, D.Y. Lee, S.E. Lee, and J.G. Park, Nanotechnology **27**, 485203 (2016).	CoFeB/MgO/CoFeB	134	RT	perp.
Y.K. Wakabayashi, K. Okamoto, Y. Ban, S. Sato, M. Tanaka, and S. Ohya, Appl. Phys. Express **9**, 123001 (2016).	$Ge_{0.935}Fe_{0.065}$/MgO/Fe	0.3	3.5K	in-plane

TMR_2017

References	**Structures**	**TMR (%)**	T_m	**in-plane or perp.**
T. Nakano, M. Oogane, T. Furuichi, and Y. Ando, Appl. Phys. Lett. **110**, 012401 (2017).	Pd/[Co/Pt]*9/Co/Ru/Co/[Pd/Co]*7/Ta/CoFeB/MgO/CoFeB	41	RT	perp.
K. Yakushiji, A. Sugihara, A. Fukushima, H. Kubota, and S. Yuasa, Appl. Phys. Lett. **110**, 092406 (2017).	Ru/Pt/Co/[Pt/Co]*7/Ir/[Co/Pt]*4/W/CoB/W/CoFeB/MgO/CoFeB/MgO	131	RT	perp.
Y.F. Liu, X. Yin, Y. Yang, D. Ewing, P.J. De Rego, and S.H. Liou, AIP Adv. **7**, 056666 (2017).	IrMn/CoFe/Ru/CoFeB/MgO/CoFeB/MgO	137	RT	in-plane
H. Sukegawa, Y. Kato, M. Belmoubarik, P.H. Cheng, T. Daibou, N. Shimomura, Y. Kamiguchi, J. Ito, H. Yoda, T. Ohkubo, S. Mitani, and K. Hono, Appl. Phys. Lett. **110**, 122404 (2017).	Fe/Mg/$MgGa_2O_4$/Fe/IrMn	121	RT	in-plane
		196	4K	in-plane
J.G. Deak, Z. Zhou, and W. Shen, AIP Adv. **7**, 056676 (2017).	PtMn/CoFe/Ru/CoFeB/MgO/CoFeB/NiFe	225	RT	in-plane
H. Almasi, C.L. Sun, X. Li, T. Newhouse-Illige, C. Bi, K.C. Price, S. Nahar, C. Grezes, Q. Hu, P. Khalili Amiri, K.L. Wang, P.M. Voyles, and W.G. Wang, J. Appl. Phys. **121**, 153902 (2017).	W/CoFeB/MgO/CoFeB	138	RT	perp.
T. Dohi, S. Kanai, F. Matsukura, and H. Ohno, Appl. Phys. Lett. **111**, 072403 (2017).	Ta/Pt/[Co/Pt]*6/Co/Ru/[Co/Pt]*2/Co/Ta/CoFeB/MgO/CoFeB	160	RT	perp.
K. Ning, H. Liu, Z. Ju, C. Fang, C. Wan, J. Cheng, X. Liu, L. Li, J. Feng, H. Wei, X. Han, Y. Yang, and T.L. Ren, AIP Adv. **7**, 015035	CoFeB/MgO/CoFeB	152.8	300K	perp.

(2017).				
J. Chatterjee, R.C. Sousa, N. Perrissin, S. Auffret, C. Ducruet, and B. Dieny, Appl. Phys. Lett. **110**, 202401 (2017).	FeCoB/MgO/FeCoB	117	RT	perp.
O. Manos, A. Böhnke, P. Bougiatioti, R. Klett, K. Rott, A. Niesen, J.M. Schmalhorst, and G. Reiss, J. Appl. Phys. **122**, 103904 (2017).	CoFe/Ta/CoFeB/MgO/CoFeB	47.2	RT	perp.
R. Xiong, B. Fang, G. Li, Y. Xiao, M. Tang, and Z. Li, Appl. Phys. Lett. **111**, 062401 (2017).	NiFe/IrMn/CoFeB/MgO/CoFeB	46	RT	in-plane
S. Tamaru, H. Kubota, K. Yakushiji, A. Fukushima, and S. Yuasa, J. Appl. Phys. **122**, 193901 (2017).	PtMn/CoFe/Ru/CoFeB/MgO/FeB/MgO	84	RT	in-plane
G. Kurij, A. Solignac, T. Maroutian, G. Agnus, R. Guerrero, L.E. Calvet, M. Pannetier-Lecoeur, and P. Lecoeur, Appl. Phys. Lett. **110**, 082405 (2017).	$La_{0.67}Sr_{0.33}MnO_3$/Nb-doped $SrTiO_3$/$La_{0.67}Sr_{0.33}MnO_3$/$La_{0.67}Sr_{0.3}Mn_{0.93}Ru_{0.07}O_3$	350	20K	in-plane
N. Ohshima, H. Sato, S. Kanai, J. Llandro, S. Fukami, F. Matsukura, and H. Ohno, AIP Adv. **7**, 055927 (2017).	Pt/[Co/Pt]*6/Co/Ru/[Co/Pt]*2/Co/Ta/CoFeB/MgO/CoFeB/Ta/CoFeB/MgO	90	RT	perp.
T. Devolder, S. Couet, J. Swerts, E. Liu, T. Lin, S. Mertens, A. Furnemont, and G. Kar, J. Appl. Phys. **121**, 113904 (2017).	NiCr/[Ni/Co]*6/Ru/Co/TaFeCoB/FeCoB/MgO/FeCoB/Ta/FeCoB/MgO	146	RT	perp.
C. Yoshida, H. Noshiro, Y. Yamazaki, and T. Sugii, AIP Adv. **7**, 065105 (2017).	CoPt/Ru/Ta/MgO/CoFeB/Ta/CoFeB/MgO/CoFeB/CoPt/Ru/CoPt	98	RT	in-plane
Z. Jin, M. Oogane, K. Fujiwara, and Y. Ando, J. Appl. Phys. **122**, 174502 (2017).	NiFe/Ru/CoFeB/MgO/CoFeB/Ru/CoFeB/IrMn	180	RT	in-plane
L. Martins, J. Ventura, R. Ferreira, and P.P. Freitas, Appl. Surf. Sci. **424**, 58 (2017).	PtMn/CoFe/Ru/CoFeB/MgO/CoFeB	103.32	RT	in-plane
S. Knudde, D.C. Leitao, S. Cardoso, and P.P. Freitas, J. Phys. D. Appl. Phys. **50**, 165001 (2017).	NiFe/CoFeB/Al-oxide/CoFeB/Ru/CoFe/IrMn	35	RT	in-plane
S. Couet, T. Devolder, J. Swerts, S. Mertens, T. Lin, E. Liu, S. Van Elshocht, and G. Sankar Kar, Appl. Phys. Lett. **111**, 152406 (2017).	[Co/Pt]*3/Co/Ru/[Co/Pt]/MgO/CoFeB/Mg/Ta/CoFeB/MgO	197	RT	perp.
P.U. Asshoff, J.L. Sambricio, A.P. Rooney, S. Slizovskiy, A. Mishchenko, A.M. Rakowski, E.W. Hill, A.K. Geim, S.J. Haigh, V.I. Fal'Ko, I.J. Vera-Marun, and I. V. Grigorieva, 2D Mater. **4**, 031004 (2017).	NiFe/hBN/graphene/Co	1	10K	in-plane
R.C. Subedi, R. Geng, H.M. Luong, W. Huang, X. Li, L.A. Hornak, and T.D. Nguyen, Appl. Phys. Lett. **110**, 053302 (2017).	$La_{2/3}Sr_{1/3}MnO_3$/VDF-TrFE/Co	-20	20K	in-plane
O. Vávra, R. Soni, A. Petraru, N. Himmel, I. Vávra, J. Fabian, H. Kohlstedt, and C. Strunk, AIP Adv. **7**, 025008 (2017).	Fe/Al_2O_3/Fe	5.2	0.3K	in-plane
T. Matou, K. Takeshima, L.D. Anh, M. Seki, H. Tabata, M. Tanaka, and S. Ohya, Appl. Phys. Lett. **110**, 212406 (2017).	$La_{0.67}Sr_{0.33}MnO_3$/$LaMnO_3$/$La_{0.67}Sr_{0.33}MnO_3$	2	3.6K	in-plane

L. Huang, Z.H. Yuan, B.S. Tao, C.H. Wan, P. Guo, Q.T. Zhang, L. Yin, J.F. Feng, T. Nakano, H. Naganuma, H.F. Liu, Y. Yan, and X.F. Han, J. Appl. Phys. **122**, 113903 (2017).	IrMn/CoFe/Ru/CoFeB/MgO/CoFeB/Ru/CoFeSiB	200	RT	in-plane
K. Singh and D. Kaur, Appl. Phys. Lett. **111**, 022902 (2017).	NiMnIn/$PbZrTiO_3$/$SrTiO_3$/NiMnSb	-39	300K	in-plane
J.Y. Chen, L. He, J.P. Wang, and M. Li, Phys. Rev. Appl. **7**, 021001 (2017).	Pd/[Co/Pd]*4/Co/MgO/(Ga,Fe)Co	0.6	RT	perp.
W. Skowroński, M. Czapkiewicz, S. Ziętek, J. Chęciński, M. Frankowski, P. Rzeszut, and J. Wrona, Sci. Rep. **7**, 10172 (2017).	[Co/Pt]*6/Co/Ru/Co[Pt/Co]*3/W/CoFeB/MgO/CoFeB/W/CoFeB/MgO	180	RT	perp.
		280	20K	perp.
S. Mao, J. Lu, X. Zhao, X. Wang, D. Wei, J. Liu, J. Xia, and J. Zhao, Sci. Rep. **7**, 43064 (2017).	MnGa/Co_2MnSi/MgO/Co_2MnSi/MnGa	10	300K	perp.
		65	10K	perp.

TMR_2018

References	**Structures**	**TMR (%)**	T_m	**in-plane or perp.**
L. Bainsla, K.Z. Suzuki, M. Tsujikawa, H. Tsuchiura, M. Shirai, and S. Mizukami, Appl. Phys. Lett. **112**, 052403 (2018).	CoFeMnSi/Mg/MgO/CoFe/IrMn	101	RT	in-plane
		521	10K	in-plane
B. Parks, M. Bapna, J. Igbokwe, H. Almasi, W. Wang, and S.A. Majetich, AIP Adv. **8**, 055903 (2018).	CoFeB/MgO/CoFeB	35	RT	in-plane
Ikhtiar, H. Sukegawa, X. Xu, M. Belmoubarik, H. Lee, S. Kasai, and K. Hono, Appl. Phys. Lett. **112**, 022408 (2018).	CoFeB/CoFe/MgO/$MgAl_2O_4$/CoFeB	242	RT	in-plane
M. Wang, W. Cai, K. Cao, J. Zhou, J. Wrona, S. Peng, H. Yang, J. Wei, W. Kang, Y. Zhang, J. Langer, B. Ocker, A. Fert, and W. Zhao, Nat. Commun. **9**, 671 (2018).	[Co/Pt]*6/Co/Ru/Co/[Pt/Co]*3/W/CoFeB/MgO/CoFeB/W/CoFeB/MgO	249	RT	perp.
D.L. Zhang, K.B. Schliep, R.J. Wu, P. Quarterman, D. Reifsnyder Hickey, Y. Lv, X. Chao, H. Li, J.Y. Chen, Z. Zhao, M. Jamali, K.A. Mkhoyan, and J.P. Wang, Appl. Phys. Lett. **112**, 152401 (2018).	Pt/FePd/W/CoFeB/MgO/CoFeB/Ta/[Co/Pd]*4	7	RT	perp.
		46	10K	perp.
K.Z. Suzuki, Y. Miura, R. Ranjbar, A. Sugihara, and S. Mizukami, J. Phys. D. Appl. Phys. **51**, 235001 (2018).	CoGa/MnGa/Mg/MgO/CoFeB	8	RT	perp.
		25	10K	perp.
K.Z. Suzuki, Y. Miura, R. Ranjbar, L. Bainsla, A. Ono, Y. Sasaki, and S. Mizukami, Appl. Phys. Lett. **112**, 062402 (2018).	CoGa/MnGa/Mn/Mg/MgO/CoFeB	18	300K	perp.
		38.4	5K	perp.
D. Tiwari, R. Sharma, O.G. Heinonen, J. Åkerman, and P.K. Muduli, Appl. Phys. Lett. **112**, 022406 (2018).	IrMn/CoFe/Ru/CoFeB/MgO/CoFeB	73	RT	in-plane
H. Lv, D.C. Leitao, Z. Hou, P.P. Freitas, S. Cardoso, T. Kämpfe, J. Müller, J. Langer, and J. Wrona, AIP Adv. **8**, 055908 (2018).	CoFeB/MgO/CoFeB	123.9	RT	perp.
M. Williamson, M. De Rozieres, H. Almasi, X. Chao, W. Wang, J.P. Wang, and M. Tsoi, AIP Adv. **8**, 055912 (2018).	CoFeB/MgO/CoFeB	100	RT	perp.

M. Sun, T. Kubota, S. Takahashi, Y. Kawato, Y. Sonobe, and K. Takanashi, AIP Adv. **8**, 055902 (2018).	$Co_2Fe_{0.4}Mn_{0.6}Si$/MgO/$Co_{50}Fe_{50}$	136	RT	in-plane
M. Bapna, B. Parks, S.D. Oberdick, H. Almasi, W. Wang, and S.A. Majetich, Phys. Rev. Appl. **10**, 024013 (2018).	CoFeB/MgO/CoFeB	128	RT	perp.
X.D. Xu, K. Mukaiyama, S. Kasai, T. Ohkubo, and K. Hono, Acta Mater. **161**, 360 (2018).	CoFeB/MgO/CoFeB	300	RT	in-plane
K. Yakushiji, E. Kitagawa, T. Ochiai, H. Kubota, N. Shimomura, J. Ito, H. Yoda, and S. Yuasa, AIP Adv. **8**, 055905 (2018).	CoFe/Ru/CoFeB/CoFe/Mg-Fe-O/CoFeB	160	RT	in-plane
Y. Huai, H. Gan, Z. Wang, P. Xu, X. Hao, B.K. Yen, R. Malmhall, N. Pakala, C. Wang, J. Zhang, Y. Zhou, D. Jung, K. Satoh, R. Wang, L. Xue, and M. Pakala, Appl. Phys. Lett. **112**, 092402 (2018).	Ir/Co/Mo/CoFeB/MgO/CoFeB/Mo/CoFeB/MgO	215	RT	perp.
Y.C. Wu, W. Kim, S. Rao, K. Garello, S. Van Beek, S. Couet, E. Liu, J. Swerts, S. Kundu, L. Souriau, F. Yasin, D. Crotti, J.K. Jochum, M.J. Van Bael, J. Van Houdt, G. Groeseneken, and G.S. Kar, Appl. Phys. Lett. **113**, 142405 (2018).	CoFeB/MgO/CoFeB	150	300K	perp.
		115	400K	perp.
K. Cao, H. Li, W. Cai, J. Wei, L. Wang, Y. Hu, Q. Jiang, H. Cui, C. Zhao, and W. Zhao, IEEE Trans. Magn. **55**, 3400304 (2019).	Pt/$[Co/Pt]_6$/Co/Ru/Co/$[Pt/Co]_3$/W/CoFeB/MgO/CoFeB/W/CoFeB/MgO	176	20K	perp.
		120	300K	perp.
		96	400K	perp.
D.L. Zhang, C. Sun, Y. Lv, K.B. Schliep, Z. Zhao, J.Y. Chen, P.M. Voyles, and J.P. Wang, Phys. Rev. Appl. **9**, 044028 (2018).	Pt/FePd/Ru/FePd/Ta/CoFeB/MgO/CoFeB/Ta/[Co/Pd]*4	25	300K	perp.
		60	5K	perp.
J.Y. Choi, D.G. Lee, J.U. Baek, and J.G. Park, Sci. Rep. **8**, 2139 (2018).	Pt/[Co/Pt]*3/Co/Ru/Co/Pt/Co/W/CoFeB/MgO/Fe/CoFeB/W/CoFeB/MgO	180	RT	perp.
T. Kanaki, H. Yamasaki, T. Koyama, D. Chiba, S. Ohya, and M. Tanaka, Sci. Rep. **8**, 7195 (2018).	GaMnAs/GaAs/GaMnAs	7	3.8K	in-plane

TMR_2019

References	**Structures**	**TMR (%)**	T_m	**in-plane or perp.**
O. Manos, P. Bougiatioti, D. Dyck, T. Huebner, K. Rott, J.M. Schmalhorst, and G. Reiss, J. Appl. Phys. **125**, 023905 (2019).	CoFe/Ta/CoFeB/MgO/CoFeB	65.3	RT	perp.
A. Chen, Y. Wen, B. Fang, Y. Zhao, Q. Zhang, Y. Chang, P. Li, H. Wu, H. Huang, Y. Lu, Z. Zeng, J. Cai, X. Han, T. Wu, X.X. Zhang, and Y. Zhao, Nat. Commun. **10**, 243 (2019).	IrMn/CoFe/Ru/CoFeB/MgO/CoFeB	235	RT	in-plane
A.K. Reza and K. Roy, J. Appl. Phys. **126**, 023901 (2019).	CoTb/MgO/CoTb/Ru/CoFe/NiMn	87	RT	in-plane
Y. Goto, T. Yanase, T. Shimada, M. Shirai,	Fe/MgO/Fe_3Sn/Co	50	9K	in-plane

and T. Nagahama, AIP Adv. **9**, 085322 (2019).		20	RT	in-plane
H. Honjo, S. Ikeda, H. Sato, M. Yasuhira, and T. Endoh, IEEE Trans. Magn. **55**, 3400904 (2019).	Pt/[Co/Pt]*n/Co/Ru/[Co/Pt]*n/Co/W/CoFeB/MgO/Free layer/MgO	170	RT	perp.
W. Wu, L. Zhang, J. Cai, B. Fang, J. Luo, and Z. Zeng, Appl. Phys. Lett. **115**, 052401 (2019).	CoFeB/MgO/CoFeB/Ru/CoFe/PtMn	130	RT	in-plane
Q. Xiang, H. Sukegawa, M. Belmoubarik, M. Al-Mahdawi, T. Scheike, S. Kasai, Y. Miura, and S. Mitani, Adv. Sci. **6**, 1901438 (2019).	Fe/$MgAl_2O_4$/Fe	32	RT	perp.
M. Bapna, B. Parks, S. Oberdick, H. Almasi, C. Sun, P. Voyles, W. Wang, and S.A. Majetich, J. Magn. Magn. Mater. **483**, 34 (2019).	CoFeB/MgO/CoFeB	125	RT	perp.
K. Mukaiyama, J.W. Jung, H. Sepehri-Amin, S. Kasai, T. Furubayashi, T. Ohkubo, and K. Hono, Appl. Phys. Lett. **114**, 172402 (2019).	$Co_2FeGa_{0.5}Ge_{0.5}$/$CuGaSe_2$/$Co_2FeGaGe_{0.5}$	100	RT	in-plane
		250	30K	in-plane
P. Rzeszut, W. Skowroński, S. Ziętek, J. Wrona, and T. Stobiecki, J. Appl. Phys. **125**, 223907 (2019).	[Co/Pt]base/W/CoFeB/MgO/W/CoFeB/MgO	135	RT	perp.
S. Mao, J. Lu, H. Wang, X. Zhao, D. Wei, and J. Zhao, J. Phys. D. Appl. Phys. **52**, 405002 (2019).	Co_2MnSi/$L1_0$-MnAl/MgO/Co_2MnSi/MnAl	10	5K	perp.
H. Saito, S.K. Narayananellore, N. Matsuo, N. Doko, S. Kon, Y. Yasukawa, H. Imamura, and S. Yuasa, Phys. Rev. Appl. **11**, 064032 (2019).	Fe/MgO/ZnO/Fe/Co	96	RT	in-plane
		127	20K	in-plane
J. Tornos, F. Gallego, S. Valencia, Y.H. Liu, V. Rouco, V. Lauter, R. Abrudan, C. Luo, H. Ryll, Q. Wang, D. Hernandez-Martin, G. Orfila, M. Cabero, F. Cuellar, D. Arias, F.J. Mompean, M. Garcia-Hernandez, F. Radu, T.R. Charlton, A. Rivera-Calzada, Z. Sefrioui, S.G.E. Te Velthuis, C. Leon, and J. Santamaria, Phys. Rev. Lett. **122**, 037601 (2019).	$La_{0.7}Sr_{0.3}MnO_3$/$BaTiO_3$/$La_{0.7}Sr_{0.3}MnO_3$	1000	14K	in-plane
A. Titova, C. Fowley, E. Clifford, Y.C. Lau, K. Borisov, D. Betto, G. Atcheson, R. Hübner, C. Xu, P. Stamenov, M. Coey, K. Rode, J. Lindner, J. Fassbender, and A.M. Deac, Sci. Rep. **9**, 4020 (2019).	$Mn_2Ru_{0.75}Ga$/Al/MgO/CoFeB	12	60K	perp.
		-1	60K	perp.

Achievement

Publications

(1) **Yuki Iida**, Jun Okabayashi and Seiji Mitani
"Perpendicular magnetic anisotropy in sputter-deposited Fe/MgO interfaces tuned by W buffer and Tb capping layers"
Appl. Phys. Lett. **113**, 252401 (2018).

(2) **Yuki Iida**, Qingyi Xiang, Jun Okabayashi, Thomas Scheike, Hiroaki Sukegawa and Seiji Mitani
"Effect of tungsten doping on perpendicular magnetic anisotropy and its voltage effect in single crystal Fe/MgO(001) interfaces"
J. Phys. D: Appl. Phys. **53**, 124001 (2020).

(3) **Yuki Iida**, Jun Okabayashi, Peng Sheng, Masamitsu Hayashi and Seiji Mitani
"Effect of lanthanum buffer layers on perpendicular magnetic anisotropy in CoFeB/MgO heterostructures"
Submitted.

(4) **Yuki Iida**, Qingyi Xiang, Thomas Scheike, Zhenchao Wen, Jun Okabayashi, Tadakatsu Ohkubo, Kazuhiro Hono, Hiroaki Sukegawa and Seiji Mitani
"Perpendicular Magnetic Anisotropy at Fe/Rock-Salt-Type Cr-Oxide Interface Formed via Oxygen-Driven Diffusion from Cr Buffer"
in preparation.

(5) Jun Okabayashi, **Yuki Iida**, Qingyi Xiang, Hiroaki Sukegawa and Seiji Mitani
"Perpendicular orbital and quadrupole anisotropies at Fe/MgO interfaces detected by x-ray magnetic circular and linear dichroisms"
Appl. Phys. Lett. **115**, 252402 (2019).

Oral presentation

(1) **Yuki Iida**, Jun Okabayashi and Seiji Mitani
"Perpendicular magnetic anisotropy of polycrystalline Fe/MgO interfaces induced by W buffer and Tb capping layers."
応用物理学会 2017 年秋季講演会, 2017.9.5, 福岡国際会議場

(2) **Yuki Iida**, Jun Okabayashi, Peng Sheng, Masamitsu Hayashi and Seiji Mitani
"Perpendicular magnetic anisotropy in as-deposited La/CoFeB/MgO layered structures."

応用物理学会 2018 年春季講演会, 2018.3.19, 早稲田大学

(3) **Yuki Iida**, Qingyi Xiang, Hiroaki Sukegawa and Seiji Mitani
"Interface perpendicular magnetic anisotropy in sputter-deposited single crystalline Fe/MgO heterostructures"
応用物理学会 2019 年秋季講演会, 2019.9.19, 北海道大学

(4) **Yuki Iida**, Jun Okabayashi, Hiroaki Sukegawa and Seiji Mitani
"Large Perpendicular Magnetic Anisotropy in Single Crystalline Fe/MgO Heterostructures via Optimized Rf-Sputtering Processes."
64th Annual Conference on Magnetism and Magnetic Materials, 2019.11.7, Las Vegas

(5) **Yuki Iida**, Qingyi Xiang, Thomas Scheike, Zhenchao Wen, Jun Okabayashi, Tadakatsu Ohkubo, Kazuhiro Hono, Hiroaki Sukegawa and Seiji Mitani
"Perpendicular magnetic anisotropy of Fe/cubic CrO/MgO heterostructures"
第 44 回日本磁気学会学術講演会 2020.12.17 オンライン

Poseter presentation

(1) **Y. Iida** and S. Mitani
"Examination of perpendicular mangetic anisotropy in Tb-inserted CoFeB/oxide interfaces."
Tsukuba Global Science Week 2016, 2016.9.17, Tsukuba International Congress Center

(2) Yuki Iida, Jun Okabayashi and Seiji Mitani
"Perpendicular magnetic anisotropy of an Fe/MgO interface induced by W buffer and Tb cap layers"
The 28th Magnetic Recording Conference, 2017.8.3, Tsukuba International Congress Center

(3) **Yuki Iida**, Jun Okabayashi and Seiji Mitani
"Perpendicular magnetic anisotropy of an Fe/MgO interface induced by W buffer and Tb cap layers."
Tsukuba Global Science Week 2017, 2017.9.25, Tsukuba International Congress Center

(4) **Yuki Iida**, Jun Okabayashi, Peng Sheng, Masamitsu Hayashi and Seiji Mitani,
"Interface perpendicular magnetic anisotropy in annealing-free CoFeB/MgO heterostructures studied by XMCD"
2017 年度量子ビームサイエンスフェスタ, 2018.3.3, 茨城県立県民文化センター

(5) **Yuki Iida**, Qingyi Xiang, Jun Okabayashi, Thomas Scheike, Xiandong Xu, Kazuhiro Hono,

Hiroaki Sukegawa and Seiji Mitani
“Perpendicular magnetic anisotropy in tungsten-inserted Fe/MgO heterostructures studied by XMCD”
2018 年度量子ビームサイエンスフェスタ, 2019.3.12, つくば国際会議場

(6) **Yuki Iida**, Jun Okabayashi, Peng Sheng, Masamitsu Hayashi and Seiji Mitani
“Perpendicular magnetic anisotropy in annealing-free La/CoFeB/MgO heterostructures.”
Intermag 2018 Marina Bay Sands Convention Center, 2018.4.27, Singapore